Computational Modeling of Planktonic and Biofilm Metabolism

Weihua Guo

Dissertation submitted to the faculty of the Virginia Polytechnic Institute and State University in partial fulfillment of the requirements for the degree of

Doctor of Philosophy

In

Biological Systems Engineering

Xueyang Feng, Chair

Zhen (Jason) He

Ryan S. Senger

Chenming (Mike) Zhang

September 27th, 2017

Blacksburg, VA

Key words: ^{13}C assisted pathway and flux analysis, planktonic and biofilm metabolism, flux balance analysis, multi-omics analysis, machine learning, CRISPR-Cas9, metabolic engineering, biofuels, cell-free protein synthesis.

Computational Modeling of Planktonic and Biofilm Metabolism

Weihua Guo

Abstract

Most of microorganisms are ubiquitously able to live in both planktonic and biofilm states, which can be applied to dissolve the energy and environmental issues (e.g., producing biofuels and purifying waste water), but can also lead to serious public health problems. To better harness microorganisms, plenty of studies have been implemented to investigate the metabolism of planktonic and/or biofilm cells via multi-omics approaches (e.g., transcriptomics and proteomics analysis). However, these approaches are limited to provide the direct description of intracellular metabolism (e.g., metabolic fluxes) of microorganisms.

Therefore, in this study, I have applied computational modeling approaches (i.e., ^{13}C assisted pathway and flux analysis, flux balance analysis, and machine learning) to both planktonic and biofilm cells for better understanding intracellular metabolisms and providing valuable biological insights. First, I have summarized recent advances in synergizing ^{13}C assisted pathway and flux analysis and metabolic engineering. Second, I have applied ^{13}C assisted pathway and flux analysis to investigate the intracellular metabolisms of planktonic and biofilm cells. Various biological insights have been elucidated, including the metabolic responses under mixed stresses in the planktonic states, the metabolic rewiring in homogenous and heterologous chemical biosynthesis, key pathways of biofilm cells for electricity generation, and mechanisms behind the electricity generation. Third, I have developed a novel platform (i.e., omFBA) to integrate multi-omics data with flux balance analysis for accurate prediction of biological insights (e.g.,

key flux ratios) of both planktonic and biofilm cells. Fourth, I have designed a computational tool (i.e., CRISTINES) for the advanced genome editing tool (i.e., CRISPR-dCas9 system) to facilitate the sequence designs of guide RNA for programmable control of metabolic fluxes. Lastly, I have also accomplished several outreaches in metabolic engineering.

In summary, during my Ph.D. training, I have systematically applied computational modeling approaches to investigate the microbial metabolisms in both planktonic and biofilm states. The biological findings and computational tools can be utilized to guide the scientists and engineers to derive more productive microorganisms via metabolic engineering and synthetic biology. In the future, I will apply ^{13}C assisted pathway analysis to investigate the metabolism of pathogenic biofilm cells for reducing their antibiotic resistance.

Computational Modeling of Planktonic and Biofilm Metabolism

Weihua Guo

General Audience Abstract

Most of microorganisms are ubiquitously able to live in both planktonic and biofilm states (i.e., floating in a flow and anchoring on a surface, respectively), which can be applied to dissolve the energy and environmental issues (e.g., producing biofuels and purifying waste water), but can also lead to serious public health problems (e.g., chronic infections). Therefore, deciphering the metabolism of both planktonic and biofilm cells are of great importance to better harness microorganism. Plenty of studies have been implemented to investigate the metabolism of planktonic and/or biofilm cells by measuring the abundances of single type of biological components (e.g., gene expression and proteins). However, these approaches are limited to provide the direct description of intracellular metabolism (e.g., enzyme activities) of microorganisms.

Therefore, in this study, I have applied computational modeling approaches to both planktonic and biofilm cells for providing valuable biological insights (e.g., enzyme activities). The biological insights include 1) how planktonic cells response to mixed stresses (e.g., acids and organics) 2) how planktonic cells produce various chemicals, and 3) how biofilm cells generate electricity by rewiring the intracellular metabolic pathways. I also developed a novel platform to utilize multiple types of biological data for improving the prediction accuracy of biological insights of both planktonic and biofilm cells. In addition, I designed a computational tool to facilitate the sequence designs of an advanced genome editing tool for precisely controlling the corresponding enzyme activities. Lastly, I have also accomplished several outreaches in metabolic engineering.

In summary, during my Ph.D. training, I have systematically applied computational modeling approaches to investigate the microbial metabolisms in both planktonic and biofilm states. The biological findings and computational tools can be utilized to guide the metabolic engineered to derive more productive microorganisms via metabolic engineering and synthetic biology. In the future, I plan to investigate how the pathogenic biofilm cells improve their antibiotic resistance and attempt to reduce such strong resistance.

Dedication

To my dear parents and girlfriend

Acknowledgements

I would like to give my greatest thanks to Dr. Xueyang Feng, my advisor and mentor, for personally training me in metabolic flux analysis. He provided the generous support on my research work and constant help in my life. He untiringly seeks opportunities to advance my research skills, collaborate with renowned scientists, and apply to fellowships. It is my fortune to have an advisor like him who is always optimistic, energetic, and backing me. I am also thankful to Dr. Zhen (Jason) He with his student Shuai Luo and Dr. Barry Goodell with his student Liangpeng Zhuang for providing me opportunities to study the environmental microorganisms; to Dr. Zengyi Shao with her students Dr. Miguel Suastegui and Meirong Gao, as well as Dr. Wei Na with her student Yingying Chen for productive collaborations; and Dr. Huimin Zhao, Dr. Tong Si, and Dr. Jiazhang Lian for collaborations in metabolic engineering and synthetic biology. I am also grateful to my committee members, Dr. Zhen (Jason) He, Dr. Ryan Senger, and Dr. Chenming (Mike) Zhang for their kind guidance and support. I am thankful for the generous funding support from Virginia Tech start-up funding (#175323).

Very special thanks to my colleges Dr. Jiayuan Sheng for teaching me research skills in synthetic biology and metabolic engineering. I also am grateful for the help provided by Dr. Mary Leigh Wolfe, Barbara Wills, Liza Spradlin, Denton Yoder, Ling Li, and Melody Clark.

This dissertation is dedicated to my parents for their unconditional love and unwavering support and to my beautiful girlfriend, Lu Wang, for her constant supports. I can never adequately thank my parents for bringing out the best in me. I would like to

express my deepest thanks and love to my dear girlfriend and to remember every moment that we spent together although at the opposite two coastlines of American continent.

Table of Contents

List of Figures

Chapter 1

Chapter 2

Chapter 3

Chapter 5

Chapter 6

List of Tables

Chapter 2

Chapter 3

Chapter 4

Chapter 6

List of Abbreviations

6PG	6-Phosphogluconate
AA	Amino Acids
AAla	Alanine
ACAL	Acetaldehyde
ACC	Acetyl-CoA carboxylase
AcCoA	Acetyl-CoA
ACE (Ace)	Acetate
AceP	Acetyl-P
ACK	Acetate kinase
ACL	ATP citrate lyase
ACS	Acetyl-CoA synthetase
ADH	Alcohol dehydrogenase
ADH1/5	Alcohol dehydrogenase 1/5
AKG	α-Ketoglutarate
ALDH	Aldehyde dehydrogenase
ARO	Pentafunctional protein ARO1p
ARO1	Pentafunctional enzyme converting DAHP to EPSP
ARO1A	ESPS synthase
ARO1B	SA kinase
ARO1C	DHQ synthase
ARO1D	DHS dehydrogenase

$ARO1_{D920A}$	Mutant ARO1 with disrupted activity of shikimate kinase subunit
ARO1E	DHQ dehydratase
ARO2	Chorismate synthase
ARO3/4	DAHP synthase isoenzymes
$ARO4_{K229L}$	Feedback insensitive DAHP synthase
ARO7	chorismate mutase.
Asp	Aspartate
C1	C1 molecule
CIT	Citrate
Cyc BO	Cytochrome bo oxidase
Cyc c	Cytochrome C
CymA	Tetraheme cytochrome anchored in inner membrane, accepts electrons from formate and transfers them to MtrA, MtrB and MtrC
cyto-PDH	Cytosolic pyruvate dehydrogenase
DAHP	3-deoxy-D-arabinoheptulosonate 7-phosphate
DHAP	Dihydroxyacetone phosphate
DHQ	Dehydroquinoate
DHS	Dehydroshikimate
E4P	Erythrose 4-Phosphate
ENO	Enolase
EPSP	5-enolpyruvyl-3-shikimate phosphate

ETH (EtOH)	Ethanol
ETHOUT	Extracellular ethanol
F6P	Fructose 6-phosphate
FAD	Fatty acids degradation enzymes.
FAS	Fatty acid synthesis enzymes
FBA	Fructose-bisphosphate aldolase
FDH	Formate dehydrogenase
FMNOX	Oxidized flavin mononucleotide
FMNRED	Reduced flavin mononucleotide
FUM	Fumarate
G1P	Glucose-1-phosphate
G3P	Glyceraldehyde 3-phosphate
G6P	Glucose 6-Phosphate
G6PDH	G6P dehydrogenase
G6PDH2	Glucose 6-phosphate dehydrogenase
GLC	Glucose
Glox	Glyoxylate
GLOX	Glyoxylate
Glu	Glutamate
Gly	Glycine
Glyc	Glycerol
GLYC	Glycerol
GLYCOUT	Extracellular glycerol

GPD	Glycerol-3-phosphate dehydrogenase
ICIT	Isocitrate
ICL	Isocitrate lyase
IM	Inner membrane
MAA	Mycosporine-like Amino Acids
MaCoA	Malonyl-CoA
MAL	Malate
MLS	Malate synthetase
MtrA,MtrB,MtrC	Three kinds of periplasmic decaheme c-type cytochrome cytochromes anchored on outer membrane
mXDH	Mutated xylitol dehydrogenase
mXR	Mutated xylose reductase
NADH-DH	NADH dehydrogenase
OAA	Oxaloacetate
OAAMIT/OAACYT	Oxaloacetate (Mitochondria/Cytosol)
OM	Outer membrane
OXA	Oxalate
OXO	2-oxoglutarate
oxPP pathway	Oxidative pentose phosphate pathway
P5P	Ribulose 5-phosphate
pc	Pyruvate carboxylase
PDC	Pyruvate decarboxylase
PDH	Pyruvate dehydrogenase

PdhR	Pyruvate dehydrogenase regulator
PEP	Phosphoenolpyruvate
PGA	3-phosphoglycerate
PGI	Phosphoglucose isomerase
PoxB	Pyruvate oxidase
PPCK (ppck)	Phosphoenolpyruvate carboxykinase
PYK (pyk)	Pyruvate kinase
Pyr	Pyruvate
PYRCYT	Pyruvate in cytosol
PYRDC	Pyruvate decarboxylase.
PYRMIT/PYRCYT	Pyruvate (Mitochondria/Cytosol)
R5P	Ribose 5-Phosphate
Ri5P	Ribulose-5-phosphate
ROS	Reactive oxygen species
Ru5P	Ribulose 5-Phosphate
S3P	Shikimate-3-phosphate
S7P	Sedoheptulose 7-phosphate
SA	Shikimic acid
SER (Ser)	Serine
SUC	Succinate
TCA cycle	tricarboxylic acid cycle.
TKL (TKL1, TKT1)	Transketolase
TRP	Formate transporter.

TRP2	Anthranilate synthase
TRP3	Indole-3-glycerol-phosphate synthase
X5P(P5P)	Xylulose 5-phosphate
XpkA	Phosphoketolase
zwf1	Glucose-6-phosphate 1-dehydrogenase

Chapter 1: Introduction

1.1 Planktonic and biofilm metabolism

1.1.1 Planktonic and biofilm states of microorganisms

The planktonic (free floating) and biofilm (anchored to a surface) states are two ubiquitous living states for both prokaryotic and eukaryotic microorganisms[1-4]. When microorganisms are initially inoculated into an aqueous environment, they quickly reproduce in the planktonic state. Biofilms are initiated when planktonic cells recognize specific or non-specific attachment sites on a surface, as well as in response to some type of stress (e.g., antibiotic treatments)[5, 6]. Biofilms start as single cells and subsequently grow to consist of multiple layers of cells [5, 7]. As more and more planktonic cells stick onto the multi-layer biofilm, over-mature cells are flushed out of the biofilm and become planktonic again. The cycling of cells between planktonic and biofilm states has been identified as the lifecycle of biofilms.

Microorganisms in the planktonic state are usually better able to directly absorb soluble nutrients (e.g., sugar and amino acids) and excrete products or waste than those in the biofilm state. Those features lead to the fast growth associated with the planktonic state and, more importantly, make it easier to culture the microorganisms and separate products of interest. Therefore, microorganisms cultured in the planktonic state (e.g., in fermenters) have been widely used to produce various products such as biofuels[8-10], proteins[11-13], drugs[14, 15], and biomaterials[16, 17]. Because microorganisms in the planktonic state can easily access any solvable chemicals present in the culture environment,

planktonic cells can be compressed or even eliminated by various stresses (e.g., strong acids, strong bases, and antibiotics)[18]. Therefore, it is important to understand how the metabolisms of planktonic cells are reprogramed in response to different stresses in order to keep such cells as the workhorses of the microbial industries.

One the other hand, matrix-enclosed biofilms may provide a self-protected niche for microorganisms, a stable environment that is relatively free of harmful stresses such as antibiotics [2, 19-25]. The increased resistance of biofilm-associated pathogens to antibiotic drugs and the potential for antibiotic-resistant microbes to cause infections in patients with indwelling medical devices make biofilms a serious public health issue[21, 24-26]. For example, biofilms play a major role in the dissemination and protection of various bacterial pathogens (e.g., *Staphylococcus*), facilitating chronic infections and enhanced antibiotic resistance[27-35]. Such pathogens cause 1.2 million infections and over 20,000 deaths each year in the United States. Although biofilms can be dangerous, they also provide opportunities. The attachment of microorganisms to living or non-living surfaces provides an alternative approach for the transfer of substrates or products[36-39], which could be applied to solve environmental issues. For instance, biofilm and granular-sludge processes are widely applied in wastewater treatment to efficiently oxidize various organic compounds in the wastewater[40-42]. Given the dangers and opportunities presented by biofilms, an in-depth understanding of biofilm metabolism is crucial for both environmental applications and public health.

1.1.2 Current approaches to understanding planktonic and biofilm metabolism

To better harness microorganisms in both the planktonic and the biofilm states, it is important to understand the physiology and intracellular metabolism of cells in each state and also the processes involved in the conversion of cells from one state to the other[43]. The planktonic state, as the most common state for microorganisms, has received the most study and provides a convenient platform to illustrate cell metabolisms. Multi-omics approaches such as transcriptomics, proteomics, metabolomics, and fluxomics have been developed based on the planktonic platform to disclose complex microbial metabolisms by measuring and analyzing the abundances of mRNAs, proteins, metabolites, and metabolic fluxes, respectively. Those approaches cannot, however, unravel the intrinsic and complicated interactions among the multi-omics layers, which poses barriers to the rational reprogramming of planktonic microorganisms to achieve specific goals.

The biofilm state is not as well studied as the planktonic state because of its complex lifecycle and intrinsic structures [43]. Since the early 1980s, researchers have studied the lifecycle of biofilms[38, 39, 44], which includes formation, maturation, and dispersion. They found that there are huge differences in genetic regulation and pathway utilization between biofilm cells and planktonic cells[4, 45, 46]. Molecular biology studies have identified key genes and regulatory circuits related to the life cycle of biofilms[3, 23, 47, 48], providing valuable insights to help decipher biofilm metabolism. Nevertheless, researchers are still far from elucidating the mystery of biofilm metabolism. In particular, very few studies have investigated the differences in metabolic pathway usage between biofilm cells and planktonic cells. It is important to know how intracellular metabolic

fluxes are regulated in biofilm cells, because that knowledge will reveal the regulatory machinery that reprograms biofilm cells to have distinct functionalities different from those of planktonic cells.

1.2 Computational modeling of microbial metabolism

It is important to decipher microbial metabolism in order to solve public health and energy issues worldwide. Several centuries' worth of microbial metabolism studies [49] have shown that microbial metabolism is an extremely complex biological phenomenon involving thousands of genes, proteins, and metabolites as well as interactions among those components. Therefore, it is very difficult to examine the entire metabolism of a given microbe by directly measuring the abundances of all the components of the metabolism. Computational modeling provides an efficient and feasible alternative approach to understanding microbial metabolism [50, 51].

In general, the computational modeling of microbial metabolism includes two major approaches (**Fig. 1**): ^{13}C metabolic flux analysis (^{13}C-MFA)[52-54] and flux balance analysis (FBA)[55-57]. Those two approaches have distinct functionalities, but both have been widely applied to the study of various biological systems[58-64] and provided numerous biological insights to better understand cell metabolism. ^{13}C-MFA aims to rigorously elucidate metabolic reprogramming (e.g., changes in the intracellular flux distribution) by implementing ^{13}C-labeling experiments to trace pathway usages[52]. FBA aims to predict phenotypes (e.g., growth rates) by reconstructing genome-scale metabolic models with an arbitrary objective function[65].

In addition, molecular modeling provides a nanoscale-to-microscale understanding of cell metabolism[66]. In particular, machine learning approaches, especially artificial

intelligence[67], are applied to understand cell metabolisms and to predict various biological properties (e.g., alternative splicing and sequence binding specificities)[68-71]. Machine learning algorithms are remarkably accurate and capable of describing highly complex systems using large-scale data[72], which makes them suitable to modeling intricate metabolisms and processing petabyte-level biological data[70, 73].

1.3 Scope of the dissertation

There have been many studies of the metabolisms of planktonic and biofilm microorganisms using various computational modeling approaches. Many key questions are still unanswered, however, including: 1) How do microorganisms reprogram their metabolisms to resist mixed stresses or synthesize specific chemicals in the planktonic state or generate electrons in the biofilm state? 2) How can transcriptomics and fluxomics be integrated via computational modeling? 3) What regulatory rules govern genome editing?

To answer those questions, I applied three computational modeling approaches (i.e., ^{13}C-MFA, FBA, and machine learning) to study both planktonic and biofilm microorganisms. In Chapter 2 of this dissertation, I provide a comprehensive review of recent advances in ^{13}C-assisted pathway and flux analysis and metabolic engineering, with a brief introduction to the technologies used in ^{13}C-assisted pathway and flux analysis and how those technologies synergize with metabolic engineering for biochemical production[74]. In Chapter 3, I apply ^{13}C-MFA to unravel the metabolic responses (i.e., changes in metabolic flux) of *Saccharomyces cerevisiae* to multiple stresses[75]. In addition, I apply ^{13}C-MFA to reveal the metabolic reprogramming of *Gloeophyllum trabeum* for oxalate biosynthesis[76]. I also use ^{13}C-MFA combined with transcriptomics analysis to investigate strain dependency in the production of aromatic compounds in *S.*

cerevisiae [77]. In Chapter 4, I use ^{13}C-assisted pathway analysis to examine intracellular metabolic reprogramming in a biofilm of *Shewanella oneidensis* strain MR-1 growing on the anode of a microbial fuel cell. Two continuous projects reveal the different intracellular metabolisms of planktonic and biofilm cells, identify key pathways in the biofilm, and demonstrate the mechanisms behind the generation of electricity by the biofilm [78, 79]. In Chapter 5, I develop a novel platform for FBA (omFBA) that has increased prediction accuracy and simultaneously integrates multi-omics data by replacing the arbitrary objective function (e.g., maximize the growth rate) with an omics-guided objective function[80]. The omFBA platform can be applied to microorganisms in either the planktonic or the biofilm state. In Chapter 6, I develop a data-driven machine learning tool for predicting clustered regularly interspaced short palindromic repeats (CRISPR)-based transcriptional regulation, which could be used to facilitate the sequence design of guide RNAs in the CRISPR system to achieve programmable control of metabolic flux[81]. In Chapter 7, I implement several outreaches to supplement the computational modeling of planktonic cells[82, 83]. In Chapter 8, I summarize my plans for future work on deciphering the intracellular metabolism of biofilm cells.

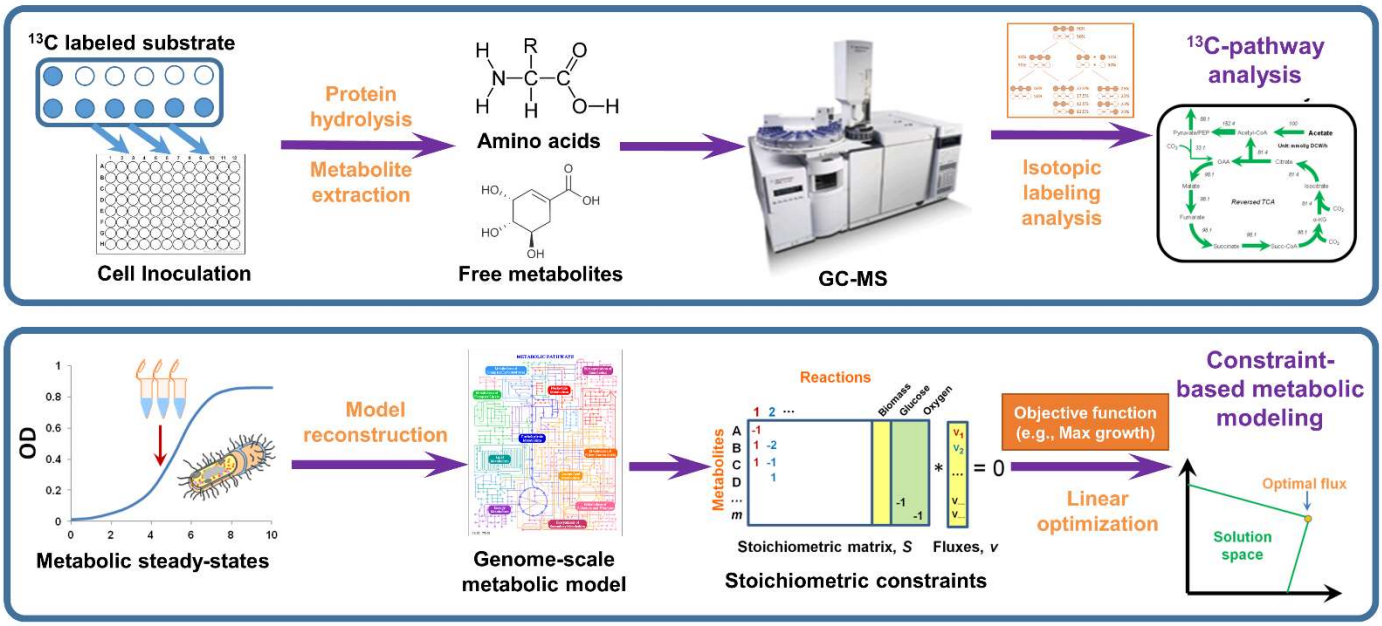

Fig. 1.1 ^{13}C-assisted pathway analysis and constraint-based metabolic modeling.

References

1. Reynolds, T.B. and G.R. Fink, *Bakers' Yeast, a Model for Fungal Biofilm Formation.* Science, 2001. **291**(5505): p. 878-881.
2. Chandra, J., et al., *Biofilm Formation by the Fungal PathogenCandida albicans: Development, Architecture, and Drug Resistance.* Journal of Bacteriology, 2001. **183**(18): p. 5385-5394.
3. Davies, D.G., et al., *The Involvement of Cell-to-Cell Signals in the Development of a Bacterial Biofilm.* Science, 1998. **280**(5361): p. 295-298.
4. McLean, J.S., et al., *Investigations of structure and metabolism within Shewanella oneidensis MR-1 biofilms.* Journal of Microbiological Methods, 2008. **74**(1): p. 47-56.
5. Karatan, E. and P. Watnick, *Signals, Regulatory Networks, and Materials That Build and Break Bacterial Biofilms.* Microbiology and Molecular Biology Reviews, 2009. **73**(2): p. 310-347.
6. Billings, N., et al., *The extracellular matrix Component Psl provides fast-acting antibiotic defense in Pseudomonas aeruginosa biofilms.* PLoS Pathog, 2013. **9**(8): p. e1003526.
7. O'Toole, G.A. and R. Kolter, *Flagellar and twitching motility are necessary for Pseudomonas aeruginosa biofilm development.* Molecular Microbiology, 1998. **30**(2): p. 295-304.
8. Lennen, R.M. and B.F. Pfleger, *Microbial production of fatty acid-derived fuels and chemicals.* Curr Opin Biotechnol, 2013. **24**(6): p. 1044-53.
9. Fillet, S. and J.L. Adrio, *Microbial production of fatty alcohols.* World Journal of Microbiology and Biotechnology, 2016. **32**(9): p. 152.
10. Sheng, J., J. Stevens, and X. Feng, *Pathway Compartmentalization in Peroxisome of Saccharomyces cerevisiae to Produce Versatile Medium Chain Fatty Alcohols.* Sci Rep, 2016. **6**: p. 26884.
11. Baneyx, F., *Recombinant protein expression in Escherichia coli.* Current Opinion in Biotechnology, 1999. **10**(5): p. 411-421.
12. Cereghino, J.L. and J.M. Cregg, *Heterologous protein expression in the methylotrophic yeast Pichia pastoris.* FEMS Microbiology Reviews, 2000. **24**(1): p. 45-66.
13. Madzak, C., C. Gaillardin, and J.-M. Beckerich, *Heterologous protein expression and secretion in the non-conventional yeast Yarrowia lipolytica: a review.* Journal of Biotechnology, 2004. **109**(1): p. 63-81.
14. Paddon, C.J., et al., *High-level semi-synthetic production of the potent antimalarial artemisinin.* Nature, 2013. **496**(7446): p. 528-532.
15. Westfall, P.J., et al., *Production of amorphadiene in yeast, and its conversion to dihydroartemisinic acid, precursor to the antimalarial agent artemisinin.* Proceedings of the National Academy of Sciences, 2012. **109**(3): p. E111-E118.
16. Aldor, I.S. and J.D. Keasling, *Process design for microbial plastic factories: metabolic engineering of polyhydroxyalkanoates.* Current Opinion in Biotechnology, 2003. **14**(5): p. 475-483.
17. Chen, G.-Q., *A microbial polyhydroxyalkanoates (PHA) based bio- and materials industry.* Chemical Society Reviews, 2009. **38**(8): p. 2434-2446.

18. Olson, M.E., et al., *Biofilm bacteria: formation and comparative susceptibility to antibiotics.* Canadian Journal of Veterinary Research, 2002. **66**(2): p. 86-92.
19. Mah, T.-F., et al., *A genetic basis for Pseudomonas aeruginosa biofilm antibiotic resistance.* Nature, 2003. **426**(6964): p. 306-310.
20. Davies, D., *Understanding biofilm resistance to antibacterial agents.* Nat Rev Drug Discov, 2003. **2**(2): p. 114-122.
21. Drenkard, E. and F.M. Ausubel, *Pseudomonas biofilm formation and antibiotic resistance are linked to phenotypic variation.* Nature, 2002. **416**(6882): p. 740-743.
22. Mah, T.-F.C. and G.A. O'Toole, *Mechanisms of biofilm resistance to antimicrobial agents.* Trends in Microbiology, 2001. **9**(1): p. 34-39.
23. Ghigo, J.-M., *Natural conjugative plasmids induce bacterial biofilm development.* Nature, 2001. **412**(6845): p. 442-445.
24. Donlan, R.M., *Biofilm Formation: A Clinically Relevant Microbiological Process.* Clinical Infectious Diseases, 2001. **33**(8): p. 1387-1392.
25. Costerton, W., et al., *The application of biofilm science to the study and control of chronic bacterial infections.* Journal of Clinical Investigation, 2003. **112**(10): p. 1466-1477.
26. Hall-Stoodley, L. and P. Stoodley, *Biofilm formation and dispersal and the transmission of human pathogens.* Trends in Microbiology, 2005. **13**(1): p. 7-10.
27. Arciola, C.R., et al., *Biofilm formation in Staphylococcus implant infections. A review of molecular mechanisms and implications for biofilm-resistant materials.* Biomaterials, 2012. **33**(26): p. 5967-5982.
28. O'Neill, E., et al., *Association between Methicillin Susceptibility and Biofilm Regulation in Staphylococcus aureus Isolates from Device-Related Infections.* Journal of Clinical Microbiology, 2007. **45**(5): p. 1379-1388.
29. de Allori, M., et al., *Antimicrobial Resistance and Production of Biofilms in Clinical Isolates of Coagulase-Negative Staphylococcus Strains.* Biological and Pharmaceutical Bulletin, 2006. **29**(8): p. 1592-1596.
30. Hall-Stoodley, L., J.W. Costerton, and P. Stoodley, *Bacterial biofilms: from the Natural environment to infectious diseases.* Nat Rev Micro, 2004. **2**(2): p. 95-108.
31. Costerton, J.W., P.S. Stewart, and E.P. Greenberg, *Bacterial Biofilms: A Common Cause of Persistent Infections.* Science, 1999. **284**(5418): p. 1318-1322.
32. Otto, M., *Staphylococcal Biofilms.* Current topics in microbiology and immunology, 2008. **322**: p. 207-228.
33. Archer, N.K., et al., *Staphylococcus aureus biofilms: Properties, regulation and roles in human disease.* Virulence, 2011. **2**(5): p. 445-459.
34. Percival, S.L., et al., *Microbiology of the skin and the role of biofilms in infection.* International Wound Journal, 2012. **9**(1): p. 14-32.
35. Davis, S.C., et al., *Microscopic and physiologic evidence for biofilm-associated wound colonization in vivo.* Wound Repair and Regeneration, 2008. **16**(1): p. 23-29.
36. Ram, R.J., et al., *Community Proteomics of a Natural Microbial Biofilm.* Science, 2005. **308**(5730): p. 1915-1920.

37. Mahadevan, R., J.S. Edwards, and F.J. Doyle, *Dynamic flux balance analysis of diauxic growth in Escherichia coli.* Biophysical Journal, 2002. **83**(3): p. 1331-1340.
38. O'Toole, G., H.B. Kaplan, and R. Kolter, *Biofilm Formation as Microbial Development.* Annual Review of Microbiology, 2000. **54**(1): p. 49-79.
39. de Beer, D., et al., *Effects of biofilm structures on oxygen distribution and mass transport.* Biotechnology and Bioengineering, 1994. **43**(11): p. 1131-1138.
40. Venkata Mohan, S., et al., *Bioelectricity generation from chemical wastewater treatment in mediatorless (anode) microbial fuel cell (MFC) using selectively enriched hydrogen producing mixed culture under acidophilic microenvironment.* Biochemical Engineering Journal, 2008. **39**(1): p. 121-130.
41. He, Z., S.D. Minteer, and L.T. Angenent, *Electricity Generation from Artificial Wastewater Using an Upflow Microbial Fuel Cell.* Environmental Science & Technology, 2005. **39**(14): p. 5262-5267.
42. Liu, Y. and J.-H. Tay, *The essential role of hydrodynamic shear force in the formation of biofilm and granular sludge.* Water Research, 2002. **36**(7): p. 1653-1665.
43. Monroe, D., *Looking for Chinks in the Armor of Bacterial Biofilms.* PLOS Biology, 2007. **5**(11): p. e307.
44. Rittmann, B.E. and P.L. McCarty, *Evaluation of steady-state-biofilm kinetics.* Biotechnology and Bioengineering, 1980. **22**(11): p. 2359-2373.
45. Yang, Y., et al., *Differential biofilms characteristics of Shewanella decolorationis microbial fuel cells under open and closed circuit conditions.* Bioresource Technology, 2011. **102**(14): p. 7093-7098.
46. Stewart, P.S. and M.J. Franklin, *Physiological heterogeneity in biofilms.* Nat Rev Micro, 2008. **6**(3): p. 199-210.
47. De Windt, W., et al., *AggA is required for aggregation and increased biofilm formation of a hyper-aggregating mutant of Shewanella oneidensis MR-1.* Microbiology, 2006. **152**(3): p. 721-729.
48. Thormann, K.M., et al., *Induction of Rapid Detachment in Shewanella oneidensis MR-1 Biofilms.* Journal of Bacteriology, 2005. **187**(3): p. 1014-1021.
49. Eknoyan, G., *Santorio Sanctorius (1561–1636) – Founding Father of Metabolic Balance Studies.* American Journal of Nephrology, 1999. **19**(2): p. 226-233.
50. Bower, J.M. and H. Bolouri, *Computational modeling of genetic and biochemical networks*. 2001: MIT press.
51. Kitano, H., *Computational systems biology.* Nature, 2002. **420**(6912): p. 206-210.
52. Zamboni, N., et al., *^{13}C-based metabolic flux analysis.* Nat. Protocols, 2009. **4**(6): p. 878-892.
53. Young, J.D., *^{13}C metabolic flux analysis of recombinant expression hosts.* Current Opinion in Biotechnology, 2014. **30**: p. 238-245.
54. Antoniewicz, M., *Methods and advances in metabolic flux analysis: a mini-review.* Journal of Industrial Microbiology & Biotechnology, 2015. **42**(3): p. 317-325.
55. Orth, J.D., I. Thiele, and B.O. Palsson, *What is flux balance analysis?* Nat Biotech, 2010. **28**(3): p. 245-248.

56. Edwards, J.S., M. Covert, and B. Palsson, *Metabolic modelling of microbes: the flux-balance approach.* Environmental Microbiology, 2002. **4**(3): p. 133-140.
57. Kauffman, K.J., P. Prakash, and J.S. Edwards, *Advances in flux balance analysis.* Current Opinion in Biotechnology, 2003. **14**(5): p. 491-496.
58. Papp, B., C. Pal, and L.D. Hurst, *Metabolic network analysis of the causes and evolution of enzyme dispensability in yeast.* Nature, 2004. **429**(6992): p. 661-664.
59. Edwards, J.S. and B.O. Palsson, *The Escherichia coli MG1655 in silico metabolic genotype: Its definition, characteristics, and capabilities.* Proceedings of the National Academy of Sciences, 2000. **97**(10): p. 5528-5533.
60. Bartek, T., et al., *Comparative ^{13}C Metabolic Flux Analysis of Pyruvate Dehydrogenase Complex-Deficient, l-Valine-Producing Corynebacterium glutamicum.* Applied and Environmental Microbiology, 2011. **77**(18): p. 6644-6652.
61. Fu, Y., et al., *Metabolic flux analysis of Escherichia coli MG1655 under octanoic acid (C8) stress.* Applied Microbiology and Biotechnology, 2015. **99**(10): p. 4397-4408.
62. Hayakawa, K., et al., *^{13}C-metabolic flux analysis in S-adenosyl-l-methionine production by Saccharomyces cerevisiae.* Journal of Bioscience and Bioengineering, 2015.
63. Cordova, L.T. and M.R. Antoniewicz, *13C metabolic flux analysis of the extremely thermophilic, fast growing, xylose-utilizing Geobacillus strain LC300.* Metabolic Engineering.
64. Crown, S.B., C.P. Long, and M.R. Antoniewicz, *Integrated ^{13}C-metabolic flux analysis of 14 parallel labeling experiments in Escherichia coli.* Metabolic Engineering, 2015. **28**: p. 151-158.
65. Schuetz, R., L. Kuepfer, and U. Sauer, *Systematic evaluation of objective functions for predicting intracellular fluxes in Escherichia coli.* Molecular Systems Biology, 2007. **3**: p. 119.
66. Schlick, T., *Molecular modeling and simulation: an interdisciplinary guide: an interdisciplinary guide*. Vol. 21. 2010: Springer Science & Business Media.
67. LeCun, Y., Y. Bengio, and G. Hinton, *Deep learning.* Nature, 2015. **521**(7553): p. 436-444.
68. Xiong, H.Y., et al., *The human splicing code reveals new insights into the genetic determinants of disease.* Science, 2015. **347**(6218).
69. Zhou, J. and O.G. Troyanskaya, *Predicting effects of noncoding variants with deep learning-based sequence model.* Nat Meth, 2015. **12**(10): p. 931-934.
70. Tarca, A.L., et al., *Machine Learning and Its Applications to Biology.* PLOS Computational Biology, 2007. **3**(6): p. e116.
71. Iniesta, R., D. Stahl, and P. McGuffin, *Machine learning, statistical learning and the future of biological research in psychiatry.* Psychological Medicine, 2016: p. 1-11.
72. Schmidhuber, J., *Deep learning in neural networks: An overview.* Neural Networks, 2015. **61**: p. 85-117.
73. Michalski, R.S., J.G. Carbonell, and T.M. Mitchell, *Machine learning: An artificial intelligence approach*. 2013: Springer Science & Business Media.

74. Guo, W., J. Sheng, and X. Feng, *13C-Metabolic Flux Analysis: An Accurate Approach to Demystify Microbial Metabolism for Biochemical Production.* Bioengineering, 2016. **3**(1): p. 3.
75. Guo, W., et al., *Investigate the Metabolic Reprogramming of Saccharomyces cerevisiae for Enhanced Resistance to Mixed Fermentation Inhibitors via ^{13}C Metabolic Flux Analysis.* PLOS ONE, 2016. **11**(8): p. e0161448.
76. Zhuang, L., et al., *Investigating oxalate biosynthesis in the wood-decaying fungus Gloeophyllum trabeum using 13C metabolic flux analysis.* RSC Advances, 2015. **5**(126): p. 104043-104047.
77. Miguel Suastegui, et al., *Investigating strain dependency in the production of aromatic compounds in Saccharomyces cerevisiae.* Biotechnol Bioeng., 2016. **Accepted**: p. 9.
78. Guo, W., et al., *13C pathway analysis of biofilm metabolism of Shewanella oneidensis MR-1.* RSC Advances, 2015. **5**(50): p. 39840-39843.
79. Luo, S., et al., *(13)C Pathway Analysis for the Role of Formate in Electricity Generation by Shewanella Oneidensis MR-1 Using Lactate in Microbial Fuel Cells.* Sci Rep, 2016. **6**: p. 20941.
80. Guo, W. and X. Feng, *OM-FBA: Integrate Transcriptomics Data with Flux Balance Analysis to Decipher the Cell Metabolism.* PLoS One, 2016. **11**(4): p. e0154188.
81. Sheng, J., et al., *Data-Driven Prediction of CRISPR-Based Transcription Regulation for Programmable Control of Metabolic Flux.* arXiv preprint arXiv:1704.03027, 2017.
82. Guo, W., et al., *Metabolic engineering of Saccharomyces cerevisiae to produce 1-hexadecanol from xylose.* Microb Cell Fact, 2016. **15**: p. 24.
83. Guo, W., J. Sheng, and X. Feng, *Mini-review: In vitro Metabolic Engineering for Biomanufacturing of High-value Products.* Computational and Structural Biotechnology Journal, 2017. **15**: p. 161-167.

Chapter 2: Synergizing ^{13}C Metabolic Flux Analysis and Metabolic Engineering for Biochemical Production

Weihua Guo[a], Jiayuan Sheng[a], Xueyang Feng[a, †]

[a] Department of Biological Systems Engineering, Virginia Tech University, Blacksburg, VA 24061, United States

[†]Correspondence to: Xueyang Feng.

Phone: +1-(540)231-2974

Email: xueyang@vt.edu

This manuscript has been published on *Springer Berlin Heidelberg: Berlin, Heidelberg.* p. 1-35.

Abstract

Metabolic engineering of industrial microorganisms to produce chemicals, fuels, and drugs has attracted increasing interests since it provides an environment-friendly and renewable route that does not depend on depleting petroleum sources. However, the microbial metabolism is so complex that metabolic engineering efforts often have difficulty in achieving a satisfactory yield, titer or productivity of the target chemical. To overcome this challenge, ^{13}C Metabolic Flux Analysis (^{13}C-MFA) has been developed to rigorously investigate the cell metabolism and quantify the carbon flux distribution in central metabolic pathways. In the past decade, ^{13}C-MFA has been widely used in academic labs and biotechnology industry to pinpoint the key issues related to microbial-based chemical production and guide the development of the appropriate metabolic engineering strategies for improving the biochemical production. In this chapter, we will introduce the basics of ^{13}C-MFA and illustrate how ^{13}C-MFA has been applied to synergize with metabolic engineering to identify and tackle the rate-limiting steps in biochemical production.

Key Words

Bottleneck, isotope, cofactor imbalance, cell metabolism, synthetic biology, biofuels.

2.1 Introduction

Producing chemicals from renewable resources would reduce strong dependence on petroleum and damage to the environment. Recently, with the development of metabolic engineering and synthetic biology, microbial production of a wide range of bulk chemicals [1-4], biofuels [5-9], and drugs [10-17], from renewable feedstock has been achieved successfully in many industrial microorganisms such as *Escherichia coli* [18-23] and *Saccharomyces cerevisiae* [24-27]. Among all of the biosynthesized chemicals, however, only a few have achieved a satisfactory production level with a titer, yield, and productivity high enough for industrial commercialization [28, 29]. Therefore, it is crucial to develop novel strategies in metabolic engineering to improve microbial-based chemical production.

One of the main reasons for the low production level of engineered microorganisms is the complexity of cell metabolism [29]. Microbial production of chemicals is more than converting the precursors to the products. Instead, the microbial metabolism needs to coordinate the carbon flux [30, 31], cofactor supply [32-34], cell maintenance [10, 35, 36], as well as other factors [37-40] to achieve the production of target chemicals at a high level. Often, the metabolic engineering strategies adopted to manipulate microbial metabolism only focus on a few known challenges (e.g., poor gene expression) but also introduce new problems (e.g., metabolic burden) that prevent the microorganisms from achieving high-level chemical production. Such complex behavior of microbial physiology presents one of the biggest obstacles in current microbial-based chemical production.

To elucidate the metabolic rewiring of microorganisms, and more importantly, to derive the appropriate strategy to engineer microorganisms for biochemical production, a technology named ^{13}C Metabolic Flux Analysis (^{13}C-MFA) has been developed in the 1990s [41-46].

Basically, ^{13}C-MFA applies carbon isotopes to trace the cell metabolism and uses mathematical modeling to uncover the carbon flux distributions in metabolic network of microorganisms [41, 42, 47-50]. By comparing the variations of metabolic fluxes among different engineered microorganisms, the key issues, such as the bottleneck pathway, could often be discovered and hence guide the bioengineers to develop more appropriate metabolic engineering strategies [51-57] to improve chemical production. In the past decade, we have witnessed many successful applications of ^{13}C-MFA on helping metabolic engineers to improve the microbial production of chemicals [31, 35, 52, 54, 58, 59], and ^{13}C-MFA has been widely recognized as one of the most important tools to diagnose microbial metabolism and develop novel metabolic engineering strategies [30, 31, 33, 35, 36, 54, 60-62].

In this chapter, we aim to summarize the synergistic tactics of ^{13}C-MFA and metabolic engineering from cases of improving microbial-based chemical production in the past decade. We will first briefly introduce the principle of ^{13}C-MFA, and then categorize the ways that ^{13}C-MFA synergizes with metabolic engineering into four groups: 1) uncovering the bottleneck steps in biochemical production; 2) identifying cofactor imbalance issues of host metabolism; 3) revealing cell maintenance requirement of industrial microorganisms; and 4) elucidating the mechanism of microbial resistance to fermentation inhibitors. We also point to emerging areas where breakthroughs of ^{13}C-MFA could potentially benefit rational metabolic engineering for improving microbial-based chemical production in the near future.

2.2 Technology Platform of ^{13}C Metabolic Flux Analysis

The technology platform of ^{13}C-MFA was first developed in 1990s [41-46]. In the past two decades, mathematical algorithms and high-throughput mass spectrometry technology have been rapidly developed and have enabled more accurate quantitative analyses of metabolic fluxes

for a broad scope of species. Because several protocols have been published to describe the procedures for both model and non-model organisms [47, 63], we focus on providing a concise introduction for ^{13}C-MFA, which includes cell culture and fermentation, isotopic analysis of metabolites, and ^{13}C-assisted pathway and flux analysis (Fig. 2.1).

2.2.1 Cell Culture and Fermentation

Cell culture on ^{13}C labeled carbon substrates is the first step for ^{13}C-MFA and plays a vital role for the entire analysis. Three key factors have been recognized in this step, namely the composition of the medium, the cultivation mode, and the selection of ^{13}C-labeled substrates.

First, a strictly minimal medium with a single carbon source is often required for the ^{13}C-labeling experiments. This is because multiple carbon substrates and unlabeled nutrients could be assimilated by microorganisms, which "dilutes" the isotopic labeling of key metabolites, mystifies the carbon fate of metabolites of interests, and increases the difficulty of both carbon consumption measurements and accurate flux calculations [64]. However, it is worth mentioning that for certain genetically engineered strains (e.g., *S. cerevisiae*) with auxotrophic markers, a trace amount of unlabeled exogenous amino acids could be supplemented into the minimal medium in order to support cell growth. Recently, several studies have reported alternative approaches for calculating the intracellular fluxes with complex medium composition and/or additional nutrients [65, 66].

Second, ^{13}C-MFA traditionally focuses on the metabolic flux distributions at the metabolic steady states, which requires both metabolic and isotopic steady states of microorganisms, i.e., the concentration and isotopic labeling of intracellular metabolites do not change. Such requirements can be met by culturing microorganisms in either of the two modes: 1) batch mode, often using shaking flask or culture tubes to culture microorganisms and harvesting biomass samples in log growth phase as a "pseudo" metabolic and isotopic steady state; and 2) chemostat mode, often

using bioreactors with continuous feeding to culture microorganisms and harvest biomass samples after 2~3 generations as the "real" metabolic and isotopic steady state. While a chemostat setup can precisely control the desired metabolic status for metabolic flux analysis, the batch mode is simpler and more cost-effective. Till now, the majority of the ^{13}C-MFA in academic labs were accomplished by sampling the ^{13}C-labeled biomass in late-log or early stationary growth phase when culturing microorganisms in batch mode [63]. Several advanced ^{13}C-assisted flux analysis approaches can also be implemented at either metabolic non-steady-state [30] or isotopic non-steady-state [67-71] to uncover the kinetic behaviors of intracellular metabolic rewiring by using novel computational tools (discussed in 2.4.2 and 2.4.3).

Third, the choice of ^{13}C-labeled substrate that should be used for ^{13}C-MFA is case-specific. In general, traditional ^{13}C-labeled glucose composition, i.e. 80% [1-^{13}C] and 20% [U-^{13}C] glucose (w/w), can easily introduce sufficient ^{13}C carbons into the metabolites of interests for accurate mass spectrometry analysis and further flux analysis [47, 72-75]. On the other hand, pure and singly labeled carbon substrates are more sensitive for detection of novel pathways because it is easier to trace labeled carbons in intermediate metabolites. For example, the [3-^{13}C] lactate was used to investigate the biofilm metabolism of *Shewanella oneidensis* MR-1 and elucidated the heavy use of C1 metabolism in biofilm cells [76]. In brief, it was expected that ^{13}C would accumulate in most metabolites because it was difficult to remove the labeled carbon of the lactate from the *S. oneidensis* cells through well-known central pathways such as the TCA cycle. However, the high concentration of unlabeled metabolites in the biofilm cells indicated that the high activity of C1 metabolism, which was the only known metabolic pathway to release the labeled carbon of lactate from *S. oneidensis* cells as $^{13}CO_2$. Additionally, multiple ^{13}C tracers are also used sometimes as they can also improve the flux resolution.

2.2.2 Isotopic Analysis of Metabolites

Experimental measurements of isotopic labeling of ^{13}C-labeled metabolites, e.g. proteinogenic amino acids, are often achieved by mass spectrometry, which detects the fractions of the total population of any molecular fragment that is unlabeled, singly labeled, doubly labeled, etc. By correcting the effects of naturally labeled isotopes on the analysis of ^{13}C-labeled metabolites, we can obtain the isotopic distributions for the metabolites of interests with high sensitivity and further use them as isotopic "fingerprints" to determine the metabolic fluxes [47, 77, 78]. Generally, three major procedures are commonly used to obtain such isotopic "fingerprints": metabolite extraction and separation; isotopic labeling detection; and correction of natural isotopomers.

Overall, many of the metabolite candidates for the flux analysis are required to be extracted from cell biomass or culture medium. Sometimes, the intracellular metabolites have low abundance and stability. Thus, a quick metabolite quenching method and sensitive mass spectrometry are often used to collect the isotopic labeling data [79]. The extracted metabolites could either be treated with the low heat derivatization group, N,O-Bis(trimethylsilyl)trifluoroacetamide (BSTFA) or N-Methyl-N-(trimethylsilyl)trifluoroacetamide (MSTFA), followed by analyzing in gas chromatography–mass spectrometry (GC-MS)[80], or directly injected without any treatment into liquid chromatography–mass spectrometry (LC-MS)[81], a machine that has much higher sensitivity than GC-MS.

For those metabolites with high abundance and stability, such as over-produced chemicals [81] and proteinogenic amino acids, the quenching step could be bypassed. Instead, the samples are often treated with N-tert-butyldimethylsilyl-N-methyltrifluoroacetamide (MTBSTFA), a cheap and commonly used derivatization group in a high heat process, followed by GC-MS analysis of

the isotopic labeling. The derivatization process will render the molecules volatile enough to enter the GC column but also introduce un-ignorable amounts of naturally labeled isotopes. Therefore, a systematic correction is required for the raw mass isotopomer spectrum prior to flux calculation. Several algorithms [82-84] have been well established to curate the isotopic labeling and remove the effects of natural isotopes so that a mass distribution vector (MDV) for each metabolite can be generated and directly used for the pathway and flux analysis.

2.2.3 ^{13}C-Assisted Pathway and Flux Analysis

Based on the corrected MDV, the metabolic behaviors of microorganisms can be elucidated both qualitatively (i.e., pathway analysis) and quantitatively (i.e., flux analysis). On one hand, the ^{13}C-assisted pathway analysis often aims to answer whether a metabolic pathway is active in non-model microorganisms by measuring the ^{13}C labeled patterns (i.e. MDVs) in key metabolites and determining the fate of biomolecule synthesis in the denoted biochemical pathways. One example of the ^{13}C-assisted pathway analysis is the discovery of C1 metabolism in biofilm *S. oneidensis* as mentioned above. On the other hand, the ^{13}C-assisted flux analysis aims to quantify the carbon fluxes in multiple metabolic pathways by simulating the ^{13}C labeled patterns (i.e. MDVs) in key metabolites and searching for the "real" metabolic fluxes that could lead to the best fit of the measured ^{13}C labeled patterns. Such quantitative analysis often reveals the network level rewiring of carbons fluxes in industrial workhorses (e.g., *E. coli*) when engineered for biochemical production. In short, while ^{13}C-assisted pathway analysis is suitable for pathway discovery in non-model microorganisms, ^{13}C-assisted flux analysis is more useful in identifying the metabolic rewiring in industrial microorganisms.

In the past decade, ^{13}C-assisted flux analysis has been widely applied to uncover the central metabolisms of various species. Accordingly to a curated database [84] that was recently

developed to collect the central carbon metabolic flux distributions investigated by ^{13}C-MFA, over 500 metabolic flux analyses have been accomplished so far for 36 organisms (Fig. 2.2). Most of the ^{13}C-MFA studies focus on investigating metabolism of *E. coli* and *S. cerevisiae*. However, there is a trend that other industrial microorganisms, such as *Clostridium* and *Cyanobacteria*, will initiate more ^{13}C-MFA studies due to their importance in biochemical production and relatively less well-known cell metabolism. Also, with the wide application of ^{13}C-MFA, many ^{13}C-MFA software packages, such as OpenFLUX2 [85], 13CFLUX2 [86], Metran [87], INCA [88], FiatFLUX [89], and Biomet Toolbox 2.0 [90], have been developed by using highly efficient mathematical algorithms (e.g., elementary metabolite unit, EMU [87, 91]) to simulate ^{13}C labeled patterns and calculating carbon fluxes in metabolic network (Table 2.1). Thus, some of the difficulties, especially the computational load, of ^{13}C-MFA have been dramatically decreased. It is reasonable to believe that the numbers of ^{13}C-MFA studies could increase by orders of magnitudes in the next decade or two.

2.3 Synergy of ^{13}C Metabolic Flux Analysis and Metabolic Engineering

The ultimate goals of metabolic engineering is to design and build engineered biological systems that can produce chemicals, materials, food, and drugs at high yield [92]. However, the lack of fundamental understanding of cellular responses during industrial fermentation often prevents metabolic engineers to achieve a satisfactory production of biochemical. In the past decade, ^{13}C-MFA has been widely used to provide insightful information about microbial metabolism and successfully helped metabolic engineers to improve biochemical production. Here, we have summarized recent successes on synergizing ^{13}C-MFA and metabolic engineering (Table 2.2-2.4), and organized them into four categories: 1) uncovering the bottleneck steps in biochemical production; 2) identifying cofactor imbalance issues of host metabolism; 3) revealing

cell maintenance requirement of industrial microorganisms; and 4) elucidating the mechanism of microbial resistance to fermentation inhibitors.

2.3.1 Uncovering the Bottleneck Steps in Biochemical Production

Bottlenecks in Acetyl-CoA Synthesis. As a central metabolite, acetyl-CoA plays an important role in a series of cellular functions. In metabolic engineering, acetyl-CoA is a key precursor in the biosynthesis of sterols, amino acids, fatty acid-derived chemicals, polyketides, and isoprenoid-derived drugs [93]. To accommodate the cellular requirement, the organisms use a variety of routes for acetyl-CoA synthesis (Fig. 2.3), such as the oxidative decarboxylation of pyruvate, the oxidation of long-chain fatty acids, and the oxidative degradation of certain amino acids. The most common way to produce the acetyl-CoA is the direct conversion from pyruvate by pyruvate dehydrogenase (PDH) [94, 95], pyruvate ferredoxin oxidoreductase (PFO), pyruvate NADPH oxidoreductase (PNO)[96], or pyruvate formate lyase (PFL)[97] under anaerobic conditions. Other acetyl-CoA synthesis pathways, e.g., acetyl-CoA synthetase (ACS) [98] and citrate lyase (ACL) [99] also play important roles in acetyl-CoA supplement for different organisms, especially for supplying the cytosolic acetyl-CoA as the precursor for various biochemical products.

In order to investigate the acetyl-CoA biosynthesis in living cells, ^{13}C-MFA was used to compare *S. cerevisiae* strains growing under purely oxidative, respiro-fermentative and predominantly fermentative conditions [100]. Based on the flux distributions, the activated pyruvate bypass pathway, i.e. converting pyruvate to acetaldehyde and then to acetate for synthesis of cytosolic acetyl-CoA, was found to be the main pathway used by *S. cerevisiae* to supply cytosolic acetyl-CoA. However, the flux in the pyruvate bypass pathway was not strong enough to supply sufficient cytosolic acetyl-CoA when engineering *S. cerevisiae* to produce acetyl-CoA-

derived chemicals, such as n-butanol. To increase the capability of producing cytosolic acetyl-CoA in *S. cerevisiae*, various metabolic engineering strategies have been adopted to further enhance cytosolic acetyl-CoA availability, including the disruption of competing pathways [51] and the introduction of heterologous biosynthetic pathways with higher catalytic efficiency and lower energy input requirement, such as cytosolic localized PDHs (cytoPDHs) [51] and ATP-citrate lyase (ACLs) [101]. In one of the studies that evaluated the effects of various acetyl-CoA synthesis pathways on n-butanol production, the cytoPDHs was found to work best and led to 3-fold increased n-butanol production in the engineered *S. cerevisiae* (Fig. 2.3A & Table 2.2) [93].

In addition to uncovering the bottleneck of cytosolic acetyl-CoA biosynthesis for wild-type yeast, ^{13}C-MFA was also used to elucidate the effect of a heterogonous acetyl-CoA enhanced pathway, i.e. phosphoketolase pathway (PHK), in a genetically modified yeast strain in which the genes *xpkA* and *ack* from *Aspergillus nidulans* were introduced [52]. The PHK pathway was originally utilized by several bacterial species [102] and filamentous fungi for glucose dissimilation as an alternative to the Embden-Meyerhof-Parnas pathway (EMP). For example, in *A. nidulans*, the utilization of this metabolic pathway led to increased carbon flow towards acetate and acetyl-CoA through the action of a phosphotransacetylase [103]. Flux distribution in the central metabolic pathways showed the positive role of the PHK pathway on improving the supply of cytosolic acetyl-CoA in the *S. cerevisiae* strain, which also accounted for the improved acetate yield. Encouraged by this discovery, the same PHK pathway was co-expressed together with a wax ester synthase (*ws2*) and successfully improved the titer of fatty acid ethyl esters by 1.7 fold [104]. Such proof-of-concept study indicated that the PHK pathway could be established as stand-alone route to divert flux from glycolysis to cytosolic acetyl-CoA supply, and hold great potential for future improving the production of acetyl-CoA-derived chemicals.

Bottlenecks in Fatty Acid Synthesis. Fatty acids are the precursors to produce transportation fuels and industrial chemicals including surfactants, solvents, and lubricants [58]. The microbial production of fatty acid-derived chemicals has recently been achieved in many industrial applications. *Escherichia coli* can serve as an excellent host for fatty acids production due to its fast growth, simple nutrient requirements, well-understood metabolism, and well-established genetic tools. But only a small amount of free fatty acids is detectable under normal conditions in the wild-type *E. coli.* The synthesis of saturated fatty acid starts with the conversion of acetyl-CoA into malonyl-CoA catalyzed by ATP-dependent acetyl-CoA carboxylase and the transesterification of malonyl-CoA into an acyl carrier protein (ACP) catalyzed by malonyl-CoA ACP transacylase (*fabD*), followed by cyclic chain elongation (Table 2.2) [105].

In spite of various fatty acid over-producing strains that have been created, most studies focus on engineering terminal enzymes in fatty acid biosynthesis pathways and little is known about how central metabolism responds to fatty acid production. To reveal the metabolic bottlenecks in fatty acid production, ^{13}C-MFA has been performed by using an engineered fatty acid over-producing *E. coli* DH1 strain with over-expression of *tesA*, and *fadR* genes and knock-out of *fadE* gene (Fig. 2.3B) [58]. This ^{13}C-MFA study clearly showed the *E. coli* metabolic flux were redistributed in response to over-production of fatty acid. Basically, compared to the wild-type *E. coli* strain, the flux in the engineered strain was significantly diverted from acetate synthesis to fatty acid synthesis, indicating that an increase in the supply of key precursors in fatty acid synthesis is crucial to increasing subsequent fatty acid synthesis. The fluxes of pentose phosphate pathway (PPP) also dramatically increased to supply large amount of reduction powers, mostly NADPH, to support the fatty acid production in the engineered strain. Finally, the flux of the anaplerotic pathway into the TCA cycle decreased 1.7-fold in the engineered strain, and

consequently, more carbon fluxes were diverted to supply cytosolic acetyl-CoA, the starting point of fatty acid biosynthesis. Overall, as indicated by ^{13}C-MFA, the supply of fatty acid precursor and NADPH was recognized as the key bottleneck in microbial engineering for fatty acid production.

In order to improve fatty acid production, numerous engineering strategies have been suggested and explored. For example, to overcome the challenge of limited supply of fatty acid precursors, the acetyl-CoA carboxylase was over-expressed to provide more malonyl-CoA, a key precursor for fatty acid synthesis, which successfully enhanced the production of fatty acids [106, 107]. In another study, the fatty acid degradation pathway was removed by knocking out *fadE* in *E. coli*. Together with the over-expression of *tesA* and *fabF*, the yield of fatty acids was enhanced by nearly 3-fold [108]. Similarly, another study showed that by co-expressing *fabZ* and a thioesterase from *Ricinus communis* in a *fadD* (a key gene in fatty acid degradation) deletion mutant, the fatty acid titer was enhanced by nearly 3-fold (Table 2.2) [109]. In sum, the precursor issue identified by ^{13}C-MFA has now been well addressed in microbial engineering for fatty acid production. The insufficient supply of NADPH, another issue revealed by ^{13}C-MFA in fatty acid production, could be the next direction that metabolic engineers need to pay attention.

Bottlenecks in Pentose Phosphate Pathway. Pentose phosphate pathway, well known as the limitation step in providing sufficient NADPH for biochemical synthesis (discussed in 2.3.2), is also the essential pathway to provide the precursors for the synthesis of nucleotides and nucleic acids from ribose 5-phosphate and aromatic amino acids (e.g., phenylalanine and tyrosine). Several aromatic compounds, such as shikimic acid, a valuable drug precursor, could be produced from metabolites in pentose phosphate pathway. To investigate the bottleneck in pentose phosphate pathway for the biosynthesis process of shikimic acid, ^{13}C-MFA was recently applied to four different engineered *S. cerevisiae* strains which were engineered to produce shikimic acids at

different amount [110]. By comparing flux distributions of the four strains with different shikimic acid productions, a higher flux through pentose phosphate pathway was positively correlated with higher production of shikimic acid. This analysis indicated that the low flux into PP pathway could be the bottleneck for the shikimic acid production. Indeed, it was found that when removing the original phenylalanine and tyrosine synthesis pathway, and overexpressing *aro1, aro4* and *tkl* genes to improve the metabolic fluxes in PP pathway, the shikimic acid was increased by nearly 2-fold in *S. cerevisiae* (Table 2.2).

Similarly, riboflavin is an important industrial bio-product from PP pathway, which has been commercially produced by engineering *Bacillus subtilis* strains [111]. ^{13}C-MFA has also been implemented for both wild type and engineered *B. subtilis* strains in the past two decades [112, 113] to unravel the metabolic rewiring in the riboflavin producing strain, which could further improve the riboflavin production. The intracellular flux distributions of a riboflavin-producing *B. subtilis* strain has been rigorously investigated via ^{13}C-MFA under three different dilution rates in chemostats [112]. It found that PP pathway was activated, which not only supplied sufficient precursors but also produced sufficient NADPH. More interestingly, cofactor NADPH was always excessively produced in *B. subtilis* strains under all the three dilution rates based on the flux analysis, especially in the low dilution rate without riboflavin production. In other words, the estimated amount of NADPH requirements was found to be less than the NADPH formations for both biomass and riboflavin production. Thus, the high production of riboflavin and purine nucleotides is attributed to the sufficient precursor supply from PP pathway in *B. subtilis*. It is worth noting that the transhydrogenase, which catalyzed the reversible conversion of NADPH to NADH, played an important role to re-oxidize the excessive NADPH that was generated due to the highly activated PP pathways.

2.3.2 Identifying Cofactor Imbalance Issues of Host Metabolism

Cofactors, e.g. NADH/NAD^+ and NADPH/$NADP^+$, play a major role as the redox carriers for catabolic and anabolic reactions as well as the important agents in transfer of energy for the cell. NADH/NAD^+ functions as a cofactor pair in over 300 redox reactions and regulates various enzymes and genetic processes [56]. Under aerobic growth, NADH acts as an electron carrier for the transportation of electrons from the carbon source to the final electron acceptor: oxygen. Under anaerobic growth with the absence of an alternative oxidizing agent, the regeneration of NAD^+ is of great significance for the redox balance, which is achieved through fermentation by using NADH to reduce metabolic intermediates [114, 115]. Thus, the balance issue of NADH/NAD^+ is crucial for both aerobic and anaerobic conditions. NADPH/$NADP^+$, as the phosphorylation products of NADH/NAD^+, drives the anabolic reactions. The enzymatic synthesis of some important compounds, e.g. fatty acids and amino acids, depends heavily on cofactor NADPH as the reducing equivalents. The major pathways supplying NADPH during heterotrophic growth on glucose are the oxidative pentose phosphate pathway, the Entner-Doudoroff pathway, and $NADP^+$-dependent isocitrate dehydrogenase in the TCA cycle [53]. Additionally, the balance between NADH and NADPH also plays an important role to provide sufficient NADPH for the anabolic reactions. NAD(P) transhydrogenase can catalyze the reversible conversion between NADH and NADPH to balance the cofactors [116]. With the expense of 1 mol ATP, NAD kinase also can catalyze the conversion from NADH to NADPH [55].

It is conceivable that in cofactor-dependent production systems, cofactor availability and balance issue plays a vital role in dictating the overall process yield. Hence, the identification of key pathways to balance the cofactor levels would be helpful for the rational design of metabolic engineering strategies to further increase biochemical production. ^{13}C-MFA is one of few

analytical tools that can rigorously determine the cofactor usage in cell metabolism and has been applied in many industrial microorganisms to reveal the cofactor imbalance issues related to biochemical production. In this section, we summarized several important discoveries of the cofactor balance issues via ^{13}C-MFA and the corresponding metabolic engineering strategies to solve such issues (Fig. 2.4 & Table 2.3).

Cofactor Imbalance in Xylose Fermentation of *S. cerevisiae.* *S. cerevisiae* with the ability to anaerobically ferment sugars to ethanol at high rates has been domesticated for millennia and continuously selected as a workhorse for bioethanol production. However, *S. cerevisiae* cannot utilize xylose anaerobically, which is the second abundant composition in lignocellulose, a renewable and non-food-competitive resource. One of the commonly used strategies to engineer *S. cerevisiae* to utilize xylose is introducing a fungal xylose pathway from xylose-utilizing yeasts such as *Pichia stipites*. Through this fungal xylose pathway, xylose could be converted to fermentable xylulose through the consecutive redox reactions catalyzed by NADPH-dependent xylose reductase (XR) and NAD^+-dependent xylitol dehydrogenases (XDH), with xylitol produced as the intermediate. However, the usage of different cofactors in the fungal xylose pathway brings a notorious cofactor imbalance issue and severely limits the xylose utilization in *S. cerevisiae*. More importantly, the cofactor imbalance issue is not standalone. Rather, as shown in a few ^{13}C-MFA studies, it is intertwined with the central metabolism to induce network-level rewiring of carbon fluxes. Basically, a systematic investigation of xylose utilization of recombinant *S. cerevisiae* strains in an oxygen limited condition for ethanol production was accomplished by ^{13}C-MFA [36]. By implementing the ^{13}C tracer experiments and running metabolic flux analysis for six recombinant strains with different origins of XR and XDH in the xylose pathway [36], a universally high activity of oxidative pentose phosphate pathway was found to supply the NADPH

for the XR. The strong activities in TCA cycle was also found and indicated that huge amount of NADH needed to be consumed by oxidative phosphorylation. Concurrent with the global metabolic rewiring, only a small amount of the carbon fluxes was diverted to ethanol production.

To solve the cofactor-imbalance issues in the xylose utilization of *S. cerevisiae*, numerous efforts in metabolic engineering have been devoted. One of the strategies is the partial alteration of the cofactor preference for these two enzymes, i.e. altering the preference of XR to use NADH or altering XDH to use $NADP^+$ as the cofactors, which would generate a cofactor-balance cycle for the initial two steps of xylose utilization to balance the cofactor utilization. The cofactor engineering strategy has proved to be functional in several studies. For example, by replacing the native *P. stipitis* XR with a mutated XR with increased preference of NADH, the ethanol yield was improved by ~40% with the decreased xylitol production [117-123]. The similar successes have also been achieved in several other attempts to increase the $NADP^+$ preference for the XDH, which have successfully improved the ethanol production by 28%~41% [124-127]. The other strategy used to tackle the cofactor imbalance issue is to engineer the cofactor-dependent metabolic pathways that could decrease the xylitol production and enhance ethanol yield. For instance, lowering the flux through the NADPH-producing pentose phosphate pathway could lead to increasing ethanol yield and decreasing xylitol production. This is attributed to an insufficient supplement of NADPH which could improve the NADH preference of XR, and thus partially balance the cofactor usage of XR and XDH [128]. In addition, replacing the NADPH-producing PP pathway (glucose-6-phosphate dehydrogenase) with a fungal $NADP^+$-dependent D-glyceraldehyde-3-phosphate dehydrogenase (NADP-GAPDH) could produce NADPH for the XR without losing any carbon, and provide more carbon for the ethanol production [129]. Improving the NAD^+ regeneration directly by introducing the heterogeneous genes could also decrease the

xylitol production and increase ethanol production [130]. Beside the two-step xylose utilization pathway, using xylose isomerase is another efficient approach for the xylose fermentation since it does not require cofactor when converting xylose to xylulose, and hence, bypasses the cofactor imbalance issue (Table 2.3). However, as indicated by a recent ^{13}C-MFA study, the lower glycolysis activity that led to inefficient re-oxidation of NADH could be potentially a new bottleneck step when using xylose isomerase in *S. cerevisiae* [131].

Cofactor Imbalance in Chemical Biosynthesis. The production of many chemicals, such as fatty acids and amino acids, requires a large amount of cofactors. Thus, cofactor imbalance issues are tightly related to not only the sugar utilization but also the chemical production. For example, by using ^{13}C-MFA to analyze the cell metabolism in wild-type and fatty acid over-producing *E. coli* strains, it was found that the engineered strain requires excessive NADPH compared to the wild-type strain, i.e. 255 units compared to 179 units NADPH with the flux of glucose uptake was normalized of 100 units. However, the sum of NADPH supplied from central metabolism could only reach 100 units [58], which clearly indicated that more NADPH production would be needed to increase fatty acid production in *E. coli*. To balance the NADPH usage, an alternative transdehydrogenase pathway that converted NADH to NADPH was activated in the engineered *E. coli*. The flux of the transdehydrogenase pathway was increased by 70% compared to that in wild-type strains (i.e. from 90 units to 153 units) to support fatty acid biosynthesis.

Realizing the importance of cofactor balance, particularly the NADPH supply, in biochemical production, metabolic engineers have adopted various strategies to overcome this challenge. One strategy is switching the specificities of glycolytic enzymes, e.g. GAPDH, from NAD^+-dependence to $NADP^+$-dependence, which could build a NADPH-producing glycolysis pathway to increase the bioavailability of NADPH and further improved the NADPH-dependent

lycopene production by ~100% (Table 2.3)[53]. Also, it is used to redirect the metabolic flux from the glycolysis pathway into the pentose phosphate pathway to enhance NADPH supply by the overexpression of *zwf* that encodes glucose-6-phosphate dehydrogenase (G6PDH) [132-134], deletion of *pfkA* and *pfkB* that encode the phosphofructokinase (PFK) [135], or deletion of *pgi* that encodes phosphoglucose isomerase [136, 137]. In addition, transhydrogenase [138, 139] or NAD kinase [53] was overexpressed to further boost the NADPH/$NADP^+$ availability in *E. coli* and other microorganisms.

In addition to the production of fatty acids, biosynthesis of amino acids, such as L-lysine and L-valine, requires NADPH as cofactors of the enzymatic reactions. *Corynebacterium glutamicum*, one of the industrial workhorses for producing amino acids, has been considered an important microorganism with extensive ^{13}C-MFA studies [46, 140-143]. Many metabolic engineering strategies provided by ^{13}C-MFA have been developed to improve the amino acids production. For example, L-lysine is one of the major products of *C. glutamicum*, which is synthesized from the pyruvate and oxaloacetate consuming 4 moles NADPH for 1 mole L-lysine. To study the intracellular metabolic rewiring of the L-lysine producing *C. glutamicum* strains, several ^{13}C-MFA studies have been implemented and uncovered that the PP pathway has been increased to supply NADPH. The anaplerotic carboxylation pathway was also enhanced to provide enough precursors for L-lysine synthesis [141, 142, 144]. Similarly, a significant increase in the PP pathway flux was also found to be associated with L-valine production in a pyruvate decarboxylase deficient *C. glutamicum* strain via ^{13}C-MFA, which again indicated that the NADPH supply was the key issue in L-valine production [54].

Based on the insightful information from ^{13}C-MFA studies, various metabolic strategies have been developed to improve the L-lysine and L-valine production. First, to overcome the

insufficient NADPH supply, the enzymes in PP pathway, such as glucose-6-phosphate dehydrogenase [145], transketolase, and transaldolase [146], as well as 1, 6-bisphosphatase [147], were overexpressed to redirect fluxes towards PP pathway to improve lysine production. In addition to the strategy of overexpressing the native enzymes in PP pathway, the alteration of cofactor specificity of GAPDH from NAD^+-dependence to $NADP^+$-dependence has successfully improved the L-lysine production by ~50% without decreasing cell growth rate [148]. To further investigate the metabolic responses of such alteration, ^{13}C-MFA was performed again to compare the intracellular flux distributions between wild-type strains and mutants with alternated GAPDH. It was found that the mutated GAPDH pathway was the major source of the NADPH in the mutated strain with the similar PP pathway flux, but with higher lysine production. At last but not least, by cloning a transhydrogenase from *E.coli* to enhance NADPH supply in *C. glutamicum*, L-valine yield in *C. glutamicum* strain was dramatically improved by ~200% (Fig. 2.4C & Table 2.3) [54]. These discoveries were consistent with the expectations of the metabolic engineering strategies, and more importantly, demonstrated that ^{13}C-MFA could indeed rationally guide the metabolic engineering and improve the microbial performance.

2.3.3 Revealing Cell Maintenance Requirement of Industrial Microorganisms

Metabolic engineering is frequently equated with the heterologous production of a series of recombinant proteins. Nowadays, with the development of synthetic biology approaches, more and more heterologous pathways have been introduced into a host cell to produce non-natural products with multiple genes inserted, deleted, replaced, or overexpressed. On one hand, the genetic manipulation could modify cell metabolism and divert more carbon flux into the desired chemicals. On the other hand, the metabolic engineering, particularly heterologous protein overexpression, could interfere the host metabolism and generate severe metabolic burdens since

the protein expression could be energetically expensive during transcription and translation. Such issues, however, has not yet been well studied in the field of metabolic engineering.

The metabolic burden of industrial microorganisms is often reflected as elevated cell maintenance energy of industrial microorganisms, as revealed in several pioneering ^{13}C-MFA studies. In one of the ^{13}C-MFA studies, *Pichia pastoris*, a methylotrophic yeast with an attractive system to produce various heterologous proteins [65-68] was investigated by introducing a mock plasmid, a low-copy plasmid to express *R. oryzae* lipase, and a high-copy plasmid to express *R. oryzae* lipase, respectively. It was found that the TCA cycle fluxes of both protein-expressing *P. pastoris* strains were much higher than the control strain to produce more ATP to sustain cell growth, confirming that the protein folding and conformational stress indeed imposed a metabolic burden on the microbial host. The similar metabolic rewiring, i.e., elevated TCA cycle fluxes to provide more ATP for cell maintenance, was also found in a S-Adenosyl-L-methionine (SAM) producing *S. cerevisiae* strain [35] and a xylose-utilization *S. cerevisiae* strain (Table 2.4) [36].

To avoid introducing metabolic burdens, metabolic engineers have explored three strategies: medium optimization, using low-copy plasmids, and promoter engineering. Optimization of cultural medium and fermentation condition could potentially remove stresses such as nutrient limitation and hence reduce the requirement for cell maintenance energy. For example, by using several novel feeding strategies to cultural SAM-producing *P. pastoris*, the production of SAM was found to be improved by ~35% [149, 150]. In addition, it has been found that the utilization of a high-copy plasmid may increase risk of plasmid instability and metabolic burden [151], since the protein over-expression requires tremendous amount of building blocks and energy, which could jeopardize the normal cell growth and increase the metabolic burden. It was found that using a low-copy plasmid sometimes could be a better choice for chemical

production. For example, in the study that aimed to engineer *E. coli* to produce lycopene [152], the cell density of the engineered *E. coli* with high-copy plasmid at stationary phase was approximately 24% lower than the one with low-copy and 30% lower than the control culture. Similarly, the titer of lycopene in the *E. coli* with high-copy plasmid was 20% lower than that with low-copy plasmid. Another method to decrease metabolic burden is to tune the promoter strengths of various genes to balance the pathways and avoid the accumulation of certain toxic intermediates as the growth inhibitor. One example uses this method to engineer a more efficient production of taxadiene in *E. coli* [10]. In general, by tuning the expression levels of two modules in the taxadiene pathway, a native upstream methylerythritol-phosphate (MEP) pathway forming isopentenyl pyrophosphate and a heterologous downstream pathway forming terpenoid, an inhibitory intermediate compound for cell growth, indole, was achieved the minimal accumulation by expressing the upstream pathway in a very low level. Correspondingly, the taxadiene production was improved by ~15-fold.

2.3.4 Elucidating the Mechanism of Microbial Resistance to Fermentation Inhibitors

Environmental stresses, such as physical heat shock [153] and chemical acidity [154], could affect the physiology and viability of microbial cells and decrease or even cease the bioprocess productivity. For example, the lignocellulosic biofuels hold promises for a sustainable fuel economy. However, the chemical stresses from the toxic compounds in processed lignocellulosic hydrolysates, e.g. weak acids, furans, and phenolic compounds [155], have hampered the economic feasibility of biofuels. Thus, it is important to identify the intracellular metabolic responses of industrial microorganisms to various stresses in order to rationally improve their resistance to inhibitors [156]. Compared to other commonly used approaches such as transcriptomics and proteomics analysis, ^{13}C-MFA is more intuitive and provides direct and

quantitative readouts of the metabolic rewiring under stress conditions. In this section, we introduce recent advances in the study of stress response using ^{13}C-MFA and the corresponding metabolic engineering strategies to improve microbial resistance to different inhibitors (Fig. 2.5).

Among various toxic compounds from the lignocellulose pretreatment and hydrolysis, furfural is an important contributor to the toxicity for *S. cerevisiae*. Although it has been found that *S. cerevisiae* has weak intrinsic ability to reduce furfural to the less-toxic furfuryl alcohol, the holistic view of metabolic responses to furfural is still missing. To further investigate the flux distribution of *S. cerevisiae* under the increasing strengths (concentrations) of furfural stress, ^{13}C-MFA has been applied for both wild-type and several evolved furfural-resistant strains in micro-aerobic and glucose-limited chemostats [39]. As revealed by ^{13}C-MFA, NADH-dependent oxireductases, which catalyzed the reduction of furfural, were the main defense mechanisms at lower concentration of furfural (<15mM), while NADPH-dependent oxireductases became the major resistance mechanism at high concentration of furfural (>15 mM). Thus, the carbon flux of pentose phosphate increased as the main physiological response to high concentrations of furfural, which indicated that the NADPH supply was the key to help *S. cerevisiae* better resist furfural stress. Inspired by this discovery, metabolic engineers overexpressed several NADPH-dependent oxireductases, particularly ADH7 and YKL071W, and successfully increased furfural resistance in the parent *S. cerevisiae* strain by 200% [39].

In another study, ^{13}C-MFA was applied to elucidate the metabolic responses of *E. coli* to octanoic acid stress [38]. When comparing the flux distributions of stressed and unstressed *E. coli* strains, a decreased flux in TCA cycle and an increased flux in pyruvate oxidative pathway for producing acetate were observed. It was hypothesized that octanoic acid triggered the membrane disruption and led to NAD^+ deficiency because of the destabilization of membrane-bound proteins,

such as NADH dehydrogenase, which would down-regulate several key NAD^+ dependent pathways, such as the malate dehydrogenase pathways in TCA cycle, and the pyruvate dehydrogenase multi-enzyme complex pathway. Also, the pyruvate pool shrank under octanoic acid stress condition, which could be attributed to the repression of the *pdhR* regulator, a regulator with high sensitivity to pyruvate in controlling the expressions of the PDH complex, NADH dehydrogenase II, and cytochrome *bo*-type oxidase encoded by *aceEF* and *lpdA*, *ndh*, and *cyoABCDE*, respectively [157]. Based on the discussion of ^{13}C-MFA results, several possible strategies to further enhance the C8 acid tolerance were proposed, including the supplement of pyruvate in the medium and the replacement of NADH/NAD^+-sensitive enzymes.

2.4 Perspectives of Synergizing ^{13}C Metabolic Flux Analysis with Metabolic Engineering

The conventional ^{13}C-MFA has been widely applied to determine microbial metabolism and guide metabolic engineers to develop numerous strategies to improve biochemical production. However, there are still several technique limitations that restrict the accuracy and flexibility of ^{13}C-MFA. For example, the ^{13}C-MFA can only be applied at metabolic and isotopic steady states [63], which could be difficult to use when the target chemicals are produced in non-steady state (e.g., drug synthesis in the stationary growth phase). In addition, most of the conventional ^{13}C-MFA studies are limited in central metabolism [158], which has very limited use when analyzing the secondary metabolism of microorganisms. To overcome these challenges, novel experimental and computational methods have recently been developed to empower ^{13}C-MFA studies. In this section, we will summarize recent breakthroughs in ^{13}C-MFA and provide a perspective for novel routes to achieve synergy of ^{13}C-MFA and metabolic engineering.

2.4.1 Expand ^{13}C-MFA into Genome Scale

The conventional ^{13}C-MFA can only be applied to determine flux distribution in the central metabolic network, mainly because of the difficulties in 1) measuring the isotopic labeling of the numerous low-abundant metabolites and 2) the huge computational burden of simulating isotopic labeling of all metabolites in genome-scale metabolic networks. However, with the rapid development of high-resolution mass spectrometry, the accurate measurement of isotopic labeling of low-abundant metabolites becomes possible, as reported by several groups [159-161]. For the computational simulation, an *E. coli* genome-scale model (imPR90068) has recently been constructed for ^{13}C-MFA [158], which spans 1,039 metabolites and 2,077 reactions. In order to calculate the genome-scale metabolic flux distribution, a total of 1.37×10^{157} isotopomers need to be simulated [158]. Thanks to the implementation of EMU method [87], the computational burden was decreased by 1~2 orders of magnitude and for the first time, the fluxes in all the metabolic pathways of *E. coli* were elucidated. Compared to the conventional ^{13}C-MFA, the genome-scale ^{13}C-MFA could rigorously determine the metabolic rewiring in secondary metabolism, from which many high-value chemicals, such as drugs, could be produced. The genome-scale ^{13}C-MFA could provide valuable information about the metabolic rewiring in response to the production of these secondary metabolites and guide the development of rational metabolic engineering strategies in a similar way as that has been used for improving bulk chemical production.

2.4.2 Isotopic Non-Stationary ^{13}C-MFA (^{13}C-INST-MFA)

^{13}C-INST-MFA is a cutting-edge technology that was recently developed [67-71] to enable the application of ^{13}C-MFA for various autotrophic systems including cyanobacteria and plants. In brief, instead of collecting ^{13}C-labeling patterns at the isotopic steady state, ^{13}C-INST-MFA tracks the dynamics of ^{13}C-labeling in intracellular metabolites and applies computational

algorithms to calculate the steady-state metabolic fluxes that can best fit the ^{13}C-labeling kinetics. ^{13}C-INST-MFA has been applied to determine the photosynthetic metabolism of *Synechocystis* sp. PCC6803 [162] and *Arabidopsis thaliana* [163]. Such autotrophic metabolism is unable to be elucidated via the conventional ^{13}C-MFA because all of the metabolites will be universally labeled at the isotopic steady state when feeding with $^{13}CO_2$ and the information about pathway usage is completely lost. The merit of ^{13}C-INST-MFA for metabolic engineering lies on the fact that the metabolisms of numerous autotrophic systems, which used to be mysterious, can now be rigorously determined. Because many autotrophic systems are promising cell factories [164-166] that convert CO_2 into valuable chemicals, we can envision that ^{13}C-INST-MFA could guide metabolic engineers to better understand and more rationally modify such systems for improving the production of autotrophic products.

2.4.3 ^{13}C-Based Dynamic Metabolic Flux Analysis (^{13}C-DMFA)

^{13}C-DMFA has recently been developed as an approach to investigate microbial metabolism at metabolic non-steady state [30]. Compared to conventional kinetic models to describe microbial dynamics [167-170], ^{13}C-DMFA could reveal the dynamic reprogramming of intracellular fluxes and thus provides in-depth understanding of microbial metabolism in pathway level. In one of the proof-of-concept studies, the *E. coli* metabolism in a fed-batch fermentation process for overproduction of 1,3-propanediol was investigated. By introducing several additional parameters to describe the fed-batch fermentation process, a time-resolved flux map was generated and showed that the intracellular flux associated with PDO pathway increased by 10% and the split ratio between glycolysis and pentose phosphate pathway decreased from 70/30 to 50/50. ^{13}C-DMFA has provided a way for metabolic engineer to investigate the dynamic metabolism during industrial fermentation, especially the fed-batch fermentation. It is also expected that ^{13}C-DMFA

could be further extended to study microbial metabolism at stationary growth phase, during which numerous high-value secondary metabolites are often produced. With the insightful information about the metabolic rewiring at non-steady state, metabolic engineers could develop more appropriate strategies to improve the biochemical production, particularly microbial-based drug production.

2.4.4 Improve Flux Resolution of ^{13}C-MFA via the Integration of Isotopic Patterns from Parallel Labeling Experiments

Parallel labeling experiment design has been widely applied in ^{13}C-MFA to improve the observability of global metabolic network by conducting multiple labeling experiments with different isotopic tracers simultaneously [171-174]. Another recent advance in ^{13}C-MFA is the integration of the data (i.e., isotopic labeling patterns) from parallel labeling experiments to improve the flux resolution [175-177]. The integration of the data from parallel labeling experiments have been combined with rapid development of the high-throughput measure techniques and computational algorithms [175-177] which would offer unique advantages compared to conventional ^{13}C-MFA [178], particularly by improving the precision of flux estimation [175, 176] and reducing the time of labeling experiments. With the more precise measurement of intracellular carbon fluxes, it is reasonable to conclude that higher resolution of microbial metabolism will be provided for metabolic engineers in near future and fine-tuned engineering strategies will be developed for general applications in improving biochemical production.

Acknowledgements

We thank Herbert Huttanus in Virginia Tech for improving the language of the paper. This study was supported by start-up fund (#175323) from Virginia Tech and Junior Faculty Award from Institute for Critical Technology and Applied Science.

References

1. Sheng, J. and X. Feng, *Metabolic engineering of yeast to produce fatty acid-derived biofuels: bottlenecks and solutions.* Front. Microbiol., 2015. **6**(554).
2. Shin, J.H., et al., *Production of bulk chemicals via novel metabolic pathways in microorganisms.* Biotechnology Advances, 2013. **31**(6): p. 925-935.
3. Weusthuis, R.A., et al., *Microbial production of bulk chemicals: development of anaerobic processes.* Trends in Biotechnology, 2011. **29**(4): p. 153-158.
4. Hermann, B.G., K. Blok, and M.K. Patel, *Producing Bio-Based Bulk Chemicals Using Industrial Biotechnology Saves Energy and Combats Climate Change.* Environmental Science & Technology, 2007. **41**(22): p. 7915-7921.
5. Stephanopoulos, G., *Challenges in Engineering Microbes for Biofuels Production.* Science, 2007. **315**(5813): p. 801-804.
6. Peralta-Yahya, P.P. and J.D. Keasling, *Advanced biofuel production in microbes.* Biotechnology Journal, 2010. **5**(2): p. 147-162.
7. Peralta-Yahya, P.P., et al., *Microbial engineering for the production of advanced biofuels.* Nature, 2012. **488**(7411): p. 320-328.
8. Lee, S.K., et al., *Metabolic engineering of microorganisms for biofuels production: from bugs to synthetic biology to fuels.* Current Opinion in Biotechnology, 2008. **19**(6): p. 556-563.
9. Stephanopoulos, G., *Metabolic engineering: Enabling technology for biofuels production.* Metabolic Engineering, 2008. **10**(6): p. 293-294.
10. Ajikumar, P.K., et al., *Isoprenoid Pathway Optimization for Taxol Precursor Overproduction in Escherichia coli.* Science, 2010. **330**(6000): p. 70-74.
11. Lee, S.Y., et al., *Metabolic engineering of microorganisms: general strategies and drug production.* Drug Discovery Today, 2009. **14**(1–2): p. 78-88.
12. Martin, V.J.J., et al., *Engineering a mevalonate pathway in Escherichia coli for production of terpenoids.* Nat Biotech, 2003. **21**(7): p. 796-802.
13. Chang, M.C.Y. and J.D. Keasling, *Production of isoprenoid pharmaceuticals by engineered microbes.* Nat Chem Biol, 2006. **2**(12): p. 674-681.
14. Demain, A.L. and S. Sanchez, *Microbial drug discovery: 80 years of progress.* J Antibiot, 2009. **62**(1): p. 5-16.
15. Ferrer-Miralles, N., et al., *Microbial factories for recombinant pharmaceuticals.* Microbial Cell Factories, 2009. **8**(1): p. 1-8.
16. Keasling, J.D., *Manufacturing Molecules Through Metabolic Engineering.* Science, 2010. **330**(6009): p. 1355-1358.
17. Huttanus, H., J. Sheng, and X. Feng, *Metabolic Engineering for Production of Small Molecule Drugs: Challenges and Solutions.* Fermentation, 2016. **2**(1): p. 4.
18. Atsumi, S., et al., *Metabolic engineering of Escherichia coli for 1-butanol production.* Metabolic Engineering, 2008. **10**(6): p. 305-311.
19. Blattner, F.R., et al., *The Complete Genome Sequence of Escherichia coli K-12.* Science, 1997. **277**(5331): p. 1453-1462.
20. Huang, C., Jr., H. Lin, and X. Yang, *Industrial production of recombinant therapeutics in Escherichia coli and its recent advancements.* Journal of Industrial Microbiology & Biotechnology, 2012. **39**(3): p. 383-399.

21. Alper, H., K. Miyaoku, and G. Stephanopoulos, *Construction of lycopene-overproducing E. coli strains by combining systematic and combinatorial gene knockout targets.* Nat Biotech, 2005. **23**(5): p. 612-616.
22. Farmer, W.R. and J.C. Liao, *Improving lycopene production in Escherichia coli by engineering metabolic control.* Nat Biotech, 2000. **18**(5): p. 533-537.
23. Clomburg, J. and R. Gonzalez, *Biofuel production in Escherichia coli: the role of metabolic engineering and synthetic biology.* Applied Microbiology and Biotechnology, 2010. **86**(2): p. 419-434.
24. Borneman, A.R., et al., *Whole-Genome Comparison Reveals Novel Genetic Elements That Characterize the Genome of Industrial Strains of Saccharomyces cerevisiae.* PLoS Genet, 2011. **7**(2): p. e1001287.
25. Ostergaard, S., L. Olsson, and J. Nielsen, *Metabolic Engineering of Saccharomyces cerevisiae.* Microbiology and Molecular Biology Reviews, 2000. **64**(1): p. 34-50.
26. Giaever, G., et al., *Functional profiling of the Saccharomyces cerevisiae genome.* Nature, 2002. **418**(6896): p. 387-391.
27. Nielsen, J. and M.C. Jewett, *Impact of systems biology on metabolic engineering of Saccharomyces cerevisiae*. Vol. 8. 2008. 122-131.
28. Chen, G.-Q., *New challenges and opportunities for industrial biotechnology.* Microbial Cell Factories, 2012. **11**: p. 111-111.
29. Kwok, R., *Five hard truths for synthetic biology.* Nature, 2010. **463**(7279): p. 288.
30. Antoniewicz, M., *Methods and advances in metabolic flux analysis: a mini-review.* Journal of Industrial Microbiology & Biotechnology, 2015. **42**(3): p. 317-325.
31. Young, J.D., *^{13}C metabolic flux analysis of recombinant expression hosts.* Current Opinion in Biotechnology, 2014. **30**: p. 238-245.
32. Wang, Y., K.-Y. San, and G.N. Bennett, *Cofactor engineering for advancing chemical biotechnology.* Current Opinion in Biotechnology, 2013. **24**(6): p. 994-999.
33. Wasylenko, T.M., W.S. Ahn, and G. Stephanopoulos, *The oxidative pentose phosphate pathway is the primary source of NADPH for lipid overproduction from glucose in Yarrowia lipolytica.* Metabolic Engineering, 2015. **30**: p. 27-39.
34. Hollinshead, W.D., et al., *Rapid metabolic analysis of Rhodococcus opacus PD630 via parallel ^{13}C-metabolite fingerprinting.* Biotechnology and Bioengineering, 2015: p. n/a-n/a.
35. Hayakawa, K., et al., *^{13}C-metabolic flux analysis in S-adenosyl-l-methionine production by Saccharomyces cerevisiae.* Journal of Bioscience and Bioengineering, 2015.
36. Feng, X. and H. Zhao, *Investigating xylose metabolism in recombinant Saccharomyces cerevisiae via 13C metabolic flux analysis.* Microbial Cell Factories, 2013. **12**(1): p. 114.
37. Lam, F.H., et al., *Engineering alcohol tolerance in yeast.* Science, 2014. **346**(6205): p. 71-75.
38. Fu, Y., et al., *Metabolic flux analysis of Escherichia coli MG1655 under octanoic acid (C8) stress.* Applied Microbiology and Biotechnology, 2015. **99**(10): p. 4397-4408.
39. Heer, D., D. Heine, and U. Sauer, *Resistance of Saccharomyces cerevisiae to High Concentrations of Furfural Is Based on NADPH-Dependent Reduction by at Least Two Oxireductases.* Applied and Environmental Microbiology, 2009. **75**(24): p. 7631-7638.
40. Çakar, Z.P., et al., *Evolutionary engineering of multiple-stress resistant Saccharomyces cerevisiae*. Vol. 5. 2005. 569-578.

41. Wittmann, C. and E. Heinzle, *Mass spectrometry for metabolic flux analysis.* Biotechnology and Bioengineering, 1999. **62**(6): p. 739-750.
42. Wiechert, W., *^{13}C Metabolic Flux Analysis.* Metabolic Engineering, 2001. **3**(3): p. 195-206.
43. Dauner, M. and U. Sauer, *GC-MS analysis of amino acids rapidly provides rich information for isotopomer balancing.* Biotechnology Progress, 2000. **16**: p. 642-649.
44. de Graaf, A.A., *Use of ^{13}C labelling and NMR Spectroscopy in Metabolic Flux Analysis*, in *NMR in Biotechnology: Theory and Applications*, J.N. Barbotin and J.C. Portais, Editors. 2000, Horizon Scientific Press: Norwich, UK.
45. Christensen, B. and J. Nielsen, *Isotopomer Analysis Using GC-MS.* Metabolic Engineering, 1999. **1**(4): p. 282-290.
46. Szyperski, T., *^{13}C-NMR, MS and metabolic flux balancing in biotechnology research.* Quarterly Reviews of Biophysics, 1998. **31**(01): p. 41-106.
47. Feng, X., et al., *Metabolic pathway determination and flux analysis in nonmodel microorganisms through ^{13}C-isotope labeling.* Methods Mol Biol, 2012. **881**: p. 309-30.
48. You, L., et al., *Metabolic pathway confirmation and discovery through ^{13}C-labeling of proteinogenic amino acids.* J Vis Exp, 2012(59): p. e3583.
49. Sauer, U., *Metabolic networks in motion: ^{13}C-based flux analysis*. Vol. 2. 2006.
50. Tang, Y.J., et al., *Advances in analysis of microbial metabolic fluxes via ^{13}C isotopic labeling.* Mass Spectrometry Reviews, 2009. **28**(2): p. 362-375.
51. Lian, J., et al., *Design and construction of acetyl-CoA overproducing Saccharomyces cerevisiae strains.* Metabolic Engineering, 2014. **24**: p. 139-149.
52. Papini, M., et al., *Physiological characterization of recombinant Saccharomyces cerevisiae expressing the Aspergillus nidulans phosphoketolase pathway: validation of activity through ^{13}C-based metabolic flux analysis.* Applied Microbiology and Biotechnology, 2012. **95**(4): p. 1001-1010.
53. Wang, Y., K.-Y. San, and G.N. Bennett, *Improvement of NADPH bioavailability in Escherichia coli by replacing NAD$^+$-dependent glyceraldehyde-3-phosphate dehydrogenase GapA with NADP$^+$-dependent GapB from Bacillus subtilis and addition of NAD kinase.* Journal of Industrial Microbiology & Biotechnology, 2013. **40**(12): p. 1449-1460.
54. Bartek, T., et al., *Comparative ^{13}C Metabolic Flux Analysis of Pyruvate Dehydrogenase Complex-Deficient, l-Valine-Producing Corynebacterium glutamicum.* Applied and Environmental Microbiology, 2011. **77**(18): p. 6644-6652.
55. Hou, J., et al., *Impact of overexpressing NADH kinase on glucose and xylose metabolism in recombinant xylose-utilizing Saccharomyces cerevisiae.* Applied Microbiology and Biotechnology, 2009. **82**(5): p. 909-919.
56. Berrı, et al., *Metabolic Engineering of Escherichia coli: Increase of NADH Availability by Overexpressing an NAD$^+$-Dependent Formate Dehydrogenase.* Metabolic Engineering, 2002. **4**(3): p. 217-229.
57. Feng, X. and H. Zhao, *Investigating xylose metabolism in recombinant Saccharomyces cerevisiae via ^{13}C metabolic flux analysis.* Microbial Cell Factories, 2013. **12**.
58. He, L., et al., *Central metabolic responses to the overproduction of fatty acids in Escherichia coli based on ^{13}C-metabolic flux analysis.* Biotechnology and Bioengineering, 2014. **111**(3): p. 575-585.

59. Ranganathan, S., et al., *An integrated computational and experimental study for overproducing fatty acids in Escherichia coli.* Metabolic Engineering, 2012. **14**(6): p. 687-704.
60. Guo, W., et al., *Investigate the Metabolic Reprogramming of Saccharomyces cerevisiae for Enhanced Resistance to Mixed Fermentation Inhibitors via ^{13}C Metabolic Flux Analysis.* PLOS ONE, 2016. **11**(8): p. e0161448.
61. Quarterman, J., et al., *Rapid and efficient galactose fermentation by engineered Saccharomyces cerevisiae.* J Biotechnol, 2016. **229**: p. 13-21.
62. Guo, W., J. Sheng, and X. Feng, *^{13}C-Metabolic Flux Analysis: An Accurate Approach to Demystify Microbial Metabolism for Biochemical Production.* Bioengineering, 2016. **3**(1): p. 3.
63. Zamboni, N., et al., *^{13}C-based metabolic flux analysis.* Nat. Protocols, 2009. **4**(6): p. 878-892.
64. Tang, Y.J., et al., *Invariability of central metabolic flux distribution in Shewanella oneidensis MR-1 under environmental or genetic perturbations.* Biotechnology Progress, 2009. **25**(5): p. 1254-1259.
65. Adler, P., et al., *Core Fluxome and Metafluxome of Lactic Acid Bacteria under Simulated Cocoa Pulp Fermentation Conditions.* Applied and Environmental Microbiology, 2013. **79**(18): p. 5670-5681.
66. Klein, T., et al., *Overcoming the metabolic burden of protein secretion in Schizosaccharomyces pombe – A quantitative approach using ^{13}C-based metabolic flux analysis.* Metabolic Engineering, 2014. **21**: p. 34-45.
67. Jazmin, L., et al., *Isotopically Nonstationary MFA (INST-MFA) of Autotrophic Metabolism*, in *Plant Metabolic Flux Analysis*, M. Dieuaide-Noubhani and A.P. Alonso, Editors. 2014, Humana Press. p. 181-210.
68. Murphy, T.A., C.V. Dang, and J.D. Young, *Isotopically nonstationary ^{13}C flux analysis of Myc-induced metabolic reprogramming in B-cells.* Metabolic Engineering, 2013. **15**: p. 206-217.
69. Jazmin, L. and J. Young, *Isotopically Nonstationary ^{13}C Metabolic Flux Analysis*, in *Systems Metabolic Engineering*, H.S. Alper, Editor. 2013, Humana Press. p. 367-390.
70. Wiechert, W. and K. Nöh, *Isotopically non-stationary metabolic flux analysis: complex yet highly informative.* Current Opinion in Biotechnology, 2013. **24**(6): p. 979-986.
71. Wiechert, W. and K. Nöh, *From Stationary to Instationary Metabolic Flux Analysis*, in *Technology Transfer in Biotechnology*, U. Kragl, Editor. 2005, Springer Berlin Heidelberg. p. 145-172.
72. Pingitore, F., et al., *Analysis of Amino Acid Isotopomers Using FT-ICR MS.* Analytical Chemistry, 2007. **79**(6): p. 2483-2490.
73. Wiechert, W. and A.A. de Graaf, *Bidirectional reaction steps in metabolic networks: I. Modeling and simulation of carbon isotope labeling experiments.* Biotechnology and Bioengineering, 1997. **55**(1): p. 101-117.
74. Wiechert, W., et al., *Bidirectional reaction steps in metabolic networks: II. Flux estimation and statistical analysis.* Biotechnology and Bioengineering, 1997. **55**(1): p. 118-135.
75. Wittmann, C. and E. Heinzle, *MALDI-TOF MS for quantification of substrates and products in cultivations of Corynebacterium glutamicum.* Biotechnology and Bioengineering, 2001. **72**(6): p. 642-647.

76. Guo, W., et al., *13C pathway analysis of biofilm metabolism of Shewanella oneidensis MR-1.* RSC Advances, 2015. **5**(50): p. 39840-39843.
77. Christensen, B., A. Karoly Gombert, and J. Nielsen, *Analysis of flux estimates based on ^{13}C-labelling experiments.* European Journal of Biochemistry, 2002. **269**(11): p. 2795-2800.
78. Christensen, B. and J. Nielsen, *Metabolic network analysis of Penicillium chrysogenum using ^{13}C-labeled glucose.* Biotechnology and Bioengineering, 2000. **68**(6): p. 652-659.
79. Bennett, B.D., et al., *Absolute quantitation of intracellular metabolite concentrations by an isotope ratio-based approach.* Nat. Protocols, 2008. **3**(8): p. 1299-1311.
80. Dauner, M. and U. Sauer, *GC-MS Analysis of Amino Acids Rapidly Provides Rich Information for Isotopomer Balancing.* Biotechnology Progress, 2000. **16**(4): p. 642-649.
81. Iwatani, S., et al., *Determination of metabolic flux changes during fed-batch cultivation from measurements of intracellular amino acids by LC-MS/MS.* Journal of Biotechnology, 2007. **128**(1): p. 93-111.
82. Millard, P., et al., *IsoCor: correcting MS data in isotope labeling experiments.* Bioinformatics, 2012. **28**(9): p. 1294-1296.
83. Wahl, S.A., M. Dauner, and W. Wiechert, *New tools for mass isotopomer data evaluation in 13C flux analysis: Mass isotope correction, data consistency checking, and precursor relationships.* Biotechnology and Bioengineering, 2004. **85**(3): p. 259-268.
84. Zhang, Z., et al., *CeCaFDB: a curated database for the documentation, visualization and comparative analysis of central carbon metabolic flux distributions explored by 13C-fluxomics.* Nucleic Acids Research, 2014.
85. Shupletsov, M.S., et al., *OpenFLUX2: ^{13}C-MFA modeling software package adjusted for the comprehensive analysis of single and parallel labeling experiments.* Microbial Cell Factories, 2014. **13**: p. 152.
86. Weitzel, M., et al., *13CFLUX2—high-performance software suite for 13C-metabolic flux analysis.* Bioinformatics, 2013. **29**(1): p. 143-145.
87. Antoniewicz, M.R., J.K. Kelleher, and G. Stephanopoulos, *Elementary metabolite units (EMU): A novel framework for modeling isotopic distributions.* Metabolic Engineering, 2007. **9**(1): p. 68-86.
88. Young, J.D., *INCA: a computational platform for isotopically non-stationary metabolic flux analysis.* Bioinformatics, 2014. **30**(9): p. 1333-1335.
89. Zamboni, N., E. Fischer, and U. Sauer, *FiatFlux – a software for metabolic flux analysis from ^{13}C-glucose experiments.* BMC Bioinformatics, 2005. **6**: p. 209-209.
90. Garcia-Albornoz, M., et al., *BioMet Toolbox 2.0: genome-wide analysis of metabolism and omics data.* Nucleic Acids Research, 2014. **42**(Web Server issue): p. W175-W181.
91. Young, J.D., et al., *An elementary metabolite unit (EMU) based method of isotopically nonstationary flux analysis.* Biotechnology and Bioengineering, 2008. **99**(3): p. 686-699.
92. Chopra, P. and A. Kamma, *Engineering life through Synthetic Biology.* In Silico Biol, 2006. **6**(5): p. 401-10.
93. Lian, J., et al., *Design and construction of acetyl-CoA overproducing Saccharomyces cerevisiae strains.* Metab Eng, 2014. **24**: p. 139-49.
94. Chen, Y., et al., *Establishing a platform cell factory through engineering of yeast acetyl-CoA metabolism.* Metab Eng, 2013. **15**: p. 48-54.

95. Jing, F., et al., *Phylogenetic and experimental characterization of an acyl-ACP thioesterase family reveals significant diversity in enzymatic specificity and activity.* BMC Biochem, 2011. **12**: p. 44.
96. Inui H, O.K., Miyatake K, Nakano Y, Kitaoka S, *Purification and characterization of pyruvate:NADP$^+$ oxidoreductase in Euglena gracilis.* J Biol Chem, 1987. **262**(19): p. 6.
97. Kozak, B.U., et al., *Replacement of the Saccharomyces cerevisiae acetyl-CoA synthetases by alternative pathways for cytosolic acetyl-CoA synthesis.* Metab Eng, 2014. **21**: p. 46-59.
98. Shiba, Y., et al., *Engineering of the pyruvate dehydrogenase bypass in Saccharomyces cerevisiae for high-level production of isoprenoids.* Metabolic Engineering, 2007. **9**(2): p. 160-168.
99. Zaidi, N., J.V. Swinnen, and K. Smans, *ATP-Citrate Lyase: A Key Player in Cancer Metabolism.* Cancer Research, 2012. **72**(15): p. 3709-3714.
100. Frick, O. and C. Wittmann, *Characterization of the metabolic shift between oxidative and fermentative growth in Saccharomyces cerevisiae by comparative ^{13}C flux analysis.* Microbial Cell Factories, 2005. **4**: p. 30-30.
101. Zaidi, N., J.V. Swinnen, and K. Smans, *ATP-citrate lyase: a key player in cancer metabolism.* Cancer Res, 2012. **72**(15): p. 3709-14.
102. Meile, L., et al., *Characterization of the D-xylulose 5-phosphate/D-fructose 6-phosphate phosphoketolase gene (xfp) from Bifidobacterium lactis.* J Bacteriol, 2001. **183**(9): p. 2929-36.
103. Panagiotou, G., et al., *Systems analysis unfolds the relationship between the phosphoketolase pathway and growth in Aspergillus nidulans.* PLoS One, 2008. **3**(12): p. e3847.
104. de Jong, B.W., et al., *Improved production of fatty acid ethyl esters in Saccharomyces cerevisiae through up-regulation of the ethanol degradation pathway and expression of the heterologous phosphoketolase pathway.* Microbial Cell Factories, 2014. **13**: p. 39-39.
105. Feng, Y. and J.E. Cronan, *Escherichia coli unsaturated fatty acid synthesis: complex transcription of the fabA gene and in vivo identification of the essential reaction catalyzed by FabB.* J Biol Chem, 2009. **284**(43): p. 29526-35.
106. Davis, M.S., J. Solbiati, and J.E. Cronan, Jr., *Overproduction of acetyl-CoA carboxylase activity increases the rate of fatty acid biosynthesis in Escherichia coli.* J Biol Chem, 2000. **275**(37): p. 28593-8.
107. Lu, X., H. Vora, and C. Khosla, *Overproduction of free fatty acids in E. coli: implications for biodiesel production.* Metab Eng, 2008. **10**(6): p. 333-9.
108. Zhang, F., et al., *Enhancing fatty acid production by the expression of the regulatory transcription factor FadR.* Metab Eng, 2012. **14**(6): p. 653-60.
109. Subrahmanyam, S. and J.E. Cronan, Jr., *Overproduction of a functional fatty acid biosynthetic enzyme blocks fatty acid synthesis in Escherichia coli.* J Bacteriol, 1998. **180**(17): p. 4596-602.
110. Suástegui, M., et al., *Investigating strain dependency in the production of aromatic compounds in Saccharomyces cerevisiae.* Biotechnology and Bioengineering, 2016. **113**(12): p. 2676-2685.
111. Perkins, J.B., et al., *Genetic engineering of Bacillus subtilis for the commercial production of riboflavin.* Journal of Industrial Microbiology and Biotechnology, 1999. **22**(1): p. 8-18.

112. Sauer, U., et al., *Metabolic fluxes in riboflavin-producing Bacillus subtilis.* Nat Biotech, 1997. **15**(5): p. 448-452.
113. Dauner, M., J.E. Bailey, and U. Sauer, *Metabolic flux analysis with a comprehensive isotopomer model in Bacillus subtilis.* Biotechnology and Bioengineering, 2001. **76**(2): p. 144-156.
114. Berrı, et al., *The Effect of Increasing NADH Availability on the Redistribution of Metabolic Fluxes in Escherichia coli Chemostat Cultures.* Metabolic Engineering, 2002. **4**(3): p. 230-237.
115. San, K.-Y., et al., *Metabolic Engineering through Cofactor Manipulation and Its Effects on Metabolic Flux Redistribution in Escherichia coli.* Metabolic Engineering, 2002. **4**(2): p. 182-192.
116. Sonderegger, M., et al., *Molecular Basis for Anaerobic Growth of Saccharomyces cerevisiae on Xylose, Investigated by Global Gene Expression and Metabolic Flux Analysis.* Applied and Environmental Microbiology, 2004. **70**(4): p. 2307-2317.
117. Watanabe, S., et al., *Ethanol production from xylose by recombinant Saccharomyces cerevisiae expressing protein-engineered NADH-preferring xylose reductase from Pichia stipitis.* Microbiology, 2007. **153**(9): p. 3044-3054.
118. Jeppsson, M., et al., *The expression of a Pichia stipitis xylose reductase mutant with higher KM for NADPH increases ethanol production from xylose in recombinant Saccharomyces cerevisiae.* Biotechnology and Bioengineering, 2006. **93**(4): p. 665-673.
119. Watanabe, S., et al., *The Positive Effect of the Decreased NADPH-Preferring Activity of Xylose Reductase from Pichia stipitis on Ethanol Production Using Xylose-Fermenting Recombinant Saccharomyces cerevisiae.* Bioscience, Biotechnology, and Biochemistry, 2007. **71**(5): p. 1365-1369.
120. Runquist, D., B. Hahn-Hägerdal, and M. Bettiga, *Increased expression of the oxidative pentose phosphate pathway and gluconeogenesis in anaerobically growing xylose-utilizing Saccharomyces cerevisiae.* Microbial Cell Factories, 2009. **8**: p. 49-49.
121. Petschacher, B. and B. Nidetzky, *Altering the coenzyme preference of xylose reductase to favor utilization of NADH enhances ethanol yield from xylose in a metabolically engineered strain of Saccharomyces cerevisiae.* Microbial Cell Factories, 2008. **7**: p. 9-9.
122. Bengtsson, O., B. Hahn-Hägerdal, and M.F. Gorwa-Grauslund, *Xylose reductase from Pichia stipitis with altered coenzyme preference improves ethanolic xylose fermentation by recombinant Saccharomyces cerevisiae.* Biotechnology for Biofuels, 2009. **2**: p. 9-9.
123. Runquist, D., B. Hahn-Hägerdal, and M. Bettiga, *Increased Ethanol Productivity in Xylose-Utilizing Saccharomyces cerevisiae via a Randomly Mutagenized Xylose Reductase.* Applied and Environmental Microbiology, 2010. **76**(23): p. 7796-7802.
124. Watanabe, S., et al., *Ethanol production from xylose by recombinant Saccharomyces cerevisiae expressing protein engineered NADP$^+$-dependent xylitol dehydrogenase.* Journal of Biotechnology, 2007. **130**(3): p. 316-319.
125. Matsushika, A., et al., *Expression of protein engineered NADP$^+$-dependent xylitol dehydrogenase increases ethanol production from xylose in recombinant Saccharomyces cerevisiae.* Applied Microbiology and Biotechnology, 2008. **81**(2): p. 243-255.
126. Krahulec, S., M. Klimacek, and B. Nidetzky, *Engineering of a matched pair of xylose reductase and xylitol dehydrogenase for xylose fermentation by Saccharomyces cerevisiae.* Biotechnology Journal, 2009. **4**(5): p. 684-694.

127. Matsushika, A., et al., *Efficient Bioethanol Production by a Recombinant Flocculent Saccharomyces cerevisiae Strain with a Genome-Integrated $NADP^+$-Dependent Xylitol Dehydrogenase Gene.* Applied and Environmental Microbiology, 2009. **75**(11): p. 3818-3822.
128. Jeppsson, M., et al., *Reduced Oxidative Pentose Phosphate Pathway Flux in Recombinant Xylose-Utilizing Saccharomyces cerevisiae Strains Improves the Ethanol Yield from Xylose.* Applied and Environmental Microbiology, 2002. **68**(4): p. 1604-1609.
129. Verho, R., et al., *Engineering Redox Cofactor Regeneration for Improved Pentose Fermentation in Saccharomyces cerevisiae.* Applied and Environmental Microbiology, 2003. **69**(10): p. 5892-5897.
130. Zhang, G.-C., J.-J. Liu, and W.-T. Ding, *Decreased Xylitol Formation during Xylose Fermentation in Saccharomyces cerevisiae Due to Overexpression of Water-Forming NADH Oxidase.* Applied and Environmental Microbiology, 2012. **78**(4): p. 1081-1086.
131. Wasylenko, T.M. and G. Stephanopoulos, *Metabolomic and ^{13}C-metabolic flux analysis of a xylose-consuming Saccharomyces cerevisiae strain expressing xylose isomerase.* Biotechnology and Bioengineering, 2015. **112**(3): p. 470-483.
132. Kim, Y.M., et al., *Engineering the pentose phosphate pathway to improve hydrogen yield in recombinant Escherichia coli.* Biotechnology and Bioengineering, 2011. **108**(12): p. 2941-2946.
133. Lee, W.-H., et al., *Enhanced production of ε-caprolactone by overexpression of NADPH-regenerating glucose 6-phosphate dehydrogenase in recombinant Escherichia coli harboring cyclohexanone monooxygenase gene.* Applied Microbiology and Biotechnology, 2007. **76**(2): p. 329-338.
134. Chin, J.W. and P.C. Cirino, *Improved NADPH supply for xylitol production by engineered Escherichia coli with glycolytic mutations.* Biotechnology Progress, 2011. **27**(2): p. 333-341.
135. Wang, Y., K.-Y. San, and G. Bennett, *Improvement of NADPH bioavailability in Escherichia coli through the use of phosphofructokinase deficient strains.* Applied Microbiology and Biotechnology, 2013. **97**(15): p. 6883-6893.
136. Chemler, J.A., et al., *Improving NADPH availability for natural product biosynthesis in Escherichia coli by metabolic engineering.* Metabolic Engineering, 2010. **12**(2): p. 96-104.
137. Kim, S., et al., *Alteration of reducing powers in an isogenic phosphoglucose isomerase (pgi)-disrupted Escherichia coli expressing NAD(P)-dependent malic enzymes and NADP-dependent glyceraldehyde 3-phosphate dehydrogenase.* Letters in Applied Microbiology, 2011. **52**(5): p. 433-440.
138. Sánchez, A.M., et al., *Effect of Overexpression of a Soluble Pyridine Nucleotide Transhydrogenase (udhA) on the Production of Poly(3-hydroxybutyrate) in Escherichia coli.* Biotechnology Progress, 2006. **22**(2): p. 420-425.
139. Chou, H.-H., C.J. Marx, and U. Sauer, *Transhydrogenase Promotes the Robustness and Evolvability of E. coli Deficient in NADPH Production.* PLoS Genet, 2015. **11**(2): p. e1005007.
140. Wiechert, W. and A.A. de Graaf, *In vivo stationary flux analysis by ^{13}C labeling experiments*, in *Metabolic Engineering*, H. Sahm and C. Wandrey, Editors. 1996, Springer Berlin Heidelberg. p. 109-154.

141. Wittmann, C. and E. Heinzle, *Application of MALDI-TOF MS to lysine-producing Corynebacterium glutamicum.* European Journal of Biochemistry, 2001. **268**(8): p. 2441-2455.
142. Klapa, M.I., J.-C. Aon, and G. Stephanopoulos, *Systematic quantification of complex metabolic flux networks using stable isotopes and mass spectrometry.* European Journal of Biochemistry, 2003. **270**(17): p. 3525-3542.
143. Quek, L.-E., et al., *OpenFLUX: efficient modelling software for ^{13}C-based metabolic flux analysis.* Microbial Cell Factories, 2009. **8**(1): p. 25.
144. Krömer, J.O., et al., *In-Depth Profiling of Lysine-Producing Corynebacterium glutamicum by Combined Analysis of the Transcriptome, Metabolome, and Fluxome.* Journal of Bacteriology, 2004. **186**(6): p. 1769-1784.
145. Becker, J., et al., *Metabolic flux engineering of l-lysine production in Corynebacterium glutamicum—over expression and modification of G6P dehydrogenase.* Journal of Biotechnology, 2007. **132**(2): p. 99-109.
146. Becker, J., et al., *From zero to hero—Design-based systems metabolic engineering of Corynebacterium glutamicum for l-lysine production.* Metabolic Engineering, 2011. **13**(2): p. 159-168.
147. Becker, J., et al., *Amplified Expression of Fructose 1,6-Bisphosphatase in Corynebacterium glutamicum Increases In Vivo Flux through the Pentose Phosphate Pathway and Lysine Production on Different Carbon Sources.* Applied and Environmental Microbiology, 2005. **71**(12): p. 8587-8596.
148. Bommareddy, R.R., et al., *A de novo NADPH generation pathway for improving lysine production of Corynebacterium glutamicum by rational design of the coenzyme specificity of glyceraldehyde 3-phosphate dehydrogenase.* Metabolic Engineering, 2014. **25**: p. 30-37.
149. Hu, X.-Q., et al., *A novel feeding strategy during the production phase for enhancing the enzymatic synthesis of S-adenosyl-l-methionine by methylotrophic Pichia pastoris.* Enzyme and Microbial Technology, 2007. **40**(4): p. 669-674.
150. Hu, X.-Q., et al., *Effects of different glycerol feeding strategies on S-adenosyl-l-methionine biosynthesis by PGAP-driven Pichia pastoris overexpressing methionine adenosyltransferase.* Journal of Biotechnology, 2008. **137**(1–4): p. 44-49.
151. Birnbaum, S. and J.E. Bailey, *Plasmid presence changes the relative levels of many host cell proteins and ribosome components in recombinant Escherichia coli.* Biotechnol Bioeng, 1991. **37**(8): p. 736-45.
152. Jones, K.L., S.W. Kim, and J.D. Keasling, *Low-copy plasmids can perform as well as or better than high-copy plasmids for metabolic engineering of bacteria.* Metab Eng, 2000. **2**(4): p. 328-38.
153. Guyot, S., et al., *Surviving the heat: heterogeneity of response in Saccharomyces cerevisiae provides insight into thermal damage to the membrane.* Environmental Microbiology, 2015: p. n/a-n/a.
154. Nugroho, R.H., K. Yoshikawa, and H. Shimizu, *Metabolomic analysis of acid stress response in Saccharomyces cerevisiae.* Journal of Bioscience and Bioengineering.
155. Parawira, W. and M. Tekere, *Biotechnological strategies to overcome inhibitors in lignocellulose hydrolysates for ethanol production: review.* Critical Reviews in Biotechnology, 2011. **31**(1): p. 20-31.

156. Çakar, Z.P., et al., *Evolutionary engineering of multiple-stress resistant Saccharomyces cerevisiae.* FEMS Yeast Research, 2005. **5**(6-7): p. 569-578.
157. King, T., et al., *Transcriptomic Analysis of Escherichia coli O157:H7 and K-12 Cultures Exposed to Inorganic and Organic Acids in Stationary Phase Reveals Acidulant- and Strain-Specific Acid Tolerance Responses.* Applied and Environmental Microbiology, 2010. **76**(19): p. 6514-6528.
158. Ravikirthi, P., P.F. Suthers, and C.D. Maranas, *Construction of an E. coli genome-scale atom mapping model for MFA calculations.* Biotechnology and Bioengineering, 2011. **108**(6): p. 1372-1382.
159. Zamboni, N. and U. Sauer, *Novel biological insights through metabolomics and 13C-flux analysis.* Current Opinion in Microbiology, 2009. **12**(5): p. 553-558.
160. Büscher, J.M., et al., *Cross-Platform Comparison of Methods for Quantitative Metabolomics of Primary Metabolism.* Analytical Chemistry, 2009. **81**(6): p. 2135-2143.
161. Christen, S. and U. Sauer, *Intracellular characterization of aerobic glucose metabolism in seven yeast species by 13C flux analysis and metabolomics.* FEMS Yeast Research, 2011. **11**(3): p. 263-272.
162. Young, J.D., et al., *Mapping photoautotrophic metabolism with isotopically nonstationary 13C flux analysis.* Metabolic Engineering, 2011. **13**(6): p. 656-665.
163. Ma, F., et al., *Isotopically nonstationary ^{13}C flux analysis of changes in Arabidopsis thaliana leaf metabolism due to high light acclimation.* Proceedings of the National Academy of Sciences, 2014. **111**(47): p. 16967-16972.
164. Brennan, L. and P. Owende, *Biofuels from microalgae—A review of technologies for production, processing, and extractions of biofuels and co-products.* Renewable and Sustainable Energy Reviews, 2010. **14**(2): p. 557-577.
165. Varman, A., et al., *Photoautotrophic production of D-lactic acid in an engineered cyanobacterium.* Microbial Cell Factories, 2013. **12**(1): p. 117.
166. Zhou, J. and Y. Li, *Engineering cyanobacteria for fuels and chemicals production.* Protein & Cell, 2010. **1**(3): p. 207-210.
167. Feng, X., Y. Tang, and K.D. Dolan, *Construction of a parsimonious kinetic model to capture microbial dynamics via parameter estimation.* Inverse Problems in Science & Engineering, 2014. **22**(2): p. 309-324.
168. Xiao, Y., et al., *Kinetic Modeling and Isotopic Investigation of Isobutanol Fermentation by Two Engineered Escherichia coli Strains.* Industrial & Engineering Chemistry Research, 2012. **51**(49): p. 15855-15863.
169. Hoefnagel, M.H.N., et al., *Metabolic engineering of lactic acid bacteria, the combined approach: kinetic modelling, metabolic control and experimental analysis.* Microbiology, 2002. **148**(4): p. 1003-1013.
170. Gombert, A.K. and J. Nielsen, *Mathematical modelling of metabolism.* Current Opinion in Biotechnology, 2000. **11**(2): p. 180-186.
171. Wittmann, C., P. Kiefer, and O. Zelder, *Metabolic Fluxes in Corynebacterium glutamicum during Lysine Production with Sucrose as Carbon Source.* Applied and Environmental Microbiology, 2004. **70**(12): p. 7277-7287.
172. Becker, J., C. Klopprogge, and C. Wittmann, *Metabolic responses to pyruvate kinase deletion in lysine producing Corynebacterium glutamicum.* Microbial Cell Factories, 2008. **7**(1): p. 8.

173. Kiefer, P., et al., *Comparative Metabolic Flux Analysis of Lysine-Producing Corynebacterium glutamicum Cultured on Glucose or Fructose.* Applied and Environmental Microbiology, 2004. **70**(1): p. 229-239.
174. Wittmann, C. and E. Heinzle, *Genealogy Profiling through Strain Improvement by Using Metabolic Network Analysis: Metabolic Flux Genealogy of Several Generations of Lysine-Producing Corynebacteria.* Applied and Environmental Microbiology, 2002. **68**(12): p. 5843-5859.
175. Leighty, R.W. and M.R. Antoniewicz, *COMPLETE-MFA: Complementary parallel labeling experiments technique for metabolic flux analysis.* Metabolic Engineering, 2013. **20**: p. 49-55.
176. Crown, S.B., C.P. Long, and M.R. Antoniewicz, *Integrated ^{13}C-metabolic flux analysis of 14 parallel labeling experiments in Escherichia coli.* Metabolic Engineering, 2015. **28**: p. 151-158.
177. Leighty, R.W. and M.R. Antoniewicz, *Parallel labeling experiments with [U-^{13}C]glucose validate E. coli metabolic network model for ^{13}C metabolic flux analysis.* Metabolic Engineering, 2012. **14**(5): p. 533-541.
178. Crown, S.B. and M.R. Antoniewicz, *Parallel labeling experiments and metabolic flux analysis: Past, present and future methodologies.* Metabolic Engineering, 2013. **16**: p. 21-32.
179. Wiechert, W., et al., *A Universal Framework for ^{13}C Metabolic Flux Analysis.* Metabolic Engineering, 2001. **3**(3): p. 265-283.
180. Cvijovic, M., et al., *BioMet Toolbox: genome-wide analysis of metabolism.* Nucleic Acids Research, 2010. **38**(suppl 2): p. W144-W149.
181. Srour, O., J.D. Young, and Y.C. Eldar, *Fluxomers: a new approach for ^{13}C metabolic flux analysis.* BMC Systems Biology, 2011. **5**: p. 129-129.
182. Kajihata, S., et al., *OpenMebius: An Open Source Software for Isotopically Nonstationary ^{13}C-Based Metabolic Flux Analysis.* BioMed Research International, 2014. **2014**: p. 10.
183. Sokol, S., P. Millard, and J.-C. Portais, *influx_s: increasing numerical stability and precision for metabolic flux analysis in isotope labelling experiments.* Bioinformatics, 2012. **28**(5): p. 687-693.
184. Gombert, A.K., et al., *Network Identification and Flux Quantification in the Central Metabolism of Saccharomyces cerevisiae under Different Conditions of Glucose Repression.* Journal of Bacteriology, 2001. **183**(4): p. 1441-1451.
185. Gill, P.E., W. Murray, and M.A. Saunders, *SNOPT: An SQP Algorithm for Large-Scale Constrained Optimization.* SIAM Review, 2005. **47**(1): p. 99-131.
186. Press, W.H., et al., *Numerical recipes in C: the art of scientific computing*. 1988: Cambridge University Press. 735.
187. Jordà, J., et al., *Metabolic flux profiling of recombinant protein secreting Pichia pastoris growing on glucose:methanol mixtures.* Microbial Cell Factories, 2012. **11**: p. 57-57.
188. Hayakawa, K., F. Matsuda, and H. Shimizu, *Metabolome analysis of Saccharomyces cerevisiae and optimization of culture medium for S-adenosyl-l-methionine production.* AMB Express, 2016. **6**(1): p. 38.

Table 2.1 Summary of ^{13}C-MFA software.

Software name	Capabilities			Labeled pattern				Key solver (algorithm)			Platform		Developer
	Steady-state	[a]INST-^{13}C-MFA	[b]PLE integration	[c]EMU	[d]MDV	[e]SFL	Cumomer	*fmincon*	IPOPT	Others	MATLAB	UNIX/Linux	
13CFLUX	●			●					●			●	Wiechert's group[179]
13CFLUX2	●			●					●			●	Wiechert's group[86]
Metran	●		●	●				●			●		Antoniewicz's group[87]
C13	●					●		●			●		Nielsen's group[180]
OpenFLUX	●				●			●			●		Krömer's group[143]
OpenFLUX2	●		●	●				●			●		Mashko's group[85]
FiatFLUX	●				●			●			●		Sauer's group[89]
FIA	●						[f]●			[g]●		●	Young's group[181]
INCA	●	●		●						[h]●	●		Young's group[88]
OpenMebius	●	●		●						[i]●	●		Shimizu's group[182]
influx_s	●						●			[j]●		●	Portais's group[183]

Notes: [a]INST-^{13}C -MFA: isotopic nonstationary ^{13}C-metabolic flux analysis. [b]PLE: Parallel labeling experiments. [c]EMU: elementary metabolite unit [87]. [d]SFL: summed fractional labeling [184]. [e]MDV: mass distribution vectors. [f]Fluxomer. [g]SNOPT [185]. [h]Customized Differential Equation Solver [91]. [i]*Levenberg-Marquardt* method[186]. [j]NLSIC [183].

Table 2.2 Summary of synergistic tactics of ^{13}C-MFA and metabolic engineering in identifying and overcoming the bottleneck steps of biochemical production.

Industrial microbial hosts	Target chemicals	Biological insights from ^{13}C-MFA						Strategies of genetic modifications		Outcomes of metabolic engineering
		Glycolysis	[b]oxPP pathways	[c]Pyr-bypass pathways	[d]ED pathways	[e]PDC pathways	[f]NADPH supply	Up-regulated	Down-regulated	
S. cerevisiae	n-Butanol	[a]NC	NC	UP [100]	NC	NC	NC	cyto-PDH[51], ACS	ADH, GPD[51]	300% increase[51]
S. cerevisiae	Amorphadiene	NC	NC	UP [100]	NC	NC	NC	ALD[98], ACS	None	70% increase [98]
S. cerevisiae	Acetyl-CoA	NC	NC	[g]UP [52]	NC	NC	NC	[g]PHK pathways [52]	None	~10% increase [52]
S. cerevisiae	Shikimic acid	UP[110]	NC	NC	NC	NC	NC	*aro1*, *aro4*, *tkl*[110]	None	600% increase[110]
E. coli	Fatty acid	NC	UP [58]	NC	UP [58]	DOWN [58]	UP	ACC, ACL, FASs[58]	FADs	200% increase

Note: [a]NC: Not changed. [b]oxPP pathways: oxidative pentose phosphate pathways. [c]Pyr-bypass pathways: pyruvate-bypass pathways, including pyruvate dehydrogenase pathways. [d]ED pathway: Entner–Doudoroff pathways. [e]PDC pathways: pyruvate decarboxylase pathways. [f]NADPH supply represents the overall NADPH net production, including oxidative PP pathways and transdehydrogenase pathways. [g]PHK pathways: Heterologous phosphoketolase (PHK) pathways. Certain metabolic engineering works were related to the ^{13}C-MFA studies but did not sequentially follow the ^{13}C-MFA studies.

Table 2.3 [b]Summary of synergistic tactics of ^{13}C-MFA and metabolic engineering in uncovering and solving the cofactor imbalance issues.

Industrial microbial hosts	Target chemicals	Biological insights from ^{13}C-MFA			Strategies of metabolic engineering			Outcomes of metabolic engineering
		[a]TCA cycle	oxPP pathways	NADPH supply	Up-regulated	Down-regulated	Others	
E. coli	Lycopene	NC	UP[53]	UP[53]	G6PDH, Transdehydrogenase [138, 139]	*pgi*[137]	None	~100% increase[53]
C. glutamicum	L-valine	NC	UP[54]	UP[54]	Transdehydrogenase[54]	None	None	>200% increase [54]
S. cerevisiae	Ethanol (Xylose utilization)	UP[36]	UP[36]	NC	None	None	Alternate the cofactor specificity of XR to NADH [117-119, 121].	~40% increase [121]

Note: [a]TCA cycle: tricarboxylic acid cycle. [b]All abbreviations and table headers in Table 3 have the same definitions in Table 2. Certain metabolic engineering works were related to the ^{13}C-MFA studies but did not sequentially follow the ^{13}C-MFA studies.

Table 2.4 [b]Summary of synergistic tactics of ^{13}C-MFA and metabolic engineering in revealing and compensating cell maintenance requirement of industrial microorganisms.

Industrial microbial hosts	Target chemicals	Biological insights from ^{13}C-MFA				Strategies of metabolic engineering	Outcomes of metabolic engineering
		TCA cycle	oxPP pathways	PDC pathways	NADPH supply		
P. pastoris	*R. oryzae* lipase	UP[187]	NC	NC	NC	• Co-substrate culture[187]	• Supply additional ~30% ATP to compensate the requirement of maintenance energy[187].
S. cerevisiae	[a]SAM	UP[35]	NC	NC	NC	• Nutrient medium optimization[188]	• 250% increase of SAM production[188]
S. cerevisiae	(Xylose utilization)	UP[36]	UP[36]	NC	UP[36]	• Nutrient medium optimization[36]	• ~50% decrease the requirement of maintenance energy[36]
S. cerevisiae	Cell growth	UP[39]	UP[39]	NC	UP[39]	• Overexpress NADPH-dependent oxireductase in parent strain.	• More than 20% decrease of biomass production[39]
E. coli	Cell growth	DOWN [38]	NC	UP[38]	UP[38]	• Decrease the cofactor (NADH/NAD$^+$) sensitivity of relevant enzymes. • Overexpress the proteins of electron transport chain. • Add other electron acceptors.	• ~ 50% increase of growth rate[38]

Note: [a]SAM: S-Adenosyl-L-Methionine. [b]All abbreviations and table headers in Table 3 have the same definitions in Table 2 and Table 3. Certain metabolic engineering works were related to the ^{13}C-MFA studies but did not sequentially follow the ^{13}C-MFA studies.

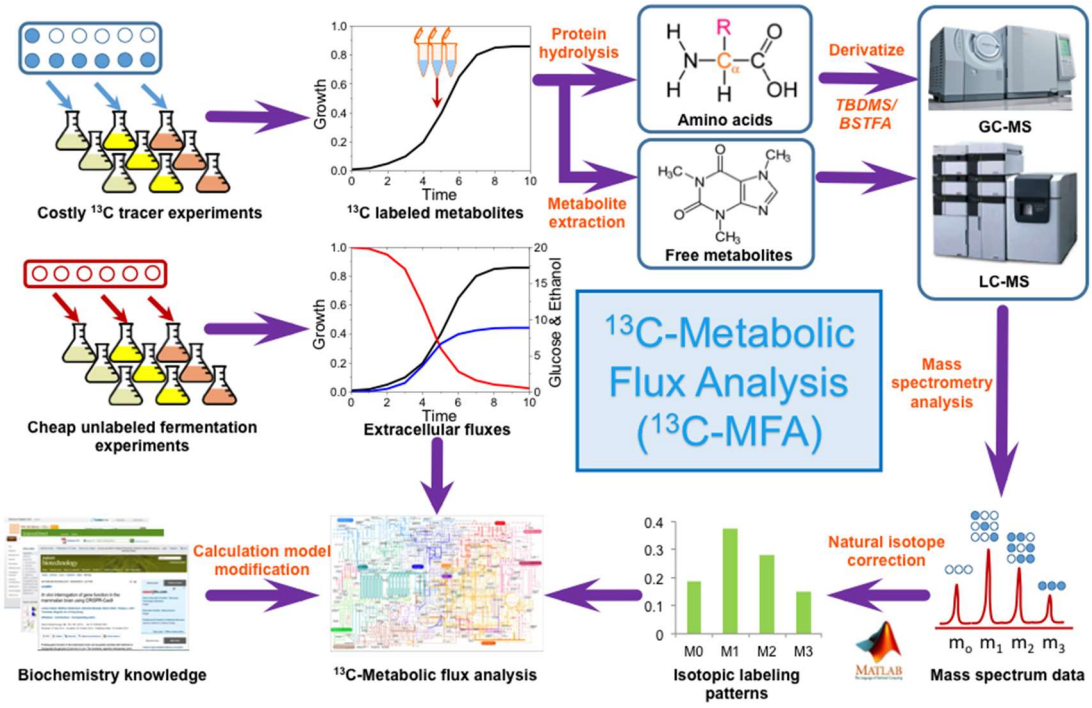

Fig. 2.1 Technology platform for ^{13}C-MFA.

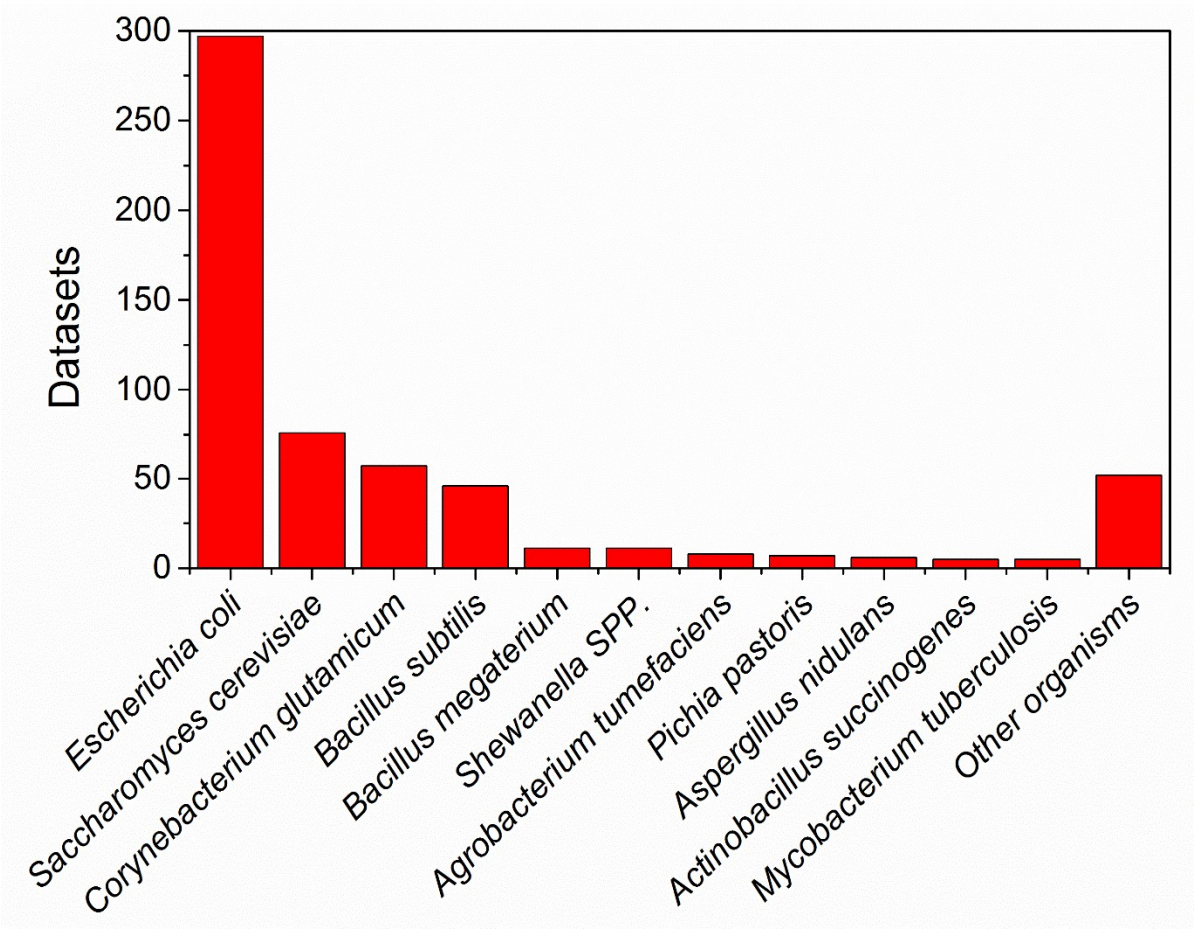

Fig. 2.2 Summary of current ^{13}C-MFA studies on different organisms.

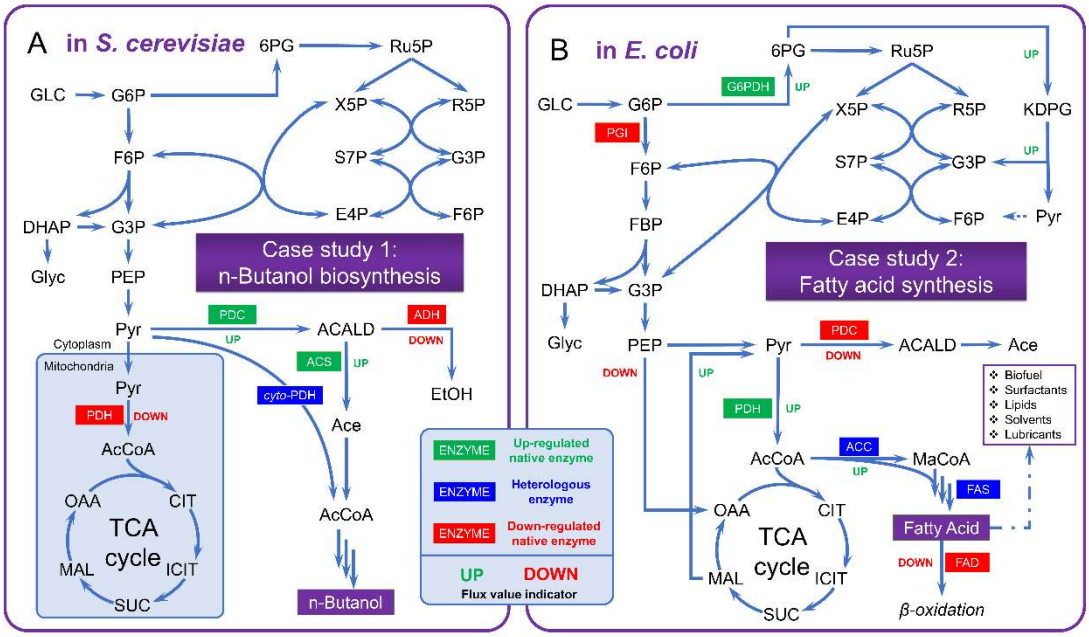

Fig. 2.3 Case studies that identify key bottleneck steps of biochemical production via ^{13}C-MFA and the corresponding metabolic engineering strategies. (A) n-Butanol biosynthesis in *S. cerevisiae*; (B) fatty acid synthesis in *E. coli*. Please note that the pathways showed in Fig. 2.3 were schematic and there could be missing pathways. Definitions of abbreviations are shown in List of Abbreviations.

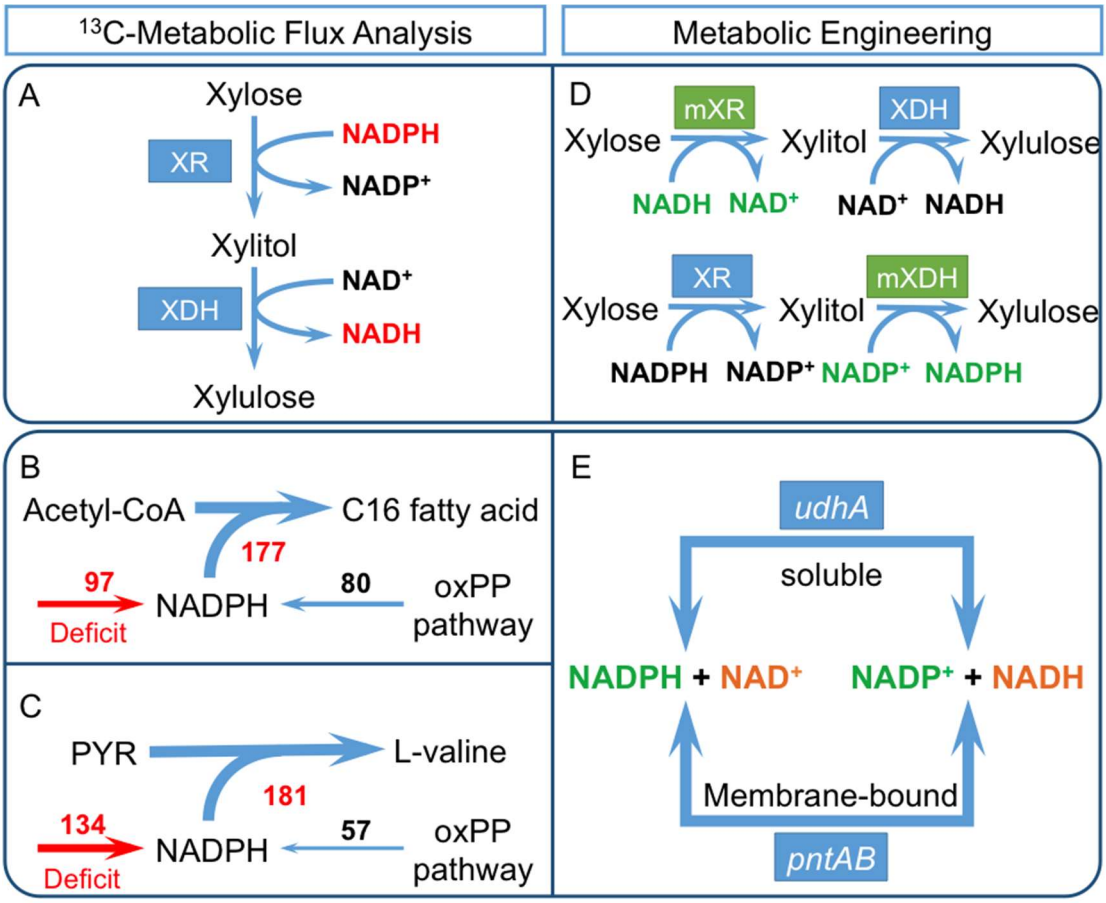

Fig. 2.4 Cofactor imbalance issues identified by ^{13}C-MFA and the corresponding metabolic engineering strategies. Left column: cofactor imbalance issues in (A) xylose utilization of *S. cerevisiae* strains, (B) fatty acid and fatty acid-derived chemical production, and (C) L-valine production. Right column: the corresponding metabolic engineering strategies to tackle cofactor imbalance issues: (D) altering the co-factor specificities of xylose reductase (XR) or xylitol dehydrogenase (XDH); (E) overexpressing transhydrogenase to balance the NADH and NADPH. Definitions of abbreviations are shown in List of Abbreviations.

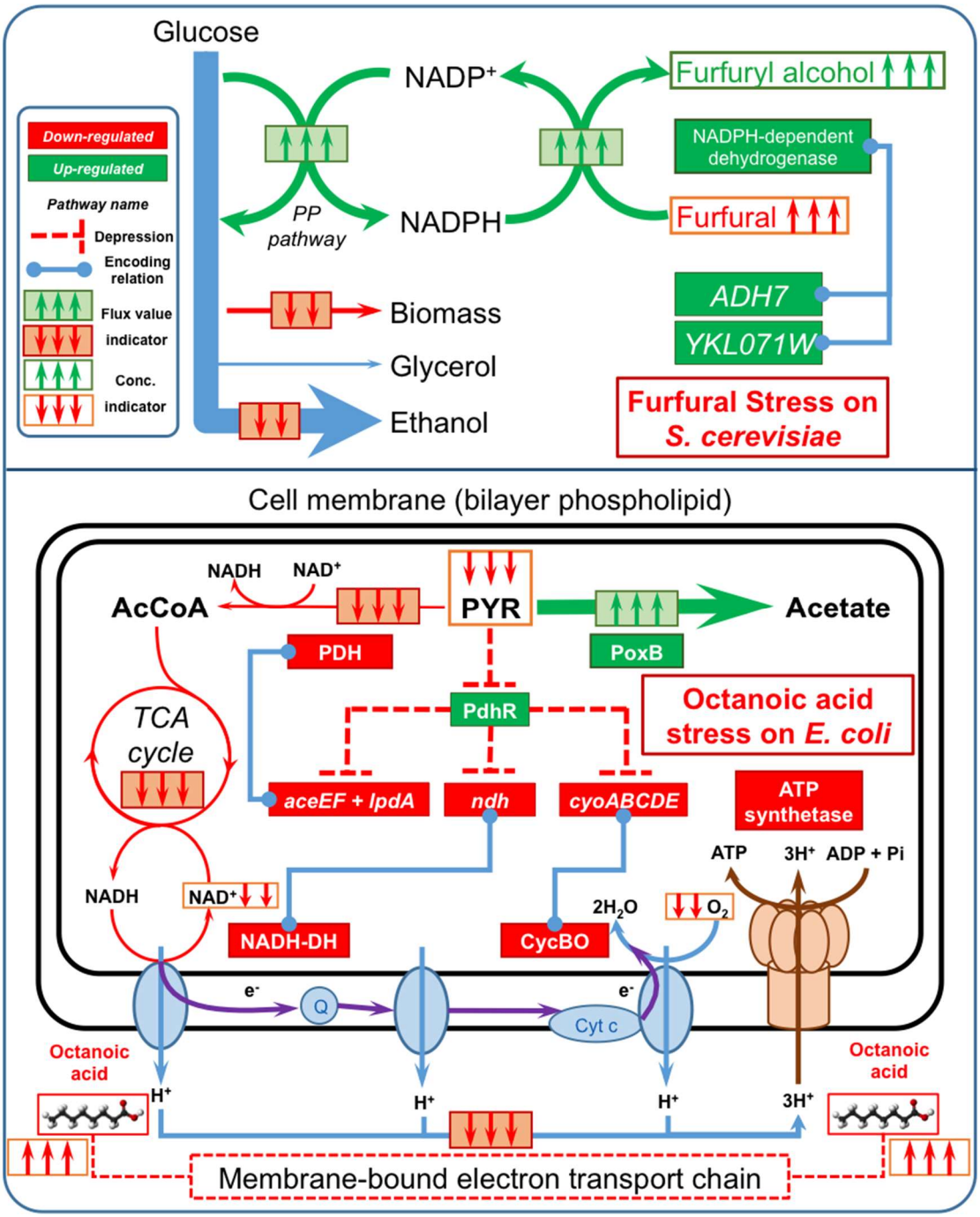

Fig. 2.5 Mechanisms of microbial stress responses identified by ^{13}C-MFA. Top: Stress responses of *S. cerevisiae* to the furfural; bottom: Stress responses of *E. coli* to octanoic acid. Definitions of abbreviations are shown in List of Abbreviations.

Chapter 3: ^{13}C Assisted Pathway and Flux Analysis for Planktonic and Biofilm Cells

3.1 ^{13}C Assisted Pathway and Flux Analysis

Based on the review in Chapter 2, it is clear to see that ^{13}C assisted pathway and flux analysis is a powerful approach to demystify the complex metabolic rewiring of microorganisms in either planktonic and biofilm state, and more importantly, to derive the appropriate strategies to engineer microorganisms for specific purposes (e.g., improving biochemical production) [1-6]. Generally, in ^{13}C assisted pathway and flux analysis, carbon isotopes have been used to trace the cell metabolism with the production of ^{13}C-labelled metabolites. The metabolic pathway usages or carbon flux distributions in metabolic network of microorganisms can then be determined using several computational algorithms by using a mathematical metabolic model and the ^{13}C-labelled patterns of the metabolites [1, 2, 7-10].

In this chapter, I applied ^{13}C assisted pathway and flux analysis to different microorganisms in either planktonic and biofilm cells for obtaining metabolic pathway usages and carbon flux distributions. I further compared variations of metabolic pathway usages or fluxes under different stresses, among different strains, in different states, and feeding with different substrates to discover several critical biological insights such as the metabolic responses under mixed stresses, the key pathways for biochemical productions (including natural products and heterologous chemicals), the metabolic rewiring of biofilm cells, and the roles of different substrates, respectively. These insights can guide the biologists and engineers to develop more appropriate strategies for enhancement of chemical production and environmental applications.

3.2 Investigate the Metabolic Reprogramming of *Saccharomyces cerevisiae* for Enhanced Resistance to Mixed Fermentation Inhibitors via ^{13}C Metabolic Flux Analysis

Weihua Guo[a], Yingying Chen[b], Na Wei[b, †], Xueyang Feng[a, †]

[a] Department of Biological Systems Engineering, Virginia Tech University, Blacksburg, VA 24061, United States

[b] Department of Civil and Environmental Engineering and Earth Sciences, University of Notre Dame, Notre Dame, IN 46556, United States

[†]Correspondence to: Na Wei and Xueyang Feng.

Phone: +1-(574)631-5164 and +1-(540)231-2974

Email: nwei@nd.edu and xueyang@vt.edu

This manuscript has been published on *PloS one* 11 (8), e0161448.

Abstract

The fermentation inhibitors from the pretreatment of lignocellulosic materials, e.g., acetic acid and furfural, are notorious due to their negative effects on the cell growth and chemical production. However, the metabolic reprogramming of the cells under these stress conditions, especially metabolic response for resistance to mixed inhibitors, has not been systematically investigated and remains mysterious. Therefore, in this study, ^{13}C metabolic flux analysis (^{13}C-MFA), a powerful tool to elucidate the intracellular carbon flux distributions, has been applied to two *Saccharomyces cerevisiae* strains with different tolerances to the inhibitors under acetic acid, furfural, and mixed (i.e., acetic acid and furfural) stress conditions to unravel the key metabolic responses. By analyzing the intracellular carbon fluxes as well as the energy and cofactor utilization under different conditions, we uncovered varied metabolic responses to different inhibitors. Under acetate stress, ATP and NADH production was slightly impaired, while NADPH tended towards overproduction. Under furfural stress, ATP and cofactors (including both NADH and NADPH) tended to be overproduced. However, under dual-stress condition, production of ATP and cofactors was severely impaired due to synergistic stress caused by the simultaneous addition of two fermentation inhibitors. Such phenomenon indicated the pivotal role of the energy and cofactor utilization in resisting the mixed inhibitors of acetic acid and furfural. Based on the discoveries, valuable insights are provided to improve the tolerance of *S. cerevisiae* strain and further enhance lignocellulosic fermentation.

3.2.1 Introduction

The production of biofuels and other bio-based chemicals from renewable resources has been widely applied to overcome the limitation of non-renewable fossil fuel energy and the challenge of global warming. Due to the fast growth and high biofuel productivity, *Saccharomyces cerevisiae* is one of the most important workhorses in producing biofuels from various carbohydrates of biomass with high abundance and low cost. However, several fermentation inhibitors generated from the pretreatment of lignocellulosic materials, such as acetic acid [11], furfural [12], and furan [13], seriously impair the biofuel production by repressing or even stopping the cell growth of *S. cerevisiae* [14-17]. More importantly, most of these inhibitors ubiquitously co-exist in the practical fermentation process. Therefore, it is important to elucidate the general metabolic responses of *S. cerevisiae* to different inhibitors, especially to mixed inhibitors, to further improve stress resistance and reduce stress impairment. Constructing a general mechanism of inhibition is important, as in reality mixed inhibitors are hard to avoid. By identifying a common target, it is thus more likely to find a way to solve the problem in practice.

A number of biological characterizations have been accomplished to unravel the effect of fermentation inhibitors and resistance mechanism in the yeast [11, 13-15, 18, 19], and several key metabolic responses have been found to be related to the stress resistance [13, 16, 17, 20-22]. It was found that acetic acid, a fermentation inhibitor commonly presenting in the lignocellulosic hydrolysate, could lead to the fermentation arrest and suppression of ethanol production for the *S. cerevisiae* strains when using glucose as the major substrate. The mechanisms for acetic acid inhibition have been investigated in *S. cerevisiae* strains [23-29]. Several strategies, such as genome screening [30-32], metabolic

engineering [33-35], and evolutionary engineering [36], have successfully been developed to improve the yeast resistance to acetic acid. Similarly, the mechanism of furfural inhibition has been studied for more than three decades [12, 13, 37-40]. It was found that the resistance of *S. cerevisiae* strains to furfural could be improved by either reducing or oxidizing the furfural to less toxic compounds [12, 37, 41]. In addition, the overexpression of the genes in pentose phosphate pathway as well as several key transcription factors has been implemented to successfully improve the tolerance to furfural in *S. cerevisiae* strains [35, 39].

Despite growing understanding of the biomolecular mechanisms of yeast resistance to single inhibitors (e.g., acetic acid or furfural), the general molecular basis of yeast resistance to mixed fermentation inhibitors remains unclear. Considering the fact that various inhibitors often co-exist in the hydrolysate and could cooperate with each other to become even more toxic to yeast than existing alone (i.e., synergistic stress), the knowledge on how yeast cells reprogram their metabolism in response to mixed fermentation inhibitors is of particular interests to biofuel and biochemical production. The key challenge in studying yeast resistance to mixed inhibitors lies in that the resistance phenotype usually involves very complex multi-genic regulations. Additionally, various fermentation inhibitors in the cellulosic hydrolysates usually have distinct toxicity mechanisms. As such, the reprogramming of yeast metabolism to resist mixed fermentation inhibitors is largely unknown. Recently, several pioneer studies have been accomplished on the transcriptional responses to mixed inhibitors of acetate and furfural [42]. However, metabolic reprogramming in responses to such mixed fermentation inhibitors remains unclear. In this scenario, metabolic flux analysis could provide a “common language”, i.e.,

intracellular metabolic flux distributions, to uncover and evaluate different inhibitory metabolic reprogramming for corresponding stress conditions. Therefore, in this study, we applied ^{13}C metabolic flux analysis (^{13}C-MFA), a powerful and accurate tool to demystify the intracellular metabolism [43-45], on two *S. cerevisiae* strains, i.e., a parent strain S-C1, and an engineered strain YC1 with improved fermentation inhibitor resistance. We used ^{13}C-MFA to systematically investigate the metabolic reprogramming of the *S. cerevisiae* strains in four conditions, namely blank condition (without any inhibitor), acetic acid, furfural, and dual-stress conditions with both acetic acid and furfural. By analyzing the carbon flux distribution as well as the energy and cofactor utilization, we elucidated the key metabolic responses under the different stress conditions. Particularly, the lack of energy and cofactor supply was found to be the main reason for the synergistic stress caused by the co-presence of acetic acid and furfural. To our best knowledge, it is the first time that ^{13}C-MFA was used to study the metabolic responses of *S. cerevisiae* under the stress of mixed fermentation inhibitors. The discovery from this work provides valuable biological insights to further improve the yeast resistance to fermentation inhibitors, especially mixed fermentation inhibitors.

3.2.2 Materials and Methods

Plasmids, Strains and Media. All the strains and plasmids used in this study were summarized in Table 3.2.1. The *S. cerevisiae* strain SR8-trp was kindly provided by Dr. Yong-Su Jin's lab. The parent strain (named as S-C1) and the engineered strain (named as YC1, a mutant with improved resistance to acetic acid and furfural) were obtained through the inverse metabolic engineering approach in our recent work [46]. Specifically, it has been demonstrated that overexpression of WHI2, a gene target encoding a cytoplasmatic

globular scaffold protein in *S. cerevisiae*, improved the resistance of yeast to acetic acid dramatically. *Escherichia coli* TOP10 strain was used for gene cloning and manipulation. *E. coli* strains were grown in Luria-Bertani medium at 37 °C and 100 μg/mL of ampicillin was added to the medium when required. Yeast strains were routinely cultivated at 30 °C in YP medium (10 g/L of yeast extract and 20 g/L of peptone) or synthetic complete (SC) medium (6.7 g/L of yeast nitrogen base, 0.6 g/L complete supplement mixture) containing 20 g/L of D-glucose. SC media containing 20 g/L agar and glucose, 20 mg/L histidine and uracil and 100 mg/L leucine without tryptophan amendment was used to select transformants using TRP1 as an auxotrophic marker.

Isotopic Labeling Experiment. The isotopic labeling experiments were accomplished by following a previously developed protocol [47]. In general, both the S-C1 and YC1 strains were cultured in a minimal medium with 20 g/L ^{13}C-glucose (a mixture of 80% [1-^{13}C] and 20% [U-^{13}C] glucose) as the sole carbon source at the oxygen-limited condition. Four conditions, i.e., blank condition without any inhibitor, acetic acid stress condition with 2 g/L acetic acid, furfural stress condition with 1g/L furfural, and the dual-stress condition with 2 g/L acetic acid and 1g/L furfural, were used to culture the yeast strains to study the metabolic responses. The cell growth was monitored by OD_{600}. The extracellular metabolite quantification using high performance liquid chromatograph (HPLC) was also conducted to assess the consumption of glucose and the production of ethanol, glycerol, and acetic acid (Table 3.2.2). For each of the culture conditions, the ^{13}C-labeled biomass was harvested during the exponential growth phase. The cell variability was checked at OD_{600} under stress conditions. The OD_{600} was found to be linearly

correlated (R^2 = 0.99) with colony-forming units (CFU) under the stress conditions (Fig. 3.2.S2), indicating the appropriateness of using OD_{600} to evaluate the cell variability.

Following harvest, isotopomer analysis of proteinogenic amino acids was conducted as previously described [47]. In brief, the biomass was hydrolyzed using 6 M HCl (20 h at 100 °C) and the amino acids were derivatized using 50 µl tetrahydrofuran and 50 µL N-(tert-butyldimethylsilyl)-N-methyl-trifluoroacetamide (Sigma-Aldrich) to form tert-butyl dimethylsilyl (TBDMS) derivatives (1h at 70°C). Gas Chromatography-Mass Spectrometry (GC-MS) was performed to analyze derivatized amino acids using a Shimadzu GC2010 GC with a SH-Rxi-5Sil column and a Shimadzu QP2010 MS. Three types of charged fragments were detected by GC-MS for various amino acids: the $[M-57]^+$ group (containing unfragmented amino acids); and the $[M-159]^+$ or $[M-85]^+$ group (containing amino acids that had lost an α-carboxyl group). For each type of fragments, the labeling patterns, i.e., mass distribution vectors (MDVs), were represented by M0, M1, M2, etc., which were fractions of non-labeled, singly-labeled, and doubly-labeled amino acids. The effects of natural isotopes on isotopomer labeling patterns were corrected by using a previously reported algorithm [48].

Metabolic Flux Analysis. The metabolic flux analysis was accomplished by following a previously developed protocol [47]. In general, the MDVs were used to calculate the summed fractional labeling (SFL) values which were directly used to calculate metabolic fluxes in Biomet Toolbox 2.0 (based on MATLAB, MathWorks, Inc. MA) [49]. The central carbon metabolic model for the MFA was developed previously [47] based on the KEGG database (http://www.genome.jp/kegg/), including glycolysis pathway, pentose phosphate pathway, anaplerotic pathways, the tricarboxylic acid (TCA)

cycle, and the transport reactions between different cell compartments (Table 3.2.S1). For metabolic flux analysis, flux estimation was repeated at least 50 times starting with different initial values generated by a genetic algorithm for all the fluxes to find a likely global solution. A fit of the simulated and measured SFLs was determined to be a global solution only after the solution fit was obtained at least twice using this method (Fig. 3.2.S1). Based on the carbon fluxes (Table 3.2.S2), the ATP, NADH, and NADPH production and consumption rates were estimated by following previous published works [47, 50]. The unpaired Student's t-test (α = 0.05) was used as the statistical method to determine the significance of the net productions of ATP and cofactors under two different conditions or of two different strains.

3.2.3 Results

Metabolic Responses to Acetic Acid Stress. When cultivating the parent *S. cerevisiae* strain, S-C1, under the acetic acid stress condition, the growth rate and glucose uptake rate were repressed by 80% and 60%, respectively (Table 3.2.2). Such suppression of the growth and glucose uptake was also observed in previous studies [13, 32, 51]. By comparing the flux distributions of S-C1 strain cultivated in blank and acetic acid stress conditions (Fig. 3.2.1), a significant increase (33%) of carbon fluxes in the pentose phosphate pathway (PP pathway) and a dramatic decrease (66%~87%) of carbon fluxes in the glycolysis pathway were observed (Fig. 3.2.1). As a result, the ethanol production decreased by >60% in the acetic acid stress condition compared to that in the blank condition. In addition, the carbon fluxes in the TCA cycle dramatically decreased (>85%) under the acetic acid stress condition, which is consistent with previous studies [23, 25]. The net production of ATP and NADH was decreased under the acetic acid stress condition

due to the decreased glycolysis and TCA cycle (Fig. 3.2.2). However, the NADPH net production was increased due to the increased PP pathways.

Similarly as that in the S-C1 strain, when cultivating the mutant *S. cerevisiae* strain, YC1, in the acetic acid stress condition, the growth rate and glucose uptake rate were depressed by 68% and 21%, respectively (Table 3.2.2). By comparing the flux distributions of YC1 strain cultivated in blank and acetic acid stress conditions (Fig. 3.2.1), a significant increase (51%) of carbon fluxes in the PP pathway and a decrease (~44%) of carbon fluxes in the glycolysis pathway were observed, which decreased the ethanol production by 32%. The TCA cycle was also decreased (~50%) under the acetic acid stress condition, which was similar as that in the wild-type strain. By calculating the consumption and production of cofactors based on the flux distribution, the net production of ATP and NADH under the acetic acid stress was found not significantly different from those under the blank condition. However, the NADPH net production was increased by ~100% due to the increased PP pathways (Fig. 3.2.2).

Comparing the metabolic responses between the S-C1 strain and YC1 strain under the acetic acid stress condition, the similar pattern of the alteration of flux distributions was observed, namely increased PP pathway, decreased glycolysis pathway, as well as the decreased TCA cycle when comparing to the blank condition (Fig. 3.2.1). This indicated that both the S-C1 strain and YC1 strain responded to the acetic acid stress in a similar manner. However, the YC1 strain demonstrated better growth rate (~100% higher than the S-C1 strain, Table 3.2.2) and glucose uptake rate (~80% higher than the S-C1 strain) under the acetic acid stress condition. Such superior performance could be related to the higher activities of the glycolysis and the TCA cycle in the mutant strain (Fig. 3.2.3), which

produced more ATP (~50% increase in net produced ATP compared to that in the S-C1 strain, Fig. 3.2.2) for relieving the oxidative stresses inflicted by acetic acid. In addition, the higher activities of PP pathway could produce more NADPH for supporting macromolecule synthesis for cell growth under acetic acid stress condition.

Metabolic Responses to Furfural Stress. When cultivating the *S. cerevisiae* S-C1 strain under the furfural stress condition, the growth rate decreased by ~50% with a slightly increased glucose uptake rate (~10%) (Table 3.2.2). Such suppressed growth but increased glucose uptake was also observed in a previous study on chemostat when feeding a high concentration of furfural [38]. By comparing the flux distributions of the S-C1 strain cultivated in blank and furfural stress condition (Fig. 3.2.1), a significant increase of carbon fluxes in the PP pathway (~80%) as well as glycolysis pathway (~12%) was observed. The carbon fluxes in TCA cycle were also increased by ~135% under the furfural stress condition. The elevated activities of glycolysis, PP pathway, and the TCA cycle led to the increased net production of ATP, NADH and NADPH in the S-C1 strain under the furfural stress condition (Fig. 3.2.2).

Similarly, when cultivating the *S. cerevisiae* YC1 strain under the furfural stress condition, the growth rate was decreased by ~56% with an increased glucose uptake rate (~30%). By comparing the flux distributions of the YC1 strain cultivated in blank and furfural stress condition (Fig. 3.2.1), an increase of the carbon fluxes in the PP pathway (~118%), glycolysis pathway (~28%), and the TCA cycle (~128%) was observed under the furfural stress condition, which is similar as that in the wild-type strain. Therefore, the net production of ATP, NADH and NADPH were also increased in the strain YC1 under the furfural stress condition (Fig. 3.2.2).

Comparing the metabolic responses between the resistant strain YC1 and control S-C1, the carbon flux distributions were similarly altered, i.e., the activities of the PP pathway, glycolysis pathway, TCA cycle were all elevated. Therefore, both strains responded to the furfural stress in a similar manner (Fig. 3.2.3). As a result of such metabolic reprogramming, the net production of ATP and NADPH was increased. The increased ATP and NADPH production could play important roles in resisting the furfural stress in the yeast. Basically, NADPH could be used as the cofactor for alcohol dehydrogenase to convert furfural to furfuryl alcohol, a less toxic compound to *S. cerevisiae*, while the over-production of ATP could relieve the oxidative stress inflicted by furfural. Noticeably, the carbon fluxes in the PP pathway and the TCA cycle were higher in the strain YC1 than that in the control strain S-C1. Although this significantly improved the YC1 cell growth, the carbon loss in the PP pathway and the TCA cycle slightly decreased the ethanol yield. The observation clearly indicated a trade-off between cell growth and the ethanol production when cultivated with furfural.

Metabolic Responses to Mixed Fermentation Inhibitors. When cultivating the *S. cerevisiae* S-C1 strain under the dual-stress condition with acetic acid and furfural, the growth rate and glucose uptake rate were dramatically decreased by 82% and 84%, respectively. By comparing the flux distributions of S-C1 strain under blank condition and the dual-stress condition (Fig. 3.2.1), we found that all the fluxes were dramatically decreased. For example, the carbon fluxes in the PP pathway, glycolysis, and TCA cycle were decreased by ~53%, ~90%, and ~85%, respectively. Compared to the flux distributions in acetic acid stress condition or furfural stress condition, the extent of carbon flux decrease was much severe in the presence of both acetic acid and furfural. The results

indicated that the mixed inhibitors of acetic acid and furfural led to synergistic stress on the S-C1 *S. cerevisiae* strain, i.e., the presence of both inhibitors is much more toxic than either individual inhibitor.

Similarly, when cultivating the *S. cerevisiae* YC1 strain under the dual-stress condition with both acetic acid and furfural, the growth rate and glucose uptake rate were dramatically decreased by 80% and 80%, respectively. The synergistic stress of acetic acid and furfural was also observed in the *S. cerevisiae* YC1 strain, in which the carbon fluxes in all of the metabolic pathways significantly decreased (Fig. 3.2.1). The severe inhibitory effects of acetic acid and furfural mixture could be highly correlated with the energy and cofactor production. In general, for both YC1 strain and S-C1 strain, the net production of ATP, NADH and NADPH were universally suppressed (Fig. 3.2.2). As a result, the oxidative stress inflicted by acetic acid and furfural could not be relieved, while on the other hand, furfural could not be sufficiently degraded to less toxic compound due to the lack of cofactor supplies (e.g., NADPH) for the alcohol dehydrogenase.

Comparisons of Yeast Metabolic Responses to Different Fermentation Inhibitors. To highlight the similarities and differences of yeast metabolic responses under different inhibitor treatments, we have compared metabolic flux distributions and corresponding ATP and cofactor balances between different stress conditions. For the stress conditions with single inhibitors, i.e., acetic acid and furfural, the growth rate and glucose uptake were dramatically impaired under the acetic acid stress compared to the unstressed condition, while cell growth was impaired but glucose uptake was improved under furfural stress condition (Table 3.2.1). As a result of improved glucose uptake, ethanol production increased under furfural stress condition but decreased under acetic acid

stress condition. In addition, more carbon flux was directed towards the glycolysis pathway under the furfural stress condition, while more carbon flux was redirected to the pentose phosphate pathway under acetic acid stress condition. In addition, more carbon going through the TCA cycle under furfural stress condition, but acetic acid impaired the TCA cycle dramatically. Due to the different metabolic flux distributions, the energy and cofactor productions also varied. Specifically, ATP net production under furfural stress was improved from the untreated condition. Whereas, under acetic acid stress, ATP net production was impaired slightly. NADH net productions of both inhibitors did not change dramatically. However, both inhibitors led to a significant increase in NADPH net production. The NADPH production under furfural stress condition was much higher than that of acetic acid stress condition due to the enhanced glucose uptake.

Next, we compared the metabolic responses to single inhibitors (i.e., acetic acid or furfural) with that to mixed inhibitors in order to highlight the different mechanisms used by yeast to resist single and mixed inhibitors. Compared to acetic acid stress condition, cell growth was similar to that of the mixed inhibitors, but glucose uptake was dramatically impaired under dual stress condition (>59%, Table 3.2.1). Due to the impaired glucose uptake rate, the net productions of ATP, NADH, and NADPH were also decreased dramatically under dual-stress condition compared to those under acetic acid stress only. Compared to furfural stress condition, both cell growth and glucose uptake under dual stress condition decreased by ~55% and ~85%, respectively. As a result, the impaired glucose uptake under dual-stress condition led to a decrease of net productions of ATP, NADH, and NADPH compared to those under furfural stress only. Overall, by comparing the metabolic responses between different inhibitors, it is evident that different inhibitors

could lead to varied metabolic responses to resist corresponding stress conditions, as discussed below.

3.2.4 Discussion

Based on the metabolic reprogramming under different stress conditions, we proposed the mechanisms that could be used by the *S. cerevisiae* strains for resisting acetic acid, furfural, or mixed inhibitors of acetic acid and furfural (Fig. 3.2.4). As for the acetic acid stress, it was found that NADPH was over-produced from the PP pathway in both the S-C1 strain and the resistant YC1 strain. Such extra NADPH could be used to support the macromolecule synthesis for cell growth. Meanwhile, the ATP production could be another important factor in resisting acetic acid stress. It is well known that acetic acid could inflict oxidative stress. At the low pH (pH<4.76) when using glucose as the substrate, the acetic acid would enter the cells by facilitated diffusion in the un-dissociated form [52]. Once in the cytosol with the neutral environment, the acetic acid would release proton. The accumulation of the intracellular proton would then induce the accumulation of the reactive oxygen species (ROS) under the aerobic or oxygen-limited condition and the dysfunction of mitochondrial by hyper-activation of Ras–cAMP–PKA pathway (Fig. 3.2.4A) [23]. In this scenario, the TCA cycle would be impaired severely due to the ROS accumulation and the mitochondrial dysfunction. Therefore, as shown in the metabolic flux analysis on the YC1 strain, the over-produced ATP from the second-half of the glycolysis (i.e., energy releasing steps) could relieve the oxidative stress and improve the resistance of yeast cells to the acetic acid stress. It is worth mentioning that introducing other ROS quenchers, e.g., oxygen, could be an effective approach to relieve the oxidative stresses induced by ROS, but with the risk of further reprogramming the intracellular metabolism. In this case,

protons from dissociated acetic acid have been considered the major stress contributor. It is also important, however, to consider acetic acid as two isolated parts, i.e., weak acid and proton donor. Evaluating the impact of the two factors of acetic acid on yeast metabolism is beyond the scope of this work. However, we are currently designing new experiments to examine the corresponding metabolic reprogramming of yeast by comparing the metabolic fluxes of yeasts when being treated with acetic acid and another inorganic acid (e.g. HCl). In addition, it is important to point out that acetic acid could also be an endogenous byproduct of biofuel production, which could be taken as a potential inhibitor for fermentation. In this study, we have omitted the synthesis of endogenous acetic acid due to the extremely low concentration compared to the exogenous acetic acid as the inhibitor. However, metabolic responses of yeast to endogenous and exogenous acetic acids could vary. We are currently developing new experiments to address this concern.

For the furfural stress, over-production of ATP and NADPH is pivotal (Fig. 3.2.4B). The stress responses inflicted by furfural are multiple, including oxidative stress, nutrient starvation, and osmotic and salt stress (Fig. 3.2.4B) [37]. As consistent with previous studies [38, 39], we found a dramatic increase of the NADPH net production (>4-fold) was observed in both the S-C1 strain and the YC1 strain (Fig. 3.2.2). These extra NADPH could be used by alcohol dehydrogenase to convert furfural to less toxic furfuryl alcohol. In the meantime, during aerobic or oxygen-limited conditions, furfural could be oxidized to furoic acid with the regeneration of NADH [21, 37]. Although the furoic acid is less toxic compared to furfural, the dissociation of furoic acid could increase the proton concentration inside the cell, and hence, lead to the oxidative stress. The over-produced ATP from energy-releasing steps in glycolysis and the TCA cycle could relieve the

oxidative stress inflicted by furfural and improve the resistance of yeast cells. It is also worth mentioning that the central metabolism was up-regulated but cell reproduction was compromised in furfural stress condition. Such phenomenon is possibly related to the enhanced glucose uptake, a step that consumed the majority of ATP. The high demand of ATP would up-regulate energy-producing pathways such as glycolysis. However, because majority ATP was used to uptake glucose, not enough ATP could be supplied to support cell growth, which led to decreased cell growth rate in furfural stress condition.

For the dual-stress with acetic acid and furfural, the two inhibitors could introduce synergistic stress. In this scenario, the glucose transport was severely limited due to the lack of ATP caused by oxidative stress (Table 3.2.2). Consequently, the activities of all the metabolic pathways were repressed, and the energy and cofactor production was hence jeopardized. Without the sufficient supply of NADPH, enzymes such as alcohol dehydrogenase could hardly convert the inhibitors into less toxic compounds. The accumulation of these inhibitors would in return reinforce the inhibitory effects, which lead to even more severe decrease on cell growth. It was also interesting to notice that the reprogramming of metabolic fluxes in YC1 compared to that of S-C1 strain was much more dramatic in the acetic acid stress condition than that of furfural stress condition or the mixed inhibitor stress condition (Fig. 3.2.3). This is consistent with how the strain YC1 was developed in our previous work[28]. Namely, the YC1 strain was initially developed and screened for improved resistance to acetic acid. However, it could be possible that when both acetic acid and furfural were present, the stress, especially the oxidative stress, could be so strong that the cell metabolism had to prioritize the resource to compensate for the

ATP loss. Therefore, the engineered metabolism in the YC1 strain was not fully exploited to demonstrate superior resistance to mixed inhibitors of acetic acid and furfural.

In summary, for the stress condition with single inhibitors, *S. cerevisiae* strains intend to overproduce the energy and cofactors to either relieve oxidative stress or to convert inhibitors to less toxic compounds. However, in the presence of mixed inhibitors, yeast cells face difficulty in producing enough ATP and NADPH to resist the heavier stresses, which deteriorate the inhibitor resistance and lead to dramatic impairment of cell growth. Using metabolic flux analysis to study yeast stress responses provides a "common language" so that different inhibitory mechanisms could be evaluated and discussed on the same platform, which is the key to enable the correlation between different phenotypes and genotypes. The engineering strategies focusing on optimizing energy and cofactor supply would be worthy in improving yeast resistance to mixed fermentation inhibitors.

3.2.5 Conclusion

In this study, we applied ^{13}C-MFA to investigate the reprogramming of cell metabolism of two *S. cerevisiae* strains in the presence of various inhibitors. In general, *S. cerevisiae* strains adopt different mechanisms to resist acetic acid stress, furfural stress, and dual-stress with both acetic acid and furfural. The resistance mechanisms heavily relied on the energy and cofactor production, especially when mixed fermentation inhibitors were present. The lack of ATP and NADPH was found to be the main reason for the poor performance of *S. cerevisiae* strains when cultivated with both acetic acid and furfural. Based on the discovery of this study, the host engineering of *S. cerevisiae* strains to improve energy and cofactor synthesis could be a potential strategy to improve yeast resistance to fermentation inhibitors in hydrolysate from lignocellulosic materials.

Acknowledgements

We thank the writing center in Virginia Tech for improving the language of the paper. This study was supported by a start-up fund (#175323) from Virginia Tech and a start-up fund from the University of Notre Dame.

Table 3.2.1. Plasmids and Strains.

Plasmids and strains	Description	References
Plasmids		
pRS424	*TRP1*, a multicopy plasmid	[53]
pRS424-*WHI2*	pRS424 with insert of S288c yeast genomic DNA fragment chrXV: 409,259-412,369 (containing complete sequence of the *WHI2* gene)	[29]
pRS424GPD	pRS424 with GPD[a] promoter	[53]
Strains		
D452-2	*MATa, leu2, his3, ura3, can1*	[54]
SR8	D452-2 expressing *XYL1, XYL2,* and *XKS1* through integration, evolutionary engineering in xylose-containing media, and *ALD6* deletion.	[55]
SR8-*trp*	SR8 with *TRP1* disrupted	Developed in Dr. Yong-Su Jin Lab
S-C1	SR8-*trp* harboring pRS424GPD, as a control	[29]
YC1	SR8-*trp* harboring pRS424-*WHI2*	[29]

[a] GPD stands for Glyceraldehyde-3-phosphate dehydrogenase, encoded by the *TDH3* gene. The *TDH3* promoter is often referred to as the *GPD* promoter, which is used in the pRS4XX series of expression vectors [53].

Table 3.2.2. Growth of S-C1 strain and YC1 strain under different stress conditions.

Stresses	Strains	Growth rates (1/h)	Specific rates (mmol/g DCW/h)			
			Glucose	Ethanol	Acetate	Glycerol
Blank	S-C1	0.117±0.017	16.00±1.64	23.03±1.22	0.00±0.00	1.69±0.10
	YC1	0.121±0.002	14.12±0.75	19.61±0.15	0.00±0.00	1.94±0.01
Acetic acid	S-C1	0.021±0.000	6.06±0.16	8.47±0.26	-0.16±0.01	0.24±0.01
	YC1	0.039±0.000	11.10±0.00	13.31±0.25	-1.13±0.04	0.58±0.00
Furfural	S-C1	0.053±0.002	18.29±1.35	27.66±1.81	0.00±0.00	2.00±0.16
	YC1	0.053±0.002	18.02±0.25	23.98±2.52	0.00±0.00	1.94±0.06
Mixed	S-C1	0.021±0.000	2.49±0.45	2.29±0.21	-0.25±0.10	0.00±0.00
	YC1	0.025±0.000	2.68±0.34	3.42±0.22	-0.19±0.02	0.74±0.03

Table 3.2.S1 The central metabolic model used in this study.

ID	Reactions
v1	GLC → G6P
v2	G6P ↔ F6P
v3	F6P ↔ DHAP + G3P
v4	DHAP ↔ G3P
v5	G3P → PEP
v6	PEP ↔ PYRCYT
v7	G6P → CO2 + P5P
v8	P5P + P5P ↔ S7P + G3P
v9	S7P + G3P ↔ F6P + E4P
v10	P5P + E4P ↔ F6P + G3P
v12	PYRCYT ↔ ACA + CO2
v13	ACA ↔ ETH
v14	ACA ↔ ACE
v15	G3P ↔ GLYC
v16	ACE → ACCOACYT
v17	PYRCYT + CO2 ↔ OAACYT
v18	PYRMIT ↔ ACCOAMIT + CO2
v19	OAAMIT + ACCOAMIT ↔ ICIT
v20	ICIT ↔ AKG + CO2
v21	AKG ↔ FUM + CO2
v22	FUM + FUM ↔ OAAMIT + OAAMIT
v24	OAAMIT ↔ OAACY
v25	ACCOACYT ↔ ACCOAMIT
v26	PYRCYT ↔ PYRMIT
v27	G3P ↔ SER
v28	SER ↔ GLY + C1
v29	OAACYT ↔ THR
v30	THR ↔ GLY + ACA
v31	PYRMIT + CO2 ↔ OAAMIT
v32	G6P → G6POUT
v33	P5P → P5POUT
v34	E4P → E4POUT
v35	G3P → G3POUT
v36	PEP → PEPOUT
v37	PYRMIT → PYRMITOUT
v38	PYRCYT → PYRCYTOUT
v39	OAACYT → OAACYTOUT
v40	AKG → AKGOUT
v41	ACCOACYT → ACCOACYTOUT
v42	ACCOAMIT → ACCOAMITOUT
v43	SER → SEROUT
v44	GLY → GLYOUT
v45	C1 → C1OUT
v46	THR → THROUT
v47	ETH → ETHOUT
v48	ACE → ACEOUT
v49	GLYC → GLYCOUT
v50	CO2 → CO2OUT

Table 3.2.S2 Metabolic fluxes of S-C1 strain and YC1 strain under different stress conditions. All the flux values were normalized to glucose uptake rates (set as 100), respectively.

ID	Blank				Acetic acid				Furfural				Mixed			
	S-C1		YC1		S-C1		YC1		S-C1		YC1		S-C1		YC1	
	Flux	STD	Flux	STD	Flux	STD	Flux	STD	Flux	STD	Flux	STD	Flux	STD	Flux	STD
v1	100.0	0.0	100.0	0.0	100.0	0.0	100.0	0.0	100.0	0.0	100.0	0.0	100.0	0.0	100.0	0.0
v2	71.9	1.3	75.6	1.2	24.5	0.6	53.7	1.1	70.4	2.2	59.9	0.6	33.2	0.0	31.6	0.0
v3	84.5	1.3	91.1	0.9	65.2	1.7	82.2	1.6	90.1	0.7	86.6	0.2	71.1	0.1	70.5	0.0
v4	84.5	1.3	91.1	0.9	65.2	1.7	82.2	1.6	90.1	0.7	86.6	0.2	71.1	0.1	70.5	0.0
v5	164.8	2.6	175.9	1.7	145.1	2.3	163.5	3.4	179.0	0.6	175.9	0.2	112.0	2.3	132.2	0.6
v6	164.8	2.6	175.9	1.7	144.5	1.5	153.5	3.4	178.9	0.7	175.9	0.2	111.4	2.1	132.2	0.6
v7	18.8	0.0	23.1	0.6	65.9	1.2	45.2	0.4	29.5	2.2	40.1	0.6	56.9	0.0	58.4	0.0
v8	6.3	0.0	7.7	0.2	20.6	0.9	14.3	0.3	9.9	0.7	13.4	0.2	18.9	0.0	19.5	0.0
v9	6.3	0.0	7.7	0.2	20.6	0.9	14.3	0.3	9.9	0.7	13.4	0.2	18.9	0.0	19.5	0.0
v10	6.3	0.0	7.7	0.2	20.1	0.3	14.3	0.3	9.8	0.7	13.4	0.2	18.9	0.0	19.4	0.0
v12	147.5	2.7	148.9	8.0	140.2	0.1	120.6	0.0	154.6	2.3	138.6	4.9	101.4	0.9	126.7	0.7
v13	144.1	0.7	139.1	0.5	139.8	0.1	120.6	0.1	149.7	0.6	127.0	0.6	101.3	0.8	128.0	0.4
v14	3.4	3.5	9.8	8.4	0.5	0.1	0.0	0.0	4.9	2.7	11.6	4.8	0.2	0.1	0.0	0.0
v15	10.4	0.0	13.8	0.0	4.0	0.0	5.2	0.0	11.0	0.0	10.7	0.0	47.7	2.3	27.6	0.3
v16	3.3	3.4	8.7	7.6	3.4	0.2	10.3	0.0	4.9	2.6	11.6	4.8	10.1	0.1	7.5	0.2
v17	1.7	1.7	0.0	0.0	0.8	0.3	9.5	4.4	0.0	0.0	11.6	0.6	4.7	0.8	3.3	0.8
v18	9.2	6.3	12.5	7.4	0.1	0.1	0.4	0.0	12.2	2.4	15.6	4.5	0.2	0.1	0.0	0.0
v19	8.1	1.4	14.5	2.3	3.5	0.1	9.5	2.1	17.1	0.5	26.7	0.6	9.9	0.5	7.3	0.3
v20	8.1	1.4	14.5	2.3	3.5	0.1	9.5	2.1	17.1	0.5	26.7	0.6	9.9	0.5	7.3	0.3
v21	0.0	0.0	0.4	0.0	2.5	0.1	8.5	2.1	5.0	0.0	5.0	0.0	8.4	0.5	5.6	0.3
v22	0.0	0.0	0.2	0.0	1.3	0.0	4.2	1.1	2.5	0.0	2.5	0.0	4.2	0.2	2.8	0.2
v24	-1.7	1.7	0.3	0.3	-0.7	0.4	2.0	5.1	0.0	0.0	-11.6	0.6	3.0	1.7	0.3	1.2
v25	3.0	3.4	7.2	8.3	3.4	0.2	10.3	0.0	4.9	2.6	11.6	4.8	10.1	0.0	7.5	0.2
v26	15.6	6.3	27.0	9.0	2.1	1.9	13.4	5.1	24.3	2.3	25.7	4.3	5.2	1.8	2.0	0.9
v27	0.0	0.0	0.1	0.1	0.0	0.0	0.0	0.0	0.1	0.1	0.0	0.0	0.0	0.0	0.5	0.1
v28	0.0	0.0	0.1	0.0	0.0	0.0	0.0	0.0	0.1	0.1	0.0	0.0	0.0	0.0	0.2	0.2
v29	0.0	0.0	0.1	0.1	0.1	0.1	6.0	5.3	0.0	0.0	0.0	0.0	0.3	0.2	1.4	0.3
v30	0.0	0.0	0.0	0.0	0.1	0.1	0.0	0.0	0.0	0.0	0.0	0.0	0.1	0.0	1.4	0.3
v31	6.4	2.0	14.4	2.5	0.3	0.4	3.0	5.1	12.1	0.5	10.1	0.3	4.5	1.3	2.0	0.9
v32	9.2	1.3	1.2	0.9	9.6	0.8	1.1	1.5	0.0	0.0	0.0	0.0	9.9	0.0	10.0	0.0
v33	0.0	0.0	0.0	0.0	4.6	3.1	2.4	0.4	0.0	0.0	0.0	0.0	0.1	0.1	0.0	0.0
v34	0.0	0.0	0.0	0.0	0.4	0.8	0.0	0.1	0.0	0.0	0.0	0.0	0.0	0.0	0.0	0.0
v35	0.0	0.0	0.0	0.0	1.5	2.9	10.0	0.0	0.0	0.1	0.0	0.0	1.3	1.1	0.2	0.3
v36	0.0	0.0	0.0	0.0	0.5	1.0	10.0	0.0	0.1	0.3	0.0	0.0	0.6	0.5	0.0	0.0
v37	0.0	0.0	0.1	0.2	1.7	1.7	10.0	0.0	0.0	0.1	0.0	0.0	0.5	0.7	0.0	0.0
v38	0.0	0.0	0.0	0.0	1.5	0.3	10.0	0.0	0.0	0.1	0.0	0.0	0.2	0.1	0.2	0.2
v39	0.0	0.0	0.2	0.3	0.0	0.0	5.5	2.1	0.0	0.0	0.0	0.0	7.4	1.7	2.2	0.9
v40	8.1	1.4	14.2	2.3	1.0	0.0	1.0	0.0	12.1	0.5	21.7	0.6	1.5	0.6	1.7	0.3
v41	0.2	0.2	1.5	1.8	0.0	0.0	0.0	0.0	0.0	0.0	0.0	0.0	0.0	0.0	0.0	0.0
v42	4.1	4.4	5.2	3.4	0.0	0.0	1.2	2.1	0.0	0.0	0.4	0.9	0.3	0.4	0.2	0.2
v43	0.0	0.0	0.0	0.1	0.0	0.0	0.0	0.0	0.0	0.0	0.0	0.0	0.0	0.0	0.3	0.3
v44	0.0	0.0	0.1	0.1	0.1	0.1	0.0	0.0	0.1	0.1	0.0	0.0	0.1	0.0	1.6	0.2
v45	0.0	0.0	0.1	0.0	0.0	0.0	0.0	0.0	0.1	0.1	0.0	0.0	0.0	0.0	0.2	0.2
v46	0.0	0.0	0.1	0.1	0.0	0.0	6.0	5.3	0.0	0.0	0.0	0.0	0.2	0.2	0.0	0.0
v47	144.1	0.7	139.1	0.5	139.8	0.1	120.6	0.1	149.7	0.6	127.0	0.6	101.3	0.8	128.0	0.4
v48	0.1	0.1	1.1	1.0	-3.0	0.1	-10.2	0.0	0.0	0.0	0.0	0.0	-9.9	0.1	-7.5	0.2
v49	10.4	0.0	13.8	0.0	4.0	0.0	5.2	0.0	11.0	0.0	10.7	0.0	47.7	2.3	27.6	0.3
v50	178.3	5.3	184.9	2.2	211.1	1.3	171.7	1.4	206.3	1.9	204.3	0.5	167.6	0.6	192.8	0.4

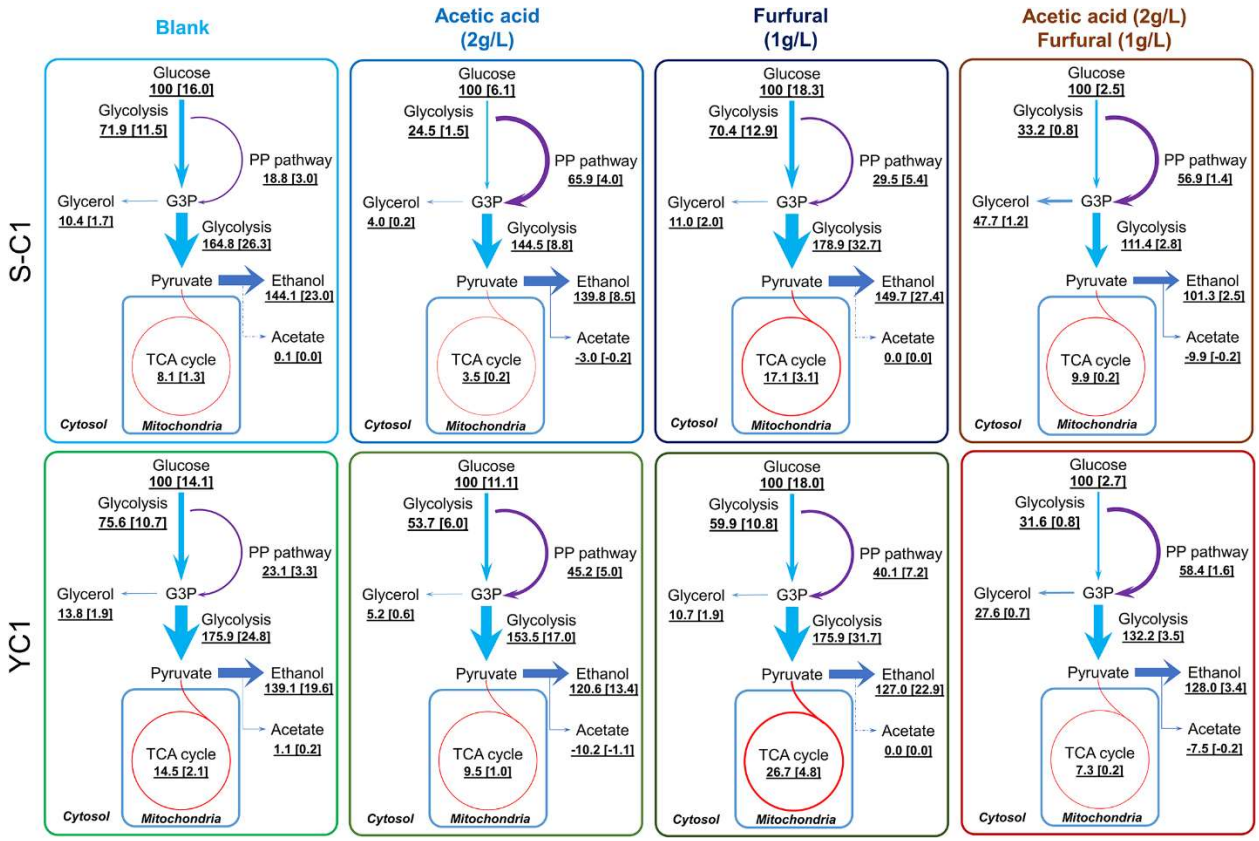

Fig. 3.2.1 Metabolic flux distribution of the S-C1 strain and YC1 strain under different stress conditions. The values outside the bracket are relative flux values normalized to glucose uptake rates as 100. Definitions of abbreviations are shown in the List of Abbreviations. The values inside the bracket are real flux values in mmol/g/h. The line widths are linearly correlated with the normalized flux values (glucose uptake rate as 100). The dashed line indicates the flux is zero.

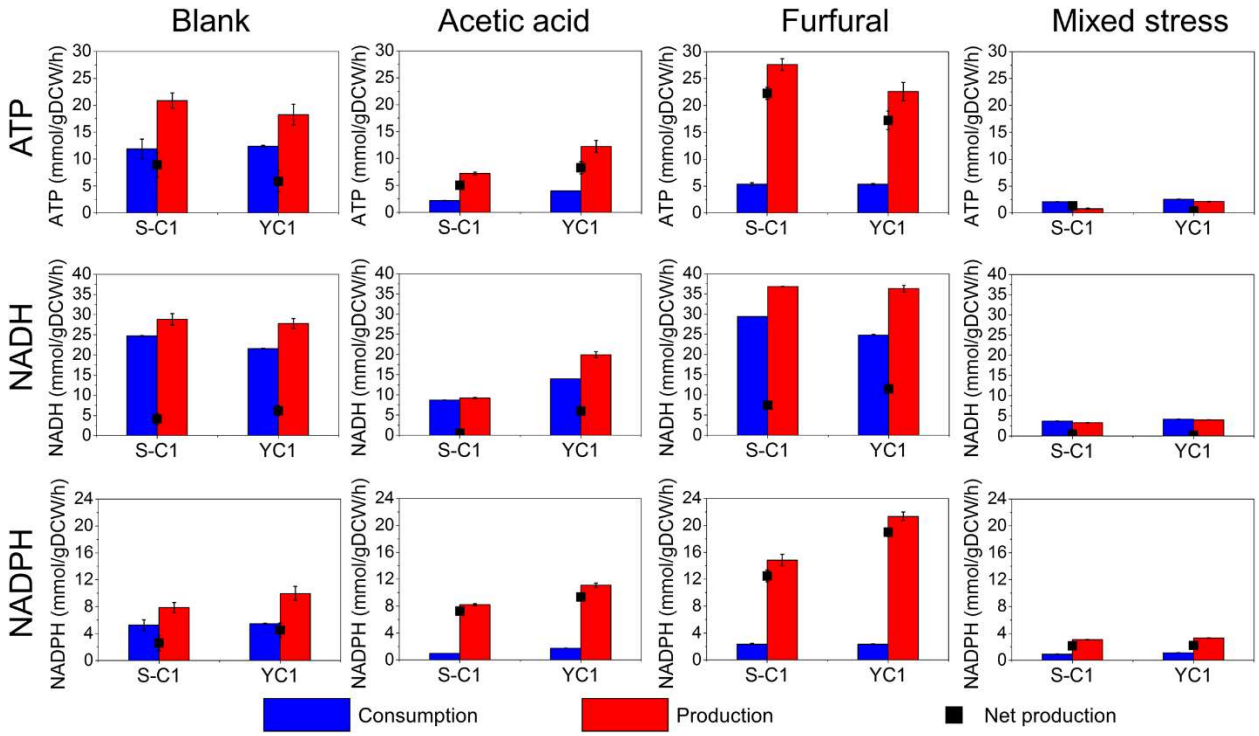

Fig. 3.2.2 Production and consumption of cofactor and energy. The consumption (blue bar), production (red bar), and net production (black dots) of ATP, NADH, and NADPH are shown for different stress conditions. The error bars present the standard deviations, which can be too small to be seen.

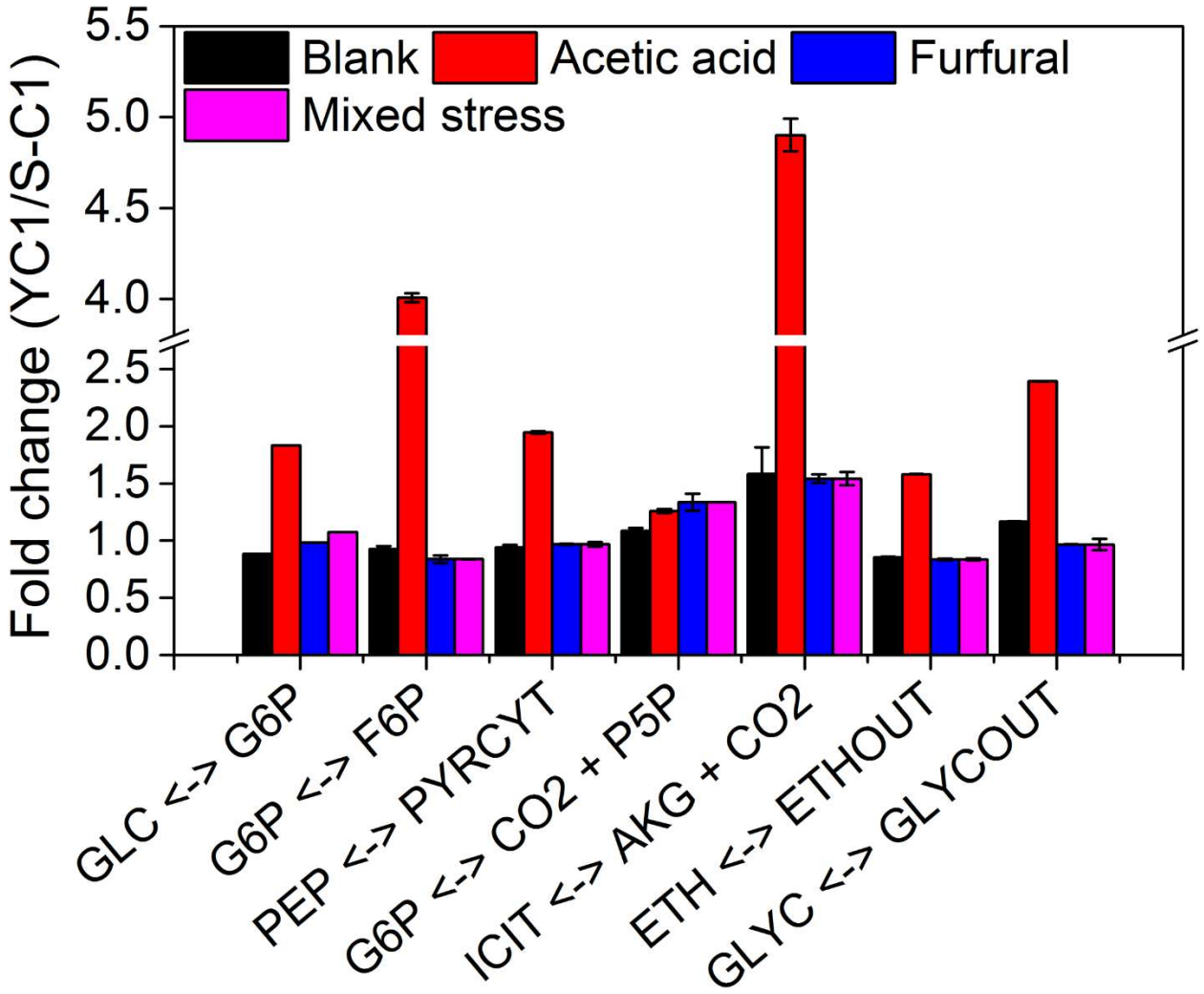

Fig. 3.2.3 Fold changes of key fluxes between the S-C1 and YC1 strain under different stress conditions. Definitions of abbreviations are shown in the List of Abbreviations.

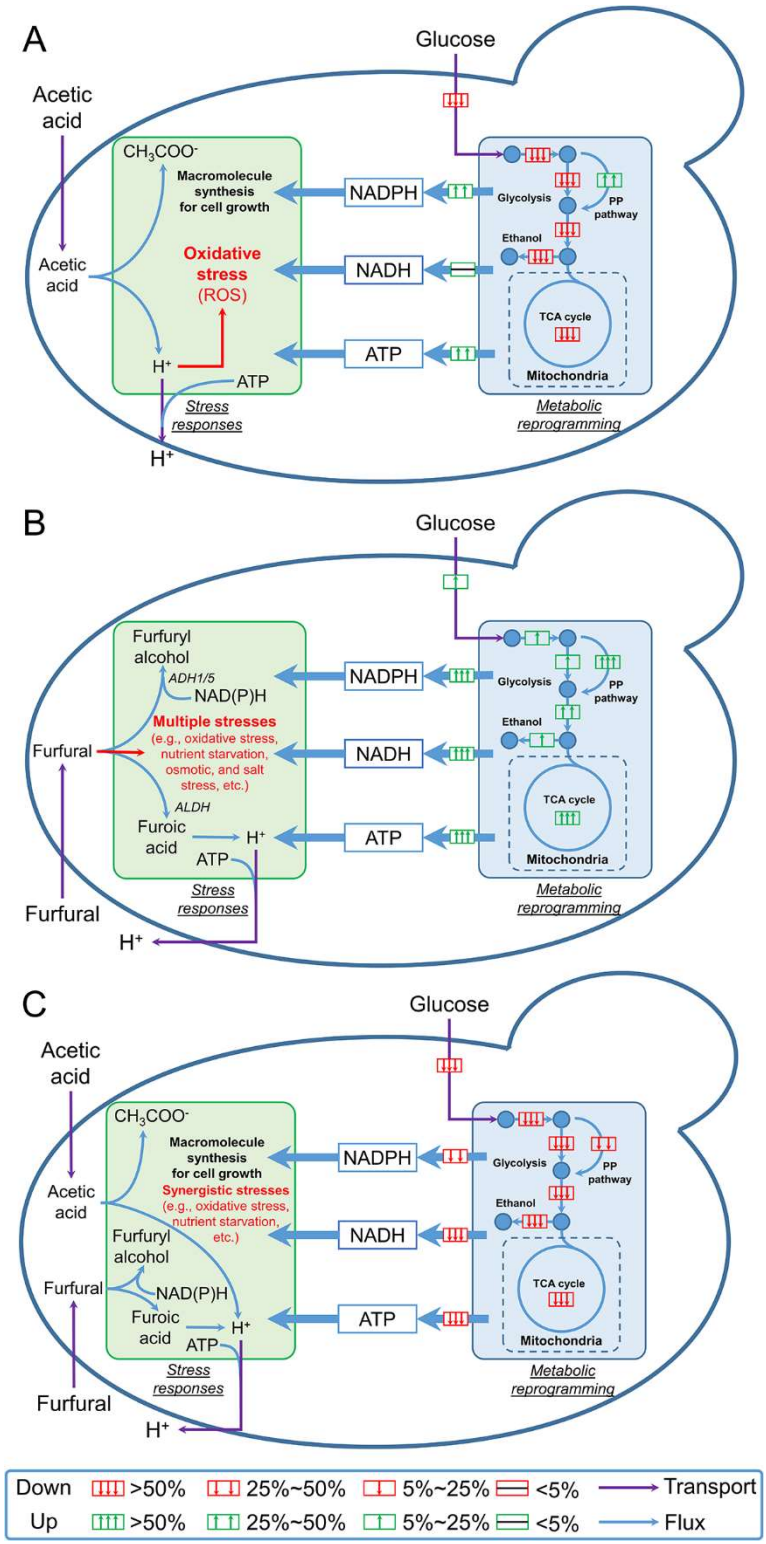

Fig. 3.2.4 Generalized mechanisms used by *S. cerevisiae* strains in different stress conditions. (A): acetic acid stress condition; (B): furfural stress condition; (C): dual-stress condition. Definitions of abbreviations are shown in the List of Abbreviations.

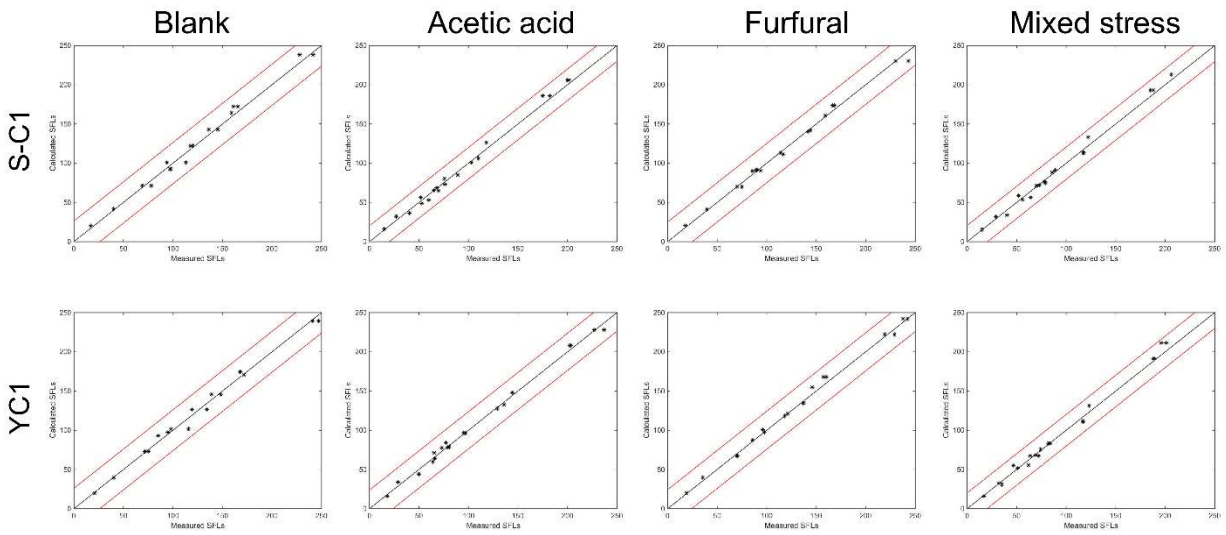

Fig. 3.2.S1 Simulated and observed SFLs for S-C1 strain and YC1 strain under different stress conditions.

.

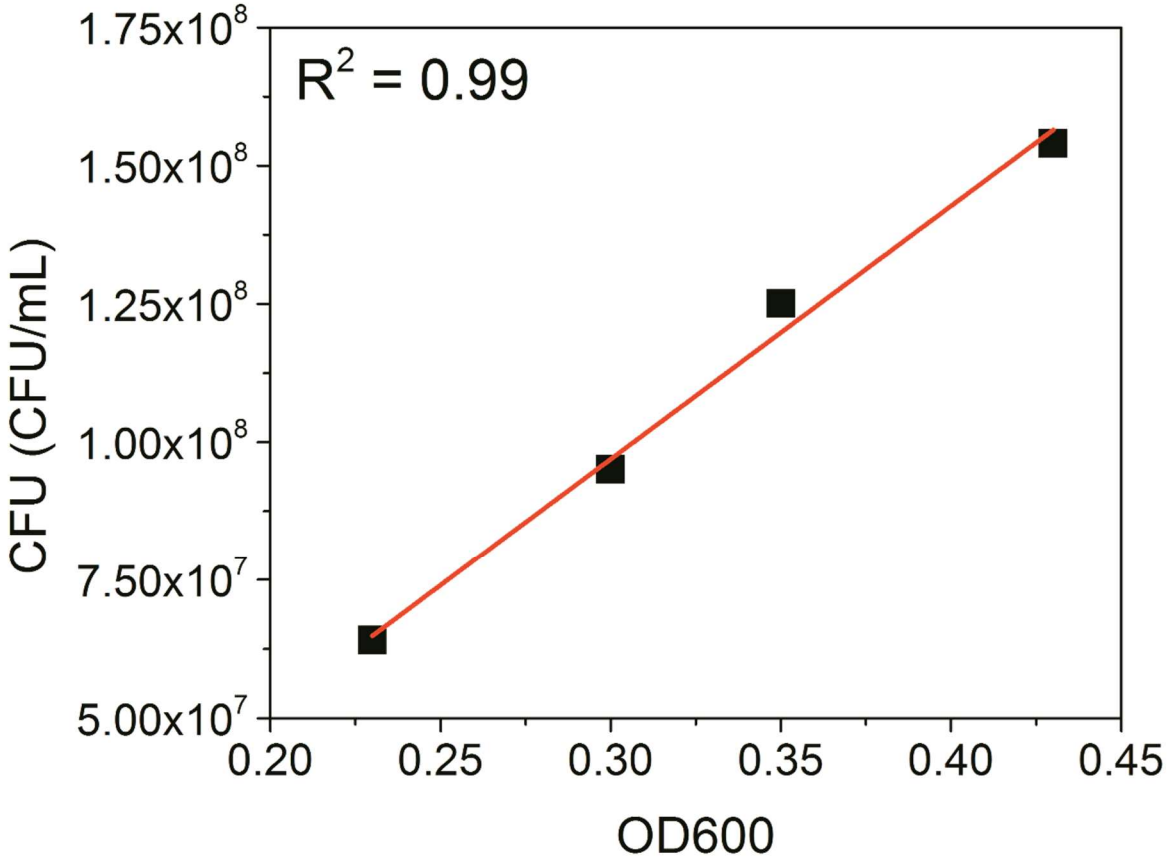

Fig. 3.2.S2 Linear correlation between OD_{600} and CFU.

3.3 Investigating Strain Dependency in the Production of Aromatic Compounds in *Saccharomyces cerevisiae.*

Miguel Suástegui[1,2], Weihua Guo[3], Xueyang Feng[3, †], Zengyi Shao[1,2, †]

[1] Department of Chemical and Biological Engineering, Iowa State University, Ames, USA.

[2] NSF Engineering Research Center for Biorenewable Chemicals (CBiRC), Ames, IA, USA.

[3] Department of Biological Systems Engineering, Virginia Polytechnic Institute and State University, Blacksburg, VA, USA.

[†]Correspondence to: Xueyang Feng and Zengyi Shao

Email: xueyang@vt.edu and zyshao@iastate.edu

This manuscript has been published on *Biotechnology and bioengineering* 113 (12), 2676-2685. Reprinted with permission of the publisher. Supplementary material of Chapter 3.3 is shown in Appendix A.

Abstract

Although *Saccharomyces cerevisiae* is the most highly domesticated yeast, strain dependency in biotechnological processes still remains as a common, yet poorly understood phenomenon. To investigate this, the entrance to the aromatic amino acid biosynthetic pathway was compared in four commonly used *S. cerevisiae* laboratory strains. The strains were engineered to accumulate shikimate by overexpressing a mutant version of the pentafunctional ARO1 enzyme with disrupted activity in the shikimate kinase subunit. Carbon tracing and ^{13}C metabolic flux analysis combined with quantitative PCR, revealed that precursor availability and shikimate production were dramatically different in the four equally engineered strains, which were found to be correlated with the strains' capacity to deal with protein overexpression burden. By implementing a strain-dependent approach, the genetic platform was reformulated, leading to an increase in yield and titer in all strains. The highest producing strain, INVSc1-SA3, produced 358 mg L^{-1} of shikimate with a yield of 17.9 mg $g^{-1}_{glucose.}$ These results underline the importance of strain selection in developing biological manufacturing processes, demonstrate the first case of high production of shikimate in yeast, and provide an appropriate platform for strain selection for future production of aromatic compounds

Key Words

shikimate pathway, protein overexpression burden, pathway balancing, ^{13}C-metabolic flux analysis

Key Points

- The aspartic acid 920 is a key residue in the catalytic pocket of the shikimate kinase subunit in the *S. cerevisiae* pentafunctional ARO1 enzyme.
- The first report of engineering *S. cerevisiae* for the production of shikimate from glucose.
- ^{13}C-fingerprinting and metabolic flux analysis to study the carbon flux into the aromatic amino acid biosynthesis pathway in yeast.
- Identification of strains' different capacities to cope with protein overexpression burden.
- Pathway balancing to enable high carbon channeling into the aromatic amino acid biosynthetic pathway.

3.3.1 Introduction

The metabolic pathways for the biosynthesis of aromatic compounds are present in many microorganisms and plants, and lead to the production of three key amino acids, *i.e.,* tryptophan, phenylalanine, and tyrosine. In certain plants such as *Papaver somniferum* (opium poppy) and *Catharanthus roseus*, these amino acids become intermediates in the production of more complex molecules that range from pigments, tannins, and alkaloids [56-58]. Given the versatile applications of these compounds and their great market opportunities [59], studying the relevant endogenous pathways has been central in metabolic engineering efforts for the production of aromatic compounds, mainly in bacteria and yeasts. Some of the molecules that have reached considerable biotechnological production levels in *Escherichia coli* include shikimate (SA) (87 g/L) [60], muconic acid (30 g/L) [61], and phenol (9.8 g/L) [62].

The production of more specialized aromatics such as flavonoids and alkaloids requires the functional expression of membrane-bound plant cytochrome P450 enzymes,

which is feasible in yeast, but remains as a challenge in *E. coli [63]*. For instance, naringenin and resveratrol can only be converted through tyrosine in *E. coli*, but can be synthesized from both tyrosine and phenylalanine in *S. cerevisiae* due to the functional expression of cytochrome P450 reductase [64, 65], and the most recent breakthrough, the biosynthesis of tyrosine-derived opioids [66], demonstrates the great potential of using yeast as a host to produce plant secondary metabolites. However, due to intrinsically complicated genetic and metabolic regulations, the efforts in engineering the central carbon metabolism to increase the production of aromatics in yeast seem somewhat ineffective. The reported yields in *S. cerevisiae* are far from reaching the theoretical values [64, 67-69], evidencing the demand for extensive strain development efforts.

A key step in the development of microbial platforms for the production of valuable chemicals is the appropriate selection of the host strain. Although it may sound trivial, it becomes more and more evident that selecting strains even among those belonging to the same species is key to ensuring optimal titers, yields, and productivities. Different *S. cerevisiae* strains, varying slightly in genetic makeups, unexpectedly display disparate behaviors [70]. The differences can be attributed to the varying capabilities of maintaining episomal plasmids [71], expressing proteins [72], hosting heterologous pathways [73], and responding to signaling processes [74]. However, the underlying basis for these varying phenotypes remains unclear and may vary case by case when engineering metabolic pathways in yeasts.

The purpose of this work was to determine an appropriate strain of *S. cerevisiae* with a high potential for producing chemicals that derive from the aromatic amino acid pathway. The main variable in play was strain ploidy, hence we compared four commonly

used laboratory strains, namely YSG50, BY4741, INVSc1, and BY4743, among which the former two are haploids, the latter are diploids, and BY4743 was directly generated from the mating of BY4741 (MATa) and BY4742 (MATα). SA was chosen as the target compound because the biosynthesis of all the aromatic amino acid-derived compounds share SA as a common precursor, and itself is the starter compound of the commercial influenza antiviral Tamiflu® [75, 76]. Although being equally engineered, the four strains produced SA at dramatically different levels. ^{13}C-metabolic flux analysis (^{13}C-MFA) was implemented to systematically characterize the metabolic differences in the SA producing strains. The results demonstrated that the flux distribution in the central metabolism was very well conserved among all strains, but that the efficacy of producing SA was strongly dependent on the ability of each strain to auto-adjust the copy numbers of the episomal vectors. The strain INVSc1 showed a distinct superiority in SA production, which might be correlated with its superior capability of dealing with protein overexpression burden. Appropriate plasmid and strain selection was essential to ensure high flux of carbon into the aromatic amino acid pathway. The results here can be further implemented to expand the palate of aromatic compounds that can be produced from the SA pathway or from the downstream branches in yeasts.

3.3.2 Materials and Methods

Strains and Media. Two haploid and two diploid strains of *S. cerevisiae* were analyzed in this study (Table 3.3.1). The haploid strains include YSG50 (*MAT□□ade2-1 ade3□22 ura3-1 his3-11,15 trp1-1 leu2-3,112 can1-100)* and BY4741 (*MATa his3Δ1 leu2Δ0 met15Δ0 ura3Δ0*); the diploid strains include InvSc1 (*MATa/□ his3□1/his3□1 leu2/leu2 trp1-289/trp1-289 ura3-52/ura-52 MAT*), and BY4743

(*MAT*a/□ *his3*□*1/his3*□*1* *leu2*□*0/leu2*□*0* *LYS2/lys2*□*0* *met15*□*0/MET15* *ura3*□*0/ura3*□*0*). The wild type strains were propagated in YPAD media (1% yeast extract, 2% peptone, 0.01% adenine, and 2% dextrose). After plasmid transformation, yeast strains were cultured in Synthetic Complete media lacking uracil and histidine (0.5% ammonium sulfate, 0.16% yeast nitrogen without amino acid and ammonium sulfate, complete amino acid supplement mix lacking uracil and histidine, and 2% dextrose). The minimal growth medium composition used for labeling experiments was the same as reported previously with 20 g/L glucose as the sole carbon substrate [77, 78]. When culturing yeast strains with ^{13}C-labeled glucose, the regular glucose was replaced with 80% [1-^{13}C] glucose and 20% [U-^{13}C] glucose (Cambridge Isotope Laboratories, Inc., Tewksbury, MA). All chemicals were purchased from Fisher Scientific (Pittsburgh, PA). *E. coli* BW25141 was cultured in Luria Bertani (LB) medium supplemented with 100 □g mL^{-1} ampicillin.

Plasmid Construction. All plasmids constructed in this study (Table 3.3.1) were derived from the pRS shuttle vector series (New England BioLabs, Ipswich, MA). To assemble the genetic cassettes, the DNA Assembler technique [79, 80] was implemented. All primers in this work were synthesized by IDT (Coralville, IA). The aspartic acid at the position of 920 in the wild type ARO1 was substituted to alanine by incorporating the mutation into PCR primers (*fwd*:gttacaaattagttgacctaGCGgagctgtttgagcaaca, *rev*: tgttgctcaaacagctcCGCtaggtcaactaatttgtaac) and the variant was cloned downstream of the *S. cerevisiae* GPD constitutive promoter and upstream of the PYK1 terminator. The expression cassette was assembled in the pRS426 backbone digested with *Xho*I, yielding the plasmid pRS426-*aro1*$_{D920A}$ (Appendix A Fig. A.S1). Plasmid pRS413-*aro4*$_{K229L}$-*tkl1*

was constructed in the previous study [81] and used here to enhance the entrance of carbon into the SA pathway. Plasmid pRS413-*aro1*$_{D920A}$-*aro4*$_{K229L}$-*tkl1* was constructed by assembling the *Xho*I digested pRS413-*aro4*$_{K229L}$-*tkl1* with the PCR-amplified *aro1*$_{D920A}$ cassette with the ends overlapping to the pRS413 backbone and TPI1 promoter. Similarly, to construct pRS426-*aro1*$_{D920A}$-*aro4*$_{K229L}$-*tkl1*, plasmid pRS426-*aro1*$_{D920A}$ was digested with *BamH*I and re-assembled by addition of the PCR cassette *aro4*$_{K229L}$-*tkl1* with the overlapping ends to the PYK terminator and the backbone of pRS426. Plasmid transformation was done by the lithium acetate technique [82].

Biomass and Metabolite Analysis. Biomass growth in minimal media was monitored by optical density changes with an absorbance reader at 600 nm (OD_{600}) (Biotek Synergy 2 Multi-Mode Microplate Reader). Samples were taken every 2 to 3 hours until the late exponential phase was reached. Cell-free samples were used to measure extracellular metabolites by Shimadzu HPLC (Columbia, MD) equipped with an Aminex HPX-87H column (Bio-Rad, Hercules, CA) and Shimadzu RID-10A refractive index detector. The column was kept at 50°C, and 5 mM sulfuric acid solution was used as the mobile phase with a constant flow rate of 0.6 mL/min. Standard samples of ethanol, glucose, glycerol, and SA were purchased from ACROS Organics™ (Geel, Belgium).

Isotopomer Analysis of Proteinogenic Amino Acids and SA. The protocol for sample preparation and amino acid analysis was followed based on Feng *et al.* [83]. During the late exponential phase, 1 mL samples were collected from the cultures grown with the labeled glucose for proteinogenic amino acid profiling. The samples were centrifuged and the biomass was hydrolyzed with 6 M HCl at 100°C for 20 h, followed by drying and derivatization with 25 □L of tetra-hydrofuran and 25 □l of tert-butyldimethylsilyl ether at

70°C for 1h. To analyze the labeled SA, 1 mL of the supernatant from the culture samples was dried overnight followed by derivatization with 60 □l of N,O-bis(trimethylsilyl)trifluoroacetamide at 70°C for 1 h. The derivatized samples were analyzed by gas chromatograph (GC2010, Shimadzu) equipped with a SH-Rxi-5Sil column (Shimadzu) and a mass spectrometer (QP2010, Shimadzu). Two types of charged fragments were detected by GC-MS for various amino acids (Appendix A Table A.S1): the $[M-57]^+$ group (containing unfragmented amino acids), and the $[M-159]^+$ or the $[M-85]^+$ group (containing amino acids that had lost an α-carboxyl group). The whole derivatized SA fragment was detected from the sample supernatant. The mass distribution vectors (MDVs) were represented by M0, M1, M2, etc., which were the corresponding fractions of non-labeled, singly labeled, doubly labeled amino acids. The effects of natural isotopes on isotopomer labeling patterns were corrected by the previously reported algorithms [84].

Metabolic Flux Analysis. MDVs were used to calculate the summed fractional labeling (SFL) values which were directly used in the MFA (Biomet Toolbox 2.0 [85], based on MATLAB (MathWorks, Inc. MA). The central carbon metabolic model for the MFA was developed based on the KEGG database (http://www.genome.jp/kegg/), and it included the glycolysis pathway, pentose phosphate pathway, anaplerotic pathways, the tricarboxylic acid (TCA) cycle, the SA synthesis pathway, and the transport reactions between different cell compartments. For our metabolic flux analysis, flux estimation was repeated at least 50 times starting with different initial values generated by a genetic algorithm for all the fluxes to find a likely global solution. A fit of the simulated and measured SFLs was determined to be a global solution only after the solution fit was obtained at least twice using this method (Appendix A Fig. A.S2).

Plasmid Copy Number Assay. The copy number of the two plasmids used in this work was quantified using quantitative PCR (qPCR). Cell cultures were grown in minimal media for 24 hours and cell amounts equivalent to 2 OD_{600} units were collected for total DNA extraction as previously described [86]. The primers were designed using the online PrimeTime© tool for qPCR assays through IDT. The primer pair p-ura3 (*fwd*: tagcagaatgggcagacattac; *rev*: ggcctctaggttcctttgttac) was used to quantify the plasmid pRS426; the primer pair p-his3 (*fwd*: gtccacacaggtatagggtttc; *rev*: gtgatggtcgtctatgtgtaagt) was used to quantify the plasmid pRS413. Plasmid copy number was normalized to total DNA with *alg9* as the reference gene (*fwd*: ccgttgccatgttgttgtatg; *rev*: gccaggaaattgtacgctaaac). A standard curve for each target was prepared using pure plasmid or genomic DNA samples.

3.3.3 Results and Discussion

Building the First Yeast Platform for SA Production. Unlike prokaryotes and higher eukaryotes, the five steps involved in SA biosynthesis in yeast are catalyzed by a single pentafunctional enzyme ARO1 [87] (Fig. 3.3.1). Knocking out individual steps of this pathway without affecting the rest of the catalytic functions in yeast could be a cumbersome task. Hence, a single amino acid substitution in the active site of the SA kinase subunit (ARO1B) could better ensure a functional mutant version of ARO1 capable of halting the conversion of SA to shikimate-3-phosphate (S3P). Initially, an amino acid sequence alignment with SA kinases from several prokaryotic and eukaryotic organisms was performed. Despite the genetic variations within these species, it was observed that the catalytic sites of the shikimate kinases (D920-*aro1* in *S. cerevisiae*) are 100% conserved (Appendix A Fig. A.S3). This residue was substituted by alanine, yielding the mutant

enzyme ARO1$_{D920A}$. The plasmid pRS426-*aro1*$_{D920A}$ was transformed into the four *S. cerevisiae* strains (YSG50, INVSc1, BY4741, and BY4743) and the resulting strains were grown in minimal media for 48 hours. However, no SA was detected in the fermentation media in any of the four strains (Figure 2). It was not a surprise because the endogenous synthesis of aromatic amino acids could have (i) channeled the accumulated SA into the downstream reactions, and (ii) feedback inhibited the first step of aromatic amino acid biosynthesis catalyzed by 3-dehydroxy-D-arabino-heptulose-7-phosphate (DAHP) synthase.

To characterize the activity of ARO1$_{D920A}$, a complementation experiment was carried out. The plasmid pRS426-*aro1*$_{D920A}$ was transformed into the strain BY4741 □*aro1* (GE Healthcare Bio-Sciences, USA) and plated onto medium lacking uracil and the three aromatic amino acids. Cell were incubated for two days and as expected no growth was observed, indicating that the novel mutant ARO1$_{D920A}$ is incapable of complementing growth in the □*aro1* background (Appendix A Fig. A.S4a). To confirm that the growth defect is caused exclusively by the disrupted kinase subunit (ARO1B) in the novel mutant ARO1$_{D920A}$, a new plasmid was constructed harboring the *E. coli* shikimate kinase gene *aroL* (pRS426-*aro1*$_{D920A}$ – *ecaroL)*. The strain BY4741 □*aro1* was transformed with the latter plasmid and after two days of culturing in media lacking uracil and aromatic amino acids, colonies were observed (Appendix A Fig. A.S4b). Complementation of growth by the *ecaroL,* was a definitive indication that the novel enzyme ARO1$_{D920A}$ remains functional in all of its subunits except for the subunit ARO1B, which catalyzes the conversion of shikimic acid to shikimate-3-phosphate.

The plasmid pRS413-*aro4*$_{K229L}$-*tkl1* was transformed into the strains (Group SA2) which carries the tyrosine-insensitive DAHP synthase to overcome the feedback inhibition, as well as the transketolase gene *tkl1* to increase the flux of the precursor erythrose-4-phosphte (E4P) [67]. These approaches have been successfully implemented in *E. coli* to produce SA and in *S. cerevisiae* for the production of dehydroshikimate-derived muconic acid [61, 67, 88, 89]. Nevertheless, SA was still not observable in any of the strains. We hypothesized that the genome-copy of *aro1* was causing a rapid channeling of SA into the production of aromatic amino acids. Hence, to completely shut down the native pathways downstream of SA, tryptophan, phenylalanine, and tyrosine were added to the minimal medium at low concentrations of 50 mg L^{-1}. The presence of these three amino acids blocked the endogenous flux into the downstream branches, and SA was finally observed (Fig. 3.3.2). This result demonstrated that despite genotypic differences, all four *S. cerevisiae* strains had undergone strong regulatory controls on the aromatic amino acid biosynthesis. It is known that the presence of external aromatic amino acids inhibits the first committed step in the biosynthesis of aromatics (ARO3 and ARO4*)* and the downstream branch points (ARO7 and TRP2/3, Fig. 1) [87]. However, inhibition may also have occurred at the step converting SA to S3P (ARO1B), most likely by the reduced transcription rates of the wild type *aro1*, thus allowing SA to accumulate in the strains overexpressing the mutant ARO1$_{D920A}$. To our knowledge, this is the first report of success in engineering yeasts to accumulate a significant amount of SA.

Comparison of Fermentation Profiles. Although all strains were able to produce SA, the titers among the strains varied drastically; the lowest being 30 mg L^{-1} in strain YSG50 and the highest, 350 mg L^{-1} in strain INVSc1. Small batch fermentations in minimal

media were first carried out to investigate how these four strains differ from each other regarding fermentation characteristics. The consumption rates of glucose and the formation rates of SA, ethanol, and glycerol among the four strains during exponential phase were compared (Table 3.3.2, Appendix A Fig. A.S4). From the fermentation profiles it was easy to arrange the strains into two groups; the strain pair of BY4741 and BY4743, and the pair of YSG50 and INVSc1. Although all four strains had similar specific growth rates (0.13-0.17 h^{-1}), the BY474x strains did have about 2-3 fold higher rates than the other pair in terms of glucose consumption and ethanol production. The rate of glycerol production varied slightly, although it was not observable in strain YSG50. The production of SA revealed the highest difference among the strains. Apparently, no correlation between strain ploidy and SA production could be drawn since strains YSG50 and BY4743 (haploid and diploid, respectively) showed the lowest productions, with yields around 0.83 and 0.32 mmol $gDCW^{-1}$, respectively. The strain BY4741 had a mid SA production with a yield of 2.38 mmol $gDCW^{-1}$, and finally, strain INVSc1 had the highest yield of 8.1 mmol $gDCW^{-1}$, 3.4-fold higher than strain BY4741, 9.8-fold higher than strain YSG50, and 25-fold higher than BY4743. These results suggested that, despite all the strains being equally engineered, either the expression of the pathway enzymes, the entrance into the aromatic amino acid pathway or both were strain dependent.

Inspection of ^{13}C Isotopic ‘‘Finger Prints’’ of Aromatic Amino Acids. The most significant difference between strains in the group SA2 arose from comparing the “fingerprints” of the aromatic amino acids, namely phenylalanine and tyrosine. Interestingly, the strains with the highest production of SA (INVSc1 and BY4741) showed the highest percentage of labeled phenylalanine and tyrosine (m1:m9), whereas the strains

with the lowest production (YSG50 and BY4743) showed a lower labeling distribution (Fig. 3.3.3). This was a clear indication that not only were the strains INVSc1 and BY4741 able to accumulate SA in higher titers, but they also had a higher pull of carbon from the downstream metabolic branch leading to the production of phenylalanine and tyrosine. It is crucial to mention that these observations were not due to different extracellular amino acid uptake, since measurement of the fermentation supernatant showed equal uptake rates (data not shown here). Analyzing the isotopic labeling patterns of leucine, another non-labeled amino acid added in the culture medium for all four strains also showed similar labeling patterns; the non-labeled leucine (m0) constituted more than 93% in all strains. This confirmed that the high producing SA strains had more active aromatic amino acid biosynthetic pathway. It is noteworthy that although the endogenous entrance of carbon into the aromatic pathway was supposedly blocked by the supplementation of aromatic amino acids, *de novo* production of tyrosine and phenylalanine was observed in all strains. Therefore, to maximize SA accumulation, future work should target the implementation of a more stringent blockage of the downstream branches.

Comparison of Flux Distributions in Key Nodes. To further investigate the metabolic differences in a quantitative manner, the isotopomer labeling patterns, i.e., mass distribution vectors, of proteinogenic amino acids were utilized to obtain the metabolic fluxes through the central carbon metabolism of the *S. cerevisiae* strains. By comparing the fluxes of the engineered strains, similar fluxes were found in the glycolytic pathway up to the formation of phosphoenolpyruvate (PEP), as well as in the oxidative pentose phosphate pathway (PPP) (Figure 4). The main variation, as expected, resulted from the flux entrance into the SA synthesis pathway (*v11*). This reflected difference in the availability of the

precursors PEP and E4P to enter the pathway. Less than 8% of the flux into PEP (*v5),* ranging from 143 to 172, was channeled into the formation of SA in all the strains. Therefore, a potential strategy to increase the availability of PEP is to lower the activity of the pyruvate kinase encoded by *pyk* (Fig. 3.3.1). This strategy has been implemented in the bacterium *Bacillus subtilis* with varying outcomes. For instance, deleting *pyk* caused a slight increase in the production of SA by 8%; failure in obtaining a higher increase can be correlated to the reduction of cell growth caused by the drastically disrupted glycolytic pathway that directly impacted the downstream tricyclic acid cycle [90]. An alternative to overcome this detrimental effect is to attenuate the activity of *pyk* instead of its complete removal. Such a strategy has been attempted in *B. subtilis via* two different approaches: (i) by expressing a mutant version of *pyk* with reduced activity [91] and (ii) by replacing the native *pyk* promoter with an inducible one [92]. Both strategies increased the availability of PEP, with the later being the least growth detrimental. A similar approach could be implemented in *S. cerevisiae*, since complete removal of *pyk* would impede the cells from growing in fermentable sugars [93].

Besides the difference in the PEP supply, another major difference occurred in the reductive PPP, which is controlled by the TKL and the transaldolase (TAL) enzymes, catalyzing the transfer of C2 and C3 units from a ketose donor to an aldose acceptor. The enzyme TKL has been shown to be indispensable in the production of aromatic amino acids; deletion of this enzyme in *S. cerevisiae* made the strain auxotrophic to aromatic amino acids [94]. Furthermore, *tkl1* has been overexpressed to increase the production of DHS-derived muconic acid in combination with the deletion of the gene *zwf1* to force carbon to enter PPP at the non-oxidative node (from fructose-6-phosphate and

glyceraldehyde-3-phosphate to xylulose-5-phosphate and E4P, Fig. 3.3.1). However, the reaction thermodynamically favors the opposite direction [95], and hence overexpression of *tkl1* with the hope of increasing the availability of E4P did not result in a considerable increase of aromatic flux. In previous work, the production of muconic acid increased from ~ 30 mg L^{-1} to 40 mg L^{-1} [67] whereas in *B. subtilis*, implementation of the same strategy to increase production of SA did not show positive results [90]. Although this strategy has been successfully implemented in *E. coli* [61, 96], a recent publication studying the production of muconic acid in a co-culture system showed that its overexpression resulted in a lower titer [97].

Expectedly, the flux through the reaction *v10* evidently differed among the strains; the lowest value, 1.1, corresponded to the highest producer, while the lowest producer showed a flux value of 17.5. This confirmed that INVSc1 had a stronger pull of carbon into the aromatic amino acid pathway, whereas in YSG50 and BY4743 more carbon returned to glycolysis at the node of E4P. An important point to highlight is that between the two precursors for aromatic compounds, E4P was clearly the limiting one. For instance, in strain INVSc1, despite that about 90% of the available E4P ended up entering the SA pathway (*v11/v9)*, it was only equivalent to 8% of the calculated available PEP (*v11*/*v5).* Thus, engineering the node to increase the availability of E4P is key to maximizing the production of aromatic compounds. This could entail pulling more carbon into the non-oxidative PPP by means of a mutant TKL incapable of converting E4P back to F6P [98], by implementing global transcriptional manipulations to increase the transcription rates of multiple genes in this node coupled with a fast-screening method [99-101], or even

selecting host yeasts (e.g. *Scheffersomyces stipitis*) with natural higher activity in the PPP [102].

Pathway Balancing for Enhanced Production of SA. Carbon tracing and ^{13}C-MFA corroborated that the four equally engineered strains had dramatically different flux distributions through the SA pathway stretching from the upstream precursor synthesis to the downstream aromatic amino acid production, which was likely caused by the differential expression of the three cloned enzymes. Initially, we hypothesized that the plasmid copy numbers could vary significantly from one strain to another, causing the major metabolic differences observed, despite all strains being equally engineered. Previous research has shown that specific genetic elements on the plasmid such as the selection marker, as well as the segregation element (centromere or 2□) play an important role in the yeast's fitness with some correlations to the strain's ploidy [71]. Since our platform consisted of plasmids harboring structural genes under the transcriptional control of strong constitutive promoters, we further reasoned that the engineered strains might have had very different capacities to deal with the energy burden posed by plasmid synthesis and enzyme overexpression. This effect was first recognized based on the observation that the optical densities at the late exponential phase of strain cultures in the group SA2 were reduced compared to the strains carrying the empty plasmids (SA0 strains, Fig. 3.3.5a), but interestingly the growth reduction did not correlate with SA production. This observation excluded SA toxicity as the major factor causing the growth reduction, suggesting that the actual copy numbers in the four strains might not reflect the behaviors of typical 2μ□and centromere as the segregation elements.

Measurement of the plasmid copy numbers revealed interesting insights on the capacity of each strain to cope with the stress caused by excessive enzyme expression. It appeared that plasmid pRS426-*aro1*$_{D920A}$ had a significant impact on the cell's fitness, and most importantly, on the production of SA. As shown in Figure 5b, the copy number ratio between the plasmid pRS426-*aro1*$_{D920A}$ and pRS413-*aro4*$_{K229L}$-*tkl1* was calculated and a clear negative correlation was identified. The strains with the highest production of SA (INVSc1 and BY4741) had a plasmid ratio closer to 1, whereas the poor-producing strains (YSG50 and BY4743) had a ratio between 3 and 7. It was also noticed that although the plasmid pRS426-*aro1*$_{D920A}$ had the 2□□segregation element, the copy number was dramatically reduced to resemble a centromere-like plasmid in all the strains. The absolute copy number of the plasmids was also compared between the strain groups SA0 and SA2 (Appendix A Fig. A.S5). The reduction in plasmid copy number was evident in all strains in the group SA2; the most significant reductions occurred in plasmids pRS426-*aro1*$_{D920A,}$ specifically the strain INVSc1-SA2, where the plasmid copy number was reduced 95% compared to the empty plasmid. Contrary to our findings, Karim et al., (2012) showed that using histidine and uracil as selection markers result in similar growth rates and plasmid copy number when comparing strains BY4741 and BY4743. In our study, we did observe major discrepancies that can be attained to (i) co-expression of two distinct episomal plasmids and (ii) constitutive overexpression of structural genes. Although the four, wildtype strains studied here have slight differences in their auxotrophic markers, no correlation with their capacity to accumulate shikimate can be observed. For instance, the only major auxotrophic difference between strains YSG50 and INVSc1 is the deletion of *ade1* in the former, yet these strains have the most evident disparity in accumulation of

shikimate. Similarly, supplementation of L-trp in the growth medium brings the strains INVSc1 and BY4743 to the same auxotrophic level, but their capacity to produce shikimic is considerably different. We hypothesized that overexpression of *aro1*$_{D920A}$ in the pRS426 background had a negative impact on SA production. Hence, only the strains capable of adjusting this plasmid to a very low copy number could produce higher amounts of SA.

To test this hypothesis, we constructed a new plasmid encoding the three genes on the pRS413 backbone (pRS413-*aro1*$_{D920A}$-*aro4*$_{K229L}$-*tkl1*). To maintain the same selective nutrients as used previously, this new plasmid, was transformed into all strains along with an empty pRS426 vector yielding the group SA3. As expected, all the strains in group SA3 showed increases in the SA titers. A 2-fold increase was observed for strains YSG50 and BY4741, and the most significant increase occurred in strain BY4743-SA3, where the SA titer was elevated 5.5-fold over the corresponding. The strain INVSc1-SA3 showed very similar titers when compared to INVSc1-SA2 (358 and 350 mgL^{-1}), indicating that such strains might have reached the maximum flux attainable into the aromatic amino acid pathway with the provided manipulations (Fig. 3.3.5c). In parallel, we reconstructed a new plasmid encoding all three genes on the pRS426 backbone (pRS426-*aro1*$_{D920A}$-*aro4*$_{K229L}$-*tkl1*), and co-transformed it with the empty pRS413 into all strains, yielding SA producing groups SA4 (Table 3.3.1). Very interestingly, a dramatic decrease in titers was observed in all strains in the group SA4. In the case of INVSc1, BY4741, and BY4743, the production dropped 94%, 96%, and 83%, respectively, whereas the strain YSG50 showed no SA accumulation (Fig. 3.3.5c). This result suggested that the stress caused by overexpressing *aro4*$_{K229L}$ and *tkl1* excessively added a new layer of stress that negatively affected cellular metabolism.

Balancing gene expression for efficient production of chemicals is a common task carried out in metabolic engineering research [71, 73, 103]. The results presented here reaffirm that pathway balance and optimization is an obligated step for the construction of efficient microbial factories. Moreover, the pipeline for optimization should also take into consideration the selection of an appropriate host strain. Recently, it has been recognized that yeast strains have the capability to auto-adjust plasmid copy number in accordance to the burden of excessive enzyme expression [104]. Our study showed that four independent, yet commonly used *S. cerevisiae* strains had disparate responses to simple metabolic manipulations, which was correlated to their ability to balance the introduced plasmids. A careful inspection of the behavior of each strain brought valuable insights into how to properly engineer the carbon entrance into the aromatic amino acid pathway.

3.3.4 Conclusion

Altogether, we were able to observe high-level accumulation of SA in three of the four strains engineered in this work. Having four S. cerevisiae strains with different capacity to produce SA, allowed us to implement a strain-dependency approach to discern the appropriate way to engineer our pathway of interest. The higher production of strains in the group SA3 was a result of rationally engineering the entrance of carbon into the aromatic amino acid biosynthetic pathway. This work emphasizes the significance of strain and plasmid selection in metabolic engineering efforts and provides insights to optimize the production of aromatic compounds in yeast.

Acknowledgements

This work is supported by the National Science Foundation Grant Numbers EEC-0813570 and EPSC-1101284, the Center for Biorenewable Chemicals and the Plant

Sciences Institute at Iowa State University, and the start-up fund (#175323) from Virginia Tech Research.

Table 3.3.1. The constructed plasmids and strains.

Plasmid	Expression Cassette	Features
pRS413-*aro4*$_{K229L}$-*tkl1*	TPI1p-ScARO4$_{K229L}$-TDH2t ADH1p-ScTKL1-ADH1t	Feedback insensitive DHAP synthase. Transketolase 1 to increase E4P pool.
pRS426-*aro1*$_{D920A}$	GPDp-ScARO1$_{D920A}$-PYK1t	Mutant version of pentafunctional ScARO1 with disrupted activity of SA kinase subunit.
pRS413-*aro1*$_{D920A}$ *aro4*$_{K229L}$-*tkl1*	GPDp-ScARO1$_{D920A}$-PYK1t TPI1p-ScARO4$_{K229L}$-TDH2t ADH1p-ScTKL1-ADH1t	Complete pathway in pRS413 backbone for accumulation of SA.
pRS426-*aro1*$_{D920A}$ *aro4*$_{K229L}$-*tkl1*		Complete pathway in pRS426 backbone for accumulation of SA.
Strains	**Genotype / Plasmid**	
YSG50	*MAT□; ade2-1; ade3□22; ura3-1; his3-11,15; trp1-1; leu2-3,112; can1-100*	
INVSc1	*MATa/□□ his3□1/his3□1; leu2/leu2; trp1-289/ trp1-289; ura3-52/ ura-52 MAT*	
BY4741	*MATa; his3Δ1; leu2Δ0; met15Δ0; ura3Δ0*	
BY4743	*MAT*a/□□□ *his3□1/his3□1; leu2□0/leu2□0; LYS2/lys2□0; met15□0/MET15; ura3□0/ura3□0*	
SA0	pRS426 & pRS413	
SA1	pRS426-*aro1*$_{D920A}$	
SA2	pRS426-*aro1*$_{D920A}$ & pRS413 *aro4*$_{K229L}$-*tkl1*	
SA3	pRS426-*aro1*$_{D920A}$- *aro4*$_{K229L}$-*tkl1* & pRS413	
SA4	pRS426 & pRS413-*aro1*$_{D920A}$-*aro4*$_{K229L}$-*tkl1*	

Table 3.3.2. **Physiological characterization of SA producing strains.** μ (h^{-1}), specific growth rate; r (mmol $gDCW^{-1}$ h^{-1}), rate of consumption or production; Y_{max} (mmol $gDCW^{-1}$), molar yield based on consumed glucose; titer (mg L^{-1}).

Strain	Glucose		Ethanol		Glycerol		SA		
	μ	r	r	Y_{max}	r	Y_{max}	r	Y_{max}	titer
YSG50-SA2	0.13	13.2	15.1	241.8	-	-	0.17	0.83	30
INVSc1-SA2	0.17	13.8	12.8	206.9	1.49	28.6	1.53	8.1	350
BY4741-SA2	0.15	28.7	34.8	246.4	4.79	36.1	1.36	2.38	150
BY4743-SA2	0.16	33.4	40.1	310.6	1.18	18.6	0.15	0.32	40

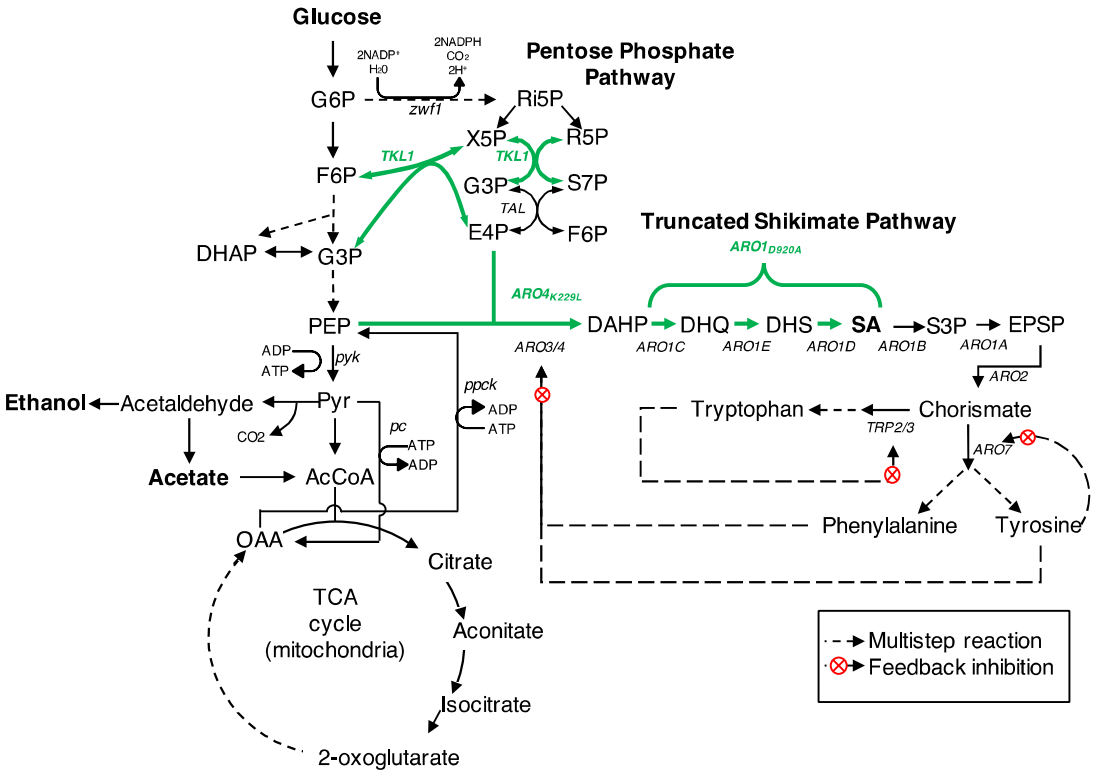

Fig. 3.3.1 Pathway depicting engineering efforts for the accumulation of SA. The arrows in green represent the overexpressed enzymes for unlocking the production of SA. Definitions of abbreviations are shown in the List of Abbreviations.

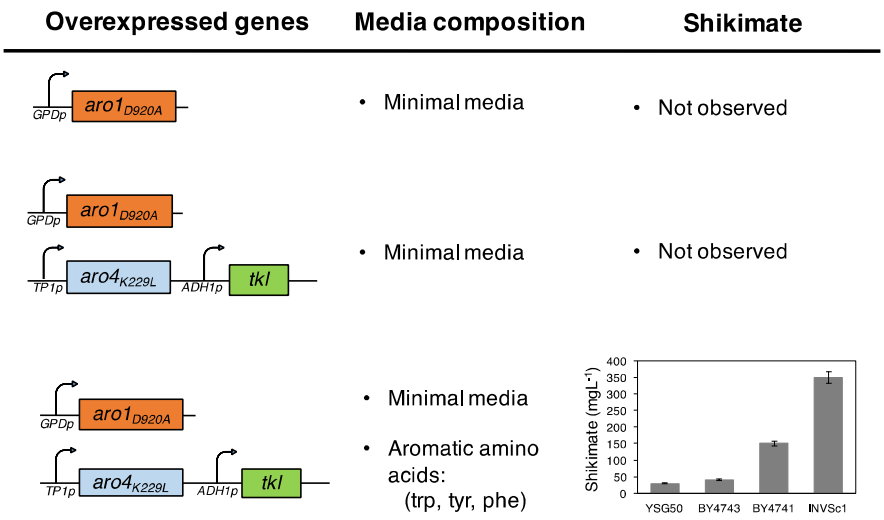

Fig. 3.3.2 Media optimization for the production of SA. To allow the accumulation of SA in all fours strains, it was necessary to incorporate the three aromatic amino acids into the growth media, through which the conversion of SA into downstream metabolites was at least partially reduced and hence the positive outcome of expressing the mutant $ARO1_{D920A}$ was observed. Samples were taken after 24 h of fermentation. The variation is represented as the standard deviation from three biological replicates.

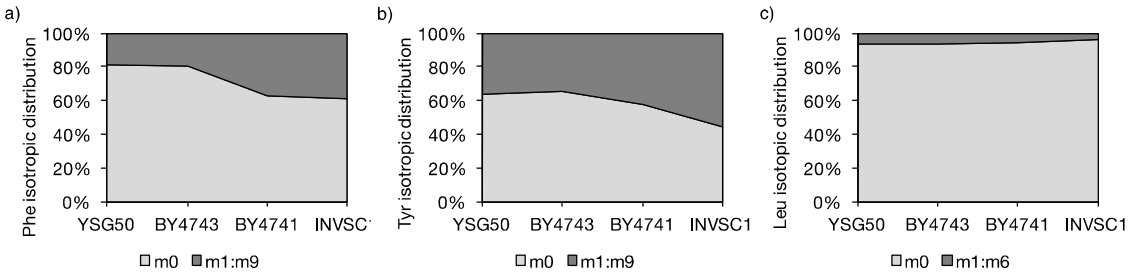

Fig. 3.3.3 Isotropic distribution of labeled and non-labeled amino acids. Strains INVSC1-SA2 and BY4741-SA2 showed higher percentages of labeled a) phenylalanine and b) tyrosine compared to YSG50-SA2 and BY4743-SA2. This corroborated the higher fluxes into the biosynthesis of aromatic compounds in the strains with higher SA accumulation levels. c) Analysis of leucine, another non-labeled amino acid, showed equal distribution across all four strains.

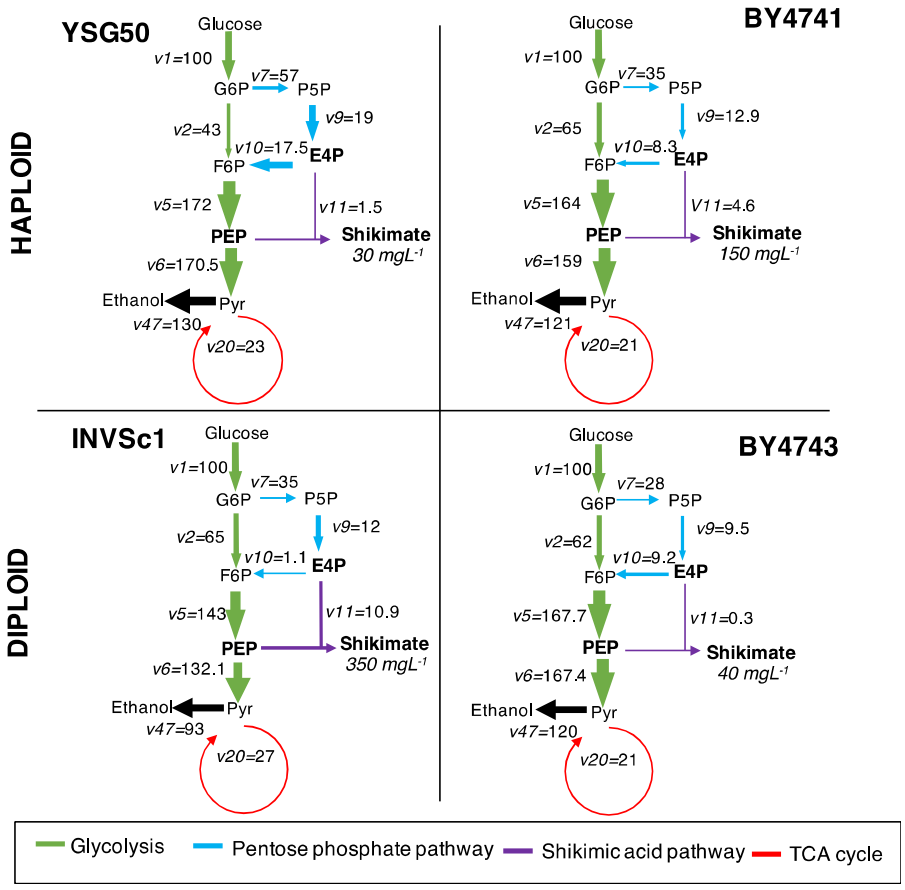

Fig. 3.3.4 Major intracellular metabolic flux distributions in the engineered strains in group SA2 (Table 3.3.1). All fermentations were performed in batch mode supplemented with 20 g L^{-1} of 80% [1-^{13}C] glucose and 20% [U-^{13}C] glucose. The fluxes are expressed as normalized values relative to specific glucose uptake rate (Table 3.3.2). These values represent a global solution obtained *via* isotopomer modeling of the ^{13}C labeled proteinogenic amino acids. To emphasize the flux differences in the SA pathway, the thickness of the arrows of reactions *v9* to *v11* was normalized by a value of 5; a value of 25 was used otherwise. P5P: pentose phosphate sugar.

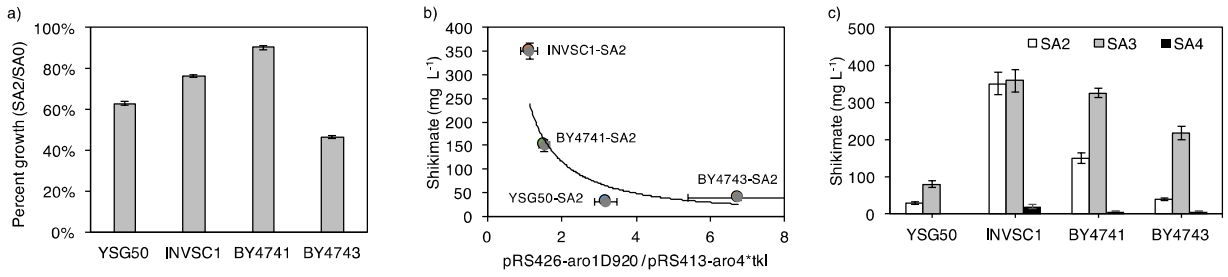

Fig. 3.3.5 Phenotypic comparison of *S. cerevisiae* engineered for the production of SA. a) Growth percentage of strains in the group SA2 versus strains carrying empty plasmids (group SA0, Table 3.3.1). b) Correlation between SA production and plasmid maintenance. The ratio between plasmid pRS426-*aro1*$_{D920A}$ and pRS413-*aro4*$_{K229L}$-*tkl* was calculated and plotted on the x-axis. c) Accumulation of SA in the strains of groups SA2, SA3, and SA4. All strains showed an increased production of SA when the genes were encoded in the plasmid pRS413 (group SA4). Conversely, incorporating all three genes into the backbone of pRS426 resulted in extremely low production of SA. Samples were taken after 24 h of growth in minimal media. Variation is represented as the standard deviation from three biological replicates.

3.4 Investigating Oxalate Biosynthesis in Wood-decaying Fungus *Gloeophyllum trabeum* Using ^{13}C Metabolic Flux Analysis

Liangpeng Zhuang,[a, *] Weihua Guo,[b, *] Makoto Yoshida[c], Xueyang Feng,[b, †] and Barry Goodell[a, †]

[a] Department of Sustainable Biomaterials, Virginia Polytechnic Institute and State University, Blacksburg, VA 24061, USA

[b] Department of Biological Systems Engineering, Virginia Polytechnic Institute and State University, Blacksburg, VA 24061, USA

[c] Department of Environmental and Natural Resource Science, Tokyo University of Agriculture and Technology, Tokyo, Japan

[†] Correspondence to: Xueyang Feng and Barry Goodell.

[*] LZ and WG contribute to this work equally.

Phone: +1-(540)231-2974 and +1-(540)231-8176

Email: xueyang@vt.edu and goodell@vt.edu

This manuscript has been published on *RSC Advances* 5 (126), 104043-104047. Chapter 3.4 is reproduced by permission of The Royal Society of Chemistry. Supplementary material of Chapter 3.4 is shown in Appendix B.

Oxalate synthesis was rigorously investigated in a wood-decaying fungus, *Gloeophyllum trabeum*, using ^{13}C metabolic flux analysis, a method not previously explored in this type of system. Peroxisomal glyoxylate dehydrogenase and cytosolic oxaloacetate acetylhydrolase were found to contribute to the majority of oxalate synthesized under low and high nitrogen conditions, respectively.

Lignocellulose is the most abundant biomass resource in terrestrial environments[105], and wood fiber has seen growing use as an industrial feedstock for value-added chemical and biofuel production[106]. However, the recalcitrant structure of lignocellulosic biomass prevents it from being converted to fermentable sugar efficiently and research in this area is still needed. Brown rot fungi are the only organisms known that can depolymerize crystalline cellulose without removal of lignin[107]. *Gloeophyllum trabeum*, a brown rot fungus with high polysaccharide depolymerization activity has promising industrial application prospects. For example, it has been used in a corn stover pretreatment step for ethanol production[108], and also in a saccharification step in ethanol production via simultaneous saccharification and fermentation (SSF)[109]. A non-enzymatic oxidative "chelator-mediated Fenton" (CMF) system is reported to be involved in brown rot fungi cellulose depolymerization processes[110], but many aspects of how this system works are unknown. The process, involves the secretion of the low molecular weight metabolites, oxalate and hydroquinone/catecholate compounds to first sequester and then reduce iron in a sequence, which results in generation of Fenton chemistry at a distance from the fungal hyphae within the lignocellulose cell wall. A highly reactive hydroxyl radical is generated and has been demonstrated to be responsible for the deconstruction of the wood cell wall in brown rot non-enzymatic decay[111-113]. Previous

research on the detection of oxalate and catechols in brown rot fungal liquid culture medium in the absence of wood has demonstrated that these compounds are generated by the fungus rather than being derivatives of wood [114-116]. Due to the important role that oxalate and catecholates play in brown rot fungal degradation mechanisms, study of their biosynthetic pathways will provide novel insight about how brown rot fungi regulate the production of these compounds to break down the recalcitrant structure of lignocellulose biomass.

In this study, we applied ^{13}C Metabolic Flux Analysis (^{13}C-MFA), a technique that has been widely applied to reveal previously unknown metabolic pathways in various non-model organisms[117-121], to provide valuable insight into the intracellular metabolisms of *G. trabeum* under different culture conditions[122-124]. We found that the major source for intracellular oxalate synthesis varied under different culture conditions. While peroxisomal glyoxylate dehydrogenase contributed to the majority of oxalate synthesized under low nitrogen conditions, cytosolic oxaloacetate acetylhydrolase was found to be the main pathway for oxalate synthesis when culturing *G. trabeum* in a high concentration of nitrogen. To our best knowledge, this is the first time that oxalate biosynthesis metabolism in *G. trabeum* has been rigorously and quantitatively determined by ^{13}C trace experiments using the metabolic flux analysis approach. Research in this area will facilitate future work in increasing the degradation efficiency for bioconversion of lignocellulosic biomass by *G. trabeum* and related organisms.

G. trabeum was cultured statically, in 150mL flasks at 36 ℃ in 20mL liquid medium containing the following basal salts per liter: 2g NH_4NO_3, 2g KH_2PO_4, 0.5g $MgSO_4 \cdot 7H_2O$, 0.1g $CaCl_2 \cdot 2H_2O$, 0.57mg H_3BO_4, 0.036 mg $CuSO_4 \cdot 5H_2O$[125], and 1%

glucose. All glassware was acid-washed and Fe and Mn was omitted to promote production of secondary metabolites. After 20 days, the medium in three flasks was homogenized and sterile water was added to bring the total volume to 150mL. The homogenate was diluted 1:40 and a 0.5 ml aliquot was used to inoculate a ^{13}C-glucose medium containing low nitrogen (LN), or high nitrogen (HN). These cultures contained 1% ^{13}C-glucose (a mixture of 80% [1-^{13}C] and 20% [U-^{13}C] glucose)[114] and the basal salts listed above with either 25mM NH_4NO_3 (HN) or 2.5mM NH_4NO_3 (LN). In separate work with HN and LN cultures using non-labeled glucose, growth was analysed by weighing the dried mycelial mass at 3-5d intervals, and HPLC of the culture filtrate was also conducted to assess glucose consumption (Table 3.4.1). The ^{13}C-labeled fungal cultures were harvested during the exponential growth phase, after 14 days. Our cultivation conditions were different to those previously used by Varela and Tien[126] in part to avoid uncontrolled levels of iron in the media and so that nitrogen levels could be modified.

Following harvest, isotopomer analysis of proteinogenic amino acids and intracellular oxalate was conducted using a previously developed protocol [127-129]. In brief, the biomass was hydrolyzed using 6 M HCl (20h at 100 °C) and the amino acids and intracellular oxalate were silyated using 50 µl tetrahydrofuran and 50 µL N-(tert-butyldimethylsilyl)-N-methyl-trifluoroacetamide (Sigma-Aldrich) to form tert-butyl dimethylsilyl (TBDMS) derivatives. Gas Chromatography-Mass Spectrometry (GC-MS) was performed to analyse fungal metabolites using a Shimadzu GC2010 GC with a SH-Rxi-5Sil column and a Shimadzu QP2010 MS. Three types of charged fragments were detected by GC-MS for various amino acids (Table S1): the $[M-57]^+$ group (containing unfragmented amino acids); and the $[M-159]^+$ or $[M-85]^+$ group (containing amino acids

that had lost an α-carboxyl group). For each type of fragments, the labeling patterns, mass distribution vectors (MDVs), were represented by M0, M1, M2, etc., which were fractions of non-labeled, singly-labeled, and doubly-labeled amino acids. The effects of natural isotopes on isotopomer labeling patterns were corrected by previously reported algorithms[130]. MDVs were used to calculate the summed fractional labelling (SFL) values which were directly used in the MFA (Biomet Toolbox 2.0[131], based on MATLAB, MathWorks, Inc. MA). The central carbon metabolic model for the MFA was developed based on the KEGG database (http://www.genome.jp/kegg/) and previous reports on metabolic pathways of brown rot fungi[132, 133], which included glycolysis pathways, pentose phosphate pathways, futile pathways, the tricarboxylic acid (TCA) cycle, the glyoxylate cycle in peroxisomes, cytosolic oxaloacetate acetylhydrolase and transport pathways among different cell compartments (Fig. 3.4.1A). Of particular interest, two oxalate biosynthesis pathways, i.e., cytosolic oxaloacetate acetylhydrolase (OAH) and peroxisomal glyoxylate dehydrogenase (GLX)[134] were examined in our metabolic models (Fig. 3.4.1A) to assess oxalate biosynthesis. These two pathways have been reported to contribute to fungal extracellular oxalate accumulation in other species[135]. Although little research has been done to elucidate the genes associated with oxalate biosynthesis pathways in *G. trabeum*, the homologs of oxaloacetate acetylhydrolase (fpOAH) and glyoxylate dehydrogenase (fpGLOXDH) in *Fomitopsis palustris* have been indicated in the *G. trabeum* genome using Blastp[136] with 77% and 67% similarity respectively, which suggested these two pathways could potentially be exploited by *G. trabeum* for oxalate synthesis. For our metabolic flux analysis, flux estimation was repeated at least 50 times starting with different initial values generated by a genetic

algorithm for all fluxes to find a likely global solution. A fit of the simulated and measured summed fractional labelings was determined to be a global solution only after the solution fit was obtained at least twice using this method (Fig. B.S1).

In addition to the MDVs detected by GC-MS, we also used a similar protocol to detect oxalate concentrations for both soluble and insoluble oxalate from the cultivation medium and cell biomass, respectively. To measure the concentrations of soluble oxalate, we dried 5mL of the medium and followed the same derivatization process for GC-MS analysis. We detected no soluble oxalate and therefore repeated this work with a more sensitive HPLC analysis. Again, no soluble oxalate was detected (at levels down to 0.01 mM), which is consistent with previous results that *G. trabeum* accumulates less oxalate compared to other brown rot fungi [137], mainly due to the presence of oxalate decarboxylase, which has previously been shown to decompose oxalate in *G. trabeum*. To measure the concentrations of insoluble oxalate, we followed similar protocols for biomass hydrolysis followed by derivatization. We found that oxalate was produced at levels of 0.19±0.09 mM and 0.56 ±0.09 mM under LN and HN conditions, respectively. The observation that greater amounts of oxalate were produced under high nitrogen levels was also consistent with previous research[138].

Based on the production of insoluble oxalate, we next investigated the central metabolic flux of *G. trabeum* when cultured using different nitrogen levels. In general, for most of the central metabolic pathways such as glycolysis and pentose phosphate pathways, the fluxes were similar despite changes in nitrogen culture levels (Fig. 3.4.1A). However, when we next evaluated the effects of peroxisomal glyoxylate dehydrogenase (GLX) and cytosolic oxaloacetate acetylhydrolase (OAH) on oxalate synthesis, we found that usage of

these two pathways was significantly different when high and low nitrogen conditions were used (Fig. 3.4.1B). While the flux ratio of OAH/GLX for the low nitrogen condition was only 0.01; it was as high as 56.2 for the high nitrogen condition (Fig. 3.4.1B), indicating that the preferred pathway for oxalate production (OAH or GLX) shifts dramatically when the fungus was grown at different nitrogen levels. Correspondingly, the fluxes of metabolic pathways related to OAH and GLX were also found to be different. For example, the metabolic flux of the futile pathway that supplies cytosolic oxaloacetate from cytosolic pyruvate in the LN condition was dramatically higher than that in the HN condition (Fig. 3.4.1C). The varied flux distribution in the peroxisomal glyoxylate dehydrogenase, cytosolic oxaloacetate acetylhydrolase and futile pathways clearly indicated that *G. trabeum* metabolism was regulated in response to the C/N ratio, which confirmed that the C/N ratio was a key factor in oxalate biosynthesis for this fungus[114].

While it is clear that the conversion of oxaloacetate to oxalate by peroxisomal glyoxylate dehydrogenase occurred in the peroxisome, oxalate synthesis via cytosolic oxaloacetate acetylhydrolase could potentially be from several sources since oxaloacetate, the precursor of oxalate in synthesis via cytosolic oxaloacetate acetylhydrolase, can be generated by either of three pathways in different regions of the cell: 1) the futile pathway, where pyruvate is converted to oxaloacetate in the cytosol to supply the TCA cycle in mitochondria; 2) the TCA cycle, where oxaloacetate is generated from malate in mitochondria; and 3) the glyoxylate cycle, where oxaloacetate is generated in the peroxisome. However, based on ^{13}C-MFA, we found the flux for oxaloacetate synthesis in the glyoxylate cycle was trivial under both LN and HN conditions (Fig. 3.4.1B), indicating that glyoxylate was mainly used to produce oxalate directly rather than being converted to

oxaloacetate in *G. trabeum*. Therefore, it is likely that the oxalate generated by cytosolic oxaloacetate acetylhydrolase is generated directly from oxaloacetate that is synthesized in the futile cycle or the TCA cycle, rather than from oxaloacetate that is synthesized in the glyoxylate cycle. In addition, in prior research with a related fungus, *F. palustris* [115, 139] under high nitrogen conditions (although with a different nitrogen source than in our research), cytosolic oxaloacetate acetylhydrolase was the dominant precursor for oxalate synthesis. Both *F. palustris* and *G. trabeum* have previously been reported to utilize the non-enzymatic "chelator-mediated Fenton" system in lignocellulose deconstruction, and therefore it is possible that these two fungi would adopt a similar regulatory system for oxalate synthesis. It has been reported that high levels of ammonium ions may inhibit the activity of glyoxylate dehydrogenase, the key enzyme for oxalate production in the glyoxylate cycle[140][141], which could explain the limited role of the peroxisomal glyoxylate dehydrogenase on oxalate synthesis when nitrogen (ammonium) concentrations were high.

To further investigate the regulation of cytosolic oxaloacetate acetylhydrolase and peroxisomal glyoxylate dehydrogenase, we performed qPCR (VBI – Virginia Tech) to determine the expression level of the genes that encode these two enzymes. We followed an established protocol[142] to extract the mRNAs of *G. trabeum* from both LN and HN conditions using a FastRNA spin kit (MP Biomaterials, USA), and measured the mRNA levels. It was found that there was no significant difference in gene expression levels between the LN and HN conditions for both cytosolic oxaloacetate acetylhydrolase and peroxisomal glyoxylate dehydrogenase (Fig. B.S2). Comparing with the distinct flux results between LN and HN conditions, this indicates that the regulation of the pathways

for oxalate synthesis was not executed at the transcriptional level. Considering the complex regulatory machinery in eukaryotic metabolism (e.g., *G. trabeum*), the peroxisomal glyoxylate dehydrogenase and cytosolic oxaloacetate acetylhydrolase could be regulated in translational, post-translational or even at the metabolic level (e.g., ammonium inhibition). The systemic investigation of the regulatory mechanism is beyond the scope of this manuscript but will be investigated by our group in the future.

In sum, this study examined the effects of peroxisomal glyoxylate dehydrogenase and cytosolic oxaloacetate acetylhydrolase on oxalate biosynthesis in *G. trabeum* using ^{13}C tracer experiments and metabolic flux analysis; approaches not previously explored in fungi for oxalate production. As revealed by the metabolic flux results, the pathway selected for oxalate biosynthesis was highly dependent on the C/N ratio, with cytosolic oxaloacetate acetylhydrolase being the dominant pathway for the oxalate synthesis under low C/N (i.e., high nitrogen) conditions, and peroxisomal glyoxylate dehydrogenase contributing to oxalate synthesis under high C/N (i.e., low nitrogen) conditions. Combined with transcriptional analysis, it was determined that such metabolic reprogramming was not transcriptionally controlled. Overall, ^{13}C-MFA proved to be a useful approach in evaluating the pathway usage in *G. trabeum* for oxalate production and could help improve our understanding of oxalate metabolism in wood-decaying fungi and to facilitate further improvement of the lignocellulose bioconversion technology with other fungal species.

Acknowledgements

This study was supported by start-up fund (#175323) from Virginia Tech. This work was also supported in part by the USDA-HATCH Project S-1041 VA-136288, and by The Research Council of Norway 243663/E50 BioMim.

Table 3.4.1. Growth behaviour of *G. trabeum* under different nitrogen conditions.

Nitrogen Conditions	Growth rate (day^{-1})	Glucose uptake (g/g DCW/day)
LN	0.14±0.03	0.24±0.002
HN	0.15±0.03	0.15±0.001

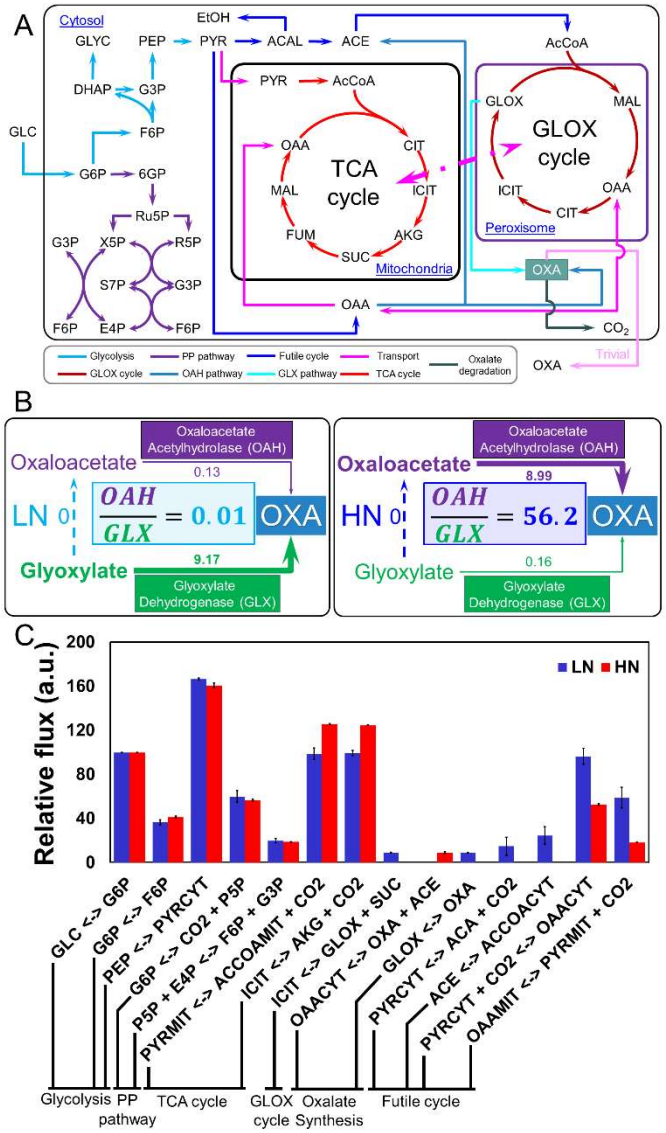

Fig. 3.4.1. Metabolic pathway map and key flux distributions for *G. trabeum* under different C/N ratios. (A) Central carbon metabolic pathways and oxalate synthesis pathways of *G. trabeum*. Transport fluxes between mitochondria and peroxisome were simplified to a single dash-dot line. (B) The flux ratio between OAH and GLX pathways for LN and HN conditions with the OAH/GLX ratio highlighted. (C) Key metabolic flux distributions for *G. trabeum* under LN and HN conditions. Definitions of abbreviations are shown in the List of Abbreviations.

3.5 ^{13}C Pathway Analysis of Biofilm Metabolism of *Shewanella oneidensis* MR-1

Weihua Guo[a, *], Shuai Luo[b, *], Zhen He[b, †] and Xueyang Feng[a, †]

[a] Department of Biological Systems Engineering, Virginia Tech University, Blacksburg, VA 24061, United States

[b] Department of Civil and Environmental Engineering, Virginia Polytechnic Institute and State University, Blacksburg, VA 24061, United States

[†]Correspondence to: Zhen He and Xueyang Feng.

[*] WG and LS contribute to this work equally.

Phone: +1-(540)231-1346 and +1-(540)231-2974

Email: zhenhe@vt.edu and xueyang@vt.edu

This manuscript has been published on *RSC Advances* 5 (50), 39840-39843. Chapter 3.5 is reproduced by permission of The Royal Society of Chemistry

Biofilm metabolism of *Shewanella* was analyzed via ^{13}C tracing experiments for the first time. The activity of C1 metabolism in the biofilm cells was found to be interestingly higher than that in planktonic cells, which could be related to utilizing C1 metabolites as electron donors when growing *Shewanella* in biofilms.

The biofilms formed by *Shewanella oneidensis* MR-1 has been extensively studied[143-147] and found to play pivotal roles in bioremediation of heavy metals[148-152] and electric power generation[153, 154]. Despite recent discoveries of *Shewanella* metabolism under aerobic and anaerobic conditions using various analytical approaches[155-158], few studies have been accomplished to investigate the metabolic pathway usage in *Shewanella* biofilms. In this study, we applied the ^{13}C pathway analysis, a reliable and well-developed technology[159], to analyze the carbon metabolism of *S. oneidensis* cells derived from biofilm and planktonic growth, respectively. Through the comparison of isotopomer labeling patterns of key proteinogenic amino acids, we found that the C1 metabolism was much more active when growing *S. oneidensis* in biofilms compared to planktonic cells, which could be related to the utilization of C1 metabolites as electron donor by *S. oneidensis* when growing in biofilms. To our best knowledge, this is the first time that the biofilm metabolism of *S. oneidensis* was rigorously determined by isotopomer analysis.

S. oneidensis MR-1 was initially grown in shake flasks with minimal medium containing 3.7 mM [3-^{13}C] sodium L-lactate (Sigma-Aldrich) for two days at 100 rpm, 30ºC. It was then transferred to completely fill up a 140 mL sealed bottle reactor and cultivated under oxygen-limited condition (stirrer at the bottom) at 30ºC. To grow *S. oneidensis* MR-1 in a biofilm, a carbon cloth (2.5 cm×4.5 cm, Zoltek, Panex® 30 Fabric,

PW06) was submerged in the medium of the sealed bottle reactor, with titanium mesh (McMaster) to support and titanium wire (Sigma-Aldrich) to bind the cloth tightly on mesh. Duplicate reactors were processed (n=2). When lactate was depleted (<0.01 mM), the minimal medium was refreshed by removing 10 mL medium from the sealed bottle reactor and injecting 10 mL fresh filter (0.22um pore size) sterilized medium. The final concentration of [3-^{13}C] sodium L-lactate was maintained at ~0.8 mM. The biomass of planktonic cells was monitored by OD_{600} using a plate reader (BioTek). The concentrations of lactate and acetate in the sealed bottle reactor were measured by high-performance liquid chromatography (HPLC, Shimadzu), following the method that has been previously developed[160] (Fig. 3.5.1). It was found that lactate was consumed to produce acetate as the sole fermentation byproduct when growing *Shewanella* in the sealed bottle bioreactor. The declining OD_{600} of the planktonic cells in the reactor indicated that more cells would be grown in the biofilms with the replenishment of the medium.

After five refreshment of the medium, both the planktonic cells and the biofilm cells were collected in duplicate from the liquid culture and the carbon cloth, respectively, followed by isotopomer analysis of proteiogenic amino acids using a previously developed protocol[127-129]. In general, the biomass was hydrolysed using 6 M HCl (24 h at 100 °C). The amino acids were derivatized in 20 µl of tetrahydrofuran and 20 µL of N-(tert-butyldimethylsilyl)-N-methyl-trifluoroacetamide (Sigma-Aldrich). A gas chromatograph (GC2010, Shimadzu) equipped with a SH-Rxi-5Sil column (Shimadzu) and a mass spectrometer (QP2010, Shimadzu) was used for analyzing the labeling profiles of metabolites. Three types of charged fragments were detected by GC-MS for Ala, Gly, Ser, Asp and Glu: the $[M-57]^+$ group (containing unfragmented amino acids); and the $[M-159]^+$

or $[M-85]^+$ group (containing amino acids that had lost an α-carboxyl group). For each type of fragments, the labeling patterns were represented by M0, M1, M2, etc., which were fractions of non-labeled, singly labeled, and doubly labeled amino acids. The effects of natural isotopes on isotopomer labeling patterns were corrected by previously reported algorithms[130].

By feeding [3-^{13}C] lactate as the sole carbon source to *S. oneidensis* under an oxygen-limited culture condition, most alanine molecules were expected to be singly labeled because pyruvate, the direct precursor of alanine, was believed to be mainly synthesized from [3-^{13}C] lactate (Fig 3.5.2 and Table 3.5.1). To our surprise, 34% alanine molecules were found to be non-labeled in the biofilm cells. As a result of the non-labeled pyruvate produced, we also found a significant amount of non-labeled aspartate and glutamate in the biofilm cells, which were synthesized from the futile cycle and the TCA cycle, respectively, by using the non-labeled pyruvate as the precursor. However, it remains unknown that how the non-labeled pyruvate was synthesized during *Shewanella* growth in biofilms.

To our best knowledge, there is only one pathway, C1 metabolism, which could lead to the synthesis of non-labeled pyruvate when growing with [3-^{13}C] lactate[145, 161-163]. Generally, pyruvate could be converted to 3-phosphoglycerate (PGA) through the gluconeogenesis, which is used to produce serine, and further converted into glycine and a C1 molecule (e.g., formate) via C1 metabolism. During the glycine synthesis from serine, the labeled carbon originated from the [3-^{13}C] lactate would get lost as C1 metabolites while glycine became mostly non-labeled, as found in this study (Fig. 3.5.2). Glycine could be continuously divided into CO_2 and C1 molecule, both of which were non-labeled in this

study. Considering the high reversibility of the C1 metabolism, the non-labeled C1 metabolites could be incorporated with non-labeled glycine to synthesize non-labeled serine (i.e., reversed C1 metabolism), which would then be used to synthesize the non-labeled pyruvate via serine dehydratase (SDH, EC 4.3.1.17)[164, 165]. This is possible in the present study because we grew *Shewanella* in biofilms with very low concentration of [3-^{13}C] lactate (~0.8 mM), which was rapidly consumed for cell growth within 5~10 hours but also produced non-labeled C1 metabolites via the C1 metabolic pathway. Once lactate utilization stage was finished, *Shewanella* growing in biofilms would use the generated C1 metabolites as the secondary carbon source to continue the production of building blocks for cell growth. As a result of the combined effects of lactate utilization and C1 metabolites utilization, the proteinogenic amino acids, such as alanine, aspartate and glutamate, demonstrated a high percentage of non-labeled molecules (34%, 31%, and 28%, respectively). It is also worth noting that although most of detected glycine (84%) is non-labeled, there was 13% single-labeled glycine detected, which could be synthesized from glyoxylate shunt of TCA cycle as that has been discovered in previous studies.[145, 161, 163]

Compared to the isotopomer labeling patterns of the biofilm cells, the non-labeled proteinogenic amino acids (e.g., Ala, Glu, and Asp) were also detected in the planktonic cells of *S. oneidensis* MR-1, which could come from two sources. First, the C1 metabolism could be active in the planktonic cells and generate non-labeled amino acids. Secondly, considering the cohesiveness of the biofilm, some cells could be washed out from the biofilm and become the planktonic cells[166, 167], which brought non-labeled amino acids as detected in the planktonic cells. Indeed,

at the end of the fifth medium replenishment, we did observe an increased OD_{600} of the planktonic cells (Fig. 3.5.1), which could be attributed to the washout of the biofilm cells. The washout was not observed in early stages since the cells attached on biofilms were not saturated, while in the late stages, the biofilm could no longer attach all the cells and the extra cells were washed out. We also found that the percentages of non-labeled proteinogenic amino acids in planktonic cells were much smaller compared to that in biofilm cells. For example, only 23% of alanine detected in the planktonic cells was non-labeled while 34% alanine was found to be non-labeled in biofilm cells. This is possible since the substrate (i.e., [3-^{13}C] lactate in this study) was more difficult to diffuse into the biofilms, more lactate would be used by the planktonic cells, which makes the lactate utilization metabolism more dominant in the planktonic cells and leads to smaller percentage of non-labeled pyruvate synthesized from C1 metabolism of planktonic cells.

The results of this study have important implications to use *S. oneidensis* MR-1 for energy production. For example, it has been well known that by forming the biofilms, *S. oneidensis* MR-1 could generate electricity from organic carbon substrates[154, 168]. The discovery from this study indicated that the C1 metabolite, especially formate, could serve as the electron donor and generate electricity during the C1 metabolism[162]. Considering the direct connection of biofilm cells and carbon cloth, the electron transfer of biofilm cells should be more active compared to planktonic cells, which could lead to active the C1 metabolism in the biofilm cells. The effects on C1 metabolites (e.g., formate) on bioelectricity generation and the exact pathway of carbon flux during bioelectricity generation are currently being investigated and expected to be reported in future. In

summary, by applying ^{13}C pathway analysis to investigate microbial metabolism of *S. oneidensis* MR-1 growing in biofilms, we discovered that the activity of C1 metabolism was interestingly higher than that in planktonic cells, which could be related to the utilization of C1 metabolites as electron donor when growing *Shewanella* in biofilms.

Table 3.5.1. Mass distribution of detected metabolites for the ^{13}C tracing experiments (n = 2) [a]

	Biofilm samples		Planktonic samples	
	M-57	**M-159/85**	**M-57**	**M-159/85**
Ala				
M0	0.34	0.35	0.21	0.22
M1	0.59	0.58	0.68	0.70
M2	0.05	0.07	0.09	0.08
M3	0.01		0.02	
Gly				
M0	0.84	0.87	0.85	0.88
M1	0.13	0.13	0.14	0.12
M2	0.03		0.01	
Ser				
M0	0.33	0.39	0.29	0.29
M1	0.58	0.56	0.66	0.66
M2	0.08	0.06	0.04	0.05
M3	0.01		0.01	
Asp				
M0	0.31	0.33	0.23	0.23
M1	0.19	0.25	0.22	0.31
M2	0.22	0.28	0.31	0.31
M3	0.25	0.14	0.21	0.15
M4	0.02		0.02	
Glu				
M0	0.28	0.29	0.19	0.20
M1	0.14	0.16	0.13	0.16
M2	0.17	0.26	0.26	0.33
M3	0.27	0.27	0.31	0.30
M4	0.12	0.03	0.10	0.02
M5	0.02		0.00	

[a] The error in mass distribution from duplicates was <5%.

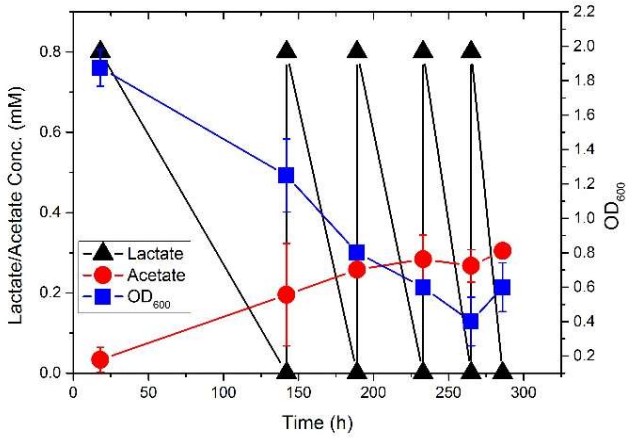

Fig. 3.5.1 Fermentation profile of *S. oneidensis* MR-1 in the sealed bottle reactor.

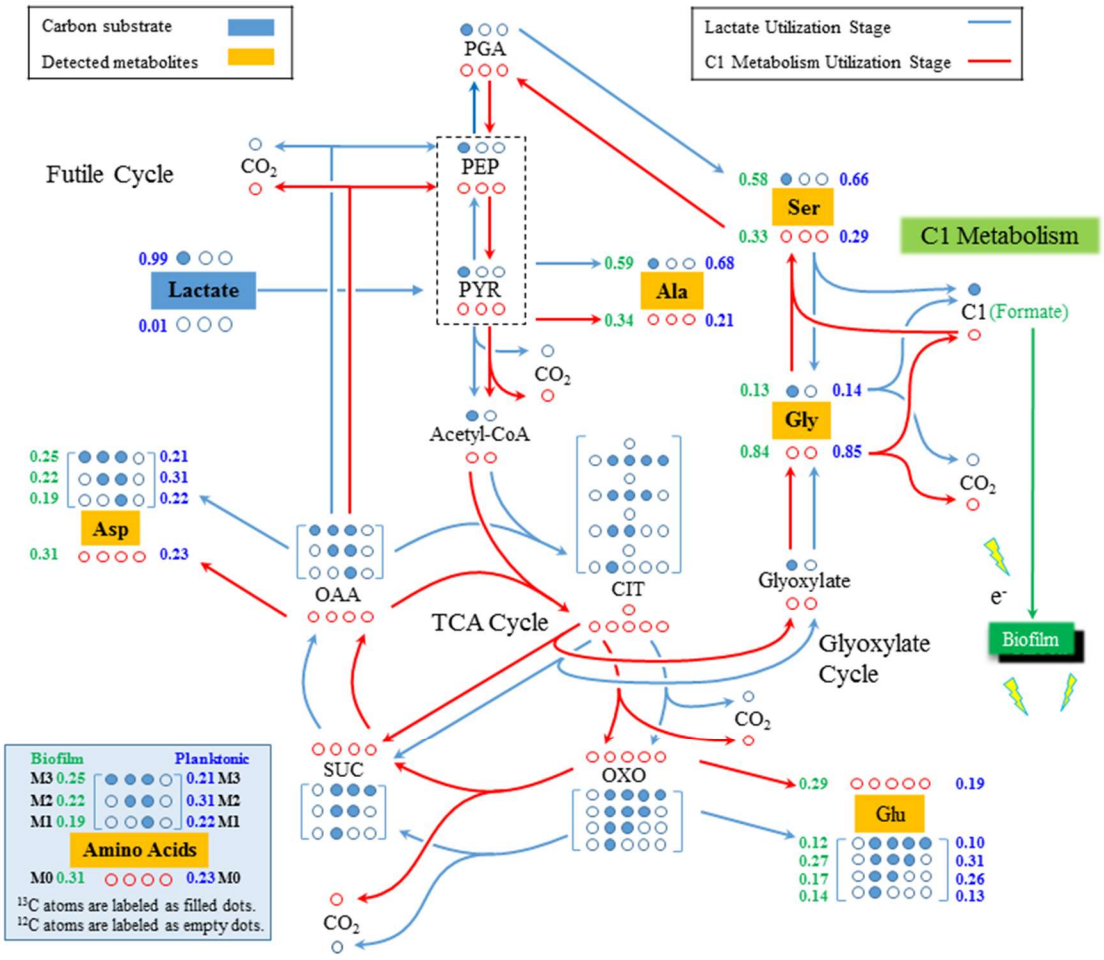

Fig. 3.5.2 Central carbon metabolic pathways of *S. oneidensis* MR-1 from biofilm and planktonic growth. The ^{13}C and ^{12}C atoms were labeled as filled and empty dots, respectively. The lactate utilization pathways were colored as blue while the C1 metabolic pathways were colored as red. The number on the left side of each isotopomer (green) was the M-57 values of proteinogenic amino acids from the biofilm cells while the number on the right side of each isotopomer (blue) was the M-57 value of proteinogenic amino acids from the planktonic cells. Definitions of abbreviations are shown in the List of Abbreviations.

3.6 ^{13}C Pathway Analysis for the Role of Formate in Electricity Generation by *Shewanella oneidensis* MR-1 Using Lactate in Microbial Fuel Cells

Shuai Luo[a, *], Weihua Guo[b, *], Kenneth Nealson[c], Xueyang Feng[b, †], and Zhen He[a, †]

[a] Department of Civil and Environmental Engineering, Virginia Polytechnic Institute and State University, Blacksburg, VA 24061, USA

[b] Department of Biological System Engineering, Virginia Polytechnic Institute and State University, Blacksburg, VA 24061, USA

[c] Department of Earth Sciences, University of Southern California, Los Angeles, CA 90089, USA.

[†]Correspondence to: Xueyang Feng and Zhen He.

[*] LS and WG contribute to this work equally.

Phone: +1-(540)231-2974 and +1-(540)231-1346

Email: xueyang@vt.edu and zhenhe@vt.edu

This manuscript has been published on *Scientific reports* 6, 20941.

Abstract

Microbial fuel cell (MFC) is a promising technology for direct electricity generation from organics by microorganisms. The type of electron donors fed into MFCs affects the electrical performance, and mechanistic understanding of such effects is important to optimize the MFC performance. In this study, we used a model organism in MFCs, *Shewanella oneidensis* MR-1, and ^{13}C pathway analysis to investigate the role of formate in electricity generation and the related microbial metabolism. Our results indicated a synergistic effect of formate and lactate on electricity generation, and extra formate addition on the original lactate resulted in more electrical output than using formate or lactate as a sole electron donor. Based on the ^{13}C tracer analysis, we discovered decoupled cell growth and electricity generation in *S. oneidensis* MR-1 during co-utilization of lactate and formate (i.e., while the lactate was mainly metabolized to support the cell growth, the formate was oxidized to release electrons for higher electricity generation). To our best knowledge, it is the first time that ^{13}C tracer analysis was applied to study microbial metabolism in MFCs and it was proved to be a valuable tool to understand the metabolic pathways affected by electron donors in the selected electrochemically-active microorganisms.

3.6.1 Introduction

Microbial fuel cells (MFCs) are an emerging technology to convert organics in the wastewater to electrical energy[169, 170]. Electrochemically active bacteria (EAB) serve as effective microbial catalysts to transfer electrons from substrates to solid electron acceptors (e.g., anode electrode) under anaerobic conditions of MFCs[171-174]. Electron transferring mechanism between EAB and the electrode is one of the most important steps in electricity generation by MFCs, and can be critically influenced by the type of the electron donors that will result in difference in the composition, structure, and metabolism of microorganisms on the anode electrode[175-177]. Therefore, understanding of the impact from electron donors on electricity generation in MFCs is important to improve the efficiency of energy recovery[178-180].

Shewanellaceae is a typical family including several model bacterial species that can generate electricity in MFCs such as *Shewanella oneidensis* MR-1[177, 181, 182]. *S. oneidensis* MR-1 can transport electrons via intracellular metabolic reactions to complete extracellular electron transfer (EET) pathways[183], via multiple electron-transferring mechanisms including direct contact on the electron acceptor[184], redox reactions of mediators (e.g., flavin) to transfer electrons[185-187], and/or conductive nanowire extension to contact the electron acceptor[188]. Versatile electron transferring abilities allow *S. oneidensis* MR-1 to use multiple organics as electron donors (e.g., lactate, pyruvate, acetate, formate) to process dissimilatory reactions to reduce insoluble metals (e.g. Fe(III), Mn(IV)) and some inorganic ions (e.g., nitrate, nitrite) as electron acceptors[150, 181, 189-191]. Among those electron donors, lactate has been extensively studied. It was found that *S. oneidensis* MR-1 prefers to catabolize lactate because of a

series of internally competent enzymatic reactions that utilize the electron donors to obtain energy for growth and electricity generation[183, 192, 193]. Under anaerobic conditions, including the anaerobic anode of MFCs, lactate can be utilized to release electrons with the involvement of NADH, specific cytochromes, as well as various complexes, and the lactate is further oxidized to acetyl-CoA, and CO_2 or formate[182, 183, 194]. To assess electricity generation efficiency, Coulombic efficiency (CE) and Coulombic recovery (CR) are quantitative indicators to show the fraction of collected electrons through EET versus total ideal electron production[195-197]. It was reported that the lactate-fed MFC inoculated with *S. oneidensis* MR-1 achieved CE at the range about 15-20%[184, 198], where there is still a lot of room to improve electricity generation efficiency.

In addition to lactate, formate is another potentially important electron donor to serve carbon and energy source for *S. oneidensis* MR-1[181, 183, 199]. *S. oneidensis* MR-1 has NAD^+-dependent formate dehydrogenase (FDH) to catalyze the formate oxidation to CO_2, and release electrons to complete EET pathway[182]. On the basis of EET started from lactate and pyruvate utilization, the catabolic metabolism of formate with the help of FDH can release and transfer more electrons to specific electron acceptors, which is possibly helpful to improve CE/CR *of S. oneidensis* MR-1 in MFCs[182, 194]. Thus, it is hypothesized that extra formate addition on lactate utilization can boost the electrical output and improve CE/CR. However, formate is seldom studied for its effect on electricity generation of *S. oneidensis* MR-1 in MFCs.

This study aims to investigate the role of formate for the catabolic metabolism and electricity generation of *S. oneidensis* MR-1 in MFC. Particularly, we applied ^{13}C tracer experiment, which is a method widely used to facilitate the elucidation of metabolic

rewiring in various non-model environmental microorganisms[7, 200, 201]. Normally, by feeding the ^{13}C labeled substrate into culture system, the carbon flow in the intracellular metabolism is traced to produce labeled metabolites (e.g., proteinogenesis amino acids). By analyzing these metabolites using gas chromatography-mass spectrometry (GC-MS) and the following natural isotopic correction of the raw mass spectrums, the isotopic labeling patterns (e.g., mass distribution vector) would be obtained and could be directly analyzed to reveal the metabolic rewiring of the target strains. Our previous study has, for the first time, applied the ^{13}C tracer experiments to a well-designed anaerobic system for revealing the distinct intracellular metabolic behaviors between the biofilm and planktonic *S. oneidensis* MR-1 cells[202]. The ^{13}C tracer experiment successfully revealed the cell metabolisms of *S. oneidensis* MR-1, and a conclusion was made that C1 metabolism such as formate oxidation is strongly related to the electron transferring to the extracellular environment. Therefore, in this study, ^{13}C tracer experiment was applied to help us rigorously analyze the effects of formate on microbial metabolism of *S. oneidensis* MR-1 using lactate for electricity generation in an MFC. As the novel contribution presented in this work, we discovered, for the first time, that the addition of formate in MFCs could indeed synergize with the lactate utilization to improve the electricity generation efficiency, which was achieved by a unique metabolism in *S. oneidensis* MR-1 to decouple cell growth and electricity generation during co-utilization of lactate and formate.

3.6.2 Results and Discussion

Combined Supply of Formate and Lactate Enhanced Current Generation. The MFC was operated for three conditions, each of which was operated for at least three repeated cycles and the current profile was recorded (Fig. 3.6.1). The added formate and

lactate in the anode chamber was completely consumed in each cycle based on the HPLC results, indicating that the current drop at the end of each cycle was caused by the complete consumption of electron donors (Fig. 3.6.1). In the control reactor that did not have electricity generation (electrodes were under an open circuit condition), the electron donors were also consumed, possibly because of oxygen intrusion from the cathode (with continuous aeration) into the control chamber acting as the electron acceptor[203]. Though the oxygen diffusion through cation exchange membrane (CEM) was very limited[204, 205], the electron donor for each cycle could still be consumed up because of very small amount (~ 0.8 mM) of carbon source added into the control and anode chambers. Electricity generation in the MFC clearly competed for electron donors, and the comparable CR (Coulombic recovery) with other MFC studies of *S. oneidensis* MR-1 indicates that the anode electrode has strong ability to compete with oxygen for the electron donors to collect electrons (data of CR were shown in the following section)[184, 198].

The peak current of the MFC was increased from 0.194 ± 0.005 mA using lactate alone to 0.231 ± 0.019 mA with additional formate as the extra electron donor (p<0.05, one-tailed two-sample t-test with unequal variance at α=0.05 for all following statistical tests). Sole supply of formate significantly decreased the peak current to 0.147 ± 0.067 mA, lower than other conditions (p<0.05). When extra lactate was added with formate at the last two cycles, the current was boosted up again, to 0.290 ± 0.056 mA, significantly higher than the current production with sole formate supply (p<0.05). The catholyte pH was stable at 7.2-7.4 due to generally low current output and strong buffering capacity of phosphate buffer saline (PBS) [206], which eliminated the limiting effects of the cathode. The profile of current generation with the combination of formate and lactate is higher than

that with only lactate or formate, indicating that formate and lactate could have achieved synergistic effect when metabolized by *S. oneidensis* MR-1 to benefit the electricity generation in the MFC.

Formate Addition Resulted in Higher Conversion Efficiency. To further understand the impact of formate on the MFC performance containing *S. oneidensis* MR-1, CR (Coulombic recovery) and TC (total coulombs) are used to reflect the conversion efficiency from electron donors to electrical output, with the equations below to calculate both indexes for each cycle (eqs. 1-3) [195-197]:

$$I = \frac{V}{R} \tag{1}$$

$$\text{TC of each cycle} = \sum I * t \tag{2}$$

$$\text{CR for consumption of formate and lactate} = \frac{\sum I*t*1000}{(\Delta C_{Formate}*N_1+\Delta C_{Lactate}*N_2)*V*F} \tag{3}$$

where in Eq. 1, V represents the voltage (V); R is the external resistance (R = 8.2 Ω); where in Eq. 2, t represents the voltage measurement interval (t=120 s) of the digital multimeter; I represents the current (A) measured for each measurement interval, with the assumption that the current is the same within a time interval; and where in Eq. 3, $\Delta C_{Formate}$ and $\Delta C_{Lactate}$ (mM) represent the moles of formate and lactate added into the reactor at the beginning of each cycle, respectively; N_1 and N_2 represent the mole of electrons transferring per mole substrate consumption, respectively, where N_1=2 (formate → CO_2 + $2H^+$ +$2e^-$)[207-209], and N_2=4 (lactate +$2H_2O$ → Acetate$^-$+ HCO_3^- + $5H^+$ +$4e^-$, incomplete oxidation in anaerobic condition) [184, 198, 210, 211]; V represents the reactor volume (0.14L); F represents the Faraday constant (96485 Coulombs per mole electrons).

Combining non-labeled formate and lactate resulted in higher CR of 34.9 ± 6.0 % than that of lactate alone (19.2 ± 0.9 %) (p<0.05), indicating that extra formate addition on

lactate supply can enhance the efficiency of substrate conversion to electrons, which can be ultimately harvested by the solid electron acceptor in the anode chamber (Fig. 3.6.2). Supplying formate as the sole electron donor was found to have a lower CR of 19.3 ± 6.8 % ($p<0.05$) than that condition of combined formate and lactate, suggesting that lactate was also needed for *S. oneidensis* MR-1 to achieve good electron transferring efficiency. The TC with formate addition to lactate was 30.8 ± 5.4 C, much higher than the sum of TC (16.5 ± 2.1 C) via solely supplying formate (5.6 ± 1.9 C) and lactate (10.9 ± 0.2 C) ($p<0.05$) (Fig. 2). These results demonstrate that the increased electricity generation with combined formate with lactate was not simply "1+1=2"; instead, the combination achieved "1+1>2". This further confirms the pivotal role of formate in the electricity generation by *S. oneidensis* MR-1. Lactate is a commonly acknowledged an electron donor in MFCs, being involved in the central metabolism of *S. oneidensis* MR-1[184, 190, 198, 212, 213], while formate is more likely an electron transferring driving stimulus, which is related to the existence of FDH to convert the formate in periplasmic region to CO_2, and finally the electrons are released extracellularly[182, 194, 214]. Therefore, to explain the synergistic effects of lactate and formate in electricity generation in MFCs, we hypothesize that lactate may be more involved in central metabolism while formate may be more related to EET.

^{13}C Tracer Experiments Facilitated the Elucidation of the Role for Formate. To examine our hypothesis, we applied ^{13}C tracer experiment to investigate the intracellular metabolism of *S. oneidensis* MR-1 when metabolizing formate and lactate in the MFC. The addition of ^{13}C formate to non-labeled lactate also improved MFC electricity generation with the peak current of 0.308 ± 0.084 mA (Fig. 3.6.3), suggesting that the labeled formate was also favored by *S. oneidensis* MR-1 to produce electricity. When the labeled formate

was used with non-label lactate, similar improvements in both CR and TC were obtained (Fig. 3.6.2). By examining the corrected mass distribution vectors from the isotopic analysis, no labeled carbon was found in the proteinogensis amino acids (Table. 3.6.1), which are the building blocks for the cell growth of both planktonic and biofilm cells in the MFC. This indicates that formate did not participate in the central metabolism to produce the building blocks for the cell growth. Instead, non-labeled lactate was mainly used for growth of the *S. oneidensis* MR-1. In other words, the cell growth and electricity generation could be decoupled when culturing *S. oneidensis* MR-1 with combined formate and lactate in MFCs. Indeed, it has been reported that lactate was a preferential carbons substrate than formate for cell growth of *S. oneidensis* MR-1. The biomass yield of *S. oneidensis* MR-1 cultivating under oxygen limited conditions reached >0.22 g/g when using lactate as the carbon substrate while only reached <0.11 g/g when using formate as the carbon substrate[215]. On the other hand, the expression levels of FDH genes in *S. oneidensis* MR-1 have been found to be up-regulated in MFCs[214]. Recently, a recombinant *S. oneidensis* MR-1 that harbored additional copies of FDH genes was found to generate electricity at a higher current density[182]. Therefore, it clearly suggested that the pivotal roles of formate played in supplying electrons through FDH in MFCs. Considering the importance of lactate and formate on cell growth and electricity generation, respectively, it is interesting but unsurprising to find in this study that these two carbon substrates could synergize with each other to improve current generation via a decoupled metabolism of cell growth and electricity generation.

According to a proposed pathway shown in Fig. 4, lactate is metabolized in the central metabolism of *S. oneidensis* MR-1 as its favorable substrate for cell growth[181,

182, 184, 190, 194, 198, 212, 213, 216], while formate is more likely used as an electron-transfer driving stimulus from either extracellular exchange or the central metabolism to release the electron in periplasm by FDH[182, 194, 214]. In this scheme, the unlabeled lactate would be directly metabolized via central metabolism to produce various unlabeled building block (e.g., unlabeled amino acids) as we observed, and the labeled formate would be transported into periplasm and oxidized by inner membrane FDH to CO_2 with the release of electrons, and eventually labeled carbon was lost in the form of CO_2 in the MFC system. The released electrons from formate would be further transported by EET to the anode electrode or riboflavin intermediate to enhance electricity generation. Therefore, such decoupled cell growth and electricity generation is responsible for the synergistic improvement of electricity generation with the addition of formate during the lactate uptake by *S. oneidensis* MR-1 in MFCs.

In summary, this study has contributed to an initial understanding of the role of formate in the electricity generation by *S. oneidensis* MR-1 using lactate in MFCs. The results show that the co-supply of two substrates would affect the EET behaviors, and ultimately the electricity generation in the MFC, implying the conception of synergy in substrates. Mutually complementary substrates may take advantage of substrate interaction in the cell metabolism, and generate a total effect greater than the sum of the individual contribution of single substrate for electricity generation. This may raise a question if other combinations of synergistic substrates also exist to enhance the MFC performance for pure or mixed culture. Moreover, ^{13}C tracer experiment proves to be an effective technique to explore the influence of substrates on EET behavior of a selected species. Future studies can target what substrate has greater stimulating effect on EET behavior qualitatively and

quantitatively to potentially improve the electricity generation. It will not only help reveal the pathway of EET and carbon flow, but also formulate a strategy for adjusting substrate combination to achieve optimal electricity generation under a certain special conditions (e.g., known composition of substrates being used for MFC application).

3.6.3 Methods

Bacterial Strains and Growing Conditions in the MFC . *S. oneidensis* MR-1 (kindly provided by Dr. Y.J. Tang's lab, Washington University, St. Louis, MO, USA) was initially grown in the shaking flasks with minimal medium containing 5mM sodium L-lactate (Sigma-Aldrich) for two days at 100 rpm and 30 °C [191, 212]. The culture medium was then transferred to completely fill up the autoclaved anode chamber and the control chamber of the MFC (see Fig. 3.6.S1), where both chambers were operated under oxygen-limited condition at 30 °C.

MFC Setup and Operation. A triple-chamber MFC was constructed by connecting three glass bottles together with two CEMs as separators (UltexCMI7000, Membranes International, Inc., GlenRock, NJ, USA) between each set of two bottles (see Fig. 3.6.S1). The liquid volume of three chambers was 140 mL/each. The middle chamber served as a cathode chamber, while one bottle containing an anode electrode connected to the cathode electrode was the functioning anode and the other bottle (also containing an anode electrode but under the open circuit condition) was the control chamber. The anode and cathode chambers were sealed with creamy epoxy to create oxygen-limited environment. The anode electrode was a piece of rectangular carbon cloth (2.5 cm × 4.5 cm PANEX® 30PW06, Zoltek Corporation, St. Louis, MO, USA), and the cathode electrode using the same carbon cloth coated with platinum/carbon as the catalyst for

oxygen reducing reaction (0.1 mg Pt cm^{-2}). The cathode chamber was continually aerated to provide sufficient oxygen for cathodic reaction. The catholyte was 50 mM PBS (2.65 g L^{-1} KH_2PO_4 and 5.35 g L^{-1} K_2HPO_4), to buffer the catholyte pH to eliminate the limiting effect of cathode.

The MFC was operated under a batch mode with the external resistance of 8.2 Ω. Non-labelled electron donors were first applied, and three conditions were tested: 1) 0.8 mM lactate in 1st - 3rd cycles; 2) 0.8 mM lactate + 0.8 mM formate in 4th - 6th and 14th - 15th cycles; 3) 0.8 mM formate in 7th - 13th cycles. Once the current dropped to the baseline (~ 0.04 mA) in each cycle, the medium in the anode chamber and the control chamber was refreshed by removing 10 mL medium with sterile syringe and then injecting 10 mL fresh filtered (0.22 μm pore size) medium into the chambers. Depending on the substrate, each cycle time period was 16 - 60 hours. To accelerate electron transfer, 0.2 μm riboflavin was added as an electron mediator to the anode and the control chambers at the beginning of the entire experiment (there was no more addition until the end of the experiment).

^{13}C Tracer Experiment. Isotopic-labelled formate as an electron donor was supplied after finishing the cycles with non-isotopic labeled electron donors in the MFC. The combination of 0.8 mM [^{13}C] sodium formate (99% purity, Cambridge Isotope Laboratory, USA) and 0.8 mM non-labeled sodium L-lactate was supplied to the anode and the control chambers at the beginning of a new cycle. After nine-cycle tests, both the liquid culture and carbon cloth in the anode and the cathode chambers were extracted to collect the planktonic and the biofilm cells, respectively, followed by the protocol developed previously for the isotopic analysis of proteiogenic amino acids[202, 217, 218]. In general, the biomass was hydrolyzed using 6 M HCl (20 h at 100 °C). The amino acids

were derivatized in 50 µl of tetrahydrofuran and 50 µL of N-(tert-butyldimethylsilyl)-N-methyl-trifluoroacetamide (Sigma-Aldrich). A gas chromatograph (GC2010, Shimadzu) equipped with a SH-Rxi-5Sil column (Shimadzu) and a mass spectrometer (QP2010, Shimadzu) was used for analyzing the labeling profiles of metabolites. Three types of charged fragments were detected by GC-MS for Ala, Gly, Ser, Asp and Glu: the $[M-57]^+$ group (containing unfragmented amino acids); and the $[M-159]^+$ or $[M-85]^+$ group (containing amino acids that had lost an α-carboxyl group). For each type of fragments, the labeling patterns were represented by M0, M1, M2, etc., which were fractions of non-labeled, singly labeled, and doubly labeled amino acids. The effects of natural isotopes on isotopic labeling patterns were corrected by previously reported algorithms[48].

Data Measurement. The voltage of the MFC was recorded by a digital multimeter (2700, Keithley Instruments, Inc., Cleveland, OH, USA) with measurement interval of 2 min. The concentrations of formate and lactate at the beginning and the end of each cycle were measured by high-performance liquid chromatorgraphy (HPLC) (Shimadzu, Columbia, MD) equipped with an Aminex HPX-87H column (Bio-Rad, Hercules, CA) and refractive index detector (RID, 10A, Shimadzu), with the following program: column temperature, 65℃; mobile phase, 0.5 mM sulfuric acid solution; flow rate, 0.6mL/min. The electrolyte pH was measured by using a pH meter (Oakton Instruments, Vernon Hills, IL, USA).

Acknowledgements

S.L. was supported by a fellowship from Water INTERface IGEP, Graduate School of Virginia Tech. The MFC and isotopic analysis work was financially supported by faculty startup fund (#175323) from Virginia Tech.

Table 3.6.1 Mass distribution vectors of the key proteogenic amino acids.

Cell sources	Anode-biofilm		Anode-planktonic		Control-biofilm		Control-planktonic	
Fragments	**M-57**	**M-159**	**M-57**	**M-159**	**M-57**	**M-159**	**M-57**	**M-159**
Ala								
M0	0.93	0.95	0.96	0.95	0.95	0.95	0.94	0.94
M1	0.06	0.03	0.04	0.02	0.05	0.03	0.05	0.03
M2	0.01	0.03	0.00	0.03	0.00	0.03	0.00	0.03
M3	0.00		0.00		0.00		0.01	
Gly								
M0	1.00	1.00	0.98	0.98	0.95	1.00	0.95	0.97
M1	0.00	0.00	0.02	0.02	0.05	0.00	0.05	0.03
M2	0.00		0.00		0.00		0.00	
Ser								
M0	0.98	0.99	0.97	0.98	0.88	0.94	0.93	0.96
M1	0.04	0.02	0.03	0.02	0.17	0.06	0.06	0.04
M2	0.00	0.00	0.00	0.00	0.00	0.00	0.01	0.00
M3	0.00		0.00		0.00		0.01	
Asp								
M0	0.96	0.94	0.92	0.94	0.84	0.91	0.88	0.93
M1	0.04	0.05	0.09	0.04	0.16	0.05	0.10	0.06
M2	0.00	0.01	0.00	0.00	0.00	0.02	0.03	0.00
M3	0.00	0.01	0.00	0.01	0.00	0.01	0.00	0.01
M4	0.00		0.00		0.00		0.00	
Glu								
M0	0.94	0.98	0.96	0.95	0.92	0.96	0.92	0.89
M1	0.06	0.01	0.03	0.05	0.10	0.03	0.08	0.10
M2	0.00	0.01	0.00	0.00	0.00	0.00	0.00	0.00
M3	0.00	0.00	0.01	0.00	0.01	0.00	0.00	0.00
M4	0.00	0.00	0.00	0.00	0.00	0.00	0.01	0.00
M5	0.00		0.00		0.00		0.00	

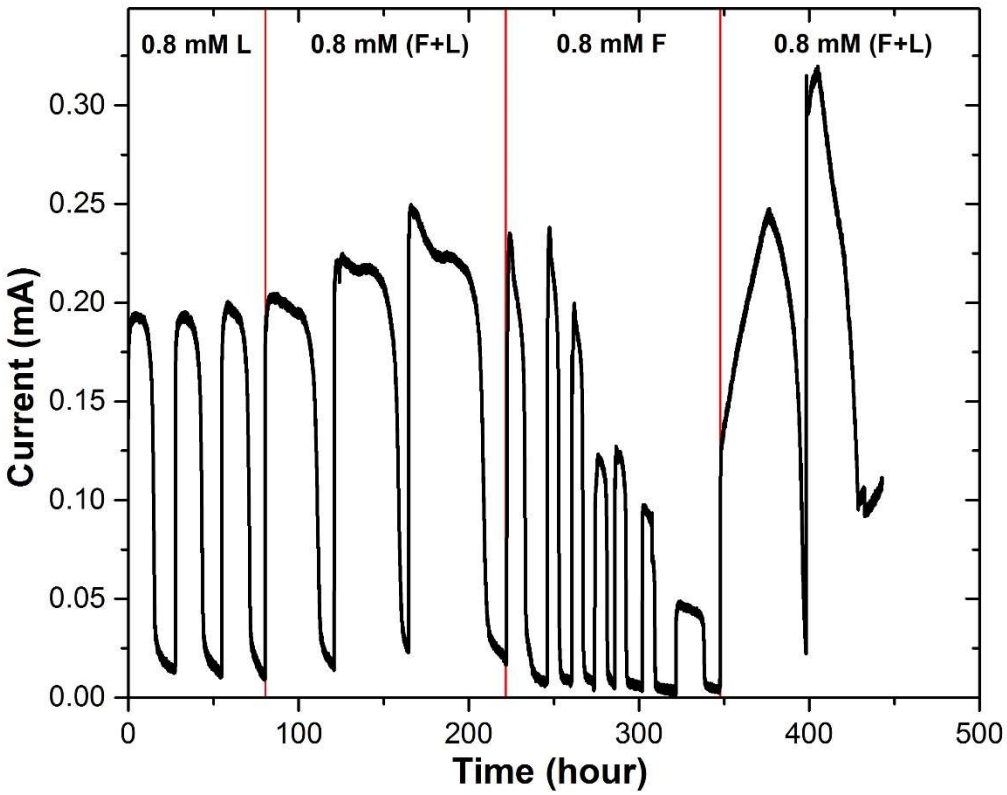

Fig. 3.6.1 Current generation in the MFC supplied with various electron donors. Note: "L" means lactate; "F" means formate; "(F+L)" means addition of both substrate together; "0.8mM" means 0.8 mM of each substrate added each cycle.

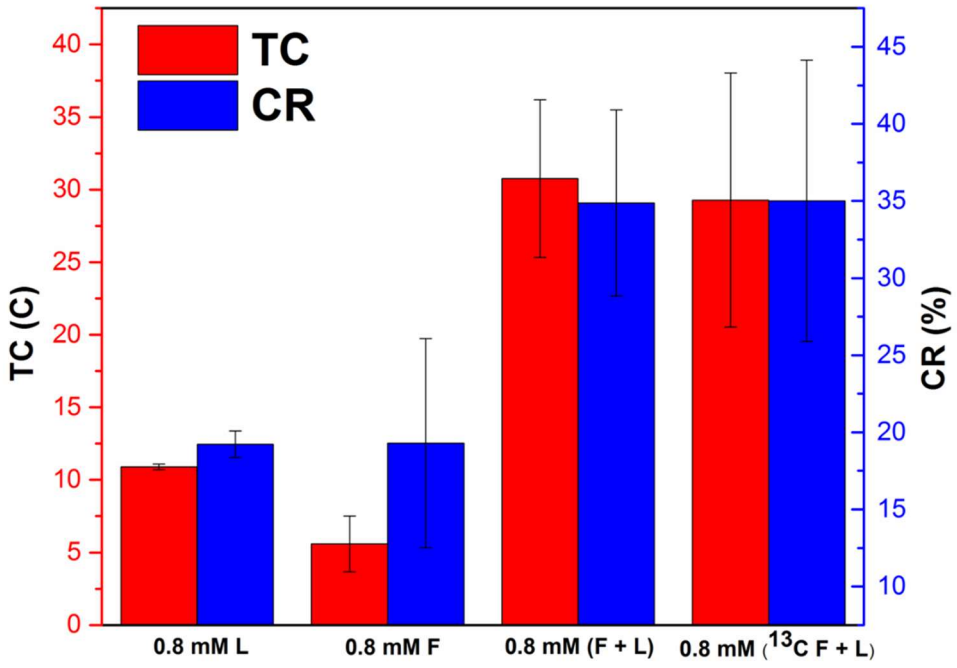

Fig. 3.6.2 CR and TC obtained in the MFC under different supplies of formate and lactate. Note: "L" means lactate; "F" means formate; "(F+L)" means addition of both substrate together; "^{13}C" represents the isotopomer addition; "0.8mM" means 0.8 mM of each substrate added each cycle.

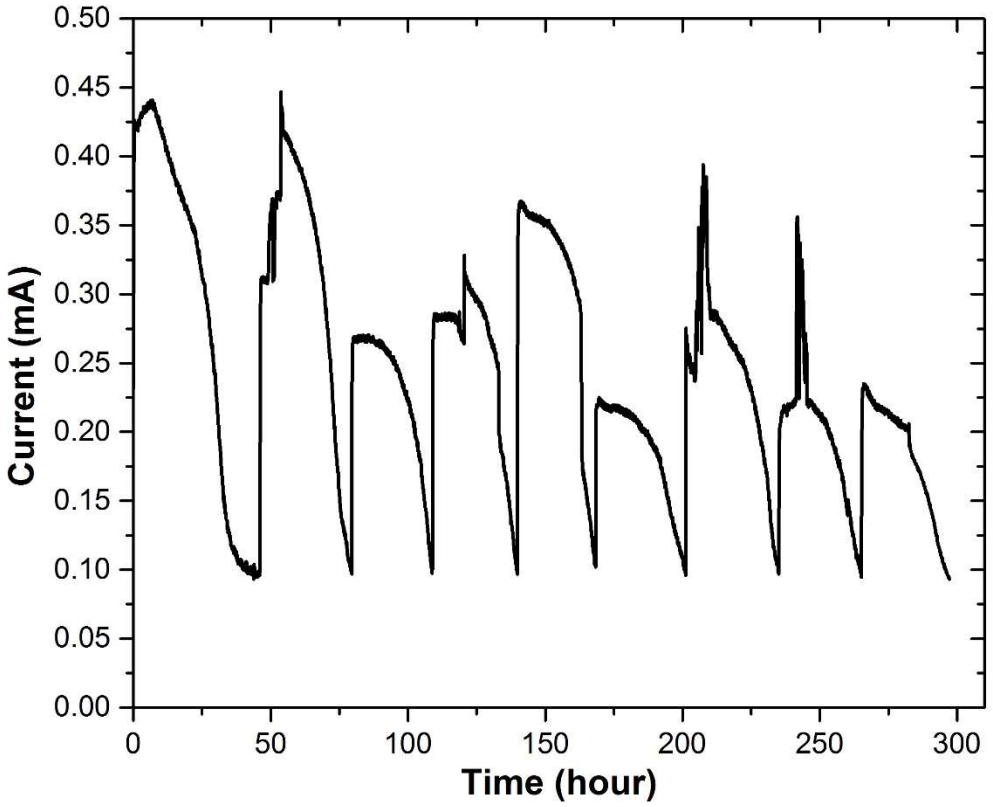

Fig. 3.6.3 Current generation in the MFC supplied with 0.8 mM ^{13}C isotopic formate and 0.8mM non-labelled lactate.

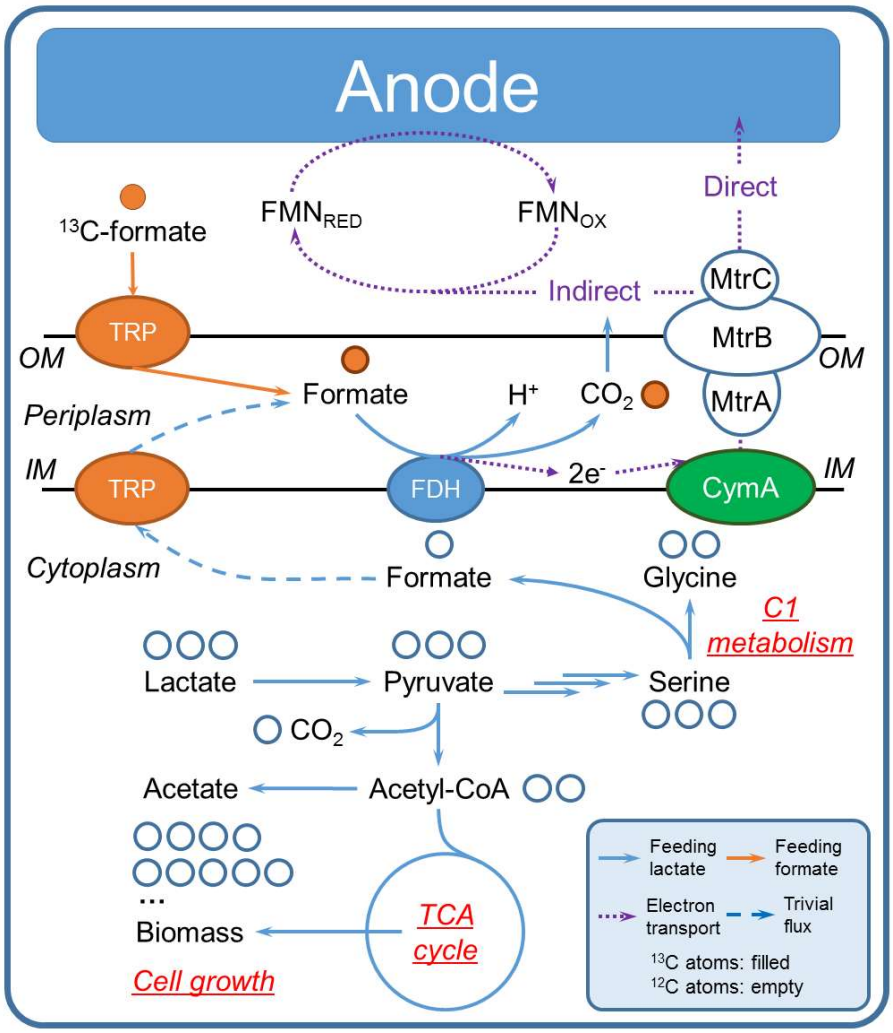

Fig. 3.6.4 Proposed pathway of formate in the metabolism of *S. oneidensis* MR-1 after ^{13}C formate experimental analysis. Definitions of abbreviations are shown in the List of Abbreviations.

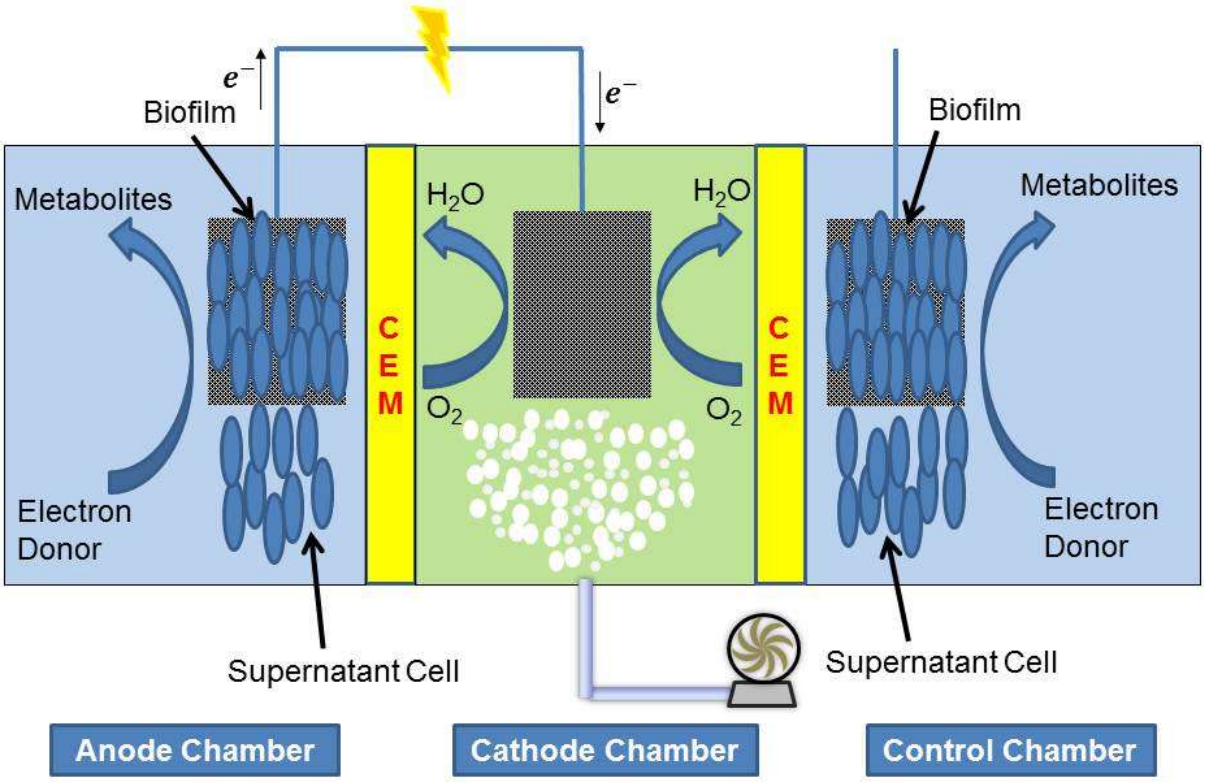

Fig. 3.6.S1 Schematic of a three-chamber system consisting of an anode chamber, a cathode chamber, and a control chamber. The electrodes in the anode and the cathode chambers were connected to form an electrical circuit (functioning MFC).

References

1. Wittmann, C. and E. Heinzle, *Mass spectrometry for metabolic flux analysis.* Biotechnology and Bioengineering, 1999. **62**(6): p. 739-750.
2. Wiechert, W., *^{13}C Metabolic Flux Analysis.* Metabolic Engineering, 2001. **3**(3): p. 195-206.
3. Dauner, M. and U. Sauer, *GC-MS analysis of amino acids rapidly provides rich information for isotopomer balancing.* Biotechnology Progress, 2000. **16**: p. 642-649.
4. de Graaf, A.A., *Use of ^{13}C labelling and NMR Spectroscopy in Metabolic Flux Analysis*, in *NMR in Biotechnology: Theory and Applications*, J.N. Barbotin and J.C. Portais, Editors. 2000, Horizon Scientific Press: Norwich, UK.
5. Christensen, B. and J. Nielsen, *Isotopomer Analysis Using GC-MS.* Metabolic Engineering, 1999. **1**(4): p. 282-290.
6. SZYPERSKI, T., *13C-NMR, MS and metabolic flux balancing in biotechnology research.* Quarterly Reviews of Biophysics, 1998. **31**(01): p. 41-106.
7. Feng, X., et al., *Metabolic pathway determination and flux analysis in nonmodel microorganisms through 13C-isotope labeling.* Methods Mol Biol, 2012. **881**: p. 309-30.
8. You, L., et al., *Metabolic pathway confirmation and discovery through ^{13}C-labeling of proteinogenic amino acids.* J Vis Exp, 2012(59): p. e3583.
9. Sauer, U., *Metabolic networks in motion: ^{13}C-based flux analysis*. Vol. 2. 2006.
10. Tang, Y.J., et al., *Advances in analysis of microbial metabolic fluxes via ^{13}C isotopic labeling.* Mass Spectrometry Reviews, 2009. **28**(2): p. 362-375.
11. Palmqvist, E., et al., *Main and interaction effects of acetic acid, furfural, and p-hydroxybenzoic acid on growth and ethanol productivity of yeasts.* Biotechnology and Bioengineering, 1999. **63**(1): p. 46-55.
12. Heer, D. and U. Sauer, *Identification of furfural as a key toxin in lignocellulosic hydrolysates and evolution of a tolerant yeast strain.* Microbial biotechnology, 2008. **1**(6): p. 497-506.
13. Almeida, J.R.M., et al., *Increased tolerance and conversion of inhibitors in lignocellulosic hydrolysates by Saccharomyces cerevisiae.* Journal of Chemical Technology & Biotechnology, 2007. **82**(4): p. 340-349.
14. Palmqvist, E. and B. Hahn-Hägerdal, *Fermentation of lignocellulosic hydrolysates. I: inhibition and detoxification.* Bioresource Technology, 2000. **74**(1): p. 17-24.
15. Maiorella, B., H.W. Blanch, and C.R. Wilke, *By-product inhibition effects on ethanolic fermentation by Saccharomyces cerevisiae.* Biotechnology and Bioengineering, 1983. **25**(1): p. 103-121.
16. Jönsson, L.J., B. Alriksson, and N.-O. Nilvebrant, *Bioconversion of lignocellulose: inhibitors and detoxification.* Biotechnology for Biofuels, 2013. **6**(1): p. 1-10.
17. Keating, J.D., C. Panganiban, and S.D. Mansfield, *Tolerance and adaptation of ethanologenic yeasts to lignocellulosic inhibitory compounds.* Biotechnology and Bioengineering, 2006. **93**(6): p. 1196-1206.

18. Krebs, H.A., S. Gurin, and L.V. Eggleston, *The pathway of oxidation of acetate in baker's yeast.* Biochemical Journal, 1952. **51**(5): p. 614-628.
19. Palmqvist, E., J.S. Almeida, and B. Hahn-Hägerdal, *Influence of furfural on anaerobic glycolytic kinetics of Saccharomyces cerevisiae in batch culture.* Biotechnology and Bioengineering, 1999. **62**(4): p. 447-454.
20. Sárvári Horváth, I., et al., *Effects of Furfural on the Respiratory Metabolism of Saccharomyces cerevisiae in Glucose-Limited Chemostats.* Applied and Environmental Microbiology, 2003. **69**(7): p. 4076-4086.
21. Hohmann, S. and W.H. Mager, *Yeast stress responses*. Vol. 1. 2003: Springer Science & Business Media.
22. Liu, Z.L., *Molecular mechanisms of yeast tolerance and in situ detoxification of lignocellulose hydrolysates.* Applied Microbiology and Biotechnology, 2011. **90**(3): p. 809-825.
23. Giannattasio, S., et al., *Molecular mechanisms of Saccharomyces cerevisiae stress adaptation and programmed cell death in response to acetic acid.* Frontiers in Microbiology, 2013. **4**.
24. Sousa, M.J., et al., *Stress and Cell Death in Yeast Induced by Acetic Acid*. Cell Metabolism - Cell Homeostasis and Stress Response. 2012.
25. Semchyshyn, H.M., et al., *Acetate but not propionate induces oxidative stress in bakers' yeast Saccharomyces cerevisiae.* Redox Report, 2011. **16**(1): p. 15-23.
26. Lee, Y.J., et al., *TCA cycle-independent acetate metabolism via the glyoxylate cycle in Saccharomyces cerevisiae.* Yeast, 2011. **28**(2): p. 153-166.
27. Bauer, B.E., et al., *Weak organic acid stress inhibits aromatic amino acid uptake by yeast, causing a strong influence of amino acid auxotrophies on the phenotypes of membrane transporter mutants.* European Journal of Biochemistry, 2003. **270**(15): p. 3189-3195.
28. Chen, Y., L. Stabryla, and N. Wei, *Improved acetic acid resistance in Saccharomyces cerevisiae by overexpression of the WHI2 gene identified through inverse metabolic engineering.* Applied and Environmental Microbiology, 2016.
29. Chen, Y., et al., *Transcriptional profiling reveals molecular basis and novel genetic targets for improved resistance to multiple fermentation inhibitors in Saccharomyces cerevisiae.* Biotechnology for Biofuels, 2016. **9**(1): p. 1-18.
30. Mira, N.P., M.C. Teixeira, and I. Sá-Correia, *Adaptive Response and Tolerance to Weak Acids in Saccharomyces cerevisiae: A Genome-Wide View.* OMICS: A Journal of Integrative Biology, 2010. **14**(5): p. 525-540.
31. Zheng, D.-Q., et al., *Drug resistance marker-aided genome shuffling to improve acetic acid tolerance in Saccharomyces cerevisiae.* Journal of Industrial Microbiology & Biotechnology, 2010. **38**(3): p. 415-422.
32. Mira, N.P., et al., *Genome-wide identification of Saccharomyces cerevisiae genes required for tolerance to acetic acid.* Microbial Cell Factories, 2010. **9**(1): p. 1-13.
33. Hasunuma, T., et al., *Metabolic pathway engineering based on metabolomics confers acetic and formic acid tolerance to a recombinant xylose-fermenting strain of Saccharomyces cerevisiae.* Microbial Cell Factories, 2011. **10**(1): p. 1-13.

34. Zhang, J.-G., et al., *Improvement of acetic acid tolerance and fermentation performance of Saccharomyces cerevisiae by disruption of the FPS1 aquaglyceroporin gene.* Biotechnology Letters, 2010. **33**(2): p. 277-284.
35. Jarboe, L.R., P. Liu, and L.A. Royce, *Engineering inhibitor tolerance for the production of biorenewable fuels and chemicals.* Current Opinion in Chemical Engineering, 2011. **1**(1): p. 38-42.
36. Martín, C., et al., *Adaptation of a recombinant xylose-utilizing Saccharomyces cerevisiae strain to a sugarcane bagasse hydrolysate with high content of fermentation inhibitors.* Bioresource Technology, 2007. **98**(9): p. 1767-1773.
37. Lin, F.-M., B. Qiao, and Y.-J. Yuan, *Comparative Proteomic Analysis of Tolerance and Adaptation of Ethanologenic Saccharomyces cerevisiae to Furfural, a Lignocellulosic Inhibitory Compound.* Applied and Environmental Microbiology, 2009. **75**(11): p. 3765-3776.
38. Heer, D., D. Heine, and U. Sauer, *Resistance of Saccharomyces cerevisiae to High Concentrations of Furfural Is Based on NADPH-Dependent Reduction by at Least Two Oxireductases.* Applied and Environmental Microbiology, 2009. **75**(24): p. 7631-7638.
39. Gorsich, S.W., et al., *Tolerance to furfural-induced stress is associated with pentose phosphate pathway genes ZWF1, GND1, RPE1, and TKL1 in Saccharomyces cerevisiae.* Applied Microbiology and Biotechnology, 2006. **71**(3): p. 339-349.
40. Banerjee, N., R. Bhatnagar, and L. Viswanathan, *Inhibition of glycolysis by furfural in Saccharomyces cerevisiae.* European Journal of Applied Microbiology and Biotechnology, 1981. **11**(4): p. 226-228.
41. Taherzadeh, M.J., et al., *Inhibition effects of furfural on aerobic batch cultivation of Saccharomyces cerevisiae growing on ethanol and/or acetic acid.* Journal of Bioscience and Bioengineering, 2000. **90**(4): p. 374-380.
42. Li, B.-Z. and Y.-J. Yuan, *Transcriptome shifts in response to furfural and acetic acid in Saccharomyces cerevisiae.* Applied Microbiology and Biotechnology, 2010. **86**(6): p. 1915-1924.
43. Guo, W., J. Sheng, and X. Feng, *13C-Metabolic Flux Analysis: An Accurate Approach to Demystify Microbial Metabolism for Biochemical Production.* Bioengineering, 2016. **3**(1): p. 3.
44. Feng, X., et al., *Metabolic Pathway Determination and Flux Analysis in Nonmodel Microorganisms Through 13C-Isotope Labeling*, in *Microbial Systems Biology*, A. Navid, Editor. 2012, Humana Press. p. 309-330.
45. Zamboni, N., et al., *^{13}C-based metabolic flux analysis.* Nat. Protocols, 2009. **4**(6): p. 878-892.
46. Chen, Y., L. Stabryla, and N. Wei, *Improved acetic acid resistance in Saccharomyces cerevisiae by overexpression of the WHI2 gene identified through inverse metabolic engineering.* Applied and environmental microbiology, 2016: p. AEM. 03718-15.
47. Feng, X. and H. Zhao, *Investigating xylose metabolism in recombinant Saccharomyces cerevisiae via 13C metabolic flux analysis.* Microbial Cell Factories, 2013. **12**(1): p. 114-123.

48. Wahl, S.A., M. Dauner, and W. Wiechert, *New tools for mass isotopomer data evaluation in 13C flux analysis: mass isotope correction, data consistency checking, and precursor relationships.* Biotechnology and Bioengineering, 2004. **85**(3): p. 259-268.
49. Cvijovic, M., et al., *BioMet Toolbox: genome-wide analysis of metabolism.* Nucleic Acids Research, 2010. **38**(suppl 2): p. W144-W149.
50. Çakir, T., B. Kirdar, and K.Ö. Ülgen, *Metabolic pathway analysis of yeast strengthens the bridge between transcriptomics and metabolic networks.* Biotechnology and Bioengineering, 2004. **86**(3): p. 251-260.
51. Casal, M., H. Cardoso, and C. Leao, *Mechanisms regulating the transport of acetic acid in Saccharomyces cerevisiae.* Microbiology, 1996. **142**(6): p. 1385-1390.
52. Lambert, R.J. and M. Stratford, *Weak-acid preservatives: modelling microbial inhibition and response.* Journal of Applied Microbiology, 1999. **86**(1): p. 157-164.
53. Mumberg, D., R. Müller, and M. Funk, *Yeast vectors for the controlled expression of heterologous proteins in different genetic backgrounds.* Gene, 1995. **156**(1): p. 119-122.
54. Nikawa, J.-i., Y. Tsukagoshi, and S. Yamashita, *Isolation and characterization of two distinct myo-inositol transporter genes of Saccharomyces cerevisiae.* Journal of Biological Chemistry, 1991. **266**(17): p. 11184-11191.
55. Kim, S.-R., et al., *Rational and evolutionary engineering approaches uncover a small set of genetic changes efficient for rapid xylose fermentation in Saccharomyces cerevisiae.* PLOS One, 2013. **8**(2): p. e57048.
56. Bohlmann, J., et al., *Anthranilate synthase from Ruta graveolens. Duplicated AS alpha genes encode tryptophan-sensitive and tryptophan-insensitive isoenzymes specific to amino acid and alkaloid biosynthesis.* Plant Physiol, 1996. **111**(2): p. 507-14.
57. Facchini, P.J., *Alkaloid biosynthesis in plants: biochemistry, cell biology, molecular regulation, and metabolic engineering applications.* Annual Review of Plant Physiology and Plant Molecular Biology, 2001. **52**: p. 29-66.
58. Maeda, H. and N. Dudareva, *The shikimate pathway and aromatic amino acid biosynthesis in plants.* Annu Rev Plant Biol, 2012. **63**: p. 73-105.
59. Evans, J., *Commercial Amino Acids*. 2014, BCC Research Wellesley MA USA. p. 214.
60. Chandran, S.S., et al., *Phosphoenolpyruvate availability and the biosynthesis of shikimic acid.* Biotechnol Prog, 2003. **19**(3): p. 808-14.
61. Niu, W., K.M. Draths, and J.W. Frost, *Benzene-free synthesis of adipic acid.* Biotechnol Prog, 2002. **18**(2): p. 201-11.
62. Kim, B., et al., *Metabolic engineering of Escherichia coli for the production of phenol from glucose.* Biotechnol J, 2014. **9**(5): p. 621-9.
63. Leonard, E., et al., *Engineering central metabolic pathways for high-level flavonoid production in Escherichia coli.* Applied and Environmental Microbiology, 2007. **73**(12): p. 3877-86.

64. Koopman, F., et al., *De novo production of the flavonoid naringenin in engineered Saccharomyces cerevisiae.* Microbial Cell Factories, 2012. **11**(1): p. 155.
65. Shin, S.Y., et al., *Production of resveratrol from tyrosine in metabolically engineered Saccharomyces cerevisiae.* Enzyme Microb Technol, 2012. **51**(4): p. 211-6.
66. Thodey, K., S. Galanie, and C.D. Smolke, *A microbial biomanufacturing platform for natural and semisynthetic opioids.* Nat Chem Biol, 2014. **10**(10): p. 837-44.
67. Curran, K.A., et al., *Metabolic engineering of muconic acid production in Saccharomyces cerevisiae.* Metabolic Engineering, 2012. **15**: p. 55-66.
68. Hansen, E.H., et al., *De novo biosynthesis of vanillin in fission yeast (Schizosaccharomyces pombe) and baker's yeast (Saccharomyces cerevisiae).* Applied and Environmental Microbiology, 2009. **75**(9): p. 2765.
69. Rodriguez, A., et al., *Establishment of a yeast platform strain for production of p-coumaric acid through metabolic engineering of aromatic amino acid biosynthesis.* Metabolic Engineering, 2015. **31**: p. 181-188.
70. Strucko, T., O. Magdenoska, and U.H. Mortensen, *Benchmarking two commonly used Saccharomyces cerevisiae strains for heterologous vanillin-β-glucoside production.* Metabolic Engineering Communications, 2015. **2**: p. 99-108.
71. Karim, A.S., K.A. Curran, and H.S. Alper, *Characterization of plasmid burden and copy number in Saccharomyces cerevisiae for optimization of metabolic engineering applications.* FEMS Yeast Research, 2013. **13**(1): p. 107-116.
72. Caesar, R., et al., *Comparative proteomics of industrial lager yeast reveals differential expression of the cerevisiae and non-cerevisiae parts of their genomes.* PROTEOMICS, 2007. **7**(22): p. 4135-4147.
73. Du, J., et al., *Customized optimization of metabolic pathways by combinatorial transcriptional engineering.* Nucleic Acids Res., 2012. **40**(18): p. e142.
74. Kummel, A., et al., *Differential glucose repression in common yeast strains in response to HXK2 deletion.* FEMS Yeast Res., 2010. **10**(3): p. 322-32.
75. Bochkov, D., et al., *Shikimic acid: review of its analytical, isolation, and purification techniques from plant and microbial sources.* J Chem Biol, 2012. **5**(1): p. 5-17.
76. McQuade, B. and M. Blair, *Influenza treatment with oseltamivir outside of labeled recommendations.* American Journal of Health-System Pharmacy, 2015. **72**(2): p. 112-6.
77. Feng, X. and H. Zhao, *Investigating glucose and xylose metabolism in Saccharomyces cerevisiae and Scheffersomyces stipitis via ^{13}C metabolic flux analysis.* AIChE Journal, 2013. **59**(9): p. 3195-3202.
78. Feng, X. and H. Zhao, *Investigating xylose metabolism in recombinant Saccharomyces cerevisiae via ^{13}C metabolic flux analysis.* Microbial Cell Factories, 2013. **12**: p. 114.
79. Shao, Z., Y. Luo, and H. Zhao, *DNA assembler method for construction of zeaxanthin-producing strains of Saccharomyces cerevisiae.* Methods Mol Biol, 2012. **898**: p. 251-62.

80. Shao, Z. and H. Zhao, *Construction and engineering of large biochemical pathways via DNA assembler.* Methods in Molecular Biology, 2013. **1073**: p. 85-106.
81. Suastegui, M., et al., *Combining Metabolic Engineering and Electrocatalysis: Application to the Production of Polyamides from Sugar.* Angewandte Chemie International Edition, 2016: p. n/a-n/a.
82. Kawai, S., W. Hashimoto, and K. Murata, *Transformation of Saccharomyces cerevisiae and other fungi: methods and possible underlying mechanism.* Bioengineered Bugs, 2010. **1**(6): p. 395-403.
83. Feng, X., et al., *Metabolic pathway determination and flux analysis in nonmodel microorganisms through ^{13}C-isotope labeling.* Methods in Molecular Biology, 2012. **881**: p. 309-30.
84. Wahl, S.A., M. Dauner, and W. Wiechert, *New tools for mass isotopomer data evaluation in (13)C flux analysis: mass isotope correction, data consistency checking, and precursor relationships.* Biotechnol Bioeng, 2004. **85**(3): p. 259-68.
85. Garcia-Albornoz, M., et al., *BioMet Toolbox 2.0: genome-wide analysis of metabolism and omics data.* Nucleic Acids Research, 2014. **42**(Web Server issue): p. W175-81.
86. Moriya, H., Y. Shimizu-Yoshida, and H. Kitano, *In vivo robustness analysis of cell division cycle genes in Saccharomyces cerevisiae.* PLoS Genet, 2006. **2**(7): p. e111.
87. Braus, G.H., *Aromatic amino acid biosynthesis in the yeast Saccharomyces cerevisiae: a model system for the regulation of a eukaryotic biosynthetic pathway.* Microbiol Rev, 1991. **55**(3): p. 349-70.
88. Chen, K., et al., *Deletion of the aroK gene is essential for high shikimic acid accumulation through the shikimate pathway in E. coli.* Bioresource Technology, 2012. **119**: p. 141-147.
89. Cui, Y.Y., et al., *Production of shikimic acid from Escherichia coli through chemically inducible chromosomal evolution and cofactor metabolic engineering.* Microbial Cell Factories, 2014. **13**: p. 21.
90. Liu, D.F., et al., *Metabolic flux responses to genetic modification for shikimic acid production by Bacillus subtilis strains.* Microbial Cell Factories, 2014. **13**(1): p. 40.
91. Fry, B., et al., *Characterization of growth and acid formation in a Bacillus subtilis pyruvate kinase mutant.* Applied Environmental Microbiology, 2000. **66**(9): p. 4045-9.
92. Zhu, T., et al., *Engineering of Bacillus subtilis for enhanced total synthesis of folic acid.* Appl Environ Microbiol, 2005. **71**(11): p. 7122-9.
93. Sprague, G.F., Jr., *Isolation and characterization of a Saccharomyces cerevisiae mutant deficient in pyruvate kinase activity.* J Bacteriol, 1977. **130**(1): p. 232-41.
94. Schaaff-Gerstenschlager, I., et al., *TKL2, a second transketolase gene of Saccharomyces cerevisiae. Cloning, sequence and deletion analysis of the gene.* Eur J Biochem, 1993. **217**(1): p. 487-92.

95. Sprenger, G.A., et al., *Transketolase A of Escherichia coli K12. Purification and properties of the enzyme from recombinant strains.* European Journal of Biochemistry, 1995. **230**(2): p. 525.
96. Patnaik, R. and J.C. Liao, *Engineering of Escherichia coli central metabolism for aromatic metabolite production with near theoretical yield.* Appl Environ Microbiol, 1994. **60**(11): p. 3903-8.
97. Zhang, H., et al., *Engineering Escherichia coli coculture systems for the production of biochemical products.* Proc Natl Acad Sci U S A, 2015. **112**(27): p. 8266-71.
98. Nilsson, U., et al., *Examination of substrate binding in thiamin diphosphate-dependent transketolase by protein crystallography and site-directed mutagenesis.* J Biol Chem, 1997. **272**(3): p. 1864-9.
99. Iraqui, I., et al., *Characterisation of Saccharomyces cerevisiae ARO8 and ARO9 genes encoding aromatic aminotransferases I and II reveals a new aminotransferase subfamily.* Molecular Genetics and Genomics, 1998. **257**(2): p. 238-48.
100. Kim, S.R., et al., *Deletion of PHO13, encoding haloacid dehalogenase type IIA phosphatase, results in upregulation of the pentose phosphate pathway in Saccharomyces cerevisiae.* Appl Environ Microbiol, 2015. **81**(5): p. 1601-9.
101. Lee, K. and J.S. Hahn, *Interplay of Aro80 and GATA activators in regulation of genes for catabolism of aromatic amino acids in Saccharomyces cerevisiae.* Mol Microbiol, 2013. **88**(6): p. 1120-34.
102. Jeffries, T.W., et al., *Genome sequence of the lignocellulose-bioconverting and xylose-fermenting yeast Pichia stipitis.* Nat Biotechnol, 2007. **25**(3): p. 319-26.
103. Kim, B., et al., *Combinatorial design of a highly efficient xylose-utilizing pathway in Saccharomyces cerevisiae for the production of cellulosic biofuels.* Appl Environ Microbiol, 2013. **79**(3): p. 931-41.
104. Carquet, M., D. Pompon, and G. Truan, *Transcription interference and ORF nature strongly affect promoter strength in a reconstituted metabolic pathway.* Frontiers in Bioengeering and Biotechnology, 2015. **3**: p. 21.
105. Isikgor, F.H. and C.R. Becer, *Lignocellulosic biomass: a sustainable platform for the production of bio-based chemicals and polymers.* Polymer Chemistry, 2015. **6**(25): p. 4497-4559.
106. Arantes, V., et al., *Lignocellulosic polysaccharides and lignin degradation by wood decay fungi: the relevance of nonenzymatic Fenton-based reactions.* J Ind Microbiol Biotechnol, 2011. **38**(4): p. 541-55.
107. Arantes, V., J. Jellison, and B. Goodell, *Peculiarities of brown-rot fungi and biochemical Fenton reaction with regard to their potential as a model for bioprocessing biomass.* Appl Microbiol Biotechnol, 2012. **94**(2): p. 323-38.
108. Gao, Z., T. Mori, and R. Kondo, *The pretreatment of corn stover with Gloeophyllum trabeum KU-41 for enzymatic hydrolysis.* Biotechnol Biofuels, 2012. **5**(1): p. 1-11.
109. Vincent, M., A.L. Pometto, 3rd, and J.H. van Leeuwen, *Ethanol production via simultaneous saccharification and fermentation of sodium hydroxide treated corn stover using Phanerochaete chrysosporium and Gloeophyllum trabeum.* Bioresour Technol, 2014. **158**: p. 1-6.

110. Eastwood, D.C., et al., *The plant cell wall-decomposing machinery underlies the functional diversity of forest fungi.* Science, 2011. **333**(6043): p. 762-5.
111. Suzuki, M.R., et al., *Fungal hydroquinones contribute to brown rot of wood.* Environmental Microbiology, 2006. **8**(12): p. 2214-2223.
112. Shimokawa, T., et al., *Production of 2, 5-dimethoxyhydroquinone by the brown-rot fungus Serpula lacrymans to drive extracellular Fenton reaction.* Holzforschung, 2004. **58**(3): p. 305-310.
113. Yelle, D.J., et al., *Multidimensional NMR analysis reveals truncated lignin structures in wood decayed by the brown rot basidiomycete Postia placenta.* Environmental Microbiology, 2011. **13**(4): p. 1091-1100.
114. Varela, E., T. Mester, and M. Tien, *Culture conditions affecting biodegradation components of the brown-rot fungus Gloeophyllum trabeum.* Archives of Microbiology, 2003. **180**(4): p. 251-256.
115. Munir, E., et al., *A physiological role for oxalic acid biosynthesis in the wood-rotting basidiomycete Fomitopsis palustris.* Proceedings of the National Academy of Sciences, 2001. **98**(20): p. 11126-11130.
116. Munir, E., et al., *New role for glyoxylate cycle enzymes in wood-rotting basidiomycetes in relation to biosynthesis of oxalic acid.* Journal of Wood Science, 2001. **47**(5): p. 368-373.
117. Guo, W., et al., *13C pathway analysis of biofilm metabolism of Shewanella oneidensis MR-1.* RSC Advances, 2015. **5**(50): p. 39840-39843.
118. Hollinshead, W.D., et al., *Rapid metabolic analysis of Rhodococcus opacus PD630 via parallel ^{13}C-metabolite fingerprinting.* Biotechnology and Bioengineering, 2015: p. n/a-n/a.
119. Crown, S.B., C.P. Long, and M.R. Antoniewicz, *Integrated ^{13}C-metabolic flux analysis of 14 parallel labeling experiments in Escherichia coli.* Metabolic Engineering, 2015. **28**: p. 151-158.
120. Cordova, L.T. and M.R. Antoniewicz, *13C metabolic flux analysis of the extremely thermophilic, fast growing, xylose-utilizing Geobacillus strain LC300.* Metabolic Engineering.
121. Saunders, E., et al., *Use of 13C Stable Isotope Labelling for Pathway and Metabolic Flux Analysis in Leishmania Parasites*, in *Parasite Genomics Protocols*, C. Peacock, Editor. 2015, Springer New York. p. 281-296.
122. Wasylenko, T.M. and G. Stephanopoulos, *Metabolomic and 13C-metabolic flux analysis of a xylose-consuming Saccharomyces cerevisiae strain expressing xylose isomerase.* Biotechnology and Bioengineering, 2015. **112**(3): p. 470-483.
123. Frick, O. and C. Wittmann, *Characterization of the metabolic shift between oxidative and fermentative growth in Saccharomyces cerevisiae by comparative (13)C flux analysis.* Microbial Cell Factories, 2005. **4**: p. 30-30.
124. Feng, X. and H. Zhao, *Investigating xylose metabolism in recombinant Saccharomyces cerevisiae via 13C metabolic flux analysis.* Microbial Cell Factories, 2013. **12**(1): p. 114.
125. Highley, T., *Influence of Carbon Source on Cellulase Activity of White-rot and Brown-rot Fungi.* Wood and Fiber Science, 1973. **5**(1): p. 50-58.

126. Varela, E. and M. Tien, *Effect of pH and Oxalate on Hydroquinone-Derived Hydroxyl Radical Formation during Brown Rot Wood Degradation.* Applied and Environmental Microbiology, 2003. **69**(10): p. 6025-6031.
127. Feng, X. and H. Zhao, *Investigating xylose metabolism in recombinant Saccharomyces cerevisiae via 13C metabolic flux analysis.* Microb. Cell Fact., 2013. **12**(1): p. 114.
128. Feng, X., et al., *Metabolic flux analysis of the mixotrophic metabolisms in the green sulfur bacterium Chlorobaculum tepidum.* J. Biol. Chem., 2010. **285**(50): p. 39544-39550.
129. Feng, X., et al., *Characterization of the central metabolic pathways in Thermoanaerobacter sp. strain X514 via isotopomer-assisted metabolite analysis.* Appl. Environ. Microbiol., 2009. **75**(15): p. 5001-5008.
130. Wahl, S.A., M. Dauner, and W. Wiechert, *New tools for mass isotopomer data evaluation in 13C flux analysis: mass isotope correction, data consistency checking, and precursor relationships.* Biotechnol. Bioeng., 2004. **85**(3): p. 259-268.
131. Garcia-Albornoz, M., et al., *BioMet Toolbox 2.0: genome-wide analysis of metabolism and omics data.* Nucleic Acids Research, 2014. **42**(Web Server issue): p. W175-W181.
132. Yoon, J.-J., T. Hattori, and M. Shimada, *A metabolic role of the glyoxylate and tricarboxylic acid cycles for development of the copper-tolerant brown-rot fungus Fomitopsis palustris.* FEMS Microbiology Letters, 2002. **217**(1): p. 9-14.
133. Watanabe, T., et al., *Oxalate Efflux Transporter from the Brown Rot Fungus Fomitopsis palustris.* Applied and Environmental Microbiology, 2010. **76**(23): p. 7683-7690.
134. Lodish, H., et al., *Molecular Cell Biology*. Sixth ed. 2007: W. H. Freeman.
135. Gadd, G.M., *Fungal Production of Citric and Oxalic Acid: Importance in Metal Speciation, Physiology and Biogeochemical Processes*, in *Advances in Microbial Physiology*, R.K. Poole, Editor. 1999, Academic Press. p. 47-92.
136. Hisamori, H., et al., *Cloning and expression analysis of a cDNA encoding an oxaloacetate acetylhydrolase from the brown-rot fungus Fomitopsis palustris.* Sustainable humanosphere: bulletin of Research Institute for Sustainable Humanosphere Kyoto University, 2013. **9**: p. 57-64.
137. Connolly, J. and J. Jellison, *Oxalate production and calcium oxalate accumulation by Gloeophyllum trabeum in buffered cultures.* Document-the International Research Group on Wood Preservation (Sweden), 1994.
138. Akamatsu, Y., M. Takahashi, and M. Shimada, *Production of oxalic acid by wood-rotting basidiomycetes grown on low and high nitrogen culture media.* Material und Organismen (Germany), 1994.
139. Tang, J.D., et al., *Short-Read Sequencing for Genomic Analysis of the Brown Rot Fungus Fibroporia radiculosa.* Applied and Environmental Microbiology, 2012. **78**(7): p. 2272-2281.
140. Raven, J.A. and F.A. Smith, *NITROGEN ASSIMILATION AND TRANSPORT IN VASCULAR LAND PLANTS IN RELATION TO INTRACELLULAR pH REGULATION.* New Phytologist, 1976. **76**(3): p. 415-431.

141. Plassard, C. and P. Fransson, *Regulation of low-molecular weight organic acid production in fungi.* Fungal Biology Reviews, 2009. **23**(1–2): p. 30-39.
142. Feng, X. and H. Zhao, *Investigating host dependence of xylose utilization in recombinant Saccharomyces cerevisiae strains using RNA-seq analysis.* Biotechnology for Biofuels, 2013. **6**(1): p. 96.
143. Beliaev, A.S., et al., *Gene and protein expression profiles of Shewanella oneidensis during anaerobic growth with different electron acceptors.* Omics., 2002. **6**(1): p. 39-60.
144. Heidelberg, J.F., et al., *Genome sequence of the dissimilatory metal ion-reducing bacterium Shewanella oneidensis.* Nat. Biotech., 2002. **20**(11): p. 1118-1123.
145. Tang, Y.J., et al., *Shewanella oneidensis MR-1 fluxome under various oxygen conditions.* Appl. Environ. Microbiol., 2007. **73**(3): p. 718-729.
146. McLean, J.S., et al., *Investigations of structure and metabolism within Shewanella oneidensis MR-1 biofilms.* J. Microbiol. Methods, 2008. **74**(1): p. 47-56.
147. Pinchuk, G.E., et al., *Constraint-Based Model of Shewanella oneidensis MR-1 Metabolism: A Tool for Data Analysis and Hypothesis Generation.* PLoS Comput. Biol., 2010. **6**(6): p. e1000822.
148. Tiedje, J.M., *Shewanella: the environmentally versatile genome.* Nat. Biotech., 2002. **20**(11): p. 1093-1094.
149. DiChristina, T., et al., *Shewanella: Novel Strategies for Anaerobic Respiration*, in *Past and Present Water Column Anoxia*, L.N. Neretin, Editor. 2006, Springer Netherlands. p. 443-469.
150. Hau, H.H. and J.A. Gralnick, *Ecology and biotechnology of the genus Shewanella.* Annu. Rev. Microbiol., 2007. **61**: p. 237-258.
151. Fredrickson, J.K., et al., *Towards environmental systems biology of Shewanella.* Nat. Rev. Micro., 2008. **6**(8): p. 592-603.
152. Hau, H.H., et al., *Mechanism and Consequences of Anaerobic Respiration of Cobalt by Shewanella oneidensis Strain MR-1.* Appl. Environ. Microbiol., 2008. **74**(22): p. 6880-6886.
153. Newton, G.J., et al., *Analyses of current-generating mechanisms of Shewanella loihica PV-4 and Shewanella oneidensis MR-1 in microbial fuel cells.* Appl. Environ. Microbiol., 2009. **75**(24): p. 7674-7681.
154. Watson, V.J. and B.E. Logan, *Power production in MFCs inoculated with Shewanella oneidensis MR-1 or mixed cultures.* Biotechnol. Bioeng., 2010. **105**(3): p. 489-498.
155. Renslow, R., et al., *Modeling biofilms with dual extracellular electron transfer mechanisms.* Phys. Chem. Chem. Phys., 2013. **15**(44): p. 19262-19283.
156. Ding, Y., et al., *Disruption of putrescine biosynthesis in Shewanella oneidensis enhances biofilm cohesiveness and performance in Cr (VI) immobilization.* Appl. Environ. Microbiol., 2014. **80**(4): p. 1498-1506.
157. Zhang, Y., et al., *Cell growth and protein expression of Shewanella oneidensis in biofilms and hydrogel-entrapped cultures.* Mol. BioSyst., 2014. **10**(5): p. 1035-1042.
158. Grobbler, C., et al., *Use of SWATH mass spectrometry for quantitative proteomic investigation of Shewanella oneidensis MR-1 biofilms grown on graphite cloth electrodes.* Syst. Appl. Microbiol., 2015. **38**(2): p. 135-139.

159. Tang, Y.J., et al., *Advances in analysis of microbial metabolic fluxes via 13C isotopic labeling.* Mass Spectrom. Rev., 2009. **28**(2): p. 362-375.
160. Newton, G.J., et al., *Analyses of Current-Generating Mechanisms of Shewanella loihica PV-4 and Shewanella oneidensis MR-1 in Microbial Fuel Cells.* Applied and Environmental Microbiology, 2009. **75**(24): p. 7674-7681.
161. Scott, J.H. and K.H. Nealson, *A biochemical study of the intermediary carbon metabolism of Shewanella putrefaciens.* J. Bacteriol., 1994. **176**(11): p. 3408-3411.
162. Serres, M.H. and M. Riley, *Genomic analysis of carbon source metabolism of Shewanella oneidensis MR-1: predictions versus experiments.* J. Bacteriol., 2006. **188**(13): p. 4601-4609.
163. Tang, Y.J., et al., *Anaerobic central metabolic pathways in Shewanella oneidensis MR-1 reinterpreted in the light of isotopic metabolite labeling.* J. Bacteriol., 2007. **189**(3): p. 894-901.
164. Simon, D., J. Hoshino, and H. Kröger, *l-serine dehydrataste from rat liver. Purification and some properties.* BBA Enzymol., 1973. **321**(1): p. 361-368.
165. Grabowski, R., A.E. Hofmeister, and W. Buckel, *Bacterial L-serine dehydratases: a new family of enzymes containing iron-sulfur clusters.* Trends Biochem. Sci., 1993. **18**(8): p. 297-300.
166. Ghannoum, M. and G.A. O'Toole, *Microbial biofilms*. 2004: ASM Press.
167. Thormann, K.M., et al., *Control of formation and cellular detachment from Shewanella oneidensis MR-1 biofilms by cyclic di-GMP.* J. Bacteriol., 2006. **188**(7): p. 2681-2691.
168. Bretschger, O., et al., *Current production and metal oxide reduction by Shewanella oneidensis MR-1 wild type and mutants.* Appl. Environ. Microbiol., 2007. **73**(21): p. 7003-7012.
169. McCarty, P.L., J. Bae, and J. Kim, *Domestic wastewater treatment as a net energy producer–can this be achieved?* Environmental science & technology, 2011. **45**(17): p. 7100-7106.
170. Logan, B.E., et al., *Microbial fuel cells: Methodology and Technology.* Environ. Sci. Technol., 2006. **40**(17): p. 5181-5192.
171. Phuc Thi Ha, Beomseok Tae, and I.S. Chang, *Performance and Bacterial Consortium of Microbial Fuel Cell Fed with Formate.* Energy & Fuels, 2008. **22**: p. 164–168.
172. Li, W., H. Yu, and Z. He, *Towards sustainable wastewater treatment by using microbial fuel cells-centered technologies.* Energy Environ. Sci., 2013. **7**(3): p. 911-924.
173. Rosenbaum, M.A. and A.W. Henrich, *Engineering microbial electrocatalysis for chemical and fuel production.* Curr Opin Biotechnol, 2014. **29**: p. 93-8.
174. Pant, D., et al., *Bioelectrochemical systems (BES) for sustainable energy production and product recovery from organic wastes and industrial wastewaters.* RSC Adv., 2012. **2**(4): p. 1248-1263.
175. He, Z., *Microbial fuel cells: now let us talk about energy.* Environ Sci Technol, 2013. **47**(1): p. 332-3.
176. Schroder, U., *Anodic electron transfer mechanisms in microbial fuel cells and their energy efficiency.* Phys Chem Chem Phys, 2007. **9**(21): p. 2619-2629.

177. Dhere, N.G., et al., *Application of acetate, lactate, and fumarate as electron donors in microbial fuel cell.* 2013. **8825**: p. 1-7.
178. Lovley, D.R., *The microbe electric: conversion of organic matter to electricity.* Curr Opin Biotechnol, 2008. **19**(6): p. 564-71.
179. Clauwaert, P., et al., *Minimizing losses in bio-electrochemical systems: the road to applications.* Applied Microbiology and Biotechnology, 2008. **79**(6): p. 901-913.
180. Kim, B.H., I.S. Chang, and G.M. Gadd, *Challenges in microbial fuel cell development and operation.* Applied Microbiology and Biotechnology, 2007. **76**(3): p. 485-494.
181. Fredrickson, J.K., et al., *Towards environmental systems biology of Shewanella.* Nat Rev Microbiol, 2008. **6**(8): p. 592-603.
182. Mordkovich, N.N., et al., *Effect of NAD+-dependent formate dehydrogenase on anaerobic respiration of Shewanella oneidensis MR-1.* Microbiology, 2013. **82**(4): p. 404-409.
183. Kouzuma, A., et al., *Catabolic and regulatory systems in Shewanella oneidensis MR-1 involved in electricity generation in microbial fuel cells.* Front Microbiol, 2015. **6**.
184. Newton, G.J., et al., *Analyses of current-generating mechanisms of Shewanella loihica PV-4 and Shewanella oneidensis MR-1 in microbial fuel cells.* Appl Environ Microbiol, 2009. **75**(24): p. 7674-81.
185. Marsili, E., et al., *Shewanella secretes flavins that mediate extracellular electron transfer.* Proceedings of the National Academy of Sciences, 2008. **105**(10): p. 3968-3973.
186. Velasquez-Orta, S.B., et al., *The effect of flavin electron shuttles in microbial fuel cells current production.* Appl Microbiol Biotechnol, 2010. **85**(5): p. 1373-81.
187. Roy, J.N., et al., *A study of the flavin response by Shewanella cultures in carbon-limited environments.* RSC Advances, 2012. **2**(26): p. 10020-10027.
188. Gorby, Y.A., et al., *Electrically conductive bacterial nanowires produced by Shewanella oneidensis strain MR-1 and other microorganisms.* Proc Natl Acad Sci U S A, 2006. **103**(30): p. 11358-63.
189. Meshulam-Simon, G., et al., *Hydrogen metabolism in Shewanella oneidensis MR-1.* Applied and environmental microbiology, 2007. **73**(4): p. 1153-1165.
190. Bretschger, O., et al., *Current production and metal oxide reduction by Shewanella oneidensis MR-1 wild type and mutants.* Appl Environ Microbiol, 2007. **73**(21): p. 7003-12.
191. Tang, Y.J., et al., *Evaluation of the effects of various culture conditions on Cr(VI) reduction by Shewanella oneidensis MR-1 in a novel high-throughput mini-bioreactor.* Biotechnol Bioeng, 2006. **95**(1): p. 176-84.
192. Hunt, K.A., et al., *Substrate-level phosphorylation is the primary source of energy conservation during anaerobic respiration of Shewanella oneidensis strain MR-1.* J Bacteriol, 2010. **192**(13): p. 3345-51.
193. Pinchuk, G.E., et al., *Genomic reconstruction of Shewanella oneidensis MR-1 metabolism reveals a previously uncharacterized machinery for lactate utilization.* Proceedings of the National Academy of Sciences, 2009. **106**(8): p. 2874-2879.

194. Pinchuk, G.E., et al., *Pyruvate and lactate metabolism by Shewanella oneidensis MR-1 under fermentation, oxygen limitation, and fumarate respiration conditions.* Appl Environ Microbiol, 2011. **77**(23): p. 8234-40.
195. Qin, M., et al., *Recovery of nitrogen and water from landfill leachate by a microbial electrolysis cell-forward osmosis system.* Bioresour Technol, 2015. **200**: p. 485-492.
196. Ge, Z., et al., *Reducing effluent discharge and recovering bioenergy in an osmotic microbial fuel cell treating domestic wastewater.* Desalination, 2013. **312**: p. 52-59.
197. Ge, Z., Q. Ping, and Z. He, *Hollow-fiber membrane bioelectrochemical reactor for domestic wastewater treatment.* Journal of Chemical Technology & Biotechnology, 2013. **88**(8): p. 1584-1590.
198. Watson, V.J. and B.E. Logan, *Power production in MFCs inoculated with Shewanella oneidensis MR-1 or mixed cultures.* Biotechnol Bioeng, 2010. **105**(3): p. 489-98.
199. Mao, L. and W.S. Verwoerd, *Theoretical exploration of optimal metabolic flux distributions for extracellular electron transfer by Shewanella oneidensis MR-1.* Biotechnology for biofuels, 2014. **7**(1): p. 1-20.
200. Zhuang, L., et al., *Investigating Oxalate Biosynthesis in Wood-decaying Fungus Gloeophyllum trabeum using 13C Metabolic Flux Analysis.* RSC Advances, 2015.
201. Tang, Y.J., et al., *Invariability of central metabolic flux distribution in Shewanella oneidensis MR-1 under environmental or genetic perturbations.* Biotechnology progress, 2009. **25**(5): p. 1254-1259.
202. Guo, W., et al., *13C pathway analysis of biofilm metabolism of Shewanella oneidensis MR-1.* RSC Adv., 2015. **5**(50): p. 39840-39843.
203. Kim, J.R., et al., *Power generation using different cation, anion, and ultrafiltration membranes in microbial fuel cells.* Environmental science & technology, 2007. **41**(3): p. 1004-1009.
204. Freguia, S., et al., *Electron and carbon balances in microbial fuel cells reveal temporary bacterial storage behavior during electricity generation.* Environmental science & technology, 2007. **41**(8): p. 2915-2921.
205. Freguia, S., et al., *Non-catalyzed cathodic oxygen reduction at graphite granules in microbial fuel cells.* Electrochimica Acta, 2007. **53**(2): p. 598-603.
206. Ahn, Y. and B.E. Logan, *Saline catholytes as alternatives to phosphate buffers in microbial fuel cells.* Bioresour Technol, 2013. **132**: p. 436-9.
207. Bandarenka, A.S., et al., *Techniques and methodologies in modern electrocatalysis: evaluation of activity, selectivity and stability of catalytic materials.* Analyst, 2014. **139**(6): p. 1274-1291.
208. Neurock, M., M. Janik, and A. Wieckowski, *A first principles comparison of the mechanism and site requirements for the electrocatalytic oxidation of methanol and formic acid over Pt.* Faraday discussions, 2009. **140**: p. 363-378.
209. Chen, Y.X., et al., *Kinetic isotope effects in complex reaction networks: formic acid electro-oxidation.* Chemphyschem, 2007. **8**(3): p. 380-5.
210. Lanthier, M., K.B. Gregory, and D.R. Lovley, *Growth with high planktonic biomass in Shewanella oneidensis fuel cells.* FEMS Microbiol Lett, 2008. **278**(1): p. 29-35.

211. Yang, Y., et al., *Physiological and electrochemical effects of different electron acceptors on bacterial anode respiration in bioelectrochemical systems.* Bioresour Technol, 2014. **164**: p. 270-5.
212. Tang, Y.J., et al., *Invariability of central metabolic flux distribution in Shewanella oneidensis MR-1 under environmental or genetic perturbations.* Biotechnol Prog, 2009. **25**(5): p. 1254-9.
213. Tang, Y.J., et al., *Anaerobic central metabolic pathways in Shewanella oneidensis MR-1 reinterpreted in the light of isotopic metabolite labeling.* J Bacteriol, 2007. **189**(3): p. 894-901.
214. Wang, V.B., et al., *Metabolite-enabled mutualistic interaction between Shewanella oneidensis and Escherichia coli in a co-culture using an electrode as electron acceptor.* Sci Rep, 2015. **5**: p. 11222.
215. Pinchuk, G.E., et al., *Constraint-based model of Shewanella oneidensis MR-1 metabolism: a tool for data analysis and hypothesis generation.* PLoS Comput Biol, 2010. **6**(6): p. e1000822.
216. Brutinel, E.D. and J.A. Gralnick, *Shuttling happens: soluble flavin mediators of extracellular electron transfer in Shewanella.* Appl Microbiol Biotechnol, 2012. **93**(1): p. 41-8.
217. Feng, X. and H. Zhao, *Investigating xylose metabolism in recombinant Saccharomyces cerevisiae via 13C metabolic flux analysis.* Microb Cell Fact, 2013. **12**(114): p. 1-12.
218. Feng, X., et al., *Characterization of the central metabolic pathways in Thermoanaerobacter sp. strain X514 via isotopomer-assisted metabolite analysis.* Applied and environmental microbiology, 2009. **75**(15): p. 5001-5008.

Chapter 4: OM-FBA: Integrate Transcriptomics Data with Flux Balance Analysis to Decipher the Cell Metabolism

Weihua Guo[a], Xueyang Feng[a, †]

[a] Department of Biological Systems Engineering, Virginia Polytechnic Institute and State University, Blacksburg, VA 24061, United States

[†]Correspondence to: Xueyang Feng.

Phone: +1-(540)231-2974

Email: xueyang@vt.edu

This manuscript has been published on *PloS one* 11 (4), e015418. Supplementary material of Chapter 4 is shown in Appendix C.

Abstract

Constraint-based metabolic modeling such as flux balance analysis (FBA) has been widely used to simulate cell metabolism. Thanks to its simplicity and flexibility, numerous algorithms have been developed based on FBA and successfully predicted the phenotypes of various biological systems. However, their phenotype predictions may not always be accurate in FBA because of using the objective function that is assumed for cell metabolism. To overcome this challenge, we have developed a novel computational framework, namely omFBA, to integrate multi-omics data (e.g. transcriptomics) into FBA to obtain omics-guided objective functions with high accuracy. In general, we first collected transcriptomics data and phenotype data from published database (e.g. GEO database) for different microorganisms such as *Saccharomyces cerevisiae*. We then developed a "Phenotype Match" algorithm to derive an objective function for FBA that could lead to the most accurate estimation of the known phenotype (e.g. ethanol yield). The derived objective function was next correlated with the transcriptomics data via regression analysis to generate the omics-guided objective function, which was next used to accurately simulate cell metabolism at unknown conditions. We have applied omFBA in studying sugar metabolism of *S. cerevisiae* and found that the ethanol yield could be accurately predicted in most of the cases tested (>80%) by using transcriptomics data alone, and revealed valuable metabolic insights such as the dynamics of flux ratios. Overall, omFBA presents a novel platform to potentially integrate multi-omics data simultaneously and could be incorporated with other FBA-derived tools by replacing the arbitrary objective function with the omics-guided objective functions.

4.1 Introduction

Cell metabolism is regulated over multiple levels with the participation of various types of cell components[1], e.g., gene expression via transcription process and the protein synthesis via translation and post-translational modification (Fig. 4.1), which mystifies genotype-phenotype correlations. Since the phenotype is the net result of these interactions, it is immensely important to unveil the different cell components and their interactions, not only for an integrated understanding of physiology, but also for the practical applications of biological systems as cell factories[2-4]. High-throughput omics data provides quantitative readouts of these cell components, including the cell's DNA sequence (i.e., genomics[5, 6]), mRNA expression (i.e., transcriptomics[7]), metabolite abundance (i.e., metabolomics[8, 9]), protein composition (i.e., proteomics[10-12]), and *in vivo* enzyme activities (i.e., fluxomics[13, 14]). This valuable biological information enables the identification and quantification of individual components of a biological system, and we are now facing the challenge of understanding the interactions among these components[1, 15] by appropriately analyzing and interpreting the omics data.

Metabolic modeling is the computational approach widely used for modeling complex metabolic networks and predicting cell phenotype based on the stoichiometric constraints of the metabolic reactions. One of the most commonly used approaches is flux balance analysis (FBA)[16], in which a genome-scale metabolic model is supplied in the form of a stoichiometric matrix that conveys the molecularity of each metabolite in each reaction. This is then followed by the identification of an arbitrary objective function to optimize, due to the underdetermined FBA system. Since the early 1990s, FBA has been widely used to simulate cell phenotypes with tremendous success because of its genome-

scale estimation and fast computation speed [16-18]. However, the arbitrary objective function remains problematic and sometimes leads to inaccurate phenotype predictions [16, 19]. To integrate the FBA approach with the omics data, several FBA-derived algorithms have been developed for phenotype prediction with one or two types of omics data. These algorithms can be broadly classified into two categories [20, 21]: 1) the switch approach (e.g., GIMME[22] and iMAT[23]), which turns reaction fluxes on or off based on threshold gene expression levels, and 2) the valve approach (e.g., E-Flux[24] and PROM[25]), which regulates reaction fluxes based on relative gene/protein expressions. One of the fundamental limitations for all of these approaches is that all make the underlying assumption that gene transcription is linearly correlated with the flux of the reactions that they encode[26]. This correlation has been found to be inaccurate by many physiological studies of cells [21, 27, 28]. In addition, most of these algorithms can integrate transcriptomics only or transcriptomics and proteomics only [27, 29]. To our best knowledge, no algorithm can simultaneously integrate multi-omics data for phenotype prediction so far. Therefore, to intently overcome the ill-defined assumptions of the genotype-phenotype correlation and to potentially integrate multi-omics data for phenotype prediction, we develop a novel FBA-derived algorithm, omFBA, to correlate the genotype, e.g., transcriptomics data, with the phenotype, e.g., growth rate and product yields, by using an omics-guided objective function.

In general, we implemented a proof-of-concept study for this novel algorithm, omFBA, to accurately predict the phenotype of a model eukaryotic microorganism, *Saccharomyces cerevisiae*, by integrating the transcriptomics data with FBA via the omics-guided objective function (Fig. 4.2). We first collected the transcriptomics data, i.e.,

exponential fold changes of gene expression levels, and the corresponding phenotype data, i.e., ethanol yields, from the GEO database and previous publications [30]. We randomly separated the datasets into two equal parts: one part was used to develop the omics-guided objective function; and the other part was used to validate the omics-guided objective function by applying the transcriptomics data to predict cell phenotypes and comparing them with the observed phenotypes. We found that omFBA accurately predicted the ethanol yields in most of the cases tested (>80%) and provided valuable insights of yeast metabolism such as the key flux ratios that were consistent with previous ^{13}C-MFA studies [31-33]. In sum, the novel algorithm we developed in this study, omFBA, could accurately predict cell phenotypes, and more importantly, provide in-depth understanding of the interactions between transcriptomics and phenotypes, which could be extended for various cell components to help achieve better understanding of cell metabolism.

4.2 Results

4.2.1 Overview of omFBA Algorithm

To develop and validate omFBA algorithm as a novel approach to integrate transcriptomics data with FBA via omics-guided objective function, we have designed a computational platform with four modules: 1) transcriptomics-phenotype data collection, 2) "phenotype match" algorithm, 3) omics-guided objective function in FBA, and 4) phenotype data validation. In brief, in Module 1, we collected the transcriptomics-phenotype correlated data from a published study, curated the data based on *p*-value, smoothed the data, and randomly separated all the datasets into two equal parts, i.e., training and validation datasets, for the development and validation of omFBA algorithm, respectively. In Module 2, we developed the "phenotype match" algorithm by first using a

dual objective function, with unknown weighting factors assigned to minimizing overall enzyme usage and maximizing ethanol yield, to simulate the cell phenotype; then searched for the "phenotype matched" weighting factors that could lead to the best fitting of cell phenotypes in the training datasets; and finally, quantitatively correlated these "phenotype matched" weighting factors with the transcriptomics data from the training datasets via multivariate regression. Next in Module 3, we applied such empirical correlation between the transcriptomics data and the "phenotype matched" weighting factors in the dual objective function in FBA, together with the transcriptomics data from validation datasets, to derive the omics-guided objective function. We then used this omics-guided objective function in the genome-scale metabolic model of *S. cerevisiae* to predict the ethanol yields and to provide in-depth biological insights, e.g., key flux ratios. In Module 4, we compared our predicted ethanol yields that were derived from transcriptomics data with the observed ones in the validation datasets for evaluation of the prediction accuracy of omFBA algorithm. We also validated the biological insights implicated by the omFBA algorithm by comparing them with the experimental discoveries from ^{13}C-metabolic flux analysis (^{13}C-MFA). To ensure our algorithm is statistically reliable, we have repeated the Module 1~4 for 40 times by randomly assigning different training and validation datasets. The detailed development of each module was shown in the following sections.

4.2.2 Module 1: Transcriptomics-Phenotype Data Collection

We have collected the transcriptomics-phenotype correlated data from a published study[30], in which Ronen and Botstein studied transcriptomics responses of *S. cerevisiae* for the substrate shift from the unfavorable galactose to favorable glucose at low and high concentrations (i.e., 0.2 g/L and 2g/L, respectively) at different time points. The

transcriptomics responses were measured by microarray and represented by the fold changes of gene expression levels of all the detectable genes (>6300 genes) after the substrate shift. We collected all these data from the GEO database (GSE4158) as the "big" gene pool for omFBA algorithm by running the GEO2R web tool [34]. Comparing to this "big" gene pool, a "small" gene pool was also defined by Ronen and Botstein [30], who selected a small set of genes that could play deciding roles in determining the yeast metabolic responses to substrate shift. We also extracted transcriptomics data of the same genes from the paper as the "small" gene pool to implement the omFBA algorithm for evaluating the impacts of transcriptomics data on the omFBA algorithm. The glucose-based ethanol yields were selected as phenotype in this study, since no other phenotype but ethanol yield was provided in the experimental data.

The *p*-values of all transcriptomics data were also collected to reflect the data quality. To filter the low-quality data, we selected the cutoff *p*-value as 0.95, the same cutoff value used in the published paper [30]. That is to say, we only used the genes that had differentiated expression level with $p<0.95$ to develop omFBA. The corresponding phenotype data, i.e., ethanol yields, was collected and calculated from the Fig 1 of the published paper, which showed the fermentation profiles after the substrate shift. We found only 8 time points were available with *p*-value-filtered transcriptomics data and the corresponding phenotype data, which captured the dynamics of transcriptional responses and phenotype changes but were not enough for developing omFBA algorithm. We have used a prebuilt function namely 'csaps' in MATLAB to smooth the kinetic profile of gene expression data and phenotype data, based on the raw data of gene expression and phenotype at the 8 time points. In general, we used cubic smoothing spline to provide a

smoothed curve with 1000 points to capture the shape of the temporal gene expression and phenotype. In this case, we could overcome the limitation of lacking gene expression data for training our OM-FBA algorithm while still maintaining the high fidelity of the kinetic profile of gene expression and phenotype. We randomly chose 500 datasets as the training datasets while the remaining 500 datasets were used for model validation.

4.2.3 Module 2: "Phenotype-Match" Algorithm

Using the training datasets developed in Module 1, we developed the "phenotype match" algorithm as a bi-level FBA algorithm to find the optimal objective function that leads to accurate simulations of the observed phenotypes. To achieve this, we first selected a dual objective function that included two items: minimizing overall enzyme usage (i.e., $\min \sum v_i^2$) and maximizing ethanol yield (i.e., $\max v_{EtOH}$), indicating the trade-off between the overall enzyme activities and the ethanol production. The similar dual objective function was previously applied to successfully predict growth kinetics of *Shewanella oneidensis* [35]. The weighting factors of these two items were unknown. However, by fine-tuning the weighting factors, we could match the phenotype predicted by FBA with the observed phenotype very well. As shown in Fig. 4.3, a good fitting was observed from the carbon metabolism shift in both low and high glucose conditions, which proved that it is feasible for the "phenotype match" algorithm to find the suitable objective functions in FBA. In addition, we correlated the observed ethanol yields with the phenotype-matched weighting factors in front of minimizing overall enzyme usage for both low and high glucose conditions, and found that a negative correlation was discovered between the weighting factors and ethanol yields. In general, when the weighting factor of minimizing overall enzyme usage increased, the ethanol production decreased, which was consistent

with trade-off between the overall enzyme activities and the ethanol production. We found the flux towards biomass formation were zero when using the bi-level optimization for minimizing enzyme usage and maximizing ethanol production. This is consistent with the experimental data since no significant change was found in cell number and size (10%) during the glucose pulse experiments [30]. In comparison, we have also implemented the FBA by applying two commonly used objective functions: maximizing the growth rate, and maximizing the ethanol yield (Fig. C.S1). The simulated ethanol yield was 0.11 g ethanol/g glucose when maximizing the growth rate, which underestimated the ethanol production in the real experiments. The simulated ethanol yield was 0.51 g ethanol/g glucose when maximizing the ethanol yield, which overestimated the ethanol production in the real experiments.

With this appropriately selected dual-objective function and the phenotype-matched weighting factors, we next calculated the correlation coefficients between these weighting factors and the transcriptomics data for each gene in both the "big pool" and the "small pool", respectively. We ranked all of the genes based on the correlation coefficients, and picked the top 3 genes with the highest absolute values of the correlation coefficients as the genetic markers (Fig. 4.4). We then applied the multiple linear regression approach to quantitatively correlate the phenotype-matched weighting factors and the expression levels of the genetic markers. The regression equation, which represents the quantitative correlation of the transcriptomics and the phenotype, was calculated and used next in Module 3 to derive the omics-guided objective function.

4.2.3 Module 3 and 4: Application and Validation of Omics-Guided Objective Function

With the regression equation derived in Module 2 to connect the expression levels of the genetic markers and the weighting factors used in the dual objective function of FBA, we could use the transcriptomics data in the validation datasets to derive the so-called "omics-guided objective function" for phenotype prediction. In general, we collected the expression levels of the genetic markers in each of the validation datasets, applied the regression equation to derive the weighting factors for the dual objective function, and then used the dual objective function in a well-established genome-scale metabolic model, iND750 [36, 37], to predict the ethanol yields.

We derived the omics-guided objective function for both the "big pool" and "small pool" of genes, respectively, in both low and high glucose conditions. For each of the 500 validation datasets, we checked the predicted ethanol yield and the observed ones. As mentioned previously, we randomly assigned the 1000 datasets into 500 training datasets and 500 validation datasets, and repeated this procedure for 40 times to make sure our predictions were statistically reliable. As shown in Fig. 4.5, we found that for all of the 40 rounds of predictions, we could obtain 80~85% (Fig 5C) and 47~63% (Fig 5D) match (i.e., <5% difference) between the predicted and observed ethanol yields when using the "big pool" of genes for deriving the omics-guided objective function to simulate glucose metabolism at low and high concentrations, respectively. When using the "small pool" of genes, 67~77% (Fig. 4.5C) and 20~25% (Fig. 4.5D) match (i.e., <5% difference) between the predicted and observed ethanol yields were observed for glucose metabolism at low and high concentrations, respectively. In addition, we also plotted the raw data of ethanol

yields (i.e., the 8 datasets that were originally collected from Ronen and Botstein 's work) versus the predicted ones in low (Fig. 4.5A) and high (Fig. 4.5B) glucose conditions and found that using either "big pool" or "small pool" of genes could lead to good fittings (R^2>0.80). It is also worth noting that the prediction accuracy for the low and high glucose condition was different. While at least 65% match with the experimental data could be achieved at low glucose condition, only 60% match at best could be achieved at high glucose condition. We have examined the reason for the difference of the prediction between low and high concentration data. We found that at the low glucose condition, ~10% of the genes had strong correlations with phenotype-matched weighting factors with the absolute value of the correlation coefficient > 0.9 (Fig.4. S2). However, at the high glucose condition, <1% of the genes had strong correlations with phenotype-matched weighting factors with the absolute value of the correlation coefficient > 0.9. Therefore, the poor correlation between gene expression and the phenotype-matched weighting factors could account for the lower match at the high glucose condition.

Since the accuracy of omFBA was not satisfactory (<60% matches) when using "small pool" of genes to predict yeast metabolism in low and high glucose condition, we next tried to investigate the factors that could affect the omFBA prediction. One factor that could potentially affect the omFBA prediction is the noisy gene expressions, which is notoriously known by biologists for decades [38-41]. To examine the impact of the variability of transcriptomics data on the omFBA algorithm, we chose three different cutoff *p*-values, i.e., 0.05, 0.67, and 0.95, to represent different variability levels of the transcriptomics data for the genes in the "small pool". By filtering the transcriptomics data using the selected cutoff *p*-values, we re-ran omFBA for 40 times and compared the

prediction accuracy in p=0.05, 0.67 and 0.95, respectively. As shown in Fig. 4.6, the prediction accuracy for ethanol yields under both low and high glucose conditions dramatically increased when we chose a smaller cutoff p-value, with >60% ethanol yields in the validation datasets could be well matched (<5% difference) with the observed ethanol yields at p=0.05. This clearly suggested that the quality of transcriptomics data could be a deciding factor for accurate prediction of cell metabolism when using omFBA. With the breakthroughs in high-throughput, high-accuracy analytical methods for omics analysis, we envision the demand for high-quality omics data would be well met in very near future.

Overall, omFBA could predict the ethanol yields solely from the transcriptomics data via the development of "omics-guided objective function". It is interesting to notice that using "big pool" of genes led to much better accuracy than using "small pool" of genes, indicating that there were still many unknown regulons in *S. cerevisiae* that played pivotal roles in controlling yeast metabolism but have not yet been fully studied. In addition to the accurate predictions of the phenotypes, omFBA could also provide valuable biological insights, e.g., dynamics of flux ratios, to unravel the intracellular metabolic rewiring. Here in this study, we selected and calculated four key flux ratios, namely PGI/G6PDH2, FBA/TKT1, ENO/PPCK, and PYK/PDC, which controlled the flux distribution in the central metabolism (Fig. 4.7). To study the key metabolic responses to the substrate shift in *S. cerevisiae*, we have correlated these key flux ratios with the "phenotype matched" weighting factors, observed ethanol yields, and the ratios of corresponding gene expressions. We found clear trends between the key flux ratio and the ethanol production. In general, when the ethanol production was increased, the ratios of glycolysis to the

pentose phosphate pathways were decreased, while the ratios of glycolysis to the futile cycle and the fermentation pathway were increased. Such observations were consistent with the previous ^{13}C-MFA studies on yeast metabolism [32, 33, 42] (Table 4.1). However, no correlations between the flux ratios and gene expression ratios were observed for either low or high glucose concentration. Such poor correlation between gene expression and metabolic fluxes has been proved by previous reports [31], and emphasized the merit of developing novel algorithm like omFBA that does not rely on the assumption of correlated gene expression and metabolic fluxes. Since the growth rates from ^{13}C-MFA studies were not exactly the same as what we observed in this study because of the different experimental set-up, e.g., culture mode (batch culture or chemostate) and growth condition (medium, sugar concentration), we did not directly compare the growth rate between our studies and the ^{13}C-MFA studies.

4.3 Discussion

4.3.1 Comparison between omFBA Algorithm and the "Big Data" Regression Approach

With the abundance of transcriptomics-phenotype datasets, a natural question one may ask is how good (or bad) is omFBA when compared to regression approach using the "big data". In brief, we could also design an algorithm using the "big data" to directly correlate the ethanol yields and the transcriptomics data in the training datasets and apply the regression equation to predict the ethanol yields solely from the transcriptomics data in the validation datasets, similarly as we did for omFBA. In fact, we have implemented such "Big Data" regression approach (Appendix C Fig. C.S3) and found that the ethanol yields could indeed be accurately predicted (e.g., 82-90% matches when using "big pool" of genes

in low glucose concentration, and 80-85% matches when using "big pool" of genes in high glucose concentration, Appendix C Fig. C.S4). Comparing omFBA to the "Big Data" regression approach, we found that the prediction accuracy of omFBA was similarly good. When comparing the genetic markers used by omFBA and the **"**Big Data" regression approach (Appendix C Table C.S1)**,** we indeed found some genes were used as the genetic markers in both approaches (Appendix C Fig. C.S5**)**, which could explain the good fittings generated from both approaches. However, one distinct advantage of omFBA compared to "Big Data" approach **is** the capability to provide valuable and reliable biological insights, such as the dynamics of flux ratios as shown in Fig. 4.7. Rather than simply fitting the cell phenotypes, omFBA also provides a way to investigate the complex gene-flux-phenotype cross talking by developing the omics-guided objective functions. Such information is particularly useful since it could decipher the interactions of various cell components and rationally guides the metabolic engineering of organisms.

In this study, we chose the top 3 genes whose expression levels were most correlated with the phenotype-matched weighting factors as our important factors. Because little is known about the how exactly the genetic markers influenced the phenotype-matched weighting factors, it is possible that the some genetic markers, which played important roles in affecting phenotype-matched weighting factors but had expression levels not well correlated with the phenotype-matched weighting factors, could be left out (i.e., omitted-variable bias). However, we would like to emphasize that purpose of this proof-of-concept study is not to develop a "perfect" model to completely decipher the mechanism of how gene expression and cell phenotype are linked. Instead, this study offered a novel

route to explore the possibility of using transcriptomics data to predict some of the metabolic behaviors (e.g., ethanol production).

4.3.2 Prerequisites of omFBA Algorithm

It is worth noting that one of the prerequisites for developing omFBA algorithm is the abundant, curated, and correlated omics-phenotype datasets, which, unfortunately, are not often available. Currently, many of the database constructed only collected one type of omics data, e.g., Gene Expression Omnibus (GEO)[34, 43-45], the European Bioinformatics Institute (EBI)[46, 47], and Many Microbe Microarrays Database (M3D)[48] for collecting gene expression data; and from the Proteomics DB[49] for collecting proteomics data. Although thousands of datasets are enabled for users to query for omics analysis (e.g., transcriptomics analysis), these datasets cannot provide the details about the phenotype such as cell growth rate, and hence, have limited applications in elucidating the correlations between transcriptomics and phenotype of microorganisms. To overcome this challenge, we have done some preliminary studies to construct the correlated omics-phenotype database, namely integrated Transcriptomic And Phenotype (iTAP) database [50], to collect the transcriptomics-phenotype correlated data. Despite the fact that the phenotype data was never reported in a standardized format and the curation of correlated transcriptomics–phenotype datasets was extremely tedious and time-consuming, till now, we have successfully correlated 57 and 143 datasets of transcriptomics and phenotype for *E. coli* and *S. cerevisiae*, respectively. As the first of its kind, the iTAP database was suitable for omFBA to provide sufficient data and allow the direct phenotype prediction from the transcriptomics analysis. We are planning to use more datasets from the iTAP database that we constructed to apply omFBA. However, one challenge in

extending omFBA to other studies is the incompleteness of the meta-data. Basically, when we constructed the iTAP database, we found that many of the studies only reported the data that was most interested to the authors, e.g., growth rates alone, and left out the rest of the valuable information such as glucose consumption rates and ethanol production rates. The paper published by Ronen and Botstein was so far the most complete meta-data we could find. Therefore, we used this database to prove the concept of omFBA. It is also worth mentioning that while only transcriptomics data was used in this study, the platform of omFBA can be easily extended to include all types of omics data because of using the regression analysis to derived omics-guided objective function. For example, when using the multi-omics datasets (e.g., transcriptomics, proteomics, metabolomics datasets), we can follow the similar flowchart of omFBA in this study to rank the top cell components, e.g., gene expression, protein synthesis, metabolite concentration, that are highly correlated with the weighing factors in the "phenotype matched" objective function, and then used such connection to simulate cell phenotypes.

In summary, we have developed a novel FBA-derived algorithm, omFBA, to integrate the transcriptomics data into FBA via the omics-guided objective function for the accurate prediction of phenotypes and the in-depth simulation of biological insights. Compared to the "Big Data" regression approach, omFBA could achieve the similarly good predication but is superior in uncovering novel biological insights such as dynamics of metabolic flux ratios. The quality of transcriptomics data was found to be an important factor that affected the omFBA prediction. Although the transcriptomics-phenotype correlated datasets required by omFBA are still limiting, we envision that such challenge could be overcome by efforts such as the construction of iTAP database. With the

correlated omics-phenotype data, omFBA algorithm could be a powerful approach to link genotype and phenotype and unravel the mysteries of cell metabolism.

4.4 Methods and Models

4.4.1 Transcriptomics and Phenotype Data Collection

To develop the omFBA algorithm, we have selected a published paper with the transcriptomics-phenotype correlated data [30]. In the paper, Ronen and Botstein studied transcriptomics responses (i.e., the fold changes of gene expression levels) of *S. cerevisiae* at different time points after the shift of the substrates in chemostat, namely, from the unfavorable galactose to favorable glucose in low and high concentrations (i.e., 0.2 g/L and 2 g/L, respectively).

The transcriptomics data, i.e., the exponential fold changes of gene expression levels with *p*-values, was obtained by running the GEO2R web tool [34] with the control group set as T=0 h (i.e., the starting time for the substrate shift). These transcriptomics data for all the time points have been collected as the "big" gene pool for the development of omFBA. In addition, the transcriptional analysis by Ronen and Botstein [30] indicated that a small set of genes could play deciding roles in determining the yeast metabolic responses to substrate shift. Therefore, we also extracted transcriptomics data of the same genes from the paper as a "small" gene pool, which could examine the impact of the pool size of the transcriptomics data on the omFBA. The *p*-value of the transcriptomics data tested the statistical significance level of the fold changes and was used to quantify the data quality. In the original published paper, the author selected 0.95 as the *p*-value cutoff value to remove the low-quality data [30]. To develop the omFBA algorithm, we followed the same

cutoff value to filter the transcriptomics data in low quality by ignoring this gene in the database.

The phenotype data, i.e., ethanol yield (w/w), has been calculated based on the glucose and ethanol concentrations for the whole time courses, i.e., from 0 to 240 minutes, extracted from figures of the original paper. We have ignored the time points in the stationary phase of both low and high concentration datasets during the development of omFBA algorithm.

After removing the time points in stationary phase, we found only 8 time points were available with *p*-value-filtered transcriptomics data and recalculated phenotype data, which captured the dynamics of transcriptional responses and phenotype changes but were not enough for developing omFBA algorithm. We then smoothed both transcriptomics and phenotype data at a linear space including 1000 points by using the prebuilt function, i.e., "*csaps*", in MATLAB (Step 2, Fig. 4.2). Based on these 1000 points, we randomly selected 500 points as the training dataset for the development of omFBA algorithm. The other 500 points have been used to validate and evaluate the omFBA algorithm.

4.4.2 Phenotype-Match Algorithm

We developed the "phenotype match" algorithm to fine-tune FBA for accurate prediction of the phenotype data with a selected dual objective function in a bi-level FBA algorithm. The dual objective function includes two items: minimizing the overall enzyme usage and maximizing the ethanol yield, which reflects the trade-off between the overall enzyme activities and the ethanol production. The following mathematical equation was used to represent the dual objective function:

$$\min c_j \sum v_i^2 - (1 - c_j) v_{EtOH} \quad (1)$$

where, v_i was all the fluxes in the genome-scale metabolic model; v_{EtOH} was the flux of the ethanol exchange; c_j was the phenotype-matched weighting factor for data point j of training dataset. This dual-objective function has been applied to a bi-level FBA algorithm as the inner objective function:

$$\min\ (Y_{sim,j} - Y_{obs,j})^2$$

$$s.t.$$

$$\begin{bmatrix} \min c_j \cdot \sum v_i^2 - (1 - c_j) \cdot v_{EtOH} \\ s.t. \\ \qquad S \cdot v = 0 \\ \qquad lb \ \leq v_i \ \leq ub \end{bmatrix}$$

$$0 \leq c_j \leq 1 \qquad (2)$$

where, $Y_{sim,j}$ and $Y_{sim,j}$ were the simulated and observed ethanol yields (*w*/*w*) from inner FBA problem and training dataset, respectively. The outer objective function in this algorithm was minimizing the variance between the simulated ethanol yields and the observed ethanol yields from the training dataset by tuning the weighting factor of the dual-objective function. The stoichiometric matrix and boundary conditions were derived from the BiGG database [37], iND750[36], a genome-scale metabolic model of *S. cerevisiae*. To evaluate whether or not different metabolic models would affect the phenotype-matched weighting factors, we chose another genome-scale metabolic model of *S. cerevisiae* (iMM904 [51]), and re-ran our phenotype-match algorithm. We found that the weighting factors derived from the original model (i.e., iND750) and the new model (i.e., iMM904) were highly correlated (Appendix C Fig. C.S6), with R^2>0.99. Also, both model used almost the same gene-protein-pathway mapping. Therefore, we concluded that the network reconstruction would not significantly, if not at all, affect the omFBA. The inner FBA

problem, as a quadratic optimization problem, was solved by the prebuilt solver, "*quadprog*", in MATLAB. The outer optimization problem was solved by the "grid search" algorithm by using an in-house MATLAB algorithm with step-wise search in a range of the weighting factor ([0, 1.00]) with 10^{-4} for each step.

Next, we calculated the correlation coefficients between the phenotype-matched weighting factors and the transcriptomics data for each gene. We selected the top 3 genes with the highest absolute values of correlation coefficients as the genetic markers. To prevent over-fitting the data, we applied F-test (one-tail with cutoff *p*-value = 0.10) [52] to determine if we should accept (or reject) a new genetic marker in the linear regression model that used the "genetic markers" to fit phenotype-matched weighting factors. We found that when using top 3 instead of top 2 "genetic markers" in the linear regression model, the fitting became significantly improved, e.g., *p*-value was 0.09 (< cutoff *p*-value) for low concentration glucose condition using big gene pool. In other word, the introduction of the top 3 "genetic markers" was necessary to improve the model fitting and the data was not over-fitted.

We then quantitatively correlated the phenotype-matched weighting factors and the expression levels of the genetic markers using the multiple linear regression approach in MATLAB ("*regress*" command), which was shown in equation 3:

$$\begin{bmatrix} c_1 \\ \vdots \\ c_j \\ \vdots \\ c_{500} \end{bmatrix} = \begin{bmatrix} G_{t1}^{\#1} & G_{t1}^{\#2} & G_{t1}^{\#3} & 1 \\ \vdots & \vdots & \vdots & \vdots \\ G_{tj}^{\#1} & G_{tj}^{\#2} & G_{tj}^{\#3} & 1 \\ \vdots & \vdots & \vdots & \vdots \\ G_{t500}^{\#1} & G_{t500}^{\#2} & G_{t500}^{\#3} & 1 \end{bmatrix} \begin{bmatrix} a_1 \\ a_2 \\ a_3 \\ b \end{bmatrix} \quad (3)$$

where, c_j was the phenotype-matched weighting factors of training dataset *j*; $G_{tj}^{\#1}, G_{tj}^{\#2}, G_{tj}^{\#3}$ were the expression levels of the three genetic markers in training dataset *j*, respectively;

and a_1, a_2, a_3, b were the regression coefficients for the genetic markers and the linear part, respectively.

4.4.3 Omics-Guided Objective Function in FBA

With the regression equation derived from the "phenotype match" algorithm, we then used the transcriptomics data from the validation datasets to derive the omics-guided weighting factors:

$$\begin{bmatrix} c_1^{om} \\ \vdots \\ c_j^{om} \\ \vdots \\ c_{500}^{om} \end{bmatrix} = \begin{bmatrix} G_{v1}^{\#1} & G_{v1}^{\#2} & G_{v1}^{\#3} & 1 \\ \vdots & \vdots & \vdots & \vdots \\ G_{vj}^{\#1} & G_{vj}^{\#2} & G_{vj}^{\#3} & 1 \\ \vdots & \vdots & \vdots & \vdots \\ G_{v500}^{\#1} & G_{v500}^{\#2} & G_{v500}^{\#3} & 1 \end{bmatrix} \begin{bmatrix} a_1 \\ a_2 \\ a_3 \\ b \end{bmatrix} \quad (4)$$

where c_j^{om} was the simulated omics-guided weighting factors of dataset j; $G_{vj}^{\#1}, G_{vj}^{\#2}, G_{vj}^{\#3}$ were the transcriptomics data of three genetic markers, respectively, of dataset j from the validation dataset; and a_1, a_2, a_3, b were the regression coefficients for the genetic markers and the linear part, respectively, which were determined in the "phenotype match" algorithm.

We then input these simulated omics-guided weighting factors into the dual-objective function to set up the omics-guided objective functions in a genome-scale metabolic model of *S. cerevisiae*, iND750:

$$\min c_j^{om} \cdot \sum v_i^2 - \left(1 - c_j^{om}\right) \cdot v_{EtOH} \quad (5)$$

$$\begin{bmatrix} s.t. \\ \quad S \cdot v = 0 \\ \quad lb \leq v_i \leq ub \end{bmatrix}$$

$$c_j^{om} determined \quad (6)$$

The ethanol yields could be predicted by solving this problem via the same quadratic solver, "*quadprog*", in MATLAB. The flux ratios PGI/ZWF1, FBA/TKL, ENO/PCK, and PYK/PDC, were calculated to represent the key metabolic responses, i.e., glycolysis to oxidative pentose phosphate pathway (PP pathway), reductive PP pathway, futile cycle, and the fermentation pathway, respectively, in yeast metabolism. The variances of fluxes were obtained by flux variance analysis. The calculation of the variances of flux ratios were following the formula to calculate the combinational standard deviation [53].

$$R = \frac{F_1}{F_2}, \frac{SD_R}{R} = \sqrt{(\frac{SD_{F_1}}{F_1})^2 + (\frac{SD_{F_2}}{F_2})^2} \quad (7)$$

where, R is the key flux ratio, F_1 and F_2 are the flux values, SD is the standard deviation of the flux.

4.4.4 Comparison of Prediction Accuracies and Genetic Markers of Big Data and omFBA Algorithm

To evaluate the prediction accuracy of omFBA algorithm, we have compared the predicted ethanol yields to the observed ones from the validation dataset. We considered a prediction as a "matched" prediction if the relative error (e_r) between the predicted and the observed ethanol yield was smaller 5%, as shown below:

$$e_r = \left|\frac{Y_{pred,j} - Y_{obs,vj}}{Y_{obs,vj}}\right| \times 100\% \leq 5\% \quad (8)$$

where, $Y_{\text{pred,vj}}$ and $Y_{\text{obs,vj}}$ are the predicted and observed ethanol yields (w/w) from the omFBA, respectively.

Acknowledgements

We thank the writing center in Virginia Tech for improving the language of the paper. This study was supported by start-up fund (#175323) from Virginia Tech.

Table 4.1 Key flux ratios compared with previous studies using ^{13}C metabolic flux analysis.

Flux ratio[a]	Correlation with increased ethanol yields		Corresponding genes	Correlation with gene expression ratios	
	omFBA	Previous studies [32, 33, 42]		omFBA	Previous studies[31]
PGI/G6PDH2	Positive	Positive	YBR196C/ YNL241C	No correlation[b]	No correlation
FBA/TKT1	Positive	Positive	YKL060C/ YPR074C	No correlation	No correlation
ENO/PPCK	Negative	Negative	YGR254W/ YKR097W	No correlation	No correlation
PYK/PYRDC	Negative	Negative	YAL038W/ YLR044C	No correlation	No correlation

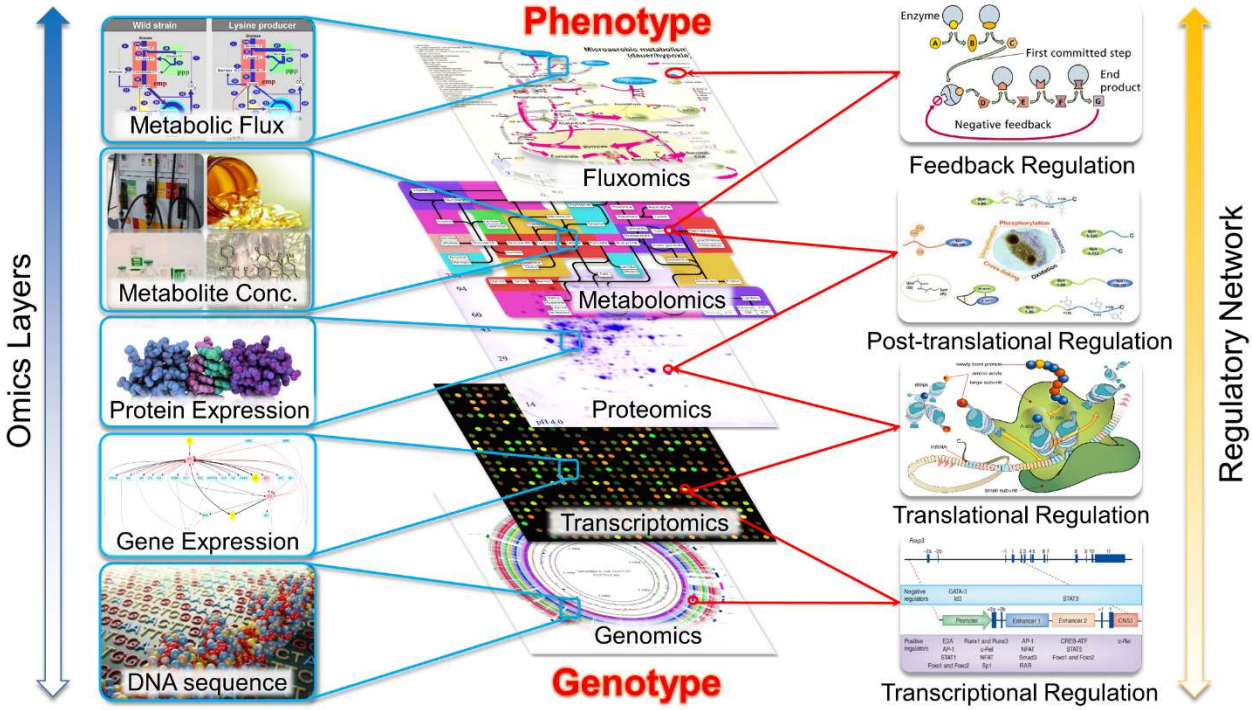

Fig. 4.1 Complex interactions of various components in cell metabolism. Multi-omics data has provided the quantitative readouts of these components, which helps us to elucidate the interactions between the multi-layer regulations.

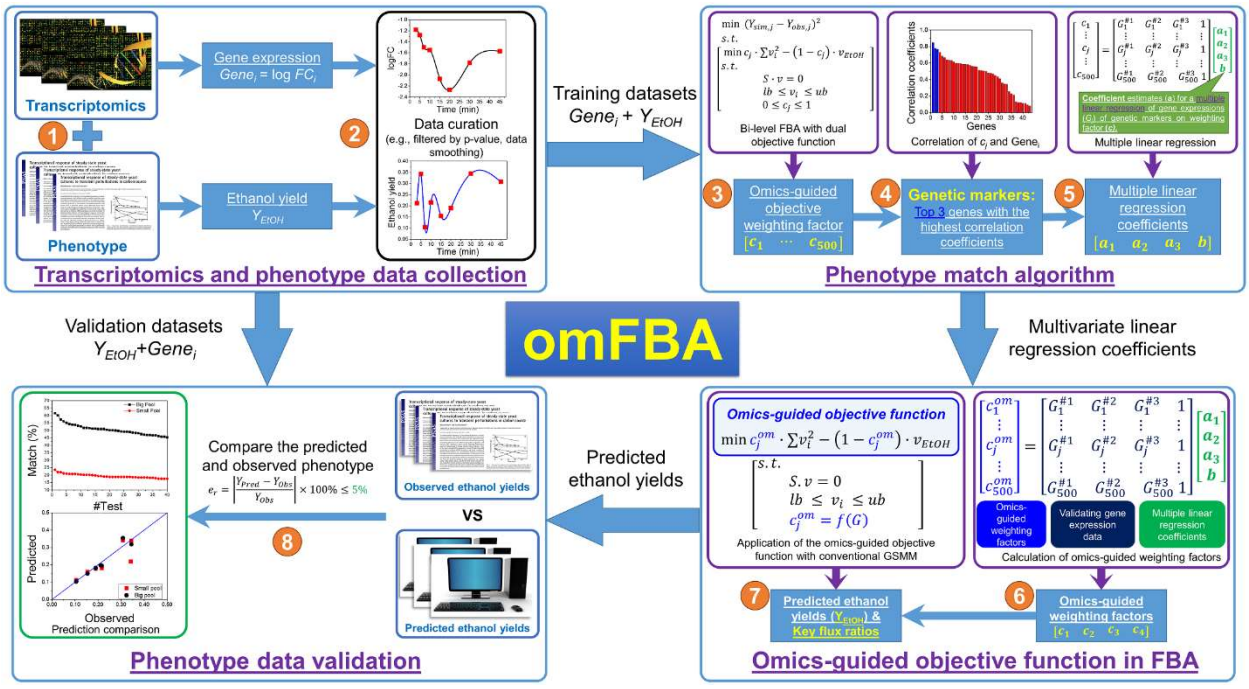

Fig. 4.2 Scheme of omFBA algorithm. Four modules are designed to implement omFBA algorithm: 1) transcriptomic-phenotype data collection (Step 1~2), 2) "phenotype match" algorithm (Step 3~5), 3) omics-guided objective function in FBA (Step 6~7), and 4) phenotype data validation (Step 8).

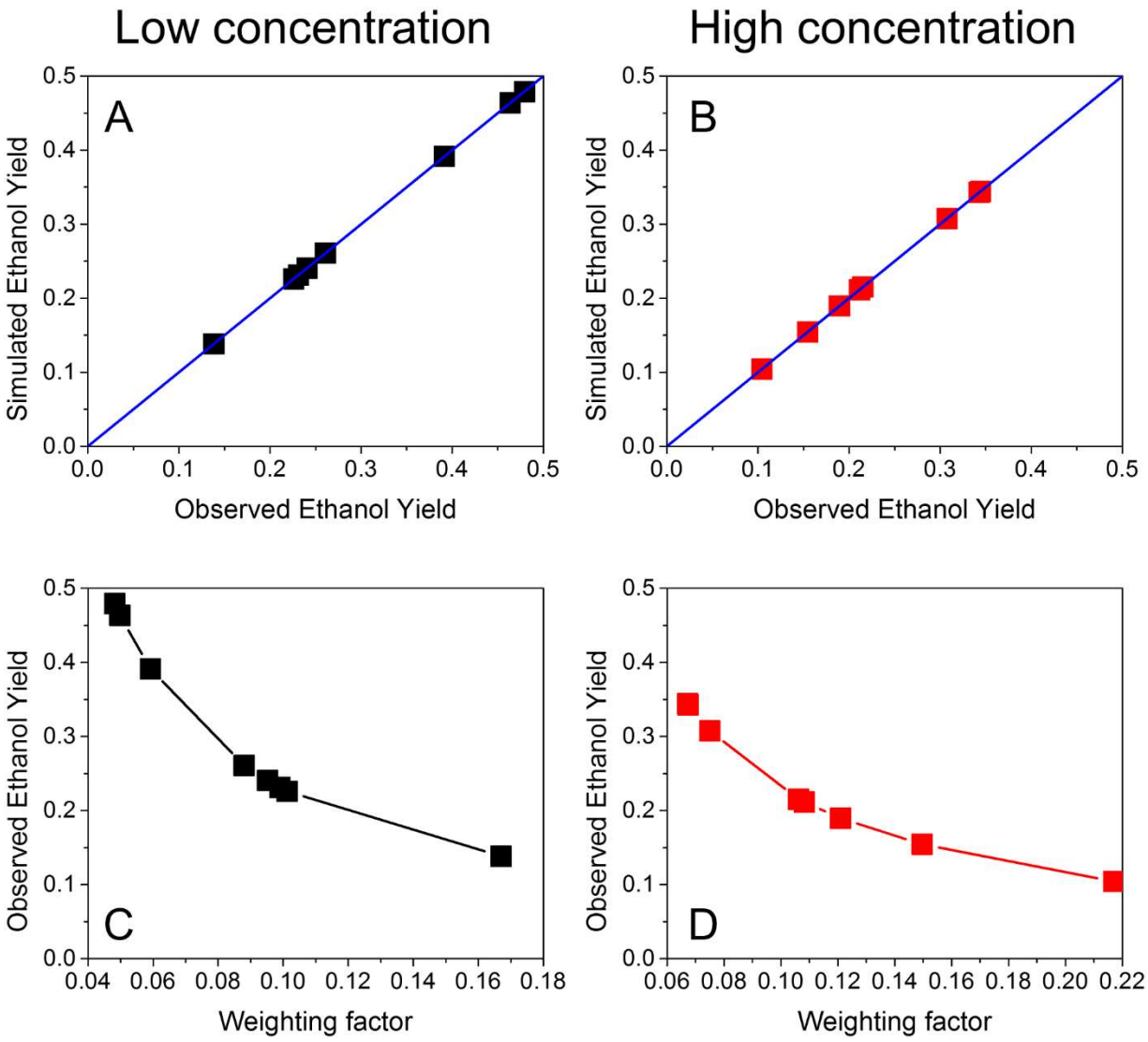

Fig. 4.3 "Phenotype match" algorithm for low and high glucose conditions. The simulated and observed ethanol yields matched well for low (A) and high (B) glucose conditions, respectively. Negative correlations between the weighting factors of minimizing the overall enzyme usage and the observed ethanol yield were found for low (C) and high (D) glucose conditions.

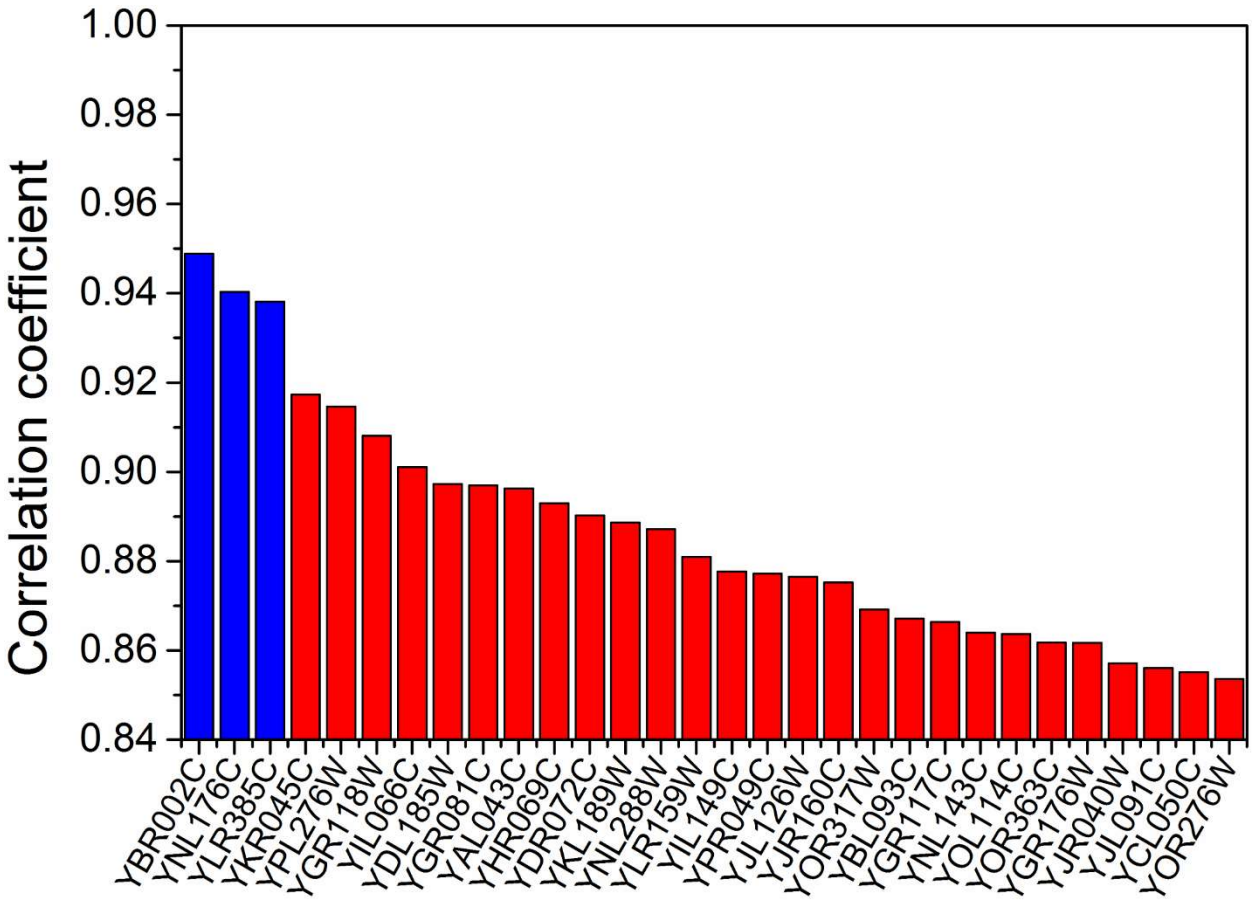

Fig. 4.4 Correlation between phenotype-matched weighting factors and gene expressions. The absolute values of the correlation coefficients in one of the training datasets were ranked from high to low (only the top 30 genes were shown here). The top 3 genes were chosen as the genetic markers to derive the omics-guided objective function (blue bars)**.**

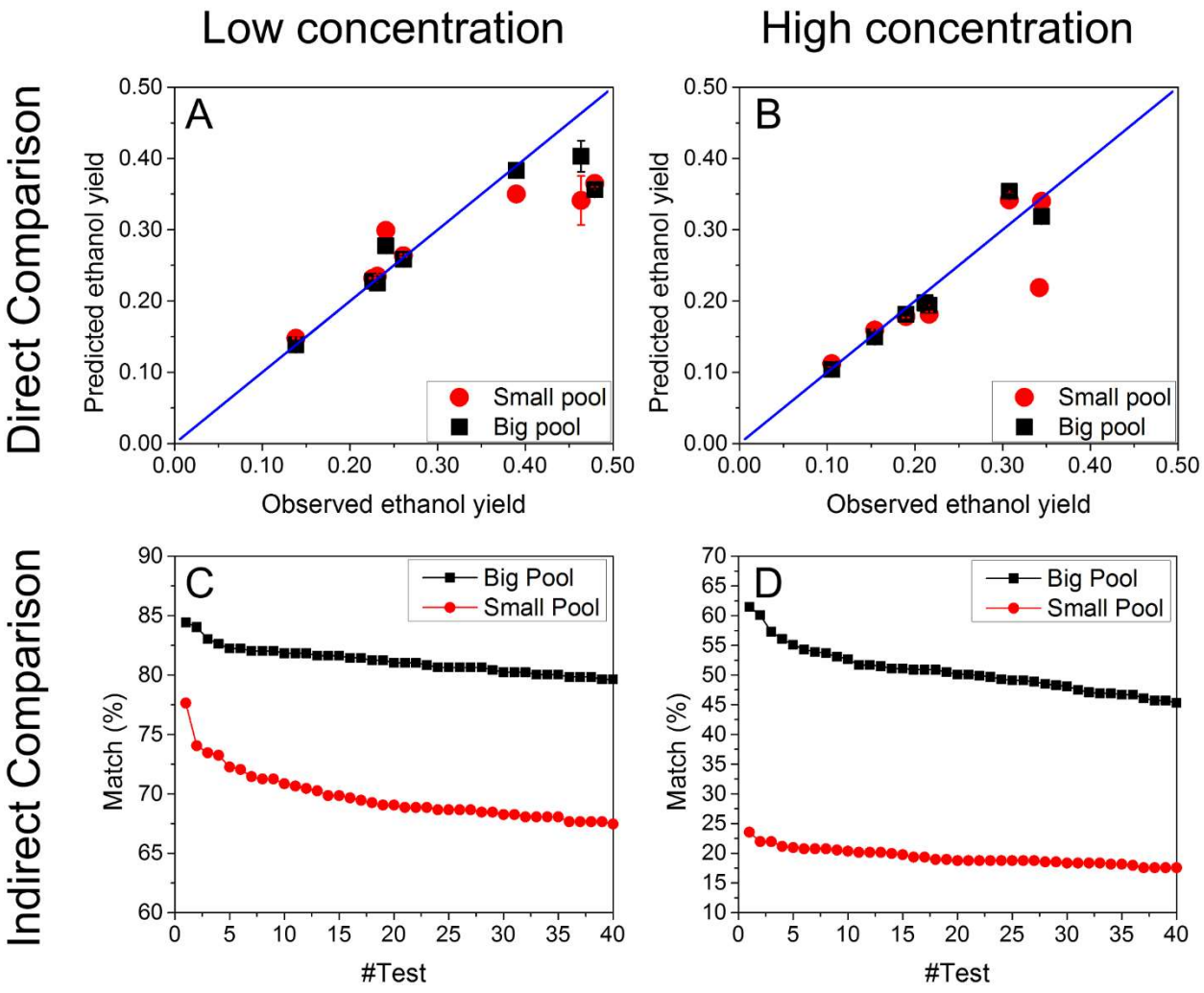

Fig. 4.5. Prediction accuracy of omFBA algorithm. Direct comparison of the predicted and observed ethanol yields in low (A) and high (B) glucose conditions. The omFBA algorithm was repeated for 40 times and the percentage of matched predictions of omFBA algorithm were calculated and ranked for low (C) and high (D) glucose conditions.

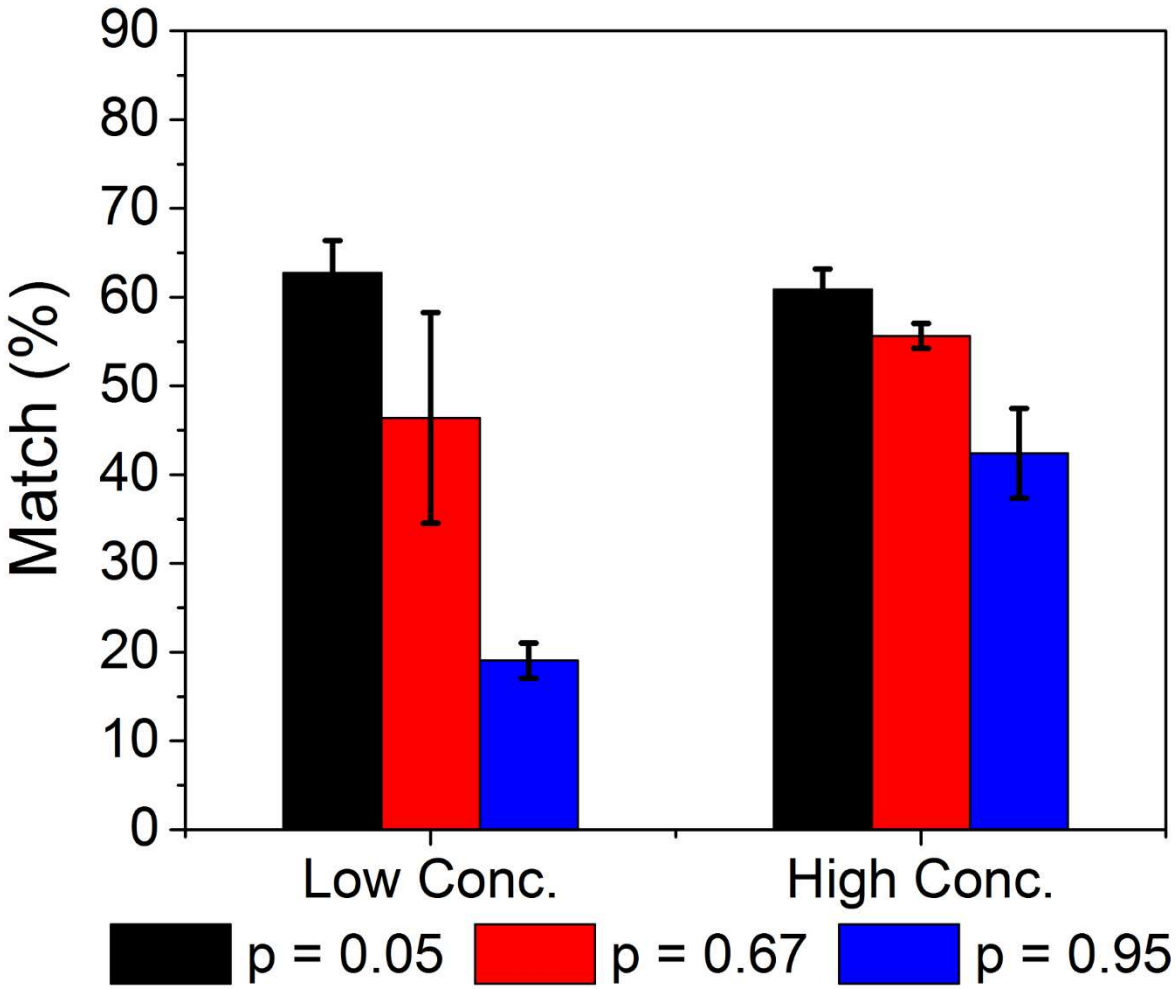

Fig. 4.6 Effect of cutoff *p*-value on omFBA prediction using "small pool" of genes. Three cutoff *p*-values, i.e., 0.05, 0.67, and 0.95, were used to filter the trancriptomics data. For each cutoff *p*-value, we re-ran the omFBA algorithm for 40 times and calculated the percentage of matches between the predicted and the observed ethanol yields in the validation datasets.

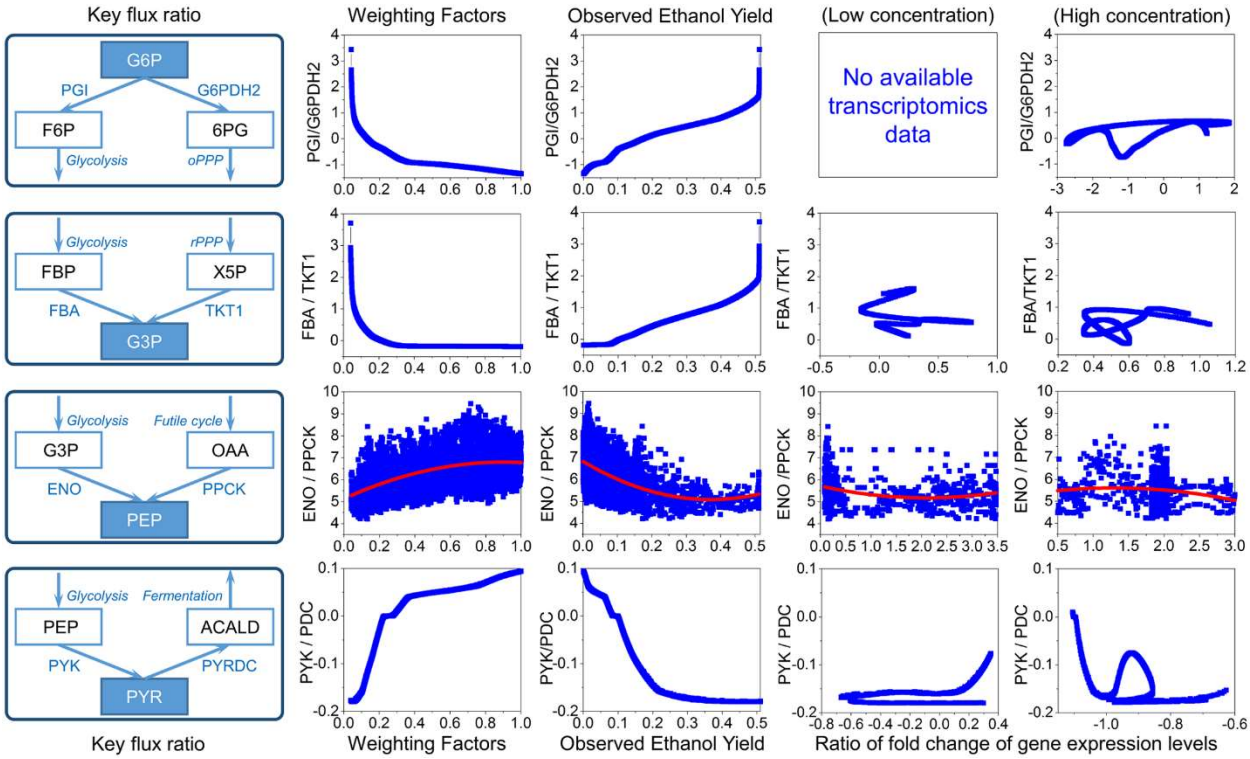

Fig. 4.7. Key flux ratio analysis. Four key flux ratios (PGI/G6PDH2, FBA/TKT1, ENO/PPCK, and PYK/PDC) were selected to be correlated with phenotype-matched weighting factors, observed ethanol yields, and the ratios of the corresponding gene expression levels for low and high glucose condition. All the values of the ratios were exponential. Definitions of abbreviations are shown in the List of Abbreviations.

References

1. Zhang, W., F. Li, and L. Nie, *Integrating multiple 'omics' analysis for microbial biology: application and methodologies.* Microbiology, 2010. **156**(2): p. 287-301.
2. Hong, K.-K. and J. Nielsen, *Metabolic engineering of Saccharomyces cerevisiae: a key cell factory platform for future biorefineries.* Cellular and Molecular Life Sciences, 2012. **69**(16): p. 2671-2690.
3. Nogales, J., B.Ø. Palsson, and I. Thiele, *A genome-scale metabolic reconstruction of Pseudomonas putida KT2440: iJN746 as a cell factory.* BMC Systems Biology, 2008. **2**: p. 79-79.
4. de Jong, B., V. Siewers, and J. Nielsen, *Systems biology of yeast: enabling technology for development of cell factories for production of advanced biofuels.* Current Opinion in Biotechnology, 2012. **23**(4): p. 624-630.
5. Morozova, O. and M.A. Marra, *Applications of next-generation sequencing technologies in functional genomics.* Genomics, 2008. **92**(5): p. 255-264.
6. Metzker, M.L., *Sequencing technologies [mdash] the next generation.* Nat Rev Genet, 2010. **11**(1): p. 31-46.
7. Wang, Z., M. Gerstein, and M. Snyder, *RNA-Seq: a revolutionary tool for transcriptomics.* Nat Rev Genet, 2009. **10**(1): p. 57-63.
8. Fiehn, O., *Metabolomics – the link between genotypes and phenotypes.* Plant Molecular Biology, 2002. **48**(1-2): p. 155-171.
9. Scalbert, A., et al., *Mass-spectrometry-based metabolomics: limitations and recommendations for future progress with particular focus on nutrition research.* Metabolomics, 2009. **5**(4): p. 435-458.
10. Zhang, Z., et al., *High-Throughput Proteomics.* Annual Review of Analytical Chemistry, 2014. **7**(1): p. 427-454.
11. Nilsson, T., et al., *Mass spectrometry in high-throughput proteomics: ready for the big time.* Nat Meth, 2010. **7**(9): p. 681-685.
12. Smith, R.D., et al., *An accurate mass tag strategy for quantitative and high-throughput proteome measurements.* Proteomics, 2002. **2**(5): p. 513-523.
13. Wiechert, W., et al., *Fluxomics: mass spectrometry versus quantitative imaging.* Current Opinion in Plant Biology, 2007. **10**(3): p. 323-330.
14. Poskar, C.H., et al., *High-Throughput Data Pipelines for Metabolic Flux Analysis in Plants*, in *Plant Metabolic Flux Analysis*, M. Dieuaide-Noubhani and A.P. Alonso, Editors. 2014, Humana Press. p. 223-246.
15. Celton, M., et al., *A comparative transcriptomic, fluxomic and metabolomic analysis of the response of Saccharomyces cerevisiae to increases in NADPH oxidation.* BMC Genomics, 2012. **13**: p. 317-317.
16. Orth, J.D., I. Thiele, and B.O. Palsson, *What is flux balance analysis?* Nat Biotech, 2010. **28**(3): p. 245-248.
17. Gianchandani, E.P., A.K. Chavali, and J.A. Papin, *The application of flux balance analysis in systems biology.* Wiley Interdisciplinary Reviews: Systems Biology and Medicine, 2010. **2**(3): p. 372-382.
18. Lakshmanan, M., et al., *Software applications for flux balance analysis.* Briefings in Bioinformatics, 2012.

19. Schuetz, R., L. Kuepfer, and U. Sauer, *Systematic evaluation of objective functions for predicting intracellular fluxes in Escherichia coli*. Vol. 3. 2007.
20. Hyduke, D.R., N.E. Lewis, and B.O. Palsson, *Analysis of omics data with genome-scale models of metabolism.* Molecular BioSystems, 2013. **9**(2): p. 167-174.
21. Saha, R., A. Chowdhury, and C.D. Maranas, *Recent advances in the reconstruction of metabolic models and integration of omics data.* Current Opinion in Biotechnology, 2014. **29**: p. 39-45.
22. Becker, S.A. and B.O. Palsson, *Context-Specific Metabolic Networks Are Consistent with Experiments.* PLoS Comput Biol, 2008. **4**(5): p. e1000082.
23. Zur, H., E. Ruppin, and T. Shlomi, *iMAT: an integrative metabolic analysis tool.* Bioinformatics, 2010. **26**(24): p. 3140-3142.
24. Colijn, C., et al., *Interpreting Expression Data with Metabolic Flux Models: Predicting <italic>Mycobacterium tuberculosis</italic> Mycolic Acid Production.* PLoS Comput Biol, 2009. **5**(8): p. e1000489.
25. Chandrasekaran, S. and N.D. Price, *Probabilistic integrative modeling of genome-scale metabolic and regulatory networks in Escherichia coli and Mycobacterium tuberculosis.* Proceedings of the National Academy of Sciences, 2010. **107**(41): p. 17845-17850.
26. Hoppe, A., *What mRNA Abundances Can Tell us about Metabolism.* Metabolites, 2012. **2**(3): p. 614-631.
27. O'Brien, E.J. and B.O. Palsson, *Computing the functional proteome: recent progress and future prospects for genome-scale models.* Current Opinion in Biotechnology, 2015. **34**: p. 125-134.
28. Kim, J. and J.L. Reed, *Refining metabolic models and accounting for regulatory effects.* Current Opinion in Biotechnology, 2014. **29**: p. 34-38.
29. Kim, M.K. and D.S. Lun, *Methods for integration of transcriptomic data in genome-scale metabolic models.* Computational and Structural Biotechnology Journal, 2014. **11**(18): p. 59-65.
30. Ronen, M. and D. Botstein, *Transcriptional response of steady-state yeast cultures to transient perturbations in carbon source.* Proceedings of the National Academy of Sciences of the United States of America, 2006. **103**(2): p. 389-394.
31. Moxley, J.F., et al., *Linking high-resolution metabolic flux phenotypes and transcriptional regulation in yeast modulated by the global regulator Gcn4p.* Proceedings of the National Academy of Sciences, 2009. **106**(16): p. 6477-6482.
32. Frick, O. and C. Wittmann, *Characterization of the metabolic shift between oxidative and fermentative growth in Saccharomyces cerevisiae by comparative 13C flux analysis.* Microbial Cell Factories, 2005. **4**(1): p. 30.
33. Raghevendran, V., et al., *Phenotypic characterization of glucose repression mutants of Saccharomyces cerevisiae using experiments with 13C-labelled glucose.* Yeast, 2004. **21**(9): p. 769-779.
34. Barrett, T., et al., *NCBI GEO: archive for high-throughput functional genomic data.* Nucleic Acids Research, 2009. **37**(suppl 1): p. D885-D890.
35. Feng, X., et al., *Integrating Flux Balance Analysis into Kinetic Models to Decipher the Dynamic Metabolism of <italic>Shewanella oneidensis</italic> MR-1.* PLoS Comput Biol, 2012. **8**(2): p. e1002376.

36. Duarte, N.C., M.J. Herrgård, and B.Ø. Palsson, *Reconstruction and Validation of Saccharomyces cerevisiae iND750, a Fully Compartmentalized Genome-Scale Metabolic Model.* Genome Research, 2004. **14**(7): p. 1298-1309.
37. King, Z.A., et al., *BiGG Models: A platform for integrating, standardizing and sharing genome-scale models.* Nucleic Acids Research, 2015.
38. Raser, J.M. and E.K. O'Shea, *Noise in Gene Expression: Origins, Consequences, and Control.* Science, 2005. **309**(5743): p. 2010-2013.
39. Blake, W.J., et al., *Noise in eukaryotic gene expression.* Nature, 2003. **422**(6932): p. 633-637.
40. Raser, J.M. and E.K. O'Shea, *Control of Stochasticity in Eukaryotic Gene Expression.* Science, 2004. **304**(5678): p. 1811-1814.
41. Fraser, H.B., et al., *Noise Minimization in Eukaryotic Gene Expression.* PLoS Biol, 2004. **2**(6): p. e137.
42. Fendt, S.-M. and U. Sauer, *Transcriptional regulation of respiration in yeast metabolizing differently repressive carbon substrates.* BMC Systems Biology, 2010. **4**(1): p. 12.
43. Edgar, R. and T. Barrett, *NCBI GEO standards and services for microarray data.* Nat Biotech, 2006. **24**(12): p. 1471-1472.
44. Barrett, T., et al., *NCBI GEO: archive for functional genomics data sets—10 years on.* Nucleic Acids Research, 2011. **39**(suppl 1): p. D1005-D1010.
45. Barrett, T., et al., *NCBI GEO: archive for functional genomics data sets—update.* Nucleic Acids Research, 2013. **41**(D1): p. D991-D995.
46. Leinonen, R., et al., *The European Nucleotide Archive.* Nucleic Acids Research, 2010.
47. Rodriguez-Tomé, P., et al., *The European Bioinformatics Institute (EBI) databases.* Nucleic Acids Research, 1996. **24**(1): p. 6-12.
48. Faith, J.J., et al., *Many Microbe Microarrays Database: uniformly normalized Affymetrix compendia with structured experimental metadata.* Nucleic Acids Research, 2008. **36**(suppl 1): p. D866-D870.
49. Wilhelm, M., et al., *Mass-spectrometry-based draft of the human proteome.* Nature, 2014. **509**(7502): p. 582-587.
50. Sundararaman, N., et al., *iTAP: integrated transcriptomics and phenotype database for stress response of Escherichia coli and Saccharomyces cerevisiae.* BMC Research Notes, 2015. **8**(1): p. 1-7.
51. Mo, M.L., B.Ø. Palsson, and M.J. Herrgård, *Connecting extracellular metabolomic measurements to intracellular flux states in yeast.* BMC Systems Biology, 2009. **3**(1): p. 1-17.
52. Ott, R. and M. Longnecker, *An introduction to statistical methods and data analysis*. 2008: Cengage Learning.
53. Kenny, J. and E. Keeping, *The Standard Deviation and Calculation of the Standard Deviation. 3. chap 6.5–6.6.* Princeton NJ, 1962: p. 77-80.

Chapter 5: Data-Driven Prediction of CRISPR-Based Transcription Regulation for Programmable Control of Metabolic Flux

Jiayuan Sheng[a, *], Weihua Guo [a, *], Christine Ash[a], Brendan Freitas[a], Mitchell Paoletti[a], and Xueyang Feng[a, †]

[a] Department of Biological Systems Engineering, Virginia Polytechnic Institute and State University, Blacksburg, VA 24061, United States

[†]Correspondence to: Xueyang Feng.

[*] JS and WG contribute to this work equally.

Phone: +1-(540)231-2974

Email: xueyang@vt.edu

This manuscript has been preprinted on *arXiv preprint* arXiv:1704.03027. Supplementary material of Chapter 5 is shown in Appendix D.

Abstract

Multiplex and multi-directional control of metabolic pathways is crucial for metabolic engineering to improve product yield of fuels, chemicals, and pharmaceuticals. To achieve this goal, artificial transcriptional regulators such as CRISPR-based transcription regulators have been developed to specifically activate or repress genes of interest. Here, we found that by deploying guide RNAs to target on DNA sites at different locations of genetic cassettes, we could use just one synthetic CRISPR-based transcriptional regulator to simultaneously activate and repress gene expressions. By using the pairwise datasets of guide RNAs and gene expressions, we developed a data-driven predictive model to rationally design this system for fine-tuning expression of target genes. We demonstrated that this system could achieve programmable control of metabolic fluxes when using yeast to produce versatile chemicals. We anticipate that this master CRISPR-based transcription regulator will be a valuable addition to the synthetic biology toolkit for metabolic engineering, speeding up the "design-build-test" cycle in industrial biomanufacturing as well as generating new biological insights on the fates of eukaryotic cells.

5.1 Introduction

Metabolic engineering has proven to be tremendously important for sustainable production of fuels[1, 2], chemicals[3, 4], and pharmaceuticals[5, 6]. One of the critical steps in metabolic engineering is reprogramming metabolic fluxes in host cells to optimize the fermentation performance such as product yield[7, 8]. To achieve this goal, several enzymes need to be activated while in the meantime others need to be repressed[9]. The multiplex and multi-directional control of enzyme expressions is largely executed through transcriptional regulation[9-12]. Recently, the type-II clustered regularly interspaced short palindromic repeats (CRISPR)/Cas9 from *Streptococcus pyogenes* (*Sp*)[13-15] has been repurposed to be a master transcriptional regulator that could activate or repress multiple genes[16-18]. By further extending the guide RNAs of SpCas9 to include effector protein recruitment sites and expressing the effector proteins in host cells[18, 19], a synthetic CRISPR-based transcriptional regulator was developed to simultaneously program the expressions of multiple genes at multiple directions (i.e., both activation and repression).

Although demonstrating great promises in controlling metabolic fluxes, the current CRISPR-based transcription regulation faces several challenges when being applied for metabolic engineering. First, it relies on a panel of well-characterized genetic parts (e.g., RNA-binding proteins) to achieve the transcriptional regulation[9, 20]. However, the rareness of such genetic parts often limits the application of current CRISPR-based transcription regulator in a metabolic network. Second, it requires the co-expression of effector proteins to activate or repress the target genes[9, 20]. Therefore, the utility of current CRISPR-based transcription regulator in metabolic engineering is mitigated by the metabolic costs associated with protein expressions[9, 20]. To address these limitations, an

ideal type of CRISPR-based transcription regulation should meet two criteria: generally applicable in any gene of interest, and requiring minimal protein expression to achieve multi-directional gene regulation.

In this study, we have developed a data-driven approach that enables the rational design of a new type of CRISPR-based transcription regulation. This CRISPR-based transcription regulator uses only a fused protein of a nuclease-deficient Cas9 (dCas9) and an effector (VP64) to achieve multi-directional and multiplex gene regulation, which eliminates the metabolic costs associated with the expression of effector proteins in previous studies[9, 20]. We found that the deployment of guide RNAs was the key factor that determined the regulatory effects of our CRISPR-based transcription regulator. We used a data-driven approach to provide accurate and target-oriented guidance on designing the guide RNAs. As we showed in our results, this approach could be applied for any gene of interest. Finally, using this system, we demonstrated a highly programmable control of metabolic fluxes when using yeast to produce versatile chemicals.

5.2 Results

5.2.1 Gene Activation and Repression by Using a CRISPR-based Transcriptional Regulator.

The CRISPR-based transcriptional regulator is composed of a codon-optimized, catalytically dead SpCa9 (i.e., dCas9) that is fused with four tandem copies of Herpes Simplex Viral Protein 16 (VP64, a commonly used eukaryotic transcription activator domain). The similar molecular design was previously reported to be able to activate gene expression in yeast[18] and mammalian cells[18]. In brief, it was found that when the dCas9-VP64 regulator was positioned in the correct sites of promoter, the target gene could

be activated by the VP64. However, we hypothesized that the effects of dCas9-VP64 could be diverse, i.e., both activation and repression could be achieved by using this master regulator (Fig. 5.1A). For example, the transcription initiation could be blocked when dCas9-VP64 is deployed to the transcription starting sites (TSS). The transcription elongation could also be inhibited when dCas9-VP64 is deployed to the open reading frame (ORF). If the hypothesis stands, we could then repurpose dCas9-VP64 as a universal regulator to activate and repress gene expressions at the same time.

To validate our hypothesis, we designed experiments by selecting 138 sites that can be targeted by dCas9-VP64 in four synthetic genetic cassettes (Fig. 5.1B): GFP under TEF1p promoter, mCherry under TPI1p promoter, Sapphire under PGK1p promoter, and Venus under PDC1p promoter. We created a library of guide RNAs and co-expressed them with the dCas9-VP64 and the target genetic cassette. For each of the tests, we measured the fluorescence of the reporter proteins and compared it to a control test in which dCas9-VP64 and the genetic cassette were expressed without guide RNA. As summarized in Fig. 5.1B and Fig. 5.1C, expression of reporter genes could indeed be programmed to be either up- or down-regulated (cutoff fold-change set as two-fold, $p<0.05$) when positioning the guide RNA at different sites on the promoter or ORF. The dynamic range of transcriptional regulation via dCas9-VP64 varied for different genetic elements, with the largest dynamic range achieving 13.8-fold (from -1.14 to 2.65 of log2 gene fold-change) in expression of TPI1p-mCherry cassette and the smallest $\log_2$ fold change dynamic range achieving 11.6-fold (from -1.82 to 1.71 of log2 gene fold-change) in expression of PGK1p-Venus cassette. We next compared the effects on transcriptional regulation when guide RNAs were positioned in the promoter region to that were positioned in the gene region (Fig. 5.1D). A

significant difference (p<0.01) was revealed: while gene expression was in general down-regulated when guide RNAs were positioned in the gene region, most of the guide RNAs (94.2%) that were positioned in the promoter region led to gene up-regulation or no effect. We also evaluated whether different PAM sites (i.e., 3'AGG, 3'TGG, 3'CGG, 3'GGG) could bias the transcriptional regulation (Fig. 5.1E). We found that most of the PAM sites (3'AGG, 3'TGG, 3'CGG) have no bias, but when guide RNAs were targeted on 3'GGG sites, the expression of selected genes tends to be more up-regulated than other PAM sites (p<0.05). Such difference, as we discussed in the section below, may be attributed to the larger percentage of guanosine in 3'GGG sites. Finally, we evaluated the metabolic costs of dCas9-VP64 by comparing the growth rates of yeast between the ones subject to transcriptional regulation (i.e., with guide RNAs) and the ones that were not. As shown in Appendix D Fig. D.S1, 131 out of the 138 tests showed no significant difference (p>0.05) on cell growth rate when being compared to that of the control strain, indicating a minimal metabolic burden when using only one synthetic protein for transcriptional regulation.

5.2.2 Data-Driven Model of Transcriptional Regulation by Using dCas9-VP64.

To determine the rule underlying transcriptional regulation by dCas9-VP64, we solicited nine design parameters on nucleotide stability, sequence of the target genetic element, PAM site location, and protein-DNA structure. These design parameters were chosen based on previous studies on the activity of SpCas9 [21, 22]. Next, we correlated these design parameters with transcriptional regulation (Appendix D Fig. D.S2A), and calculated the Pearson's correlation coefficients (PCC). The top 3 correlated design parameters were location, GC content (GC%), and PAM site of GGG. Next, we aimed to develop a predictive model that could use the design parameters to describe the effects of

guide RNAs positioning on gene expressions. Our first attempt is a linear regression model, which utilized all the nine design parameters (i.e., GC%, location, number of base G, number of base A, ΔG, AGG, TGG, CGG, and GGG) to simulate the corresponding fold changes of gene expressions as we collected from the four synthetic genetic cassettes (Appendix D Fig. D.S2B). However, the fitting of the linear regression model was very bad, as demonstrated by the low PCC (0.41) between observed and simulated fold changes (Appendix D Fig. D.S2B). This clearly indicated that the biomolecular interactions of RNA-protein and DNA-protein in the dCas9-VP64 system were highly nonlinear, which cannot be captured by the simple linear regression model.

We then used machine learning to derive an empirical model to quantitatively predict the nonlinear correlation between design parameters and transcriptional regulation by dCas9-VP64. As a data-driven modeling approach, machine learning is advantageous than linear model in solving complex problems in two aspects[23-25]: requiring no *a priori* knowledge of the system, and capable of resolving complex systems with high non-linearity and multi-dimensionality. In this study, we used the pairwise data of the design parameters of guide RNAs and the corresponding fold-change of gene expressions to train the computer for developing a mathematical model that could accurately predict the causal effects of inputs (i.e., regulated gene expression in this study). We used decision tree method to build a machine-learning algorithm and adopted ten-fold cross validation to evaluate the prediction accuracy of our model (Fig. 5.2A). The model construction and model evaluation were conducted by following a toolkit developed in MATLAB™ (i.e., "*fitrtree*" and "*predict*" in Statistics and Machine Learning Toolbox), which automatically adjust the nodes and connections of the decision tree to optimize the fitting[26, 27]. Using

the 138 pairwise data collected from the synthetic genetic cassettes (i.e., TEF1p-GFP, TPI1p-mCherry, PDC1p-Sapphire, and PGK1p-Venus), we found that the prediction accuracy was dramatically improved with PCC reaching 0.80 (Fig. 5.2B) for overall prediction of gene regulation and 0.72~0.93 for predicting gene regulation of individual genetic cassettes (Fig. 5.2C). Also, we found that the prediction accuracy of our machine-learning algorithm was improved with the enlargement of data size (Fig. 5.2D). For example, when 20 pairwise datasets were chosen, the PCC was merely 0.66. However, when the number of pairwise datasets reached 80, the PCC was improved to 0.78. This demonstrated the unique advantage of data-driven algorithm, i.e., increased prediction accuracy with more data.

To further test if our machine-learning algorithm could be generally applied for predicting the transcriptional regulation of other genes, we designed another synthetic genetic cassette that expressed tdTomato under Eno2p promoter. We used the machine-learning algorithm to predict the regulated gene expressions when guide RNAs of dCas9-VP64 were positioned at different locations of Eno2p-tdTomate cassette, followed by constructing the genetic cassettes and conducting experimental measurements. Of the 99 guide RNAs tested, our machine-learning algorithm could achieve similarly high prediction accuracy with PCC between the predicted and the measured gene expressions reaching 0.87 (Fig. 5.2E). This success demonstrated that our data-driven model could be generally applicable to guide the biomolecular design of dCas9-VP64 system to achieve customized gene regulation.

We also packaged our machine-learning algorithm into an open-source toolbox (Appendix D Fig. D.S3), CRISTINES (CRISPR-Cas9 Transcriptional Inactivation aNd

Elevation System), which is a MATLAB-based toolbox and free for downloading at https://sites.google.com/a/vt.edu/biomolecular-engineering-lab/software. CRISTINES is able to analyze the input DNA sequences, identify the design parameters of the dCas9-VP64 system, and use the embedded decision-tree algorithm to provide the top five guide RNAs that would lead to the strongest up-regulation and down-regulations, respectively. We anticipated that CRISTINES could help biologists worldwide to customize their design based on the target gene of interest.

5.2.3 Design dCas9-VP64 to Reprogram Metabolic Fluxes in Yeast.

We next applied dCas9-VP64 system in yeast metabolic engineering to test if the metabolic fluxes could be flexibly reprogrammed using our CRISPR-based transcription regulator. We chose the highly branched bacterial violacein biosynthetic pathway as our model pathway[28] (Fig. 5.3A), which uses five enzymes (VioA, VioB, VioE, VioD, and VioC) to produce four high-value products (violacein, proviolacein, deoxyviolacein, and prodeoxyviolacein). By controlling the expression levels of the five enzymes, the metabolic fluxes flowing into different branch pathways could be varied and thus leading to different yield of the four products. In this study, we reconstituted the violacein pathway in yeast by expressing the five enzymes under constitutive promoters (i.e., TEF1p, PGK1p, ENO2p, TPI1p, and PDC1p). According to our data-driven model CRISTINES, we could computationally predict the gene expression and thus predict the metabolic fluxes in the violacein pathway. Here, we designed three guide RNAs for four genes in the violacein pathway (VioA, VioE, VioD, and VioC). These three guide RNAs targeted on different promoter sites and were predicted to result in high, medium and low expression of each target gene, respectively. Correspondingly, the functional output states of the violacein

pathway were predicted to vary. For example, up-regulating VioA and down-regulating VioD would increase the fluxes into deoxyviolacein and prodeoxyviolacein, but decrease the fluxes into violacein and proviolacein. To validate our predictions on metabolic flux reprogramming, we co-expressed the dCas9-VP64 system with the violacein pathway, and used various guide RNAs to fine tune gene expressions. For each of the tests, we measured the titer of violacein, proviolacein, deoxyviolacein, and prodeoxyviolacein produced by yeast. As shown in Fig. 5.3B and 5.3C, our prediction fit well with the experimental measurements, with PCC reaching 0.84. We noticed some of the predictions on metabolic fluxes were not as good as we expected. This could be attributed to the posttranscriptional regulation of the five enzymes in the violacein pathway. Overall, we demonstrated that our master CRISPR-based transcription regulator was indeed able to program metabolic fluxes. More importantly, our data-driven algorithm allows users to design metabolic pathways with deterministic fates *in silico*.

5.3 Discussion

Using data-driven approach to investigate biomolecular interactions of CRISPR-based systems has recently been showcased in several studies, such as rational design of guide RNAs for maximizing editing activity and minimizing off-target effects of SpCas9[29, 30]. This approach is advantageous compared to conventional deterministic models because it does not require *a priori* knowledge on the mechanisms of RNA-protein and DNA-protein interactions[31, 32], which still remains largely unknown in spite of numerous studies on SpCas9 structures[33-37]. Also, because the biomolecular interactions among Cas9 protein and nucleic acids are highly nonlinear, the linear regression model cannot capture the essence of CRISPR-based transcription regulation. As

shown in our results, a machine-learning method could overcome this issue and capture the nonlinearity of the model. Not only did we achieve high accuracy when predicting the regulatory effects of CRISPR-based transcription regulator, but we also demonstrated that this method was not specific to a few selected genes and could be generally applicable. Future work will determine if the results obtained from yeast could provide useful lessons in other eukaryotic systems such as mammalian cells.

We expect that our method will provide a valuable tool for metabolic engineering, especially yeast metabolic engineering at this stage. *S. cerevisiae* is a widely used industrial workhorse for producing a broad spectrum of chemicals that represents over quarter trillion dollars market[38]. The experimental and analytical approaches described here raise the possibility of genome-scale reprogramming of metabolic fluxes, which will dramatically speed up the "design-build-test" cycle in industrial biomanufacturing[39]. We also expect our method could be used to rewire the fate of yeast cells, such as cell cycle, and thus generate new biological insights on the fundamentals of metabolic diseases, aging and apoptosis by using yeast as a disease model.

5.4 Methods and Models

5.4.1 Strain and Plasmid Construction in *Saccharomyces cerevisiae*.

dCas9 was codon-optimized for expression in *S. cerevisiae* and cloned into a pRS413 backbone under control of the GAL1 promoter. The RNA-guided transcription factors were built by fusing four repeats of the minimal domain of the herpes simplex viral protein 16 (VP16) to the C-terminus of dCas9 (dCas9_VP64)[18]. The reporter genes eGFP under the control of the TEF1p promoter, sapphire under PDC1p, mCherry under TPI1p, and venus under PGK1p were cloned into pRS416 plasmid by using the DNA assembler

method[40, 41]. The reporter plasmid for verification was built by cloning tdTomato under the control of ENO2p into pRS416 plasmid. To build gRNA-expressing plasmids, empty gRNA expressing vectors were first made by cloning the pRPR1 promoter (an RNA-polymerase-III-dependent promoter), the gRNA handle (flanked by HindIII and Xho1 sites), and the RPR1 terminator into the SacI and KpnI sites of the pRS425 plasmid. Sequences of the constructs that were used in this study were listed in Appendix D Table D.S1. Strains constructed in this study were listed in Appendix D Table D.S2.

5.4.2 Fluorescence Assays

To assess expression of the reporter constructs, yeast cells expressing different gRNAs (or no gRNA as control) were grown overnight (250 rpm, 30°C) in 3 mL SC medium supplemented with glucose with appropriate selection (three independent cultures for each sample). Ten microliters of these cultures were then transferred into fresh media, supplemented with galactose and grown for 20 h (250 rpm, 30°C) before analysis by plate reader. The wave lengths of the different reporter genes are eGFP: λ_{ex} 488 nm, λ_{em} 507nm; Sapphire: λ_{ex} 399 nm, λ_{em} 511nm; Venus λ_{ex} 515 nm, λ_{em} 528nm; tdTomato λ_{ex} 554 nm, λ_{em} 581nm; mCherry λ_{ex} 587 nm, λ_{em} 610 nm. All of the fold-changes of the synthetic genetic cassettes, including the four cassettes for model training and the ENO2p-tdTomato cassette for model validation, were listed in Appendix D Table D.S3 and Appendix D Table D.S4.

5.4.3 Qualitative Analysis of Key Parameters.

The exponential fold changes of different gRNA designs have been separated into two categories, the promoter region (location < 0, n = 52) and the gene coding region (location > 0, n = 86). The unpaired two-tail t-test was used to calculate the significance of

the fold changes between these two groups. For the analysis of the PAM type, the same t-test was used for each PAM types (n_{AGG} = 42, n_{TGG} = 69, n_{CGG} = 21, n_{GGG} = 6).

5.4.4 Modeling

The multiple linear regression model was implemented by the "*regress*" command in MATLAB. To evaluate the prediction power, the ten-fold cross validation was implemented for the linear model. The Pearson's correlation coefficient between observed and predicted fold changes was calculated by MATLAB. The binary regression decision tree model was developed by using "*fitrtree*" command in MATLAB with all the default setting of options. The details of the decision tree model were shown in Appendix D Table D.S5. The ten-fold cross validation was implemented for this model with the same manner. A detailed tutorial of CRISTINES was included in the supplementary information.

5.4.5 Ten-Fold Cross Validation

All the datasets from the four synthetic genetic cassettes (n = 151) were randomly divided into ten folds (nine folds with 15 datasets each and one-fold with 16 datasets). Nine of the ten folds were used as training datasets, and the one-fold remaining was used as validation datasets. By iteratively repeating the above process for ten times, all the folds could be used as validation datasets. The Pearson's correlation coefficient between the observed fold changes and predicted fold changes of were calculated by MATLAB.

5.4.6 Analysis of Products from Violacein Pathway.

Yeast strains for violacein biosynthesis were constructed and product distributions were analyzed as described previously with minor modifications. The parent yeast strain for these experiments was BY4741. The five-gene cassette of violacein pathway was constructed using the DNA assembler method: VioA under TEF1p; VioB under PGK1p;

VioC under ENO2p; VioD under TPI1p and VioE under PDC1p. Yeast strains with violacein pathway genes and the CRISPR system with constitutive dCas9 expression were grown in SC medium containing 5% galactose. After 3 days at 30 °C, approximately 2 mL of yeast cultures were harvested and the cells were collected and suspended in 250 μL of methanol, boiled at 95 °C for 15 minutes, and vortexed twice during the incubation. Solutions were centrifuged twice to remove cell debris, and the products from violacein pathway (i.e., violacein, proviolacein, deoxyviolacein, and prodeoxyviolacein) in the supernatant were analyzed by HPLC on an Agilent Rapid Resolution SB-C18 column as described previously, measuring absorbance at 565 nm[42].

Acknowledgements

We thank the Writing Center in Virginia Tech for improving the language of the paper. This study was supported by start-up fund (#175323) and the ICTAS Junior Faculty Award from Virginia Tech.

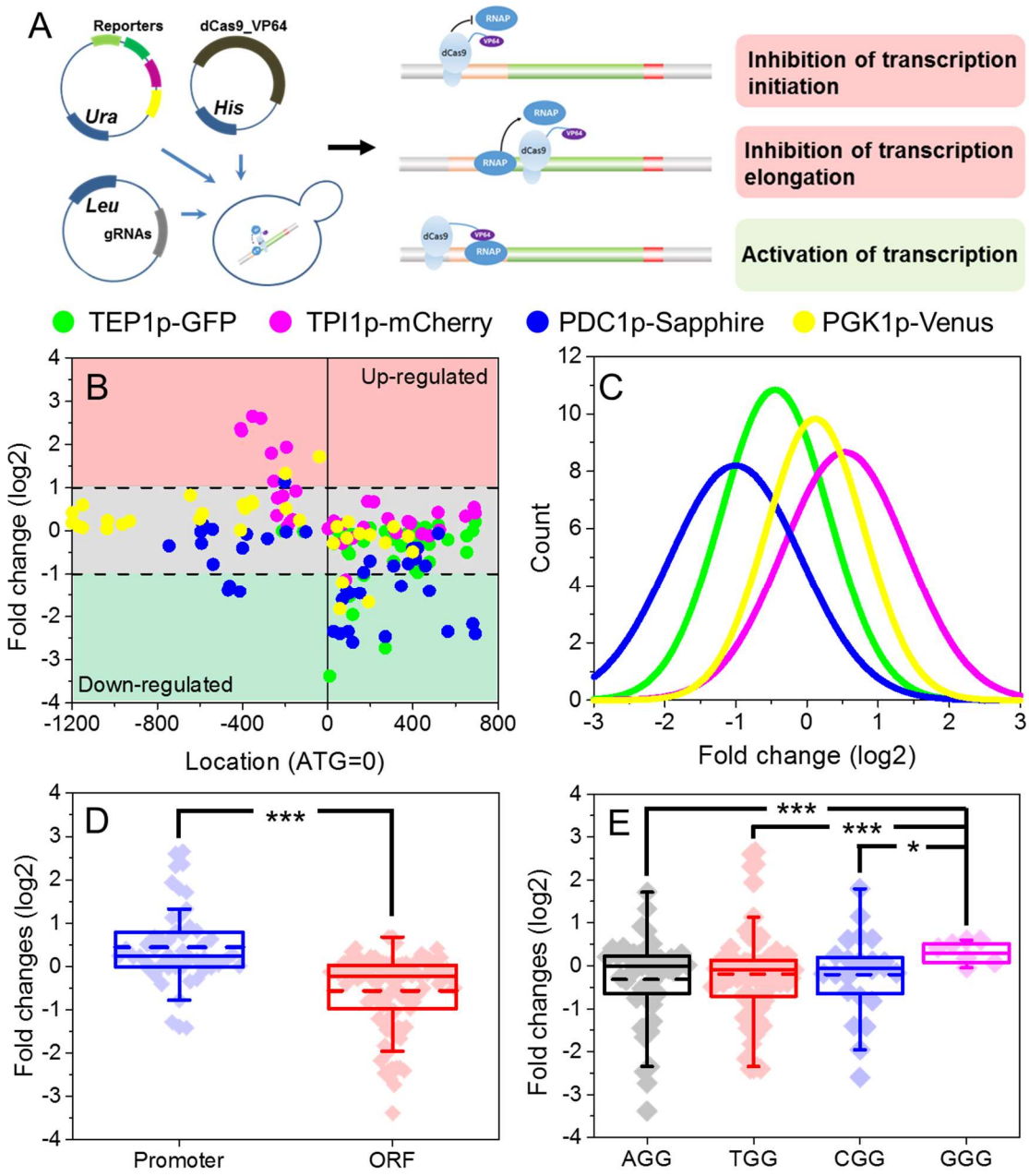

Fig. 5.1 Multi-directional transcriptional regulation by dCas9-VP64. (A) Hypothesized mechanism of transcriptional regulation by dCas9-VP64 to achieve both gene activation and gene repression. (B) The measured fold changes of gene expressions from the four synthetic genetic cassettes based on the PAM position. (C) The distributions of fold changes of gene expressions. (D) Comparison of fold changes of gene expressions from two groups: PAM sites located in the promoter regions and PAM sites located in the

ORF region. ***: $p < 0.01$. (E) Effects of different PAM sites on transcriptional regulation by dCas9-VP64. *: $p < 0.05$.

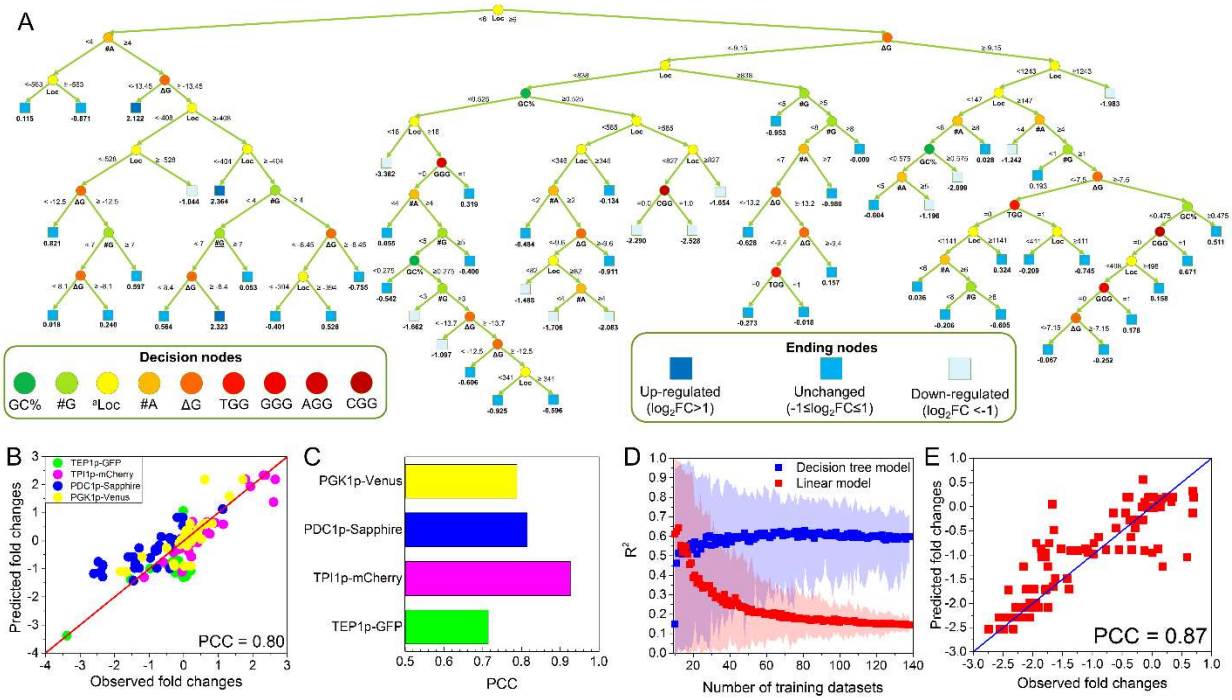

Fig. 5.2 Data-driven model of transcriptional regulation by using dCas9-VP64. (A) Binary regression tree model trained with all the screening data from the four synthetic genetic cassettes. The regression tree model consisted of 58 decision nodes and used six design parameters of guide RNAs as input. (B) and (C) Prediction accuracy of the regression tree model from ten-fold cross validation. (D) Impact of data size on model prediction. For data-driven model, the prediction increased with the inclusion of more datasets. For linear model, the prediction decreased when more datasets were used. The shadow areas indicate the 95% confidence interval of model prediction. (E) Validation of the regression tree model by comparing the simulated and experimentally measured gene regulations on Eno2p-tdTomato cassette subject to dCas9-VP64 regulation.

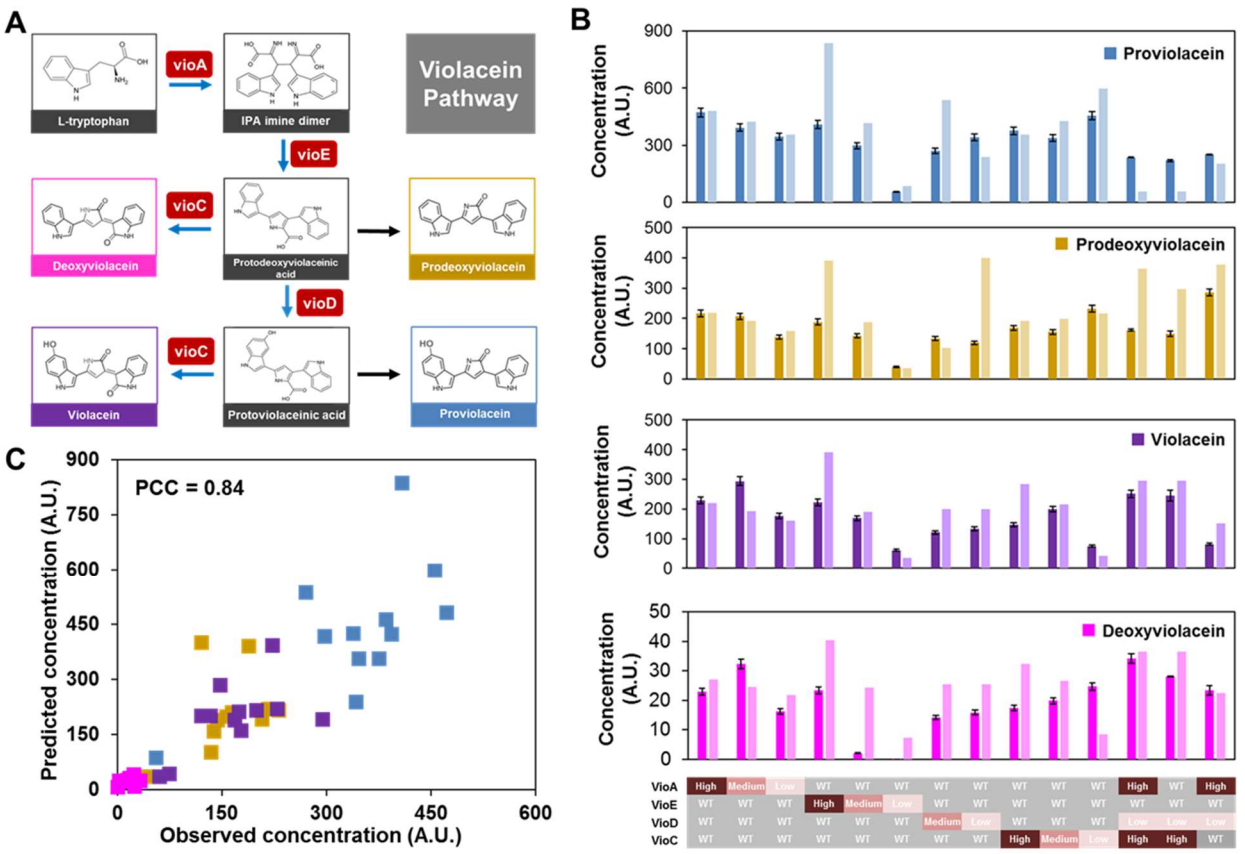

Fig. 5.3 Design dCas9-VP64 to reprogram metabolic fluxes in yeast. (A) Violacein pathway in yeast used in this study to demonstrate the programmable control of metabolic fluxes by using dCas9-VP64. Five enzymatic steps (vioA, vioB, vioC, vioD, and vioE) and two non-enzymatic steps led to four products from the violacein pathway: proviolacein, prodeoxyviolacein, violacein, and deoxyviolacein. (B) A panel of genes subject to regulation of dCas9-VP64 were chosen to control metabolic fluxes to various products from the violacein pathway. WT: wild type gene without any regulation; High: highly up-regulated gene expression by dCas9-VP64; Medium: medium-level up-regulated gene expression by dCas9-VP64; Low: down-regulated gene expression by dCas9-VP64. (C) The compassion between the model-predicted and experimentally measured products from the violacein pathway. The high correlation coefficient (PCC=0.84) indicated that the data-

driven model could accurately predict the effects of artificial Cas9-based regulator on metabolic flux reprogramming.

References

1. Lee, S.K., et al., *Metabolic engineering of microorganisms for biofuels production: from bugs to synthetic biology to fuels.* Current Opinion in Biotechnology, 2008. **19**(6): p. 556-563.
2. Keasling, J.D. and H. Chou, *Metabolic engineering delivers next-generation biofuels.* Nat Biotechnol, 2008. **26**(3): p. 298-9.
3. Vuoristo, K.S., et al., *Metabolic Engineering of TCA Cycle for Production of Chemicals.* Trends Biotechnol, 2016. **34**(3): p. 191-7.
4. Chen, X., et al., *Metabolic engineering of Escherichia coli: a sustainable industrial platform for bio-based chemical production.* Biotechnol Adv, 2013. **31**(8): p. 1200-23.
5. Yadav, V.G. and G. Stephanopoulos, *Metabolic Engineering: The Ultimate Paradigm for Continuous Pharmaceutical Manufacturing.* ChemSusChem, 2014. **7**(7): p. 1847-1853.
6. Khosla, C. and J.D. Keasling, *Metabolic engineering for drug discovery and development.* Nat Rev Drug Discov, 2003. **2**(12): p. 1019-25.
7. Keasling, J.D., *Manufacturing Molecules Through Metabolic Engineering.* Science, 2010. **330**(6009): p. 1355-1358.
8. Zadran, S. and R.D. Levine, *Perspectives in metabolic engineering: understanding cellular regulation towards the control of metabolic routes.* Appl Biochem Biotechnol, 2013. **169**(1): p. 55-65.
9. Zalatan, J.G., et al., *Engineering complex synthetic transcriptional programs with CRISPR RNA scaffolds.* Cell, 2015. **160**(1-2): p. 339-50.
10. McNerney, M.P., D.M. Watstein, and M.P. Styczynski, *Precision metabolic engineering: The design of responsive, selective, and controllable metabolic systems.* Metab Eng, 2015. **31**: p. 123-31.
11. Broun, P., *Transcription factors as tools for metabolic engineering in plants.* Curr Opin Plant Biol, 2004. **7**(2): p. 202-9.
12. Kim, J. and J.L. Reed, *OptORF: Optimal metabolic and regulatory perturbations for metabolic engineering of microbial strains.* BMC Syst Biol, 2010. **4**: p. 53.
13. Cong, L., et al., *Multiplex genome engineering using CRISPR/Cas systems.* Science, 2013. **339**(6121): p. 819-23.
14. Jiang, W., et al., *RNA-guided editing of bacterial genomes using CRISPR-Cas systems.* Nat Biotechnol, 2013. **31**(3): p. 233-9.
15. Gilbert, L.A., et al., *CRISPR-mediated modular RNA-guided regulation of transcription in eukaryotes.* Cell, 2013. **154**(2): p. 442-51.
16. Larson, M.H., et al., *CRISPR interference (CRISPRi) for sequence-specific control of gene expression.* Nat Protoc, 2013. **8**(11): p. 2180-96.
17. Qi, L.S., et al., *Repurposing CRISPR as an RNA-guided platform for sequence-specific control of gene expression.* Cell, 2013. **152**(5): p. 1173-83.
18. Farzadfard, F., S.D. Perli, and T.K. Lu, *Tunable and multifunctional eukaryotic transcription factors based on CRISPR/Cas.* ACS Synth Biol, 2013. **2**(10): p. 604-13.

19. Bikard, D., et al., *Programmable repression and activation of bacterial gene expression using an engineered CRISPR-Cas system.* Nucleic Acids Res, 2013. **41**(15): p. 7429-37.
20. Gao, Y., et al., *Complex transcriptional modulation with orthogonal and inducible dCas9 regulators.* Nat Methods, 2016. **13**(12): p. 1043-1049.
21. Montague, T.G., et al., *CHOPCHOP: a CRISPR/Cas9 and TALEN web tool for genome editing.* Nucleic Acids Research, 2014. **42**(W1): p. W401-W407.
22. Labun, K., et al., *CHOPCHOP v2: a web tool for the next generation of CRISPR genome engineering.* Nucleic Acids Research, 2016. **44**(W1): p. W272-W276.
23. Russell, S.J. and P. Norvig, *Artificial Intelligence: A Modern Approach*. 2003: Pearson Education. 1132.
24. Langley, P., *The changing science of machine learning.* Machine Learning, 2011. **82**(3): p. 275-279.
25. Mohri, M., A. Rostamizadeh, and A. Talwalkar, *Foundations of machine learning*. 2012: MIT press.
26. Breiman, L., et al., *Classification and regression trees*. 1984: CRC press.
27. Loh, W.-Y. and Y.-S. Shih, *Split selection methods for classification trees.* Statistica sinica, 1997: p. 815-840.
28. Hoshino, T., *Violacein and related tryptophan metabolites produced by Chromobacterium violaceum: biosynthetic mechanism and pathway for construction of violacein core.* Appl Microbiol Biotechnol, 2011. **91**(6): p. 1463-75.
29. Cho, S.W., et al., *Analysis of off-target effects of CRISPR/Cas-derived RNA-guided endonucleases and nickases.* Genome Res, 2014. **24**(1): p. 132-41.
30. Haeussler, M., et al., *Evaluation of off-target and on-target scoring algorithms and integration into the guide RNA selection tool CRISPOR.* Genome Biol, 2016. **17**(1): p. 148.
31. Delebecque, C.J., et al., *Organization of intracellular reactions with rationally designed RNA assemblies.* Science, 2011. **333**(6041): p. 470-4.
32. Farasat, I. and H.M. Salis, *A Biophysical Model of CRISPR/Cas9 Activity for Rational Design of Genome Editing and Gene Regulation.* PLoS Comput Biol, 2016. **12**(1): p. e1004724.
33. Nishimasu, H., et al., *Crystal structure of Cas9 in complex with guide RNA and target DNA.* Cell, 2014. **156**(5): p. 935-49.
34. Jinek, M., et al., *Structures of Cas9 endonucleases reveal RNA-mediated conformational activation.* Science, 2014. **343**(6176): p. 1247997.
35. Slaymaker, I.M., et al., *Rationally engineered Cas9 nucleases with improved specificity.* Science, 2016. **351**(6268): p. 84-8.
36. Jiang, F., et al., *Structures of a CRISPR-Cas9 R-loop complex primed for DNA cleavage.* Science, 2016. **351**(6275): p. 867-71.
37. Jiang, F., et al., *STRUCTURAL BIOLOGY. A Cas9-guide RNA complex preorganized for target DNA recognition.* Science, 2015. **348**(6242): p. 1477-81.
38. Hittinger, C.T., *Saccharomyces diversity and evolution: a budding model genus.* Trends Genet, 2013. **29**(5): p. 309-17.
39. Petzold, C.J., et al., *Analytics for Metabolic Engineering.* Frontiers in Bioengineering and Biotechnology, 2015. **3**: p. 135.

40. Shao, Z., H. Zhao, and H. Zhao, *DNA assembler, an in vivo genetic method for rapid construction of biochemical pathways.* Nucleic Acids Res, 2009. **27**(2): p. e16.
41. Shao, Z., Y. Luo, and H. Zhao, *Rapid characterization and engineering of natural product biosynthetic pathways via DNA assembler.* Mol Biosyst, 2011. **7**(4): p. 1056-9.
42. Lee, M.E., et al., *Expression-level optimization of a multi-enzyme pathway in the absence of a high-throughput assay.* Nucleic Acids Res, 2013. **41**(22): p. 10668-78.

Chapter 6: Outreaches in Metabolic Engineering

6.1 Metabolic Engineering of *Saccharomyces cerevisiae* to Produce 1-Hexadecanol from Xylose

Weihua Guo[a, *], Jiayuan Sheng[a, *], Huimin Zhao[b, †], Xueyang Feng[a, †]

[a] Department of Biological Systems Engineering, Virginia Polytechnic Institute and State University, Blacksburg, VA 24061, United States

[b] Department of Chemical and Biomolecular Engineering, University of Illinois at Urbana-Champaign, Urbana, IL 61801, United States

[†]Correspondence to: Huimin Zhao and Xueyang Feng.

[*] JS and WG contribute to this work equally.

Phone: +1-(217) 333-2631 and +1-(540)231-2974

Email: zhao5@illinois.edu and xueyang@vt.edu

This manuscript has been published on *Microbial cell factories* 15 (1), 24. Supplementary material of Chapter 6.1 is shown in Appendix E.

Abstract

Background. An advantageous but challenging approach to overcome the limited supply of petroleum and relieve the greenhouse effect is to produce bulk chemicals from renewable materials. Fatty alcohols, with a billion-dollar global market, are important raw chemicals for detergents, emulsifiers, lubricants, and cosmetics production. Microbial production of fatty alcohols has been successfully achieved in several industrial microorganisms. However, most of the achievements were using glucose, an edible sugar, as the carbon source. To produce fatty alcohols in a renewable manner, non-edible sugars such as xylose will be a more appropriate feedstock.

Results. In this study, we aim to engineer a *Saccharomyces cerevisiae* strain that can efficiently convert xylose to fatty alcohols. To this end, we first introduced the fungal xylose utilization pathway consisting of xylose reductase (XR), xylitol dehydrogenase (XDH), and xylulose kinase (XKS) into a fatty alcohol-producing *S. cerevisiae* strain (XF3) that was developed in our previous studies to achieve 1-hexadecanol production from xylose at 0.4 g/L. We next applied promoter engineering on the xylose utilization pathway to optimize the expression levels of XR, XDH, and XKS, and increased the 1-hexadecanol titer by 171%. To further improve the xylose-based fatty alcohol production, two optimized *S. cerevisiae* strains from promoter engineering were evolved with the xylose as the sole carbon source. We found that the cell growth rate was improved at the expense of decreased fatty alcohol production, which indicated 1-hexadecanol was mainly produced as a non-growth associated product. Finally, through fed-batch fermentation, we successfully achieved 1-hexadecanol production at over 1.2 g/L using xylose as the sole

carbon source, which represents the highest titer of xylose-based 1-hexadecanol reported in microbes to date.

Conclusions. A fatty alcohol-producing *S. cerevisiae* strain was engineered in this study to produce 1-hexadecanol from xylose. Although the xylose pathway we developed in this study could be further improved, this proof-of-concept study, for the first time to our best knowledge, demonstrated that the xylose-based fatty alcohol could be produced in *S. cerevisiae* with potential applications in developing consolidated bioprocessing for producing other fatty acid-derived chemicals.

Key Words

Yeast, promoter engineering, evolutionary engineering, fatty alcohols.

6.1.1 Introduction

Producing bulk chemicals from renewable resources could reduce strong dependence on petroleum and the damage to the environment [1, 2]. As important chemicals with a billion-dollar market globally [3, 4], fatty alcohols have been widely used to produce detergents, emulsifiers, lubricants, cosmetics, and have the potential to be used as fuels [5]. Currently, fatty alcohols are produced in two ways. One is direct extraction from natural plant oils [6], and the other is chemical synthesis from petrochemical sources. These methods have limitations due to either competition with the food supply, environmental concerns [7], or fast depletion of fossil sources [8].

Recently, with the development of metabolic engineering and synthetic biology, microbial production of fatty alcohols from renewable feedstock has been achieved successfully in both *Escherichia coli* [4, 9] and *Saccharomyces cerevisiae* [3, 10]. So far, the highest titer of fatty alcohols produced was 1.95 g/L [11] and 1.1 g/L [10] by *E. coli* and *S. cerevisiae* respectively. A significantly higher titer of fatty alcohols was recently reported to be produced by *R. toloroides* [12]. In *E. coli*, fatty alcohols have been produced by introducing heterologous enzymes such as fatty acyl-CoA reductase (FAR) [13], carboxylic acid reductase (CAR) [14] together with aldehyde reductases (AR) , or acyl-CoA reductase (ACR) together with aldehyde reductases (AR) [4, 15]. Compared to that in *E. coli*, the synthetic route (i.e., steps of enzymatic reactions) of fatty acyl-CoA is shorter in yeast, which allows more efficient conversion of carbohydrate substrates to fatty acids and fatty acid-derived biofuels [9]. Also, as a well characterized robust industrial host, yeast can grow under low pH and various harsh fermentation conditions [16]. Therefore, there has been an increasing interest on developing yeast, such as *S. cerevisiae*, as a cell

factory for fatty acid-derived biofuel production. In *S. cerevisiae*, a mouse FAR has been expressed to produce 1-hexadecanol [10]. Through over-expression of acetyl-CoA carboxylase (ACC) and fatty-acyl-CoA synthases (FAS), the engineered *S. cerevisiae* strain produced 98.0 mg/L total fatty alcohol from 20 g/L glucose in batch culture in minimal medium [3]. Recently, by manipulating the structural genes in yeast lipid metabolism, tuning the regulation of phospholipid synthesis, and increasing the supply of key precursors, 1-hexadecanol was produced at 1.1 g/L using glucose as the carbon source in a fed-batch fermentation [10].

One of the limitations for current research on metabolic engineering to produce fatty acid-derived chemicals is that almost all of the achievements were based on glucose as the carbon source. To produce biofuels and biochemicals in a renewable manner, non-edible sugars such as xylose will be a more appropriate feedstock. Recently, engineering *S. cerevisiae* to utilize xylose is of great interest to the biofuel industry and could solve the major bottleneck in complete and efficient conversion of cellulosic sugars present in solubilized cell wall of plants into biofuels [17]. The sugar D-xylose, derived from hydrolysis of hemicellulose, is the second most abundant sugar in the plant cell wall consisting of up to 35% of the total carbohydrate from lignocellulose biomass [18]. However, since the yeast *S. cerevisiae* cannot metabolize xylose, heterologous xylose utilization pathway needs to be introduced into *S. cerevisiae* to achieve this objective. Two different pathways for the catabolism of D-xylose have been established in *S. cerevisiae*: the fungal xylose pathway consisting of xylose reductase (XR), xylitol dehydrogenase (XDH), and xylulose kinase (XKS) [17, 19-21], and the xylose pathway using the enzyme, xylose isomerase, to convert D-xylose directly into D-xylulose [22, 23], followed by the

phosphorylation of D-xylulose to D-xylulose-5-phosphate. Recently, xylose isomerase has been successfully used in an industrial yeast strain [24].

In this study, we aim to engineer a *S. cerevisiae* strain that can efficiently convert xylose to fatty alcohols, by expressing a heterologous fungal xylose pathway into a 1-hexadecanol-producing *S. cerevisiae* strain that has been previously developed. We chose a *S. cerevisiae* strain, namely XF3, as our host since it has been engineered to produce 1-hexadecanol at over 1 g/L from glucose, and introduced xylose reductase (XR), xylitol dehydrogenase (XDH), and xylulose kinase (XKS) into XF3 to utilize xylose as the sole carbon source. Then, by applying combinatorial promoter engineering and evolutionary engineering, the production of 1-hexadecanol was enhanced by 171%. Finally, over 1.2 g/L 1-hexadecanol was produced in a fed-batch fermentation using xylose as the sole carbon source, which is at the similar level when using the glucose as the carbon source [10]. To our best knowledge, it is first time that yeast was engineered to use a pentose sugar for producing fatty acid-derived biofuels.

6.1.2 Materials and Methods

Yeast Strains, Media, and Transformation. The yeast strains used in this study were derived from BY4742 (Table 6.1.1). Yeast and bacterial strains were stored in 25% glycerol at -80 °C.*E. coli* DH5α strain was used to maintain and amplify plasmids, and recombinant strains were cultured at 37 °C in Luria-Bertani (LB) broth. Ampicillin at 100 μg/mL was added to the medium when required. Yeast BY4742 strains were cultivated in YPAD medium. Yeast cells were transformed with plasmids listed in Table 1 using the LiAc/PEG method as described previously [25]. To select the yeast transformants, a synthetic complete (SC) medium was used, which contains 0.17% yeast nitrogen base,

0.5% ammonium sulfate, and the appropriate amino acids dropout mix (MP Biomedicals, Solon, OH). A single colony was picked and cultivated in 5 mL SC medium containing 20 g/L glucose. The cells were cultivated at 30 °C in disposable culture tubes shaken at 250 rpm for 2 days.

Plasmid Construction. A yeast homologous recombination-based method, DNA assembler [26], was used to construct the recombinant plasmids. Briefly, DNA fragments sharing homologous regions to adjacent DNA fragments were co-transformed into *S. cerevisiae* along with the linearized backbone to assemble several elements in a single step [27]. Oligonucleotides used in this study were listed in Appendix E Table E.S1 and the recombinant plasmids constructed in this study were listed in Table 6.1.1. To construct the library for promoter engineering, the csXR was amplified with forward primer (XF_FP_csXR_ADH1t) and reverse primer (XF_RP_csXR_ADH1t); the ctXDH was amplified with forward primer (XF_FP_ TEF1p _CYC1t) and reverse primer (XF_RP_ctXDH_CYC1t); the ppXKS was amplified with forward primer (XF_FP_ppXKS_ADH2t) and reverse primer (XF_FP_ppXKS_ADH2t). The resulting PCR fragments have a 40 bp region homologous to constitutive yeast promoters and terminators, respectively. The constitutive yeast PDC1p promoters with different strengths for csXR were amplified with forward primer (XF_FP_PDC1p) and reverse primer (XF_RP_PDC1p) and using mutant PDC1p templates [28]. The different versions of TEF1p promoters for ctXDH and ENO2p promoters for ppXKS were achieved using the same methods. The DNA Assembler method was next used to construct the xylose utilization plasmids pRS416-PDC1p (L/M/H)-csXR-ADH1t-TEF1p(L/M/H)-ctXDH-CYC1t-ENO2p(L/M/H)-ppXKS-ADH2t with the proper combinations of each fragment

(Fig. 6.1.1B). The sequences of all mutated promoters were listed in Appendix E Table E.S2.

Determination of 1-Hexadecanol Production. The 1-hexadecanol was detected using a method previously described [3]. In general, for screening the 1-hexadecanol production in different strains, the engineered yeast strains were pre-cultured in 3 mL synthetic complete (SC) medium including all the appropriate nucleotides and amino acids, with 2% glucose for three days until saturation. The cells were then centrifuged and washed twice with double-distilled water. The cell pellets were next inoculated into 5 mL fresh SC medium with 40 g/L xylose in disposable glass tubes overlaid with 10% dodecane to prevent the evaporation of fatty alcohols and enrich the fatty alcohol in the organic layer to ease the measurement [3]. The concentrations of 1-hexadecanol were quantified at 48 h [3]. The glass tubes of yeast cultures were allowed to sit for 2 min until the organic layer could be clearly visualized. Then, 3 μL of dodecane was withdrawn from the organic layer and diluted by 100 times using ethyl acetate and analyzed by GC–MS (ShimadzuGC-MS-QP2010) with a DB-Wax column with 0.25 μm film thickness, 0.25 mm diameter, and 30 m length (Agilent Inc., Palo Alto, CA). Tridecane at a concentration of 2 mg/L was used as the internal standard. The GC program was as follows: an initial temperature of 50 °C was maintained for 1.5 min, followed by ramping to 180 °C at a rate of 25 °C /min. The temperature was then ramped to 250 °C at a rate of 10 °C /min, where the temperature was held for 3 min.

Evolutionary Engineering. To improve xylose utilization of the engineered strain, the optimized strain was cultured and serial-transferred into 50 mL of fresh SC medium with 40 g/L xylose as the sole carbon source in a closed 100 mL flask. The cells were

grown until the early stationary phase (~3 days) and spread on SC-xylose plates. After 3-days growth, the biggest colony was inoculated into a fresh medium and grown until the early stationary phase. Then the cells were sub-cultured with 5% inoculums in biological triplicates into fresh medium for the second round evolutionary engineering using the SC medium with 40 g/L xylose. The cells were grown for 3 days with typical OD_{600} in the range of 1.5-2.5. For each round of cell culture, the cell growth rate and fatty alcohol titer were measured using the method described above. We checked the plasmids intactness for each generation of the evolved strains by colony PCR, amplifying the cassettes for each gene, and confirming the intactness by DNA electrophoresis. All the plasmids were found to be intact (Appendix Fig. E.S1).

Batch and fed-batch fermentation. Both XF3XP and XF3XP07 yeast strains were first grown in 100 mL SC medium including all the appropriate nucleotides and amino acids, with 20 g/L glucose for 2 days. Then, cells from 5 mL of culture were centrifuged, washed twice with double-distilled water, and inoculated into 5 mL fresh SC medium with 40 g/L xylose in glass disposable tubes overlaid with 0.5 mL dodecane for batch fermentation. The initial ODs were similar, i.e., 2.38 ± 0.05 and 2.45 ± 0.06, with no significant difference (p-value >0.05). Samples were taken at various time points to measure the 1-hexadecanol concentration, OD_{600}, and xylose concentration. At each time point, the glass tubes of yeast cultures were allowed to sit for 2 min until the organic layer could be clearly visualized. To measure the 1-hexadecanol concentration, 3 μL of dodecane was withdrawn from the organic layer and then diluted by 100 times using ethyl acetate followed by the analysis using the GC–MS protocol mentioned above. To monitor OD_{600}, 20 μL of yeast culture was taken from the water layer and mixed with 180 μL of double-

distilled water, followed by measuring the absorbance at 600 nm using a Biotek Synergy 2 Multi-Mode Microplate Reader (Winooski, VT). To measure the concentration of xylose, 100 μL of yeast culture was taken from the water layer and mixed with 900 μL of double-distilled water, which was then centrifuged at 13,000 rpm for 5 min. The supernatant was taken and analyzed by Shimadzu HPLC (Columbia, MD) equipped with an Aminex HPX-87H column (Bio-Rad, Hercules, CA) and Shimadzu RID-10A refractive index detector. The column was kept at 50 °C, and 5 mM sulfuric acid solution was used as a mobile phase with a constant flow rate of 0.6 mL/min. Each data point represents the mean of triplicate samples. In this discontinuous fed-batch fermentation, additional xylose (0.5 mL with concentration of 200 g/L) and dodecane (0.05 mL) were fed every 12 hrs. Samples were taken after the replenishment to measure 1-hexadecanol concentration, OD_{600}, and xylose concentration using the similar methods as that for batch fermentation. The biological triplicates were implemented in both batch and fed-batch fermentation for all the strains.

6.1.3 Results and Discussion

Constructing a Xylose Utilization Pathway in a Fatty Alcohol-Producing Strain. In order to produce the xylose-based 1-hexadecanol, we first introduced the fungal xylose utilization pathway [29] into a 1-hexadecanol-producing *S. cerevisiae* strain, XF3 [10] (Fig. 6.1.1). The xylose utilization pathway was selected from our previous study [29], which included a XR from *Candida shehatae*, a XDH from *Candida tropicalis* and a XKS from *Pichia pastoris*. The XF3 strain produced 1-hexadecanol at over 1.1 g/L from glucose in *S. cerevisiae* as reported in our previous study [10]. The 1-hexadecanol production in XF3 was achieved by heterologously expressing a FAR from barn owls, over-expressing acetyl-CoA carboxylase (*ACC1* gene), knocking out a negative regulator, *RPD3* gene, in

phospholipid synthesis, and over-expressing ATP-citrate lyases (*ACL1* gene and *ACL2* gene) from *Yarrowia lipolytica* to enhancing the supply of cytosolic acetyl-CoA (Fig. 6.1.1A). By introducing the fungal xylose utilization pathway into XF3 strain, we successfully generated a *S. cerevisiae* strain (XF3XP) to produce the 1-hexadecanol from xylose as the sole carbon source at 0.4 g/L (Table 6.1.2). The xylose-based fatty alcohol titer was lower than the glucose-based 1-hexadecanol titer [10] and only 15 g/L xylose was consumed to produce 1-hexadecanol, indicating the xylose utilization could be a rate-limiting step for fatty alcohol production. We also introduced another fungal xylose pathway in which the promoter strengths of XR, XDH, and XKS were previously optimized to increase xylose-based ethanol production (XF3XPi, Table 6.1.2). We found that although 1-hexadecanol production could be increased to 0.48 g/L, the xylose utilization was even worse than the wild-type pathway with less than 5 g/L xylose consumed. This is possibly due to the fact that the regulatory mechanism adopted by *S. cerevisiae* to control xylose-based fatty alcohol production was different from that to control xylose-based ethanol production. Therefore, the metabolic engineering of *S. cerevisiae* for biofuel production is target-specific.

Promoter Engineering to Improve 1-Hexadecanol Production from Xylose. In order to further improve the 1-hexadecanol production, we implemented a synthetic biology approach called Customized Optimization of Metabolic Pathways by Combinatorial Transcriptional Engineering (COMPACTER) [28] to precisely control the gene expression levels of XR, XDH, and XKS. Basically, we chose three constitutive promoters, P_{PDC1}, $P_{TEF1,}$ and P_{ENO2} to express XR, XDH and XKS genes, respectively. For each of the constitutive promoters, we mutated the original promoters to create a promoter

library with varying strengths. We then selected promoters with high, medium, and low strengths (Appendix E Fig. E.S2) for P_{PDC1}, $P_{TEF1,}$ and P_{ENO2}, respectively, and constructed totally 27 synthetic xylose pathways (3×3×3=27) in *S. cerevisiae* with all of the promoter combinations of P_{PDC1}, $P_{TEF1,}$ and P_{ENO2} with different strengths. (Fig. 6.1.1B and Table 6.1.1). We next compared the growth rates and 1-hexadecanol titers of all the recombinant *S. cerevisiae* strains to that of the control strains, XF3XP (Fig. 6.1.2). It is worth noticing that the purpose of combinatorial promoter screening was to find the highest fatty alcohol production strain from xylose instead of the best xylose utilization strain. Therefore, we did not measure the xylose utilization rates here. We found that the growth rates of most of the promoter-engineered strains were reduced to some extent, and the 1-hexadecanol production for most of the recombinant strains was not significantly improved. However, strain XF3X07 and XF3X25 produced 1-hexadecanol at 171% and 140% higher than that of the control strains with a slightly deceased growth rates (0.073 h^{-1} and 0.080 h^{-1}) compared with the growth rates of control strains (0.093 h^{-1}). Both XF3X07 and XF3X25 used a high-level TEF1 promoter to express XDH and a low-level ENO2 promoter to express XKS. Nevertheless, XF3X07 used a low-level PDC1 promoter to express XR while XF3X25 used a high-level PDC1 promoter. This discovery is consistent with previous studies showing that the XDH enzymes were rate-limiting steps in converting xylose to biomass and ethanol [30, 31]. Interestingly, despite of higher titer of 1-hexadecanol in XF3X07 compared to XF3XPi, the xylose-based 1-hexadecanol yields were similar in XF3XP07 and XF3XPi (p>0.1). This indicated that the combinatorial promoter engineering mainly improved the xylose uptake rate instead of optimizing the host pathways to improve the conversion of xylose to 1-hexadecanol.

We correlated the strengths of promoters for XR, XDH, and XKS with the two measured parameters, 1-hexadecanol concentrations and growth rates (Appendix E Fig. E.S3). No correlation was observed between promoter strengths and 1-hexadecanol concentrations. Neither did we find the correlation between promoter strengths and growth rates. We also correlated 1-hexadecanol concentrations and growth rates, but found no correlation between them either (Appendix E Fig. E.S4). Therefore, it is unfeasible to solely use the results of promoter screening to make predictions on the choice of promoters that should be used for xylose-based production of 1-hexadecanol. This is because the introduction of xylose pathways would trigger the global metabolic rewiring, as we found previously when investigating metabolic responses to different xylose utilization pathways via ^{13}C metabolic flux analysis[32]. This global metabolic rewiring involves the reprogramming of not only xylose pathway itself but also the downstream pathways, which made the xylose metabolism too complex to be correlated with the activity of xylose utilization pathway itself.

Evolutionary Engineering to Improve 1-Hexadecanol Production from Xylose. We next chose XF3X07 and XF3X25 as our target strains for further evolutionary engineering to improve the 1-hexadecanol production. Evolutionary engineering has been widely used to improve the pentose utilization and xylose-based ethanol production in *S. cerevisiae* successfully [33-35]. Considering the poor xylose uptake in our engineered strains, we implemented the evolutionary engineering to investigate whether fatty alcohol production is growth-associated, and if so, to further improve the xylose-based fatty alcohol production. Similar as the study of combinatorial promoter screening, our goal of evolutionary engineering is to seek a yeast strain that could produce fatty alcohols from

xylose as much as possible. Therefore, we did not measure the xylose utilization rates. In general, we serially transfer the strain XF3X07 and XF3X25 to synthetic medium with 40 g/L xylose twice. Namely, the optimized strain was the second generation evolved from the wild-type strain. We found that the growth rates of two strains increased gradually (~25% and ~35%) for every round as expected. However, such increase was associated with reduced 1-hexadecanol production. For example, the highest growth rate was reached for both XF3X07 and XF3X25 with the lowest titer of 1-hexadecanol in the second round (Fig. 6.1.3). The growth rates of the evolved strains in the last round were significantly increased for XF3XP07 and XF3XP25 (p<0.05). However, the 1-hexadecanol productions were not significantly changed (p>0.05). Such discrepancy indicated that 1-hexadecanol, unlike ethanol, was not a growth-associated product. Since evolutionary engineering selects the mutant strain with higher growth rate, the 1-hexadecanol production failed to be further improved via adaptive evolution due to the de-coupling between the cell growth rate and the fatty alcohol production. In addition, we applied flux balance analysis to calculate the ATP, NADH, and NADPH synthesis under different 1-hexadecanol productions (Fig. E.S5). We found that the NADPH and ATP synthesis were positively correlated with 1-hexadecanol production, while NADH synthesis did not change too much with the 1-hexadecanol synthesis. Overall, the evolutionary engineering approach would be helpful to improve the cell growth and growth-associated products such as ethanol, but not for non-growth associated products such as fatty acid-derived chemicals.

Batch and Fed-Batch Fermentation for 1-Hexadecanol Production. With XF3XP07 as our best strain to produce xylose-based 1-hexadecanol, we next characterized its 1-hexadecanol production using batch and fed-batch fermentation. In batch

fermentation, we found that 0.79 g/L 1-hexadecanol was produced from 7.8 g/L xylose, with a cell growth rate at 0.073 h^{-1} (Table 6.1.2). This 1-hexadecanol titer of XF3XP07 is significantly higher than the ones of XF3XP and XF3XPi strain (p<0.05). More interestingly, comparing the xylose uptakes of the XF3XP and XF3XPi, we found the XF3XP strain consumed three-fold more xylose than the XF3XPi strain. This additional xylose was mainly used to produce more ethanol in XF3XP strains (Table 6.1.2). In addition, we have measured the accumulation of intracellular 1-hexadecanol, which was less than 5% of the extracellular concentration of 1-hexadecanol from the organic layer. Such low accumulation is consistent with several previous studies when yeast was cultured with an organic layer [36], although it is also reported that *S. cerevisiae* strains could accumulate a large amount of fatty alcohols intracellularly when cultured without the organic layer [37].

In fed-batch fermentation, we used resting cells for fermentation, i.e., the cell density was kept at high level to prevent using the xylose to produce biomass. Although the fermentation at high cell density might limit the oxygen supply for the fermentation, which is an important factor for the optimal expression of the xylose pathway genes [38], the marginal net growth rate of yeast cells could be more important in fed-batch fermentation because it was found in this study that fatty alcohol production was not growth-associated and hence by removing the biomass production, yeast cells could serve as biocatalysts to convert xylose to 1-hexadecanol with high efficiency. We found that a long lag phase lasting around 40 h in the fed-batch fermentation, which could be due to the repression of residue glucose from the inoculum since we cultured XF3XP and XF3XP07 with 20 g/L glucose before transferring the cells into the medium with xylose, and hence

cells needed a long time to accustom to xylose from glucose (Fig. 6.1.4). For the XF3XP strain, 1-hexadecanol has been produced quickly with a low xylose consumption, and achieved ~0.6 g/L of 1-hexadecanol at 48 h (Fig. 6.1.4A). For the XP3XP07 strain, after the long lag phase, 1-hexadecanol was produced rapidly with the increased xylose uptake and reached the highest titer of 1-hexadecanol at 1.2 g/L at the 69 h (Fig. 6.1.4B). However, when continuing the fed-batch fermentation for both strains, both the 1-hexadecanol concentrations and xylose uptake rates were decreased. The observed low xylose consumption rate accompanied with the decrease of OD_{600} suggested a starvation because of the incapability to further uptake the carbon substrate and the probable limitation by other nutrients such as nitrogen and phosphate after the 50 h of the fermentation. In our previous study[10], we found that fatty alcohols could be taken up by *S. cerevisiae,* which could be the reason for the decreased fatty alcohol production when xylose utilization became limited.

Comparing the xylose-based fatty alcohol production to the glucose-based one in the previous study, the similar titer of fatty alcohol from fed-batch fermentation has been observed, demonstrating the successful integration of xylose utilization pathway and the fatty alcohol production pathway. However, the yields of xylose-based fatty alcohols in both batch (0.10±0.02 g/g) and fed-batch fermentation (0.08 ±0.01 g/g) were much higher than that of glucose-based ones (~0.03 g/g and <0.01 g/g), respectively. The theoretical maximum yields through this production pathway from xylose and glucose were ~0.34 and ~0.35 (g/g), respectively. In this case, the yield from xylose reached nearly one third of the theoretical yield, while the yield from glucose only reached less than 10% of the theoretical yield. The bypass of ethanol production when feeding xylose instead of glucose likely

attributed to the high yield of xylose-based 1-hexadecanol, which could divert more carbons to be utilized in the fatty alcohol production rather than ethanol production.

6.1.4 Conclusions

A fatty alcohol-producing *S. cerevisiae* strain was engineered in this study to produce 1-hexadecanol from xylose. To achieve this, a xylose utilization pathway consisting of XR, XDH and XK was heterologously expressed in *S. cerevisiae*, followed by optimization of the xylose-based fatty alcohol production through promoter engineering and evolutionary engineering to improve 1-hexadecanol production by 171%. Through fed-batch fermentation, the highest titer of 1-hexadecanol reached 1.2 g/L with xylose used as the sole carbon source. Although the xylose pathway we developed in this study was still not optimal, this proof-of-concept study, for the first time to our best knowledge, indicated that the xylose-based fatty alcohol could be achieved in *S. cerevisiae* with potential applications in developing consolidated bioprocessing for producing fatty acid-derived chemicals.

Acknowledgements

We thank the writing center in Virginia Tech for improving the language of the paper. This study was supported by start-up fund (#175323) from Virginia Tech (X.F.) and Energy Biosciences Institute (OO7G21) (H.Z.).

Table 6.1.1 Plasmids and strains used in this study.

Plasmids used in this study

Name	Description	Reference
pTaFAR_ACC1	pRS425-TEF1p-TaFAR-TEF1t-PGK1p-ACC1-HXT7t	Feng et al. (2015)[36]
pYlACL	pRS423-TPI1p-YlACL1-TPI1t-TEF1p-YlACL2-TEF1t	Lian et al. (2014)[39]
pXF3X01	pRS416-PDC1p(L)-csXR-ADH1t-TEF1p(L)-ctXDH-CYC1t-ENO2p(L)-ppXKS-ADH2t	This study
pXF3X02	pRS416-PDC1p(L)-csXR-ADH1t-TEF1p(L)-ctXDH-CYC1t-ENO2p(M)-ppXKS-ADH2t	This study
pXF3X03	pRS416-PDC1p(L)-csXR-ADH1t-TEF1p(L)-ctXDH-CYC1t-ENO2p(H)-ppXKS-ADH2t	This study
pXF3X04	pRS416-PDC1p(L)-csXR-ADH1t-TEF1p(M)-ctXDH-CYC1t-ENO2p(L)-ppXKS-ADH2t	This study
pXF3X05	pRS416-PDC1p(L)-csXR-ADH1t-TEF1p(M)-ctXDH-CYC1t-ENO2p(M)-ppXKS-ADH2t	This study
pXF3X06	pRS416-PDC1p(L)-csXR-ADH1t-TEF1p(M)-ctXDH-CYC1t-ENO2p(H)-ppXKS-ADH2t	This study
pXF3X07	pRS416-PDC1p(L)-csXR-ADH1t-TEF1p(H)-ctXDH-CYC1t-ENO2p(L)-ppXKS-ADH2t	This study
pXF3X08	pRS416-PDC1p(L)-csXR-ADH1t-TEF1p(H)-ctXDH-CYC1t-ENO2p(M)-ppXKS-ADH2t	This study
pXF3X09	pRS416-PDC1p(L)-csXR-ADH1t-TEF1p(H)-ctXDH-CYC1t-ENO2p(H)-ppXKS-ADH2t	This study
pXF3X10	pRS416-PDC1p(M)-csXR-ADH1t-TEF1p(L)-ctXDH-CYC1t-ENO2p(L)-ppXKS-ADH2t	This study
pXF3X11	pRS416-PDC1p(M)-csXR-ADH1t-TEF1p(L)-ctXDH-CYC1t-ENO2p(M)-ppXKS-ADH2t	This study
pXF3X12	pRS416-PDC1p(M)-csXR-ADH1t-TEF1p(L)-ctXDH-CYC1t-ENO2p(H)-ppXKS-ADH2t	This study
pXF3X13	pRS416-PDC1p(M)-csXR-ADH1t-TEF1p(M)-ctXDH-CYC1t-ENO2p(L)-ppXKS-ADH2t	This study
pXF3X14	pRS416-PDC1p(M)-csXR-ADH1t-TEF1p(M)-ctXDH-CYC1t-ENO2p(M)-ppXKS-ADH2t	This study
pXF3X15	pRS416-PDC1p(M)-csXR-ADH1t-TEF1p(M)-ctXDH-CYC1t-ENO2p(H)-ppXKS-ADH2t	This study
pXF3X16	pRS416-PDC1p(M)-csXR-ADH1t-TEF1p(H)-ctXDH-CYC1t-ENO2p(L)-ppXKS-ADH2t	This study
pXF3X17	pRS416-PDC1p(M)-csXR-ADH1t-TEF1p(H)-ctXDH-CYC1t-ENO2p(M)-ppXKS-ADH2t	This study
pXF3X18	pRS416-PDC1p(M)-csXR-ADH1t-TEF1p(H)-ctXDH-CYC1t-ENO2p(H)-ppXKS-ADH2t	This study
pXF3X19	pRS416-PDC1p(H)-csXR-ADH1t-TEF1p(L)-ctXDH-CYC1t-ENO2p(L)-ppXKS-ADH2t	This study
pXF3X20	pRS416-PDC1p(H)-csXR-ADH1t-TEF1p(L)-ctXDH-CYC1t-ENO2p(M)-ppXKS-ADH2t	This study
pXF3X21	pRS416-PDC1p(H)-csXR-ADH1t-TEF1p(L)-ctXDH-CYC1t-ENO2p(H)-ppXKS-ADH2t	This study
pXF3X22	pRS416-PDC1p(H)-csXR-ADH1t-TEF1p(M)-ctXDH-CYC1t-ENO2p(L)-ppXKS-ADH2t	This study
pXF3X23	pRS416-PDC1p(H)-csXR-ADH1t-TEF1p(M)-ctXDH-CYC1t-ENO2p(M)-ppXKS-ADH2t	This study
pXF3X24	pRS416-PDC1p(H)-csXR-ADH1t-TEF1p(M)-ctXDH-CYC1t-ENO2p(H)-ppXKS-ADH2t	This study
pXF3X25	pRS416-PDC1p(H)-csXR-ADH1t-TEF1p(H)-ctXDH-CYC1t-ENO2p(L)-ppXKS-ADH2t	This study
pXF3X26	pRS416-PDC1p(H)-csXR-ADH1t-TEF1p(H)-ctXDH-CYC1t-ENO2p(M)-ppXKS-ADH2t	This study
pXF3X27	pRS416-PDC1p(H)-csXR-ADH1t-TEF1p(H)-ctXDH-CYC1t-ENO2p(H)-ppXKS-ADH2t	This study
pXF3XP	pRS416-PDC1p-csXR-ADH1t-TEF1p-ctXDH-CYC1t-ENO2p-ppXKS-ADH2t	This study
pXF3XPi	pRS416-PDC1p*-csXR-ADH1t-TEF1p*-ctXDH-CYC1t-ENO2p*-ppXKS-ADH2t	Jing et al. (2012)[40]

Strains used in this study

Name	Genotype	Plasmids	Reference
BY4742	*MATα his3Δ1 leu2Δ0 lys2Δ0 ura3Δ0*		
XF3	BY4742 *ΔRPD3*: pTaFAR_ACC1, pYlACL		Feng et al. (2014)
XF3XP	Same as XF3	pXF3XP	This study
XF3XPi	Same as XF3	pXF3XPi	This study
XF3X01	Same as XF3	pXF3X01	This study
XF3X02	Same as XF3	pXF3X02	This study
XF3X03	Same as XF3	pXF3X03	This study
XF3X04	Same as XF3	pXF3X04	This study
XF3X05	Same as XF3	pXF3X05	This study
XF3X06	Same as XF3	pXF3X06	This study
XF3X07	Same as XF3	pXF3X07	This study
XF3X08	Same as XF3	pXF3X08	This study
XF3X09	Same as XF3	pXF3X09	This study
XF3X10	Same as XF3	pXF3X10	This study
XF3X11	Same as XF3	pXF3X11	This study
XF3X12	Same as XF3	pXF3X12	This study
XF3X13	Same as XF3	pXF3X13	This study
XF3X14	Same as XF3	pXF3X14	This study
XF3X15	Same as XF3	pXF3X15	This study
XF3X16	Same as XF3	pXF3X16	This study
XF3X17	Same as XF3	pXF3X17	This study
XF3X18	Same as XF3	pXF3X18	This study
XF3X19	Same as XF3	pXF3X19	This study
XF3X20	Same as XF3	pXF3X20	This study
XF3X21	Same as XF3	pXF3X21	This study
XF3X22	Same as XF3	pXF3X22	This study
XF3X23	Same as XF3	pXF3X23	This study

XF3X24	Same as XF3	pXF3X24	This study
XF3X25	Same as XF3	pXF3X25	This study
XF3X26	Same as XF3	pXF3X26	This study
XF3X27	Same as XF3	pXF3X27	This study

* Mutated promoters used for ethanol production [40].

Table 6.1.2 Batch fermentation profiles of engineered *S. cerevisiae* strains.

Strains	Xylose consumed (g/L)	Growth rate (h^{-1})	1-Hexadecanol (g/L)	Ethanol (g/L)
XF3XP	14.9 ± 0.3	0.093 ± 0.009	0.40 ± 0.10	1.41 ± 0.32
XF3XPi	4.5 ± 0.4	0.096 ± 0.010	0.48 ± 0.09	0.48 ± 0.07
XF3XP07	7.8 ± 1.3	0.073 ± 0.007	0.79 ± 0.10	0.00 ± 0.00

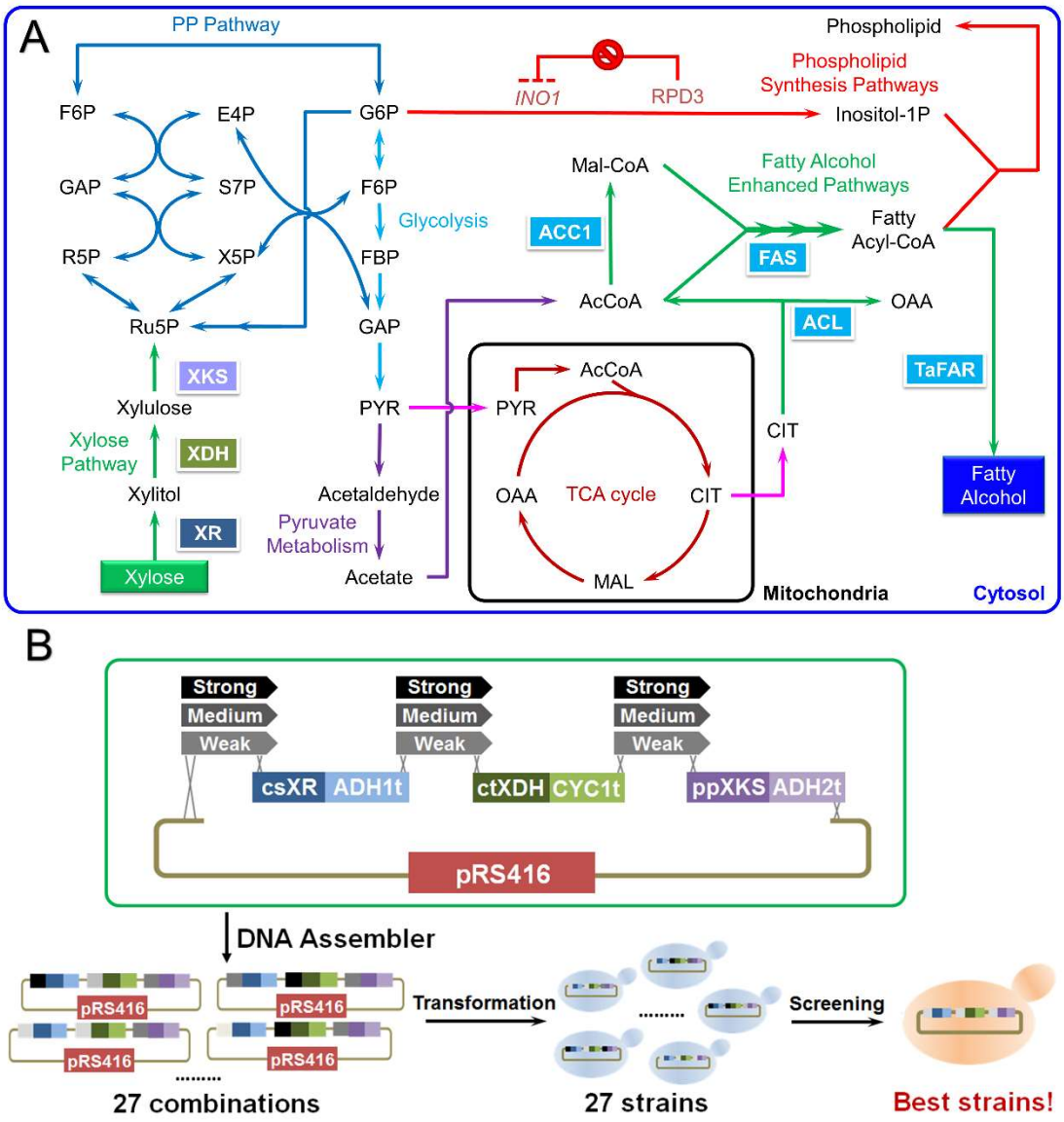

Fig. 6.1.1 Overview of the approaches for xylose-based fatty alcohol production and improvement. (A) Scheme for the introduction of xylose utilization pathway to a fatty alcohol-producing S. cerevisiae strain. The xylose utilization pathway was constituted with three fungal enzymes, XR, XDH and XKS, from our previous study. This pathway has been confirmed to use xylose as the sole carbon source. The XF3 strain was selected from our previous study in which we over-expressed a bird FAR to produce the 1-hexdecanol and engineered the yeast lipid metabolism to further improve the fatty alcohol production. (B) Plasmid design for promoter engineering to further improve the xylose-based fatty

alcohol production. We designed 27 different plasmids to exhaust all of the combinations of the promoters in front of XR, XDH, and XKS whose strengths were low, medium and high, respectively. The fatty alcohol production and growth behavior were monitored in these 27 recombinant strains.

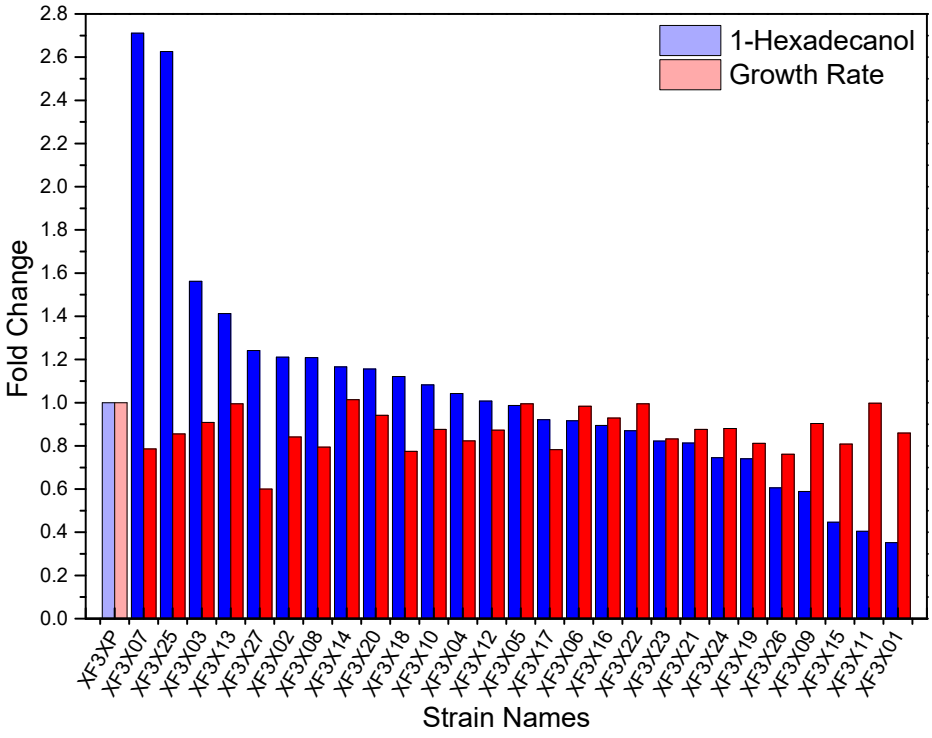

Fig. 6.1.2 1-Hexadecanol produced and growth rates of engineered *S. cerevisiae* strains via promoter engineering. All the strains were cultured in the SC-xylose (4%) medium for 48 h. The bars with lighter color were the values for the control strain (i.e., XF3XP) with the xylose utilization pathway using the native promoters.

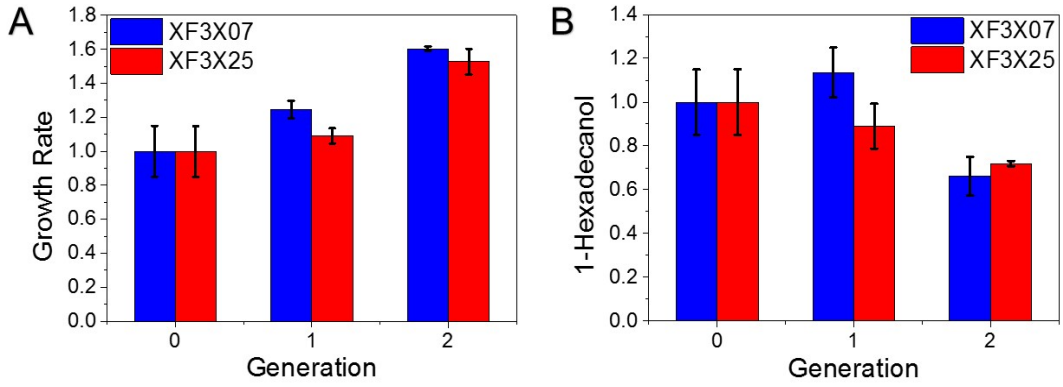

Fig. 6.1.3 Evolutionary engineering of XF3X07 and XF3X25. 1-Hexadecanol production (A) and growth rates (B) of the XF3X07 and XF3X25 in each round were normalized with 1-hexadecanol titer and growth rates of the XF3X07 and XF3X25 in round zero, respectively.

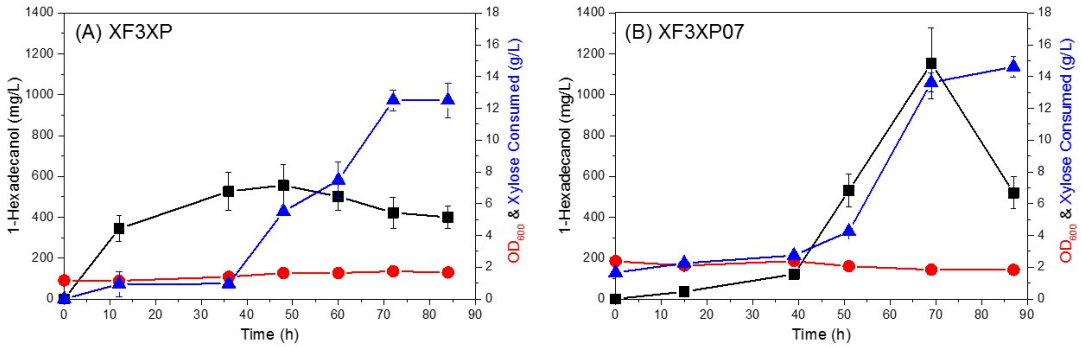

Fig. 6.1.4 Fed-batch fermentation of xylose-based 1-hexadecanol production by (A) XF3XP and (B) XF3XP07. Ethanol was detected as the only byproduct other than 1-hexadecanol. Black square: the 1-hexadecanol concentration; blue triangle: the xylose consumed; red dot: OD_{600}.

6.2 Mini-review: *In vitro* Metabolic Engineering for Biomanufacturing of High-Value Products

Weihua Guo[a, *], Jiayuan Sheng[a, *],Xueyang Feng[a, †]

[a] Department of Biological Systems Engineering, Virginia Polytechnic Institute and State University, Blacksburg, VA 24061, United States

[†]Correspondence to: Xueyang Feng.

[*] JS and WG contribute to this work equally.

Phone: +1-(540)231-2974

Email: xueyang@vt.edu

This manuscript has been published on *Computational and structural biotechnology journal* 15 161-167.

Abstract

With the breakthroughs in biomolecular engineering and synthetic biology, many valuable biologically active compound and commodity chemicals have been successfully manufactured using cell-based approaches in the past decade. However, because of the high complexity of cell metabolism, the identification and optimization of rate-limiting metabolic pathways for improving the product yield is often difficult, which represents a significant and unavoidable barrier of traditional *in vivo* metabolic engineering. Recently, some *in vitro* engineering approaches were proposed as an alternative strategy to solve this problem. In brief, by reconstituting a biosynthetic pathway in a cell-free environment with the supplement of cofactors and substrates, the performance of each biosynthetic pathway could be evaluated and optimized systematically. Several value-added products, including chemicals, nutraceuticals, and drug precursors, have been biosynthesized as proof-of-concept demonstrations of *in vitro* metabolic engineering. This mini-review summarizes the recent progresses on the emerging topic of *in vitro* metabolic engineering and comments on the potential application of cell-free technology to speed up the "design-build-test" cycles of biomanufacturing.

Key Words.

Cell-free, Biosynthesis, Metabolic Pathways, Design-Build-Test Cycle.

6.2.1 Introduction

For decades, scientists and engineers use metabolic engineering as a powerful approach to optimize industrial fermentation processes through the introduction of directed genetic changes using recombinant DNA technology. This has become an attractive, sustainable way to produce molecules[2, 41, 42], especially when chemical synthesis is difficult[43, 44]. Metabolic engineering aims to endow cells with improved properties and performance[45] while synthetic biology could create new biological parts, modules, devices and systems, in addition to re-engineering cellular components and machinery that nature has provided[46]. Through the integration of metabolic engineering and synthetic biology, efficient microbial cell factories can be constructed to produce biofuels, biomaterials and drug precursors[47].

As high valued products, biologically active compound is one kind of the most attractive engineering targets nowadays because many of them demonstrate important pharmacological activities or biotechnological significance[48]. However, due to the complexity of their structures which contains multiple chiral centers and labile connectivity[49], researchers seek microbial production instead of total chemical synthesis or semi-synthesis from isolated precursors. However, these products often lack optimal production titer and high yield. Till now, except for a few examples such as introducing heterologous pathways into yeast for the large scale production of an anti-malaria drug artemisinin[50], few valuable biologically active compounds could be produced at high yield and reach into the stage of large-scale biomanufacturing. Commodity chemicals is another large group of chemicals that attracts researchers to use cell-based metabolic engineering for manufacturing, mainly due to concerns of depleting fossil fuels and climate

changes[51]. Biomass produced from plants is the most abundant renewable resource and is considered to be the cost-competitive energy and carbon sources that could be converted to produce biofuels and biochemicals instead of fossil fuels[52]. Recent breakthroughs in synthetic biology and metabolic engineering led to the production of a series of bulk chemicals such as 1,4-butanediol[53], and isobutanol[54]. However, cell proliferation is the primary goal of microorganisms while bioconversions are the side effects. These inherent constraints of living microorganisms prevent them from implementing some important chemical reactions (e.g., H_2 production from glucose and water) and prohibit them from achieving the theoretical yield of commodity chemicals.

The unsatisfactory results of large-scale biomanufacturing of high-value products and commodity chemicals are largely due to two challenges: complex cell-wide regulation of metabolic pathways, and difficulty in balancing biosynthesis of target products and innate cell physiology. First, a lot of organisms are difficult to be engineered because of unknown regulation patterns and the lack of engineering tools for non-model organisms[55]. Even for model microorganisms like *Escherichia coli* and *Saccharomyces cerevisiae,* which are well studied and equipped with a broad spectrum of biomolecular tools to allow metabolic engineering easily, the effects of heterologous expression of pathways are often unpredictable to guarantee a high productivity, as witnessed in metabolic engineering of *S. cerevisiae* to produce n-butanol[56] and engineering carbon dioxide fixation in *E. coli*.[57] In order to identify optimal biosynthetic systems and discover the best sets of enzymes, the "design-build-test (DBT)" cycles[58] are often used. However, the DBT cycles usually take months to finish, as culturing cells is time consuming. Second, a key challenge in metabolic engineering is balancing the tug-of-war

that exists between the cell's physiological and evolutionary objectives on one side and the engineer's process objectives on the other[59]. Such conflict of resource allocation sometimes cannot be well addressed and toxic intermediates could be built up in the unbalanced pathway thus the manufacturing of high-value products often ends up with a low titer and yield and a high cost.

Many emerging technologies seek to address these challenges. Among them, cell-free biotechnology is one of the promising approaches that offer complementary advantages to *in vivo* metabolic engineering, especially in its potentials of speeding up the DBT cycles[60]. In general, the cell-free biotechnology bypasses the cell growth, and thus becomes time saving to permit more DBT cycles and avoids the conflict of resource allocation between cell growth and biosynthesis of target products. The cell-free biotechnology also uses an open reaction environment, which allows the easy and precise adjustment of components such as cofactors and intermediates during a biosynthetic reaction[61]. The cell-free biotechnology was first developed in 1961 for the purpose of elucidating the codon usage[62] and was repurposed for protein production since the end of the 1990s[63-66]. Recently in late 2000s, the cell-free biotechnology was further re-engineered to produce both biologically active compound and commodity chemicals[67],[68, 69]. In this mini-review, we summarized the experimental set-up and computational modeling of two *in vitro* metabolic engineering approaches: cell-free synthetic enzyme engineering and cell-free protein synthesis (CFPS)-based metabolic engineering (Fig. 6.2.1).

6.2.2 Cell-Free Synthetic Enzyme Engineering

The principle of cell-free synthetic enzyme engineering is to purify the individual enzymes of a biosynthetic pathway, reconstitute the pathway and study its performance *in vitro*. For more than 100 years, biologists have sought to excise complete enzymatic pathways from their native cellular environments for biochemistry research[70]. *In vitro* analysis of metabolic pathways is becoming a powerful method to gain fundamental understanding of biochemical transformations, to reveal the mechanisms of enzymatic reactions and kinetics, and to identity key metabolites and feedback control of enzyme activities.

Functional Investigation of Natural Enzymes and Metabolisms. As a powerful method to investigate natural enzymes and metabolisms, some remarkable achievements have been reported. One remarkable example is the study of the bacterial fatty acid synthases. Although being investigated extensively at the genetic and enzymatic level, it is still not easy to manipulate enhanced production of specific fatty acids because of the complex cell-wide regulation of fatty acid synthesis. In 2010, Liu et al. revealed the strong dependence of fatty acid synthesis on malonyl-CoA availability and several important phenomena in fatty acid synthesis by a quantitative investigation of the fatty acid biosynthesis and regulation in a cell-free synthetic enzyme system[71]. Following these discoveries, Yu and colleagues reported an *in vitro* reconstitution of the fatty acid synthase derived from *E. coli* by overexpressing all nine fatty acid biosynthesis (Fab) enzymes and the acyl carrier protein (ACP) in the natural *E. coli* host, and purifying the enzymes to homogeneity. Upon supplementing the ten protein species with acetyl-CoA, malonyl-CoA and NADPH, C14-C18 fatty acids were observed in the system, evidenced by ^{14}C-isotope

incorporation experiments and subsequently via UV-spectrophotometry[72]. The reconstituted multi-enzyme system has also highlighted that the fine-tuning of each individual components could substantially influence the partitioning between unsaturated and saturated fatty acid products. Similar to fatty acid biosynthesis, another pathway which synthesizes isoprenoids as key metabolites in both primary and secondary metabolisms, was reconstituted *in vitro*. Basically, in order to develop a route to synthesize the jet fuel farnesene, Zhu and colleagues reconstituted the mevalonate (MVA) pathway in a cell-free synthetic enzyme system *in vitro* by expressing and purifying eight enzymes of the MVA pathway as well as the α-farnesene synthase from an *E. coli* host[73]. The purified enzymes worked in tandem with the requisite NADPH and ATP cofactors to produce farnesene, as confirmed by gas chromatography-mass spectrometry. It was found that the isopentenyldiphosphate (IPP) isomerase was the most influential factor on the turnover rate of this pathway.

In addition to bacterial pathways, some eukaryotic pathways were also reconstituted *in vitro*. The biosynthetic pathways of dhurrin, which plays an important role in plant defense against pathogens[74], and camalexin, which is cytotoxic against aggressive prostate cancer cell lines[75], have been studied in cell-free synthetic enzyme system. Kahn and colleagues reconstituted the entire dhurrin biosynthetic pathway *in vitro* using enzymes from the natural host organism[76]. Through tedious enzyme purification processes, the researchers were able to obtain all three enzymes, CYP79, glycosyltransferase and P450ox, in the microsomal fraction of the *S. bicolor* lysates. It was found that the microsomal environment could allow functional expression of catalytically active CYP79 and P450ox, and thus dhurrin synthesis was observed by radioactive TLC

analysis when combining the three enzymes with ^{14}C-tyrosine, UDP-glucose, and NADPH. In another study, Camalexin pathway was constructed *in vitro* by purifying thee enzymes: CYP79B2, which catalyzes decarboxylation and N-hydroxylation of tryptophan to indole-3-acetaldoxamine (IAOx); a second P450 enzyme, which was previously unknown and is believed to catalyze an oxidative coupling of cysteine to IAOx; and CYP71A15, which decarboxylates and cyclizes the resulting cysteine-indole-3-acetonitrile (Cys-IAN) compound to form the thiazole ring structure within camalexin. By using a combination of gene expression data and protein sequence analysis, Klein and coworkers were able to identify a P450 enzyme capable of performing the C-S coupling reaction and to reconstitute the entire camalexin pathway *in vitro* for the first time[77].

Production of Commercially Biocommodities. Perhaps a more advanced and systematic application of cell-free synthetic enzyme engineering, especially for reconstituting long biosynthetic pathways that involves a large number of enzymes for chemical production purposes[51], is the development of Synthetic Pathway Biotransformation (SyPaB)[47]. The development cycle of SyPaB is composed of five parts: (i) pathway reconstruction, (ii) enzyme selection, (iii) enzyme engineering, (iv) enzyme production, and (v) process engineering. The entire SyPaB process can be improved in an iterative manner, which allows gradual improvement to an efficient industrial process. The DBT cycles of SyPaB has proved to be much faster than the *in vivo* systems[47]. As demonstrated in the pioneer work of high-yield cell-free hydrogen production in Zhang's lab, bulk chemicals could be potentially manufactured in a cost-effective manner[78]. This cell-free hydrogen synthetic pathway contains four modules: 1) a chain-shortening phosphorylation reaction for producing glucose-1-phosphate (G-1-P)

catalyzed by glucan phosphorylase; 2) conversion of G-1-P to glucose-6-phosphate (G-6-P) catalyzed by phosphoglucomutase; 3) a pentose phosphate pathway containing 10 enzymes for producing 12 NADPH per G-6-P; and 4) hydrogen generation from NADPH catalyzed by hydrogenase. The maximum hydrogen production rate reached 3.92 mmol of hydrogen per hour per liter of reactor. When cellobiose was used as the substrate with a reaction time of 150 h for a complete reaction, the overall yields of H_2 was 11.2 mol per mole of anhydroglucose unit of cellobiose, corresponding to 93.1% of the theoretical yields. This yield was more than 2 times higher than the yield from microbial fermentations which is limited to 4 H_2 per mole of glucose[79, 80]. In another study, Honda and his coworkers designed an *in vitro* non-natural, ATP balanced pathway for n-butanol production from glucose[81]. This pathway comprised 16 thermostable enzymes with three modules: 1) generation of two pyruvate and two NADH from one glucose molecule without ATP accumulation, 2) generation of acetyl-CoA from pyruvate; and 3) *n*-butanol production from two acetyl-CoAs. As a result, one molecule of glucose was able to produce one molecule of n-butanol, two molecules of CO_2 and one molecule of water. Recently, Opgenorth *et al.* described a robust, efficient synthetic glucose breakdown pathway and implemented it to produce bioplastic PHB[82]. The designed PBG cycle produces a net of 2 acetyl-CoA, 4 NAD(P)H, and 0 ATP for each glucose molecule and 66.6% theoretical molar yield of carbon due to the release of CO_2. Because the PBG pathway generated more reducing equivalents than are needed to produce PHB (4 NADPH per glucose produced but only 1 NADPH needed), the authors designed a NAD(P)H purge valve regulatory nodes which composed of a mixture of dehydrogenases to prevent the buildup of NADPH. Reactions were initiated with 60.7 glucose and continuously monitored in 10-h cycles by

absorbance at 600 nm. It was observed that by the end of the third cycle, the reaction stopped by the depletion of glucose with a production of 57 ± 6 mM PHB (monomer equivalents), corresponding to a 94% yield. When reactions were initiated with 109.2 mM glucose, the system maintained >50% of the maximum activity over the entire 55 h run at room temperature and generated 93.8 ± 6.1 mM PHB, corresponding to an 86% yield. The high yield emphasized the importance of cofactor recycling for SyPaB system. Compared to the microbial production of PHB using *Cupriavidus necator*[83], cell-free synthetic enzyme engineering has higher (94%) yield but lower titer (~10 g/L) than microbial bioprocess (60% yield and 83 g/L titer).

In order to further understand and predict performance of biological systems, computational modeling has been commonly applied[84]. Cell-free synthetic enzyme engineering can be modeled at multiple levels from molecules to modules to systems[85, 86]. Compared to *in vivo* cell metabolism, the relative simplicity of *in vitro* biological systems makes them far easier to simulate processes and predict optimal enzyme ratios for maximizing product yield and accelerating volumetric productivity. This simplicity could be concluded into five aspects: 1) it is free of complex transcriptional or translational regulations; 2) lower background noises in the defined system; 3) accurate measurements of metabolic components; 4) better defined model parameters, and 5) smaller modeling scales compared to *in vivo* systems. With the development of high-speed computers and the accumulation of huge biological data, numerous computational tools have been developed to simulate the *in vivo* cell metabolism and to facilitate the design of *in vivo* metabolic engineering[87]. One of the most famous computational modeling approaches is the flux balance analysis, which simulates cell metabolism at genome-scale to provide

the potential target genes for better production of chemicals[88, 89]. In addition, another commonly used computational model is the kinetic model, in which a group of differential equations are used to describe the dynamic behaviors of concentrations of biological components (e.g., metabolites, mRNA, and peptides) and are solved by a set of differential equations with defined kinetic parameters of biological reactions or processes[90]. To explicitly solve such model, defined kinetic parameters are necessary, which are commonly estimated by fitting the experimental data with kinetic models. With the estimated parameters, the dynamic responses of objective biological components can be simulated in specific conditions. However, one of the limitations of the kinetic model is the difficulty in obtaining the kinetic parameters, especially the intracellular kinetic parameters. Ensemble modeling[91], a novel computational approach constructing the ensemble of all kinetic models with the same steady state, has been developed to analyze the kinetics allowable by thermodynamics and to further facilitate the strain design for metabolic engineering[92-96]. All approaches have been applied in *in vivo* metabolic engineering with tremendous success for rational design of the host cell[84, 87]. However, only a few pioneered studies aim at developing computational modeling approaches to predict the behaviors of *in vitro* synthetic systems, even with the fact that *in vitro* synthetic systems could be easier and more precisely described via kinetic models compared to *in vivo* system[84, 85]. Recently, a non-linear kinetic model was used to describe the dynamic behavior of a SyPaB system, which was able to convert the glucose and xylose from corn stover to H_2 and CO_2, by estimating the kinetic parameters with the best fitting of experimental data[78]. The key enzymes with the largest impact of the final hydrogen yield and rate were identified by a global sensitivity analysis based on the kinetic model. By

tuning enzyme loading based on the identified key enzymes, the volumetric hydrogen productivity was improved ~3-fold[78]. This improvement demonstrates the value of computational modeling approach to the SyPaB system. In addition to enhancing the performance of SyPaB systems, computational modeling of cell-free synthetic enzyme system was also able to help derive and test new modeling approach[84, 85]. A cutting-edge study attempted to derive a genome-scale cell-free kinetic modeling approach to simulate the biosynthetic capability of important industrial organisms (e.g., *E. coli*) based on the advantages of kinetic modeling in cell-free synthetic enzyme systems[85]. In brief, the authors integrated complex allosteric regulations, which were encoded by simple effective rules and Hill-like transfer function, with traditional kinetic modeling. By modeling the kinetic profiles of several hypothetical cell-free metabolic networks, it was found that their integrated kinetic modeling approach could capture both the classic regulatory machinery (i.e., product-induced feedback regulation) and the complex allosteric machinery (i.e., non-competitive inhibition). Recently, a forward design method has been reported to establish an *in vitro* glycolysis biological process, which was constituted of 10 enzymes[97]. The researchers combined online mass spectrometry and continuous system operation to apply standard system theory input functions and used the detailed dynamic system responses to parameterize a model of sufficient quality for forward design. This allows the facile optimization of a ten-enzyme cascade to produce an important intermediate in monosaccharide synthesis, dihydroxyacetone phosphate (DHAP)[97].

In summary, cell-free synthetic enzyme engineering is advantageous to *in vivo* metabolic engineering in speed, simplicity, and easiness of manipulation. However, there

are still several drawbacks associated with cell-free synthetic enzyme engineering such as SyPaB. For example, in order to get the purified enzymes, researchers still need to spend numerous time and effort in plasmids construction, expression optimization and protein purification. Also, SyPaB was assembled in a complete artificial manner, which could lead to the instability of certain purified enzymes and coenzymes[47]. More importantly, the artificial environment could be dramatically different from the intracellular environment, which makes the results obtained from SyPaB optimization difficult to be transferred into *in vivo* metabolic engineering. The cell-free synthetic enzyme system itself, on the other hand, is arguably difficult in being scaled up for biomanufacturing[98, 99].

6.2.3 Cell-free Protein Synthesis (CFPS)-based Metabolic Engineering

A key difference between the cell-free synthetic enzyme engineering and the CFPS-based metabolic engineering is that the laborious *in vivo* protein expression and purification steps could be bypassed in the latter, which further speed up the DBT cycles. After decades of improving, current CFPS is well established, which could yield 200–2,300 mg/mL protein in the batch mode reaction[100-108] and allow the CFPS-based metabolic engineering. Recently, Jewett et al.[59] reported this novel CFPS-based metabolic engineering framework for building biosynthetic pathways by directly synthesizing each enzyme of a biosynthetic pathway *in vitro* with the use of cell-free lysates and mixing multiple crude lysates to initiate the DBT cycle. A panel of cell-free lysates are selectively enriched and prepared in parallel, in each of which a target enzyme is overexpressed by using CFPS technology. Their cell-free lysates were next mixed in a combinatorial manner to construct a mevalonate biosynthetic pathway involved in isoprenoid synthesis[109]. Using this method, Jewett's group rapidly screened enzyme variants, optimized enzyme

ratios, and explored cofactor landscapes for improving pathway performance. In the optimized system, mevalonate was synthesized at 17.6 g/L (119 mM) within 20 h compared to the initial titer of 1.6 g/L generated in 9 h. The fast prototyping and "debugging" of enzymatic pathways in this CFPS-based metabolic engineering framework offer unique advantages for metabolic engineering and synthetic biology applications because of the dramatically improved speed of DBT cycles. Encouraged by the successes of using CFPS-based metabolic engineering framework to produce mevalonate, this system was also applied to prototyping *n*-butanol biosynthesis[59]. It showed that *E. coli* lysates could support a highly active 17-step CoA-dependent *n*-butanol pathway derived from *Clostridia* metabolism involving CoA intermediates *in vitro*[59]. In this system, endogenous glycolytic enzymes convert glucose to acetyl-CoA for *n*-butanol synthesis, another *E. coli* enzyme (AtoB) converts acetyl-CoA to acetoacetyl-CoA, and heterologous enzymes (Hbd, Crt, Ter, AdhE) convert acetoacetyl-CoA to *n*-butanol. It was found that by adding both NAD and CoA with glucose to initiate n-butanol synthesis, the cell-free system could produce 1.2 g/L *n*-butanol. In order to improve pathway performance, the researchers replaced some of initial Ter and AdhE enzymes with a variety of homologs. In less than a day, they studied 4 Ter and 3 AdhE homologs by using CFPS-based metabolic engineering framework. Also they demonstrated the possibility of using linear DNA templates (i.e., linear DNAs such as PCR products containing the whole expression cassette of the desired gene) instead of plasmids for pathway prototyping (i.e., an early-stage method to study the constitution and function of a metabolic pathway), which would further expedite the process as the laborious cloning steps could be avoided. Finally, the *n*-butanol production was improved by 200% of the initial starting conditions (up to 1.5 g/L) by optimizing the

performance of different enzymes sets and adjusting the physicochemical environment.

Currently, no computational modeling approach has been reported to model the CFPS-based metabolic engineering framework[59, 110]. However, the CFPS-based metabolic engineering framework can be considered as the combination of two different procedures, i.e., cell free protein synthesis and the SyPaB. In this case, it is possible to combine a CFPS model with the SyPaB models that are described in previous section to simulate and predict the performance of CFPS-based metabolic engineering. In spite of the unknown kinetic parameters of CFPS systems and the unclear composition of cell lysates[84], several studies have been implemented to develop various computational modeling approaches for both PURE system[111] and CFPS systems[111-113]. For example, one of the pioneered studies was recently implemented to derive a kinetic model to describe the gene expression dynamics in a commercial CFPS system producing green fluorescent protein (GFP) as the target[114]. By measuring the GFP expression and mRNA levels in the CFPS system, the authors estimated the unknown kinetic parameters in the model and predicted both DNA concentration and the experimental time as the key factors impacting the protein titer of CFPS.[114] In addition, computational models of CFPS systems can also elucidate the unknown impact of biological phenomena[84, 115]. In recent studies, it was found that increasing molecular crowding of CFPS system caused by crowding reagents or coacervation of encapsulated circuits, can improve the titer of protein production dramatically[115]. By modeling the transcription-translation reactions of CFPS system with the kinetic modeling approach, the author demonstrated that the improved protein production induced by coacervation was caused by the increased association constant of T7 polymerase as well as the kinetic transcription constant in the coacervated

compartments[115]. Another hybrid kinetic model that combined a biological model with a agent-based model (or chemical kinetic model) has been developed to describe the *in vitro* protein synthesis and enabled the investigation of the polysome dynamics under the non-steady-state and non-continuum conditions[86]. We also want to point out that in addition to modeling the whole protein synthesis processes such as transcription and translation, many studies were also focusing on other bio-processes, e.g., peptide chain elongation[116] and ribosome recycle[117, 118], which play pivotal roles in the entire protein synthesis.

When using kinetic models to simulate CFPS process, one of the major limitations is the ignorance of the transcriptional and translational regulations (e.g., transcription factors) by using the kinetic parameters with constant values[119] to reflect time-dependent processes. In addition, the predictive capability of kinetic models is limited due to the unknown parameters[119]. Therefore, it is necessary to find an alternative algorithm with higher predictive capability to facilitate the design of CFPS systems. Machine learning, a central field of artificial intelligence, is an ideal choice for predictive analysis to devise complex systems with high non-linearity and multi-dimensionality[120-122]. Generally, machine learning can automatically learn the instinct correlations between the inputs and outputs of the systems, leading to a predictive model or algorithm with high prediction accuracy. For example, by training the machine-learning algorithm with paired inputs (e.g., CFPS experimental designs and properties of target proteins) and outputs (e.g., protein productions), the trained algorithm can predict the outputs from system inputs with high accuracy. Although CFPS are already simplified from the *in vivo* protein synthesis, it still has highly non-linear regulations and large-dimensional impact factors for the protein

production[120]. Recently, a pioneering study has applied a machine learning algorithm (neural network) to the CFPS systems with paired data of different experimental designs and corresponding protein productions for learning CFPS systems and optimizing protein production[90]. The authors first set up a CFPS system to synthesize enhanced GFP (eGFP) by using commercial *E. coli* CFPS kits with fixed basic reaction system. Next, the authors chose 11 variable components in CFPS system and specified a vector of values for each component to build up a space of possible experiments. By using a robotic workstation for liquid handling, a larger number of CFPS experiments was implemented in a high-throughput manner[120]. Starting with randomly selected 49 experiments, the machine-learning algorithm started to learn the CFPS experiments and offered optimized designs of CFPS systems with improved eGFP production. With the optimized experimental design, the workstation implemented the next generation of experiments to generate new experimental data and to validate the predictions. By repeating this DBT cycles for eight times, the machine learning algorithm provided an optimized experimental design with ~3.5-fold improvement of eGFP production. Besides the improved protein production, the large-scale CFPS experiments and machine learning algorithm also uncovered kinetic biological insights to better understand the CFPS system[120]. This is the first time machine learning algorithms have been integrated with CFPS systems without an arbitrary hypothesis, which demonstrates the capabilities and advantages of machine learning algorithms for better understanding the CFPS process.

6.2.4 Summary and Perspectives

Compared to traditional *in vivo* metabolic engineering, *in vitro* metabolic engineering has unique advantages in speeding up the DBT cycles. The key conceptual

innovation of *in vitro* metabolic engineering is that the components in the DBT cycle can be purified enzymes or cell-free lysates rather than genetic constructs, thus avoiding engineering the complex cell metabolism and the tedious pathway construction. For the two *in vitro* metabolic engineering approaches discussed in this study, the major obstacles for cell-free enzymatic pathway engineering are the lack of stable building blocks as standardized parts and instability of costly coenzymes. By engineering thermo-stable enzymes and using them in *in vitro* metabolic engineering, the high productivity is likely to be maintained[47, 123]. CFPS-based metabolic engineering is arguably more advantageous because it could free the researchers from tedious protein purification and bypass the cofactor issues in a cytosol mimic environment. However, *in vitro* metabolic engineering approaches face the challenge of scaling up. Because of the high cost associated with the energy source (e.g. ATP) used in the cell-free system, the large-scale biomanufacturing is too expensive even when producing high-value products. Additionally, when using cell-free synthetic enzyme engineering, the stability of the enzymes could cause the reduced productivity during biosynthesis. Nevertheless, novel strategies from synthetic biology and protein engineering are being developed to address both challenges. For example, Caschera et al. have designed by coupling polyphosphate and maltodextrin for bypassing substrate level phosphorylation based on expensive energy sources (Phosphoenolpyruvic acid (PEP) and 3-PGA)[124]. Swartz et. al demonstrated that the cost NTP could be substituted with economic NMP and by shifting the energy source from expensive compounds to glucose. Thus, the cost-benefit of cell-free protein synthesis (g-product / $ reagent cost) is as much as 2.4 times higher than for reactions using costly PEP[106]. After decades' effort, cell-free protein synthesis could reach 2.3 mg/ml protein

in the batch mode reaction which was comparable to *in vivo* expression levels.[125] Finally, although the scale-up of cell-free protein synthesis for *in vitro* metabolic remains a challenge to be demonstrated, a milestone of the scale-up of CFPS has been achieved to expression complex high valued proteins in a 100 L reactor[98]. Refactoring the *in vitro* optimized pathway back into the host cells might be a future direction to address this scale-up problem. However, issues of lethality, toxicity of some metabolic intermediates and the compartmentalization of some pathways in the eukaryotic organisms should be aware during this process and might need additional DBT cycles to further improve the productivity. Meanwhile, to simulate and guide the design of *in vitro* metabolic engineering, data-driven algorithms (e.g., machine learning and statistical learning) represent promising approaches, especially with the fast and high-throughput biological measurements of experimental data[122]. The data-driven algorithms can take advantage of the "Big Data" to uncover the biological insights behind the biological systems, and to derive the predictive models for predicting the outputs from corresponding inputs. Currently, one of the bottlenecks to develop the data-driven models is the limitation of high-quality and well-curated data[121]. Although several studies of *in vitro* metabolic engineering have been implemented and published, there is no database that curates these studies in a standardized manner, which obstructs the development of data-driven algorithms. The construction of such database requires both time and labors. However, it is still feasible to construct large-scale database including thousands of datasets in three to five years. With sufficient experimental data and an appropriate data-driven algorithm, the internal complex interactions in the *in vitro* biological systems could be captured and explicitly elucidated in near future. It is worth noting that, biased data for training the data-

driven algorithm will mislead the data-driven models. Therefore, using the equally distributed data to train the data-driven models is necessary to derive a data-driven algorithm with high prediction accuracy. To conclude, *in vitro* metabolic engineering, although still being on the infant stage, has great potentials in speeding up the DBT cycles of biomanufacturing and serves as an alternative approach to *in vivo* metabolic engineering.

Acknowledgements

This study was supported by a start-up fund (#175323) and the ICTAS Junior Faculty Award from Virginia Tech.

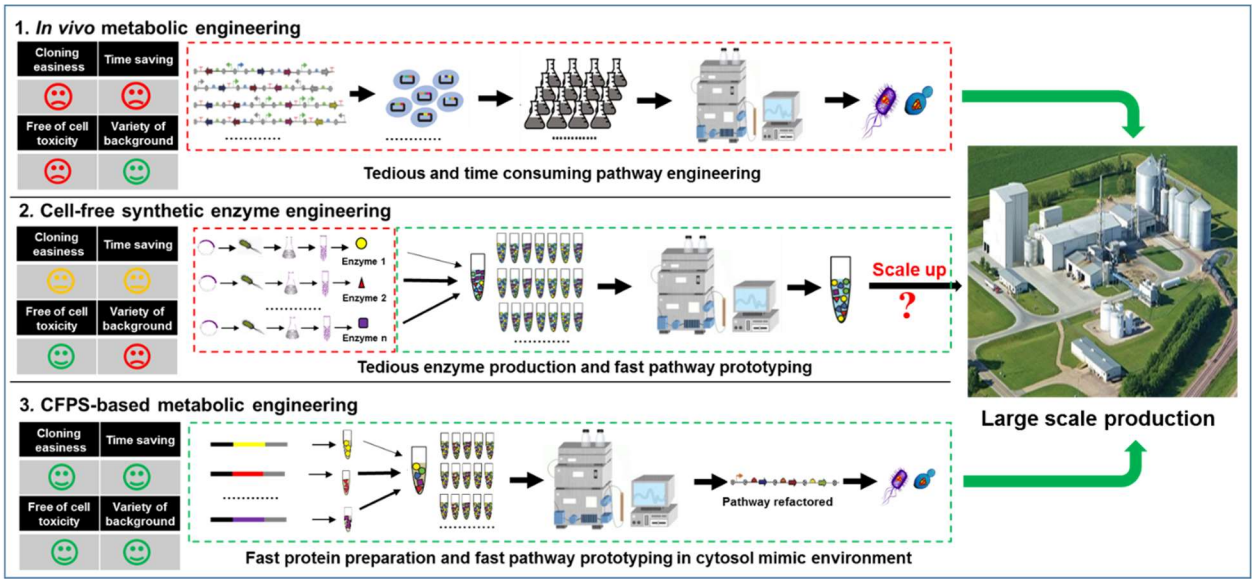

Fig. 6.2.1 Summary of *in vitro* metabolic engineering (ME) approaches. 1. *In vivo* metabolic engineering, in which model microorganisms like *Escherichia coli* and *Saccharomyces cerevisiae* are often accompanied with inefficient and time-consuming pathways construction, transformation and fermentation; 2. Cell-free synthetic enzyme engineering, which allows fast pathway prototyping; however, molecular cloning and enzyme production could be time consuming and the high cost associated with production could make the process scale-up questionable. 3. The cell-free protein synthesis (CFPS)-based metabolic engineering, which could accelerate the pathway prototyping in a cytosol mimic environment by using enzymes that are directly produced in a cell-free system and assembling pathways in a "mix-and-match" fashion.

References

1. Liu, R., et al., *Metabolic engineering of fatty acyl-ACP reductase-dependent pathway to improve fatty alcohol production in Escherichia coli.* Metab Eng, 2014. **22**: p. 10-21.
2. Du, J., Z. Shao, and H. Zhao, *Engineering microbial factories for synthesis of value-added products.* J Ind Microbiol Biotechnol, 2011. **38**(8): p. 873-90.
3. Runguphan, W. and J.D. Keasling, *Metabolic engineering of Saccharomyces cerevisiae for production of fatty acid-derived biofuels and chemicals.* Metab Eng, 2014. **21**: p. 103-13.
4. Youngquist, J.T., et al., *Production of medium chain length fatty alcohols from glucose in Escherichia coli.* Metab Eng, 2013. **20**: p. 177-86.
5. Mudge, S.M., S.E. Belanger, and A.M. Nielsen, *Fatty Alcohols: Anthropogenic and Natural Occurrence in the Environment*. 2008, The Royal Society of Chemistry: Cambridge, UK.
6. Rupilius, W. and S. Ahmad, *Palm oil and palm kernel oil as raw materials for basic oleochemicals and biodiesel.* Eur J Lipid Sci Technol, 2007. **109**(4): p. 433-439.
7. Fitzherbert, E., et al., *How will oil palm expansion affect biodiversity?* Trends Ecol Evol, 2008. **23**(10): p. 538-545.
8. Hill, J., et al., *Environmental, economic, and energetic costs and benefits of biodiesel and ethanol biofuels.* Proc Natl Acad Sci U S A, 2006. **103**(30): p. 11206-10.
9. Zhang, F., S. Rodriguez, and J.D. Keasling, *Metabolic engineering of microbial pathways for advanced biofuels production.* Curr Opin Biotechnol, 2011. **22**(6): p. 775-83.
10. Feng, X., J. Lian, and H. Zhao, *Metabolic engineering of Saccharomyces cerevisiae to improve 1-hexadecanol production.* Metab Eng, 2015. **27**: p. 10-9.
11. Cao, Y.X., et al., *Biosynthesis of odd-chain fatty alcohols in Escherichia coli.* Metab Eng, 2015.
12. Fillet, S., et al., *Fatty alcohols production by oleaginous yeast.* Journal of Industrial Microbiology & Biotechnology, 2015. **42**(11): p. 1463-1472.
13. Zheng, Y., et al., *Optimization of fatty alcohol biosynthesis pathway for selectively enhanced production of C12/14 and C16/18 fatty alcohols in engineered Escherichia coli.* Microb Cell Fact, 2012. **11:65**.
14. Akhtar, M.K., N.J. Turner, and P.R. Jones, *Carboxylic acid reductase is a versatile enzyme for the conversion of fatty acids into fuels and chemical commodities.* Proc Natl Acad Sci U S A, 2013. **110**(1): p. 87-92.
15. Liu, A., et al., *Fatty alcohol production in engineered E. coli expressing Marinobacter fatty acyl-CoA reductases.* Appl Microbiol Biotechnol, 2013. **97**(15): p. 7061-71.
16. Hong, K.K. and J. Nielsen, *Metabolic engineering of Saccharomyces cerevisiae: a key cell factory platform for future biorefineries.* Cell Mol Life Sci, 2012. **69**(16): p. 2671-90.
17. Wei, N., et al., *Enhanced biofuel production through coupled acetic acid and xylose consumption by engineered yeast.* Nat Commun, 2013. **4**: p. 2580.

18. Jeffries, T. and Y. Jin, *Metabolic engineering for improved fermentation of pentoses by yeasts.* Appl Microbiol Biotechnol, 2004. **63**(5): p. 495-509.
19. Eliasson, A., et al., *Anaerobic xylose fermentation by recombinant Saccharomyces cerevisiae carrying XYL1, XYL2, and XKS1 in mineral medium chemostat cultures.* Appl Environ Microbiol, 2000. **66**(8): p. 3381-6.
20. Kim, B., et al., *Combinatorial design of a highly efficient xylose-utilizing pathway in Saccharomyces cerevisiae for the production of cellulosic biofuels.* Appl Environ Microbiol, 2013. **79**(3): p. 931-41.
21. Garcia Sanchez, R., et al., *Improved xylose and arabinose utilization by an industrial recombinant Saccharomyces cerevisiae strain using evolutionary engineering.* Biotechnol Biofuels, 2010. **3**: p. 13.
22. Kuyper, M., et al., *High-level functional expression of a fungal xylose isomerase: the key to efficient ethanolic fermentation of xylose by Saccharomyces cerevisiae?* FEMS Yeast Res, 2003. **4**(1): p. 69-78.
23. Zhou, H., et al., *Xylose isomerase overexpression along with engineering of the pentose phosphate pathway and evolutionary engineering enable rapid xylose utilization and ethanol production by Saccharomyces cerevisiae.* Metab Eng, 2012. **In press**.
24. Demeke, M.M., et al., *Development of a D-xylose fermenting and inhibitor tolerant industrial Saccharomyces cerevisiae strain with high performance in lignocellulose hydrolysates using metabolic and evolutionary engineering.* Biotechnology for Biofuels, 2013. **6**(1): p. 1-24.
25. Gietz, R. and R. Schiestl, *High-efficiency yeast transformation using the LiAc/SS carrier DNA/PEG method.* Nat Protoc, 2007. **2**(1): p. 31-4.
26. Shao, Z., H. Zhao, and H. Zhao, *DNA assembler, an in vivo genetic method for rapid construction of biochemical pathways.* Nucleic Acids Res, 2009. **27**(2): p. e16.
27. Shao, Z., Y. Luo, and H. Zhao, *Rapid characterization and engineering of natural product biosynthetic pathways via DNA assembler.* Mol Biosyst, 2011. **7**(4): p. 1056-9.
28. Du, J., et al., *Customized optimization of metabolic pathways by combinatorial transcriptional engineering.* Nucleic Acids Res, 2012. **40**(18): p. e142.
29. Feng, X. and H. Zhao, *Investigating host dependence of xylose utilization in recombinant Saccharomyces cerevisiae strains using RNA-seq analysis.* Biotechnol Biofuels, 2013. **6:95**.
30. Young, E., S. Lee, and H. Alper, *Optimizing pentose utilization in yeast: the need for novel tools and approaches.* Biotechnol Biofuels, 2010. **3**(24).
31. Toivari, M.H., et al., *Endogenous Xylose Pathway in Saccharomyces cerevisiae.* Applied and Environmental Microbiology, 2004. **70**(6): p. 3681-3686.
32. Feng, X. and H. Zhao, *Investigating xylose metabolism in recombinant Saccharomyces cerevisiae via 13C metabolic flux analysis.* Microbial Cell Factories, 2013. **12**(1): p. 114.
33. Kuyper, M., et al., *Evolutionary engineering of mixed-sugar utilization by a xylose-fermenting Saccharomyces cerevisiae strain.* FEMS Yeast Res, 2005. **5**(10): p. 925-34.

34. Scalcinati, G., et al., *Evolutionary engineering of Saccharomyces cerevisiae for efficient aerobic xylose consumption.* FEMS Yeast Res, 2012. **12**(5): p. 582-97.
35. Sonderegger, M. and U. Sauer, *Evolutionary engineering of Saccharomyces cerevisiae for anaerobic growth on xylose.* Appl Environ Microbiol, 2003. **69**(4): p. 1990-8.
36. Feng, X., J. Lian, and H. Zhao, *Metabolic engineering of Saccharomyces cerevisiae to improve 1-hexadecanol production.* Metabolic Engineering, 2015. **27**(0): p. 10-19.
37. Tang, X. and W.N. Chen, *Enhanced production of fatty alcohols by engineering the TAGs synthesis pathway in Saccharomyces cerevisiae.* Biotechnology and Bioengineering, 2015. **112**(2): p. 386-392.
38. Latimer, L.N., et al., *Employing a combinatorial expression approach to characterize xylose utilization in Saccharomyces cerevisiae.* Metabolic Engineering, 2014. **25**: p. 20-29.
39. Lian, J., et al., *Design and construction of acetyl-CoA overproducing Saccharomyces cerevisiae strains.* Metab Eng, 2014. **24**: p. 139-49.
40. Du, J., et al., *Customized optimization of metabolic pathways by combinatorial transcriptional engineering.* Nucleic Acids Research, 2012. **40**(18): p. e142.
41. Becker, J. and C. Wittmann, *Bio-based production of chemicals, materials and fuels -Corynebacterium glutamicum as versatile cell factory.* Curr Opin Biotechnol, 2012. **23**(4): p. 631-40.
42. Wendisch, V.F., M. Bott, and B.J. Eikmanns, *Metabolic engineering of Escherichia coli and Corynebacterium glutamicum for biotechnological production of organic acids and amino acids.* Curr Opin Microbiol, 2006. **9**(3): p. 268-74.
43. Erickson, B., Nelson, and P. Winters, *Perspective on opportunities in industrial biotechnology in renewable chemicals.* Biotechnol J, 2012. **7**(2): p. 176-85.
44. Nielsen, J., et al., *Engineering synergy in biotechnology.* Nat Chem Biol, 2014. **10**(5): p. 319-322.
45. Koffas, M., et al., *Metabolic engineering.* Annu Rev Biomed Eng, 1999. **1**: p. 535-57.
46. Andrianantoandro, E., et al., *Synthetic biology: new engineering rules for an emerging discipline.* Mol Syst Biol, 2006. **2**: p. 2006 0028.
47. Zhang, Y.H., *Production of biocommodities and bioelectricity by cell-free synthetic enzymatic pathway biotransformations: challenges and opportunities.* Biotechnol Bioeng, 2010. **105**(4): p. 663-77.
48. Mishra, B.B. and V.K. Tiwari, *Natural products: an evolving role in future drug discovery.* Eur J Med Chem, 2011. **46**(10): p. 4769-807.
49. Pickens, L.B., Y. Tang, and Y.H. Chooi, *Metabolic engineering for the production of natural products.* Annu Rev Chem Biomol Eng, 2011. **2**: p. 211-36.
50. Ro, D.K., et al., *Production of the antimalarial drug precursor artemisinic acid in engineered yeast.* Nature, 2006. **440**: p. 940-943.
51. Zhang, Y.H., *Production of biofuels and biochemicals by in vitro synthetic biosystems: Opportunities and challenges.* Biotechnol Adv, 2015. **33**(7): p. 1467-83.

52. Wyman, C.E., *BIOMASS ETHANOL: Technical Progress, Opportunities, and Commercial Challenges.* Annual Review of Energy and the Environment, 1999. **24**(1): p. 189-226.
53. Yim, H., et al., *Metabolic engineering of Escherichia coli for direct production of 1,4-butanediol.* Nat Chem Biol, 2011. **7**(7): p. 445-52.
54. Atsumi, S., T. Hanai, and J.C. Liao, *Non-fermentative pathways for synthesis of branched-chain higher alcohols as biofuels.* Nature, 2008. **451**(7174): p. 86-89.
55. Lee, J.Y., et al., *Metabolic engineering of Clostridium acetobutylicum M5 for highly selective butanol production.* Biotechnol J. , 2009. **4**(10): p. 1432-40.
56. Dong, H., et al., *Engineering Escherichia coli Cell Factories for n-Butanol Production*, in *Bioreactor Engineering Research and Industrial Applications I: Cell Factories*, Q. Ye, J. Bao, and J.-J. Zhong, Editors. 2016, Springer Berlin Heidelberg: Berlin, Heidelberg. p. 141-163.
57. Schwander, T., et al., *A synthetic pathway for the fixation of carbon dioxide in vitro.* Science, 2016. **354**(6314): p. 900-904.
58. Kwok, R., *Five hard truths for synthetic biology.* Nature, 2010. **463**(7279): p. 288-90.
59. Karim, A.S. and M.C. Jewett, *A cell-free framework for rapid biosynthetic pathway prototyping and enzyme discovery.* Metab Eng, 2016. **36**: p. 116-26.
60. Hodgman, C.E. and M.C. Jewett, *Cell-free synthetic biology: thinking outside the cell.* Metab Eng, 2012. **14**(3): p. 261-9.
61. Sun, Z.Z., et al., *Linear DNA for rapid prototyping of synthetic biological circuits in an Escherichia coli based TX-TL cell-free system.* ACS Synth Biol, 2014. **3**(6): p. 387-97.
62. Nirenberg, M.W. and J.H. Matthaei, *The dependence of cell-free protein synthesis in E. coli upon naturally occurring or synthetic polyribonucleotides.* Proc Natl Acad Sci U S A, 1961. **47**: p. 1588-602.
63. Iizuka, N., et al., *Cap-dependent and cap-independent translation by internal initiation of mRNAs in cell extracts prepared from Saccharomyces cerevisiae.* Mol Cell Biol, 1994. **14**(11): p. 7322-30.
64. Kim, D.M. and J.R. Swartz, *Prolonging cell-free protein synthesis with a novel ATP regeneration system.* Biotechnol Bioeng, 1999. **66**(3): p. 180-8.
65. Kim, D.M. and J.R. Swartz, *Prolonging cell-free protein synthesis by selective reagent additions.* Biotechnol Prog, 2000. **16**(3): p. 385-90.
66. Kim, D.M. and J.R. Swartz, *Regeneration of adenosine triphosphate from glycolytic intermediates for cell-free protein synthesis.* Biotechnol Bioeng, 2001. **74**(4): p. 309-16.
67. Zhang, Y.H., *Reviving the carbohydrate economy via multi-product lignocellulose biorefineries.* J Ind Microbiol Biotechnol, 2008. **35**(5): p. 367-75.
68. Schultheisz, H.L., et al., *Pathway engineered enzymatic de novo purine nucleotide synthesis.* ACS Chem Biol, 2008. **3**(8): p. 499-511.
69. Zhang, Y.H.P., *A sweet out-of-the-box solution to the hydrogen economy: is the sugar-powered car science fiction?* Energy & Environmental Science, 2009. **2**(3): p. 272-282.

70. Lowry, B., C.T. Walsh, and C. Khosla, *In Vitro Reconstitution of Metabolic Pathways: Insights into Nature's Chemical Logic.* Synlett, 2015. **26**(8): p. 1008-1025.
71. Liu, T., H. Vora, and C. Khosla, *Quantitative analysis and engineering of fatty acid biosynthesis in E. coli.* Metab Eng, 2010. **12**(4): p. 378-86.
72. Yu, X., et al., *In vitro reconstitution and steady-state analysis of the fatty acid synthase from Escherichia coli.* Proc Natl Acad Sci U S A, 2011. **108**(46): p. 18643-8.
73. Zhu, F., et al., *In vitro reconstitution of mevalonate pathway and targeted engineering of farnesene overproduction in Escherichia coli.* Biotechnol Bioeng, 2014. **111**(7): p. 1396-405.
74. Wittstock, U. and J. Gershenzon, *Constitutive plant toxins and their role in defense against herbivores and pathogens.* Current Opinion in Plant Biology, 2002. **5**(4): p. 300-307.
75. Smith, B.A., et al., *The phytoalexin camalexin mediates cytotoxicity towards aggressive prostate cancer cells via reactive oxygen species.* J Nat Med, 2013. **67**(3): p. 607-18.
76. Kahn, R.A., et al., *Isolation and reconstitution of cytochrome P450ox and in vitro reconstitution of the entire biosynthetic pathway of the cyanogenic glucoside dhurrin from sorghum.* Plant Physiol, 1997. **115**(4): p. 1661-70.
77. Klein, A.P., G. Anarat-Cappillino, and E.S. Sattely, *Minimum set of cytochromes P450 for reconstituting the biosynthesis of camalexin, a major Arabidopsis antibiotic.* Angew Chem Int Ed Engl, 2013. **52**(51): p. 13625-8.
78. Rollin, J.A., et al., *High-yield hydrogen production from biomass by in vitro metabolic engineering: Mixed sugars coutilization and kinetic modeling.* Proceedings of the National Academy of Sciences, 2015. **112**(16): p. 4964-4969.
79. Maeda, T., V. Sanchez-Torres, and T.K. Wood, *Hydrogen production by recombinant Escherichia coli strains.* Microb Biotechnol, 2012. **5**(2): p. 214-25.
80. Rollin, J.A., et al., *High-yield hydrogen production from biomass by in vitro metabolic engineering: Mixed sugars coutilization and kinetic modeling.* Proc Natl Acad Sci U S A, 2015. **112**(16): p. 4964-9.
81. Krutsakorn, B., et al., *In vitro production of n-butanol from glucose.* Metabolic Engineering, 2013. **20**: p. 84-91.
82. Opgenorth, P.H., T.P. Korman, and J.U. Bowie, *A synthetic biochemistry module for production of bio-based chemicals from glucose.* Nat Chem Biol, 2016. **12**(6): p. 393-5.
83. Pradella, J.G., et al., *Carbon source pulsed feeding to attain high yield and high productivity in poly(3-hydroxybutyrate) (PHB) production from soybean oil using Cupriavidus necator.* Biotechnol Lett, 2012. **34**(6): p. 1003-7.
84. Lewis, D.D., et al., *Synthetic Biology Outside the Cell: Linking Computational Tools to Cell-Free Systems.* Frontiers in Bioengineering and Biotechnology, 2014. **2**(66).
85. Wayman, J., A. Sagar, and J. Varner, *Dynamic Modeling of Cell-Free Biochemical Networks Using Effective Kinetic Models.* Processes, 2015. **3**(1): p. 138.

86. Semenchenko, A., G. Oliveira, and A.P.F. Atman, *Hybrid agent-based model for quantitative in-silico cell-free protein synthesis.* Biosystems, 2016. **150**: p. 22-34.
87. Gombert, A.K. and J. Nielsen, *Mathematical modelling of metabolism.* Current Opinion in Biotechnology, 2000. **11**(2): p. 180-186.
88. Orth, J.D., I. Thiele, and B.O. Palsson, *What is flux balance analysis?* Nat Biotech, 2010. **28**(3): p. 245-248.
89. Guo, W. and X. Feng, *OM-FBA: Integrate Transcriptomics Data with Flux Balance Analysis to Decipher the Cell Metabolism.* PLoS One, 2016. **11**(4): p. e0154188.
90. Vital-Lopez, F.G., et al., *A computational procedure for optimal engineering interventions using kinetic models of metabolism.* Biotechnology progress, 2006. **22**(6): p. 1507-1517.
91. Tran, L.M., M.L. Rizk, and J.C. Liao, *Ensemble Modeling of Metabolic Networks.* Biophysical Journal, 2008. **95**(12): p. 5606-5617.
92. Contador, C.A., et al., *Ensemble modeling for strain development of l-lysine-producing Escherichia coli.* Metabolic Engineering, 2009. **11**(4–5): p. 221-233.
93. Lee, Y., J.G. Lafontaine Rivera, and J.C. Liao, *Ensemble Modeling for Robustness Analysis in engineering non-native metabolic pathways.* Metabolic Engineering, 2014. **25**: p. 63-71.
94. Rizk, M.L. and J.C. Liao, *Ensemble Modeling for Aromatic Production in Escherichia coli.* PLOS ONE, 2009. **4**(9): p. e6903.
95. Theisen, M.K., J.G. Lafontaine Rivera, and J.C. Liao, *Stability of Ensemble Models Predicts Productivity of Enzymatic Systems.* PLOS Computational Biology, 2016. **12**(3): p. e1004800.
96. Bogorad, I.W., et al., *Building carbon–carbon bonds using a biocatalytic methanol condensation cycle.* Proceedings of the National Academy of Sciences, 2014. **111**(45): p. 15928-15933.
97. Hold, C., S. Billerbeck, and S. Panke, *Forward design of a complex enzyme cascade reaction.* Nat Commun, 2016. **7**: p. 12971.
98. Zawada, J.F., et al., *Microscale to manufacturing scale-up of cell-free cytokine production--a new approach for shortening protein production development timelines.* Biotechnol Bioeng, 2011. **108**(7): p. 1570-8.
99. Dudley, Q.M., A.S. Karim, and M.C. Jewett, *Cell-free metabolic engineering: biomanufacturing beyond the cell.* Biotechnol J, 2015. **10**(1): p. 69-82.
100. Jewett, M.C., et al., *An integrated cell-free metabolic platform for protein production and synthetic biology.* Mol Syst Biol, 2008. **4**: p. 220.
101. Jewett, M.C. and J.R. Swartz, *Mimicking the Escherichia coli cytoplasmic environment activates long-lived and efficient cell-free protein synthesis.* Biotechnol Bioeng, 2004. **86**(1): p. 19-26.
102. Bundy, B.C., M.J. Franciszkowicz, and J.R. Swartz, *Escherichia coli-based cell-free synthesis of virus-like particles.* Biotechnol Bioeng, 2008. **100**(1): p. 28-37.
103. Albayrak, C. and J.R. Swartz, *Cell-free co-production of an orthogonal transfer RNA activates efficient site-specific non-natural amino acid incorporation.* Nucleic Acids Res, 2013. **41**(11): p. 5949-63.

104. Calhoun, K.A. and J.R. Swartz, *An Economical Method for Cell-Free Protein Synthesis using Glucose and Nucleoside Monophosphates.* Biotechnology Progress, 2005. **21**(4): p. 1146-1153.
105. Kim, D.M. and J.R. Swartz, *Prolonging cell-free protein synthesis with a novel ATP regeneration system.* Biotechnology and bioengineering, 1999. **66**(3): p. 180-188.
106. Calhoun, K.A. and J.R. Swartz, *Energizing cell-free protein synthesis with glucose metabolism.* Biotechnol Bioeng, 2005. **90**(5): p. 606-13.
107. Kwon, Y.C. and M.C. Jewett, *High-throughput preparation methods of crude extract for robust cell-free protein synthesis.* Sci Rep, 2015. **5**: p. 8663.
108. Pardee, K., et al., *Portable, On-Demand Biomolecular Manufacturing.* Cell, 2016. **167**(1): p. 248-259.e12.
109. Dudley, Q.M., K.C. Anderson, and M.C. Jewett, *Cell-Free Mixing of Escherichia coli Crude Extracts to Prototype and Rationally Engineer High-Titer Mevalonate Synthesis.* ACS Synth Biol, 2016.
110. Goering, A.W., et al., *In Vitro Reconstruction of Nonribosomal Peptide Biosynthesis Directly from DNA Using Cell-Free Protein Synthesis.* ACS Synthetic Biology, 2016.
111. Mavelli, F., R. Marangoni, and P. Stano, *A Simple Protein Synthesis Model for the PURE System Operation.* Bulletin of Mathematical Biology, 2015. **77**(6): p. 1185-1212.
112. Karzbrun, E., et al., *Coarse-Grained Dynamics of Protein Synthesis in a Cell-Free System.* Physical Review Letters, 2011. **106**(4): p. 048104.
113. Matsuura, T., et al., *Quantifying epistatic interactions among the components constituting the protein translation system.* Molecular Systems Biology, 2009. **5**(1).
114. Stogbauer, T., et al., *Experiment and mathematical modeling of gene expression dynamics in a cell-free system.* Integrative Biology, 2012. **4**(5): p. 494-501.
115. Sokolova, E., et al., *Enhanced transcription rates in membrane-free protocells formed by coacervation of cell lysate.* Proceedings of the National Academy of Sciences, 2013. **110**(29): p. 11692-11697.
116. Zouridis, H. and V. Hatzimanikatis, *A Model for Protein Translation: Polysome Self-Organization Leads to Maximum Protein Synthesis Rates.* Biophysical Journal, 2007. **92**(3): p. 717-730.
117. Margaliot, M. and T. Tuller, *Ribosome flow model with positive feedback.* Journal of The Royal Society Interface, 2013. **10**(85).
118. Garai, A., et al., *Stochastic kinetics of ribosomes: Single motor properties and collective behavior.* Physical Review E, 2009. **80**(1): p. 011908.
119. Ay, A. and D.N. Arnosti, *Mathematical modeling of gene expression: a guide for the perplexed biologist.* Critical reviews in biochemistry and molecular biology, 2011. **46**(2): p. 137-151.
120. Caschera, F., et al., *Coping with complexity: Machine learning optimization of cell-free protein synthesis.* Biotechnology and Bioengineering, 2011. **108**(9): p. 2218-2228.
121. Michalski, R.S., J.G. Carbonell, and T.M. Mitchell, *Machine learning: An artificial intelligence approach*. 2013: Springer Science & Business Media.

122. Iniesta, R., D. Stahl, and P. McGuffin, *Machine learning, statistical learning and the future of biological research in psychiatry.* Psychological Medicine, 2016: p. 1-11.
123. Liu, W., et al., *Fast identification of thermostable beta-glucosidase mutants on cellobiose by a novel combinatorial selection/screening approach.* Biotechnol Bioeng, 2009. **103**(6): p. 1087-94.
124. Caschera, F. and V. Noireaux, *A cost-effective polyphosphate-based metabolism fuels an all E. coli cell-free expression system.* Metab Eng, 2015. **27**: p. 29-37.
125. Caschera, F. and V. Noireaux, *Synthesis of 2.3 mg/ml of protein with an all Escherichia coli cell-free transcription-translation system.* Biochimie, 2014. **99**: p. 162-8.

Chapter 7: General Conclusions and Future Works

The deciphering of planktonic and biofilm metabolism is playing an increasingly important role in reducing dependency on fossil energy and protecting the security of public health. In the past three years, I have developed and applied computational modeling approaches to investigate the metabolisms of planktonic and biofilm cells as part of my Ph.D. training. In general, I have applied ^{13}C-MFA to 1) investigate intracellular metabolic responses to multiple stresses[1], 2) reveal the metabolisms underlying the biosynthesis of natural and heterologous products [2], and 3) discover strain dependencies in metabolic engineering [3]. I have also used ^{13}C-assisted pathway analysis to systematically study various pathway usages in planktonic and biofilm cells of *S. oneidensis* strain MR-1 in a microbial fuel-cell system and to discover the key pathways and substrate for electricity generation in the biofilm cells [4, 5]. To integrate multi-omics data with FBA, I have developed an innovative framework for FBA (omFBA) to accurately predict biological insights (i.e., key flux ratios) by replacing the arbitrary objective function (e.g., maximize the growth rate) with an omics-guided objective function[6]. I have subsequently used omFBA in a proof-of-concept study to predict ethanol production using different substrates in yeast. Furthermore, I have applied a machine learning approach to predict CRISPR-based transcriptional regulation in an innovative attempt at computational modeling for the CRISPR-based system. The computational tool that I developed is able to facilitate the sequence design of the guide RNA in the CRISPR system to achieve programmable control of metabolic flux[7], which will accelerate the application of CRISPR-based systems to genome editing. In addition to my computational modeling work, I have leveraged my

expertise in metabolic engineering to develop a novel yeast strain that utilizes xylose as the sole carbon source to produce 1-hexadecanol[8].

In the future, I plan to continue my research on deciphering the metabolic reprogramming of pathogenic biofilm cells in clinical infections. I will focus on three key questions. The first question is: Which metabolic pathways are reprogrammed when cells switch from the planktonic state to the biofilm state in the absence of antibiotics? To answer that question, I will apply ^{13}C-assisted pathway analysis to elucidate the differences in pathway usage between planktonic and biofilm cells. The second question is: Do different strains of pathogenic biofilm cells adopt a common pattern of metabolic reprogramming in clinical infections? To answer that question, I will use ^{13}C-assisted pathway analysis to systematically investigate the metabolic reprogramming among various pathogenic strains of biofilm cells that are commonly observed in clinical infections. The third question is: How do biofilm cells reprogram their metabolism to enhance their resistance to antibiotics? To answer that question, I will characterize the differences in pathway usage between planktonic and biofilm cells in the presence of antibiotics.

References

1. Guo, W., et al., *Investigate the Metabolic Reprogramming of Saccharomyces cerevisiae for Enhanced Resistance to Mixed Fermentation Inhibitors via ^{13}C Metabolic Flux Analysis.* PLOS ONE, 2016. **11**(8): p. e0161448.
2. Zhuang, L., et al., *Investigating oxalate biosynthesis in the wood-decaying fungus Gloeophyllum trabeum using 13C metabolic flux analysis.* RSC Advances, 2015. **5**(126): p. 104043-104047.
3. Miguel Suastegui, et al., *Investigating strain dependency in the production of aromatic compounds in Saccharomyces cerevisiae.* Biotechnol Bioeng., 2016. **Accepted**: p. 9.
4. Guo, W., et al., *13C pathway analysis of biofilm metabolism of Shewanella oneidensis MR-1.* RSC Advances, 2015. **5**(50): p. 39840-39843.
5. Luo, S., et al., *(13)C Pathway Analysis for the Role of Formate in Electricity Generation by Shewanella Oneidensis MR-1 Using Lactate in Microbial Fuel Cells.* Sci Rep, 2016. **6**: p. 20941.
6. Guo, W. and X. Feng, *OM-FBA: Integrate Transcriptomics Data with Flux Balance Analysis to Decipher the Cell Metabolism.* PLoS One, 2016. **11**(4): p. e0154188.
7. Sheng, J., et al., *Data-Driven Prediction of CRISPR-Based Transcription Regulation for Programmable Control of Metabolic Flux.* arXiv preprint arXiv:1704.03027, 2017.
8. Guo, W., et al., *Metabolic engineering of Saccharomyces cerevisiae to produce 1-hexadecanol from xylose.* Microb Cell Fact, 2016. **15**: p. 24.

Appendix A: Supplementary Material of Chapter 3.3

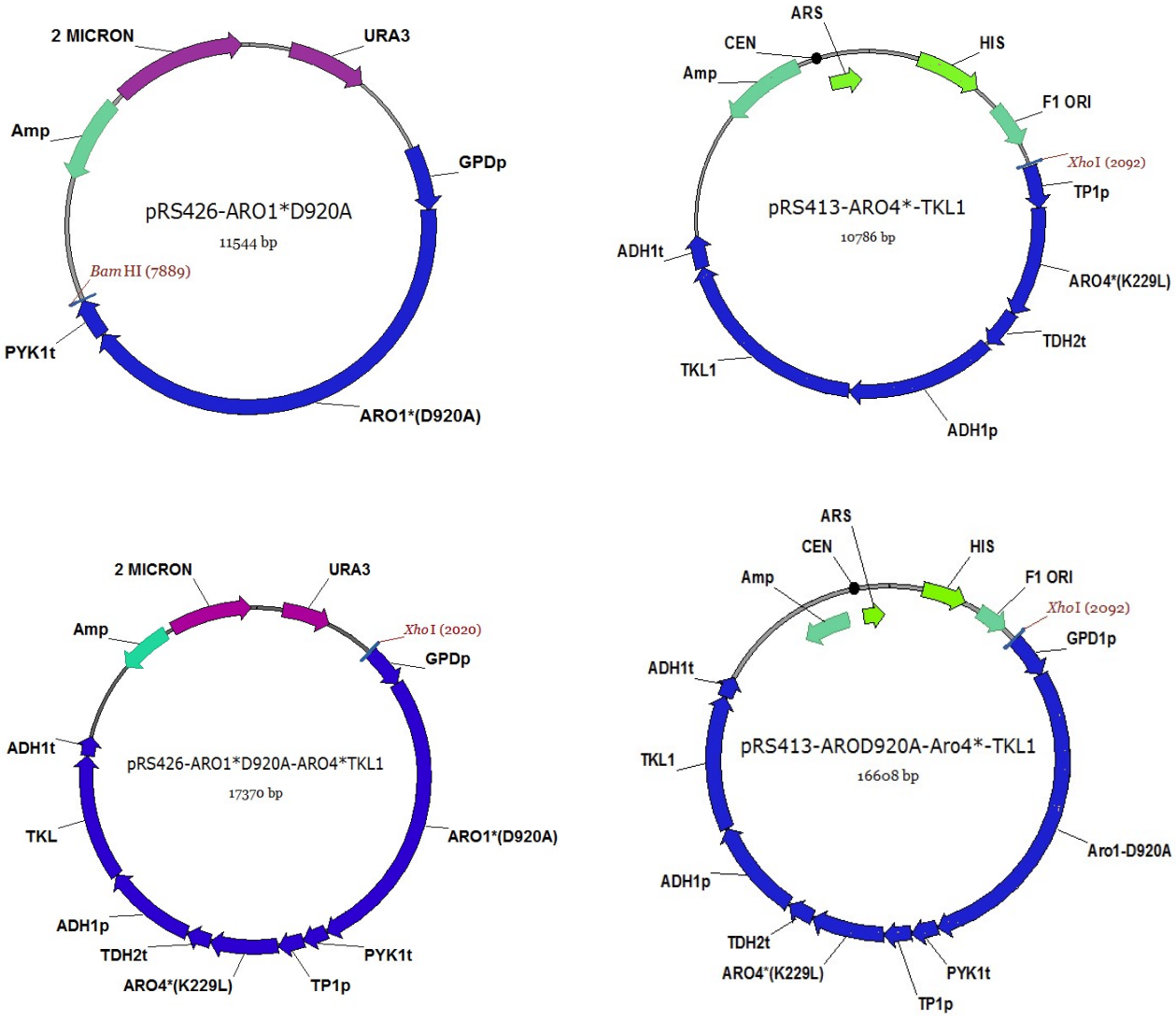

Fig. A.S1 Plasmids used in this work.

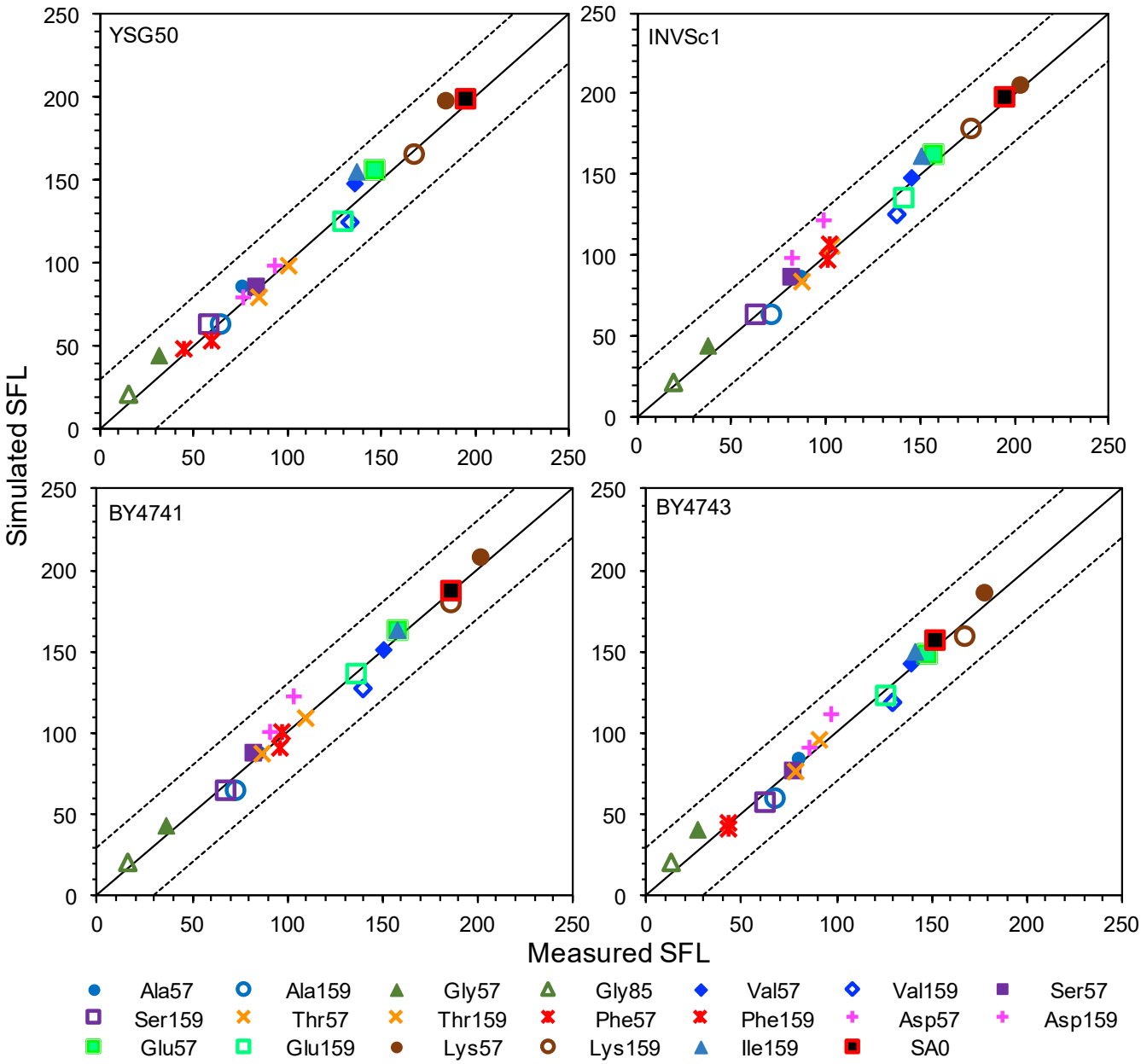

Fig. A.S2 - Fitting between measured and simulated summed fractional labeling (SFL) of strains in group SA2 (Table 3.3.1).

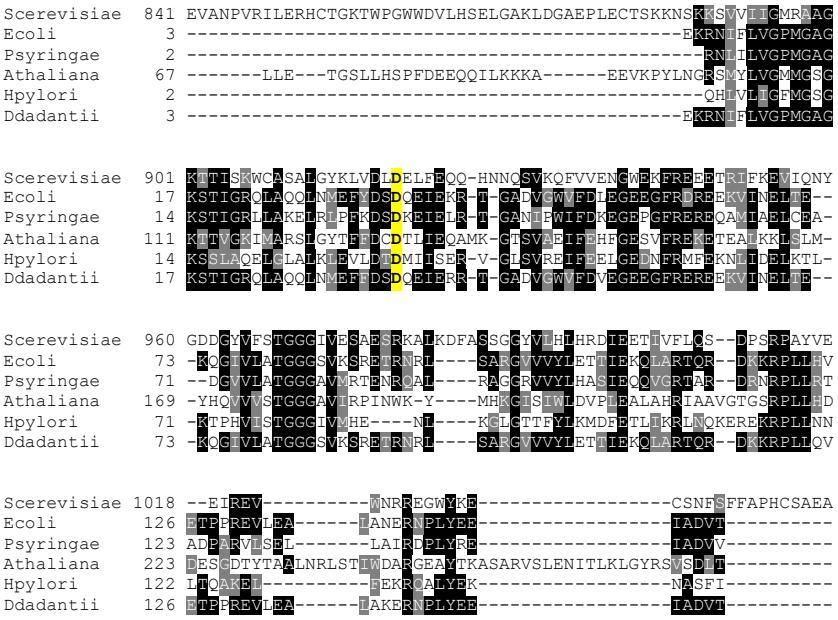

Fig. A.S3 Sequence alignment of shikimate kinases from different species. The aspartic acid residue (D920 in *S. cerevisiae*) is conserved in the five selected species, from which the corresponding residue has been reported to be the catalytic residue. UNIPROT accesion number: *S. cerevisiae: aro1*B subunit (P08566), *Escherichia coli* (P0A6D7), *Pseudomonas syringae* (Q87V14), *Arabidopsis thaliana* (Q8GY88), *Helicobacter pylori* (P56073), and *Dickeya dadantii* (E0SJR7).

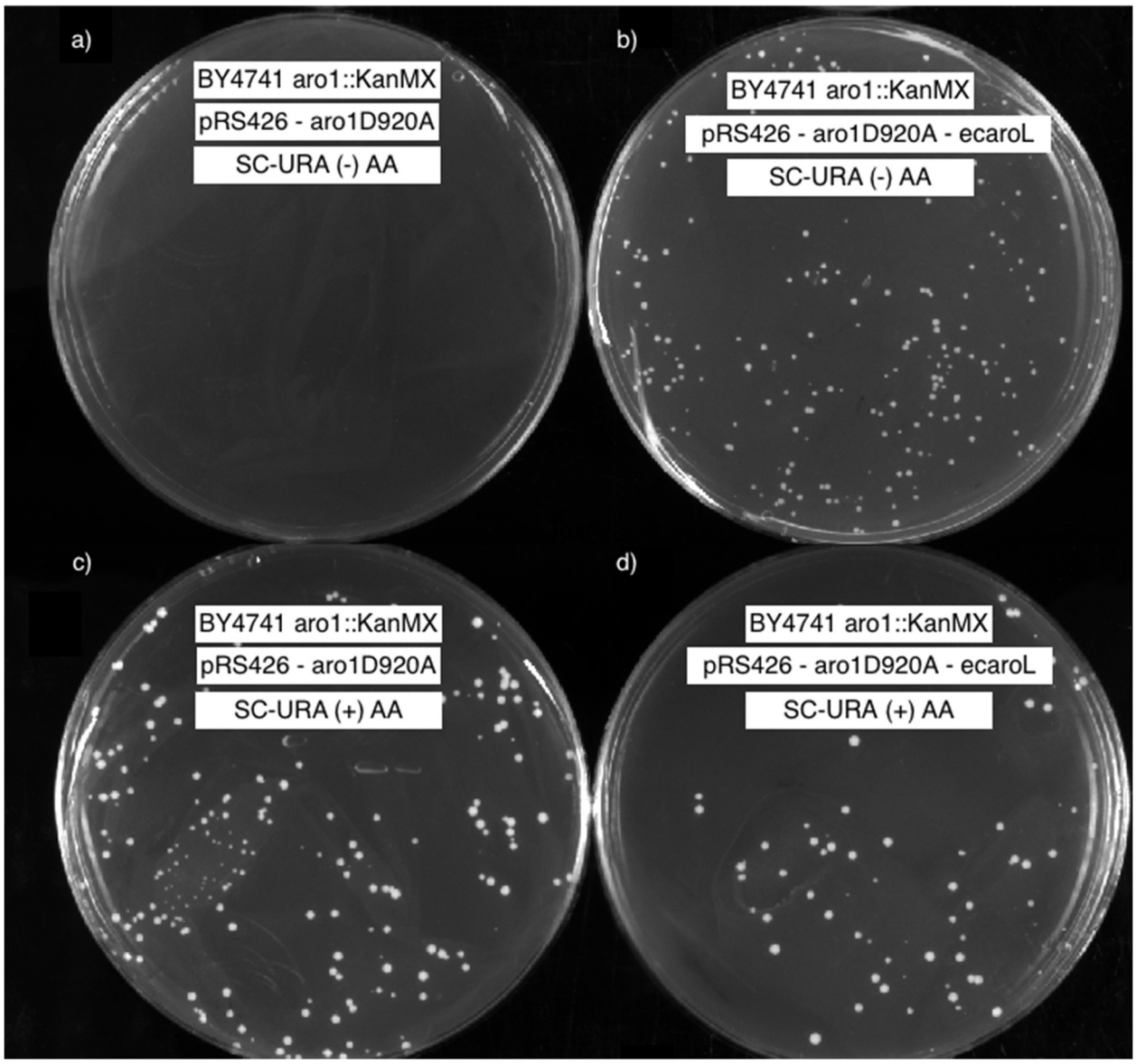

Fig. A.S4 Characterization of the novel mutant enzyme ARO1D920A. A) The strain BY4741 aro1 harboring plasmid pRS426-*aro1*$_{D920A}$ cannot grow in medium lacking aromatic amino acids (AA). B) Complementation of growth was achieved by constructing the plasmids pRS426-*aro1*$_{D920A}$ – *ecaroL,* which harbors the *E. coli* shikimate kinase gene *aroL.* C-D) Control plates containing aromatic amino acids.

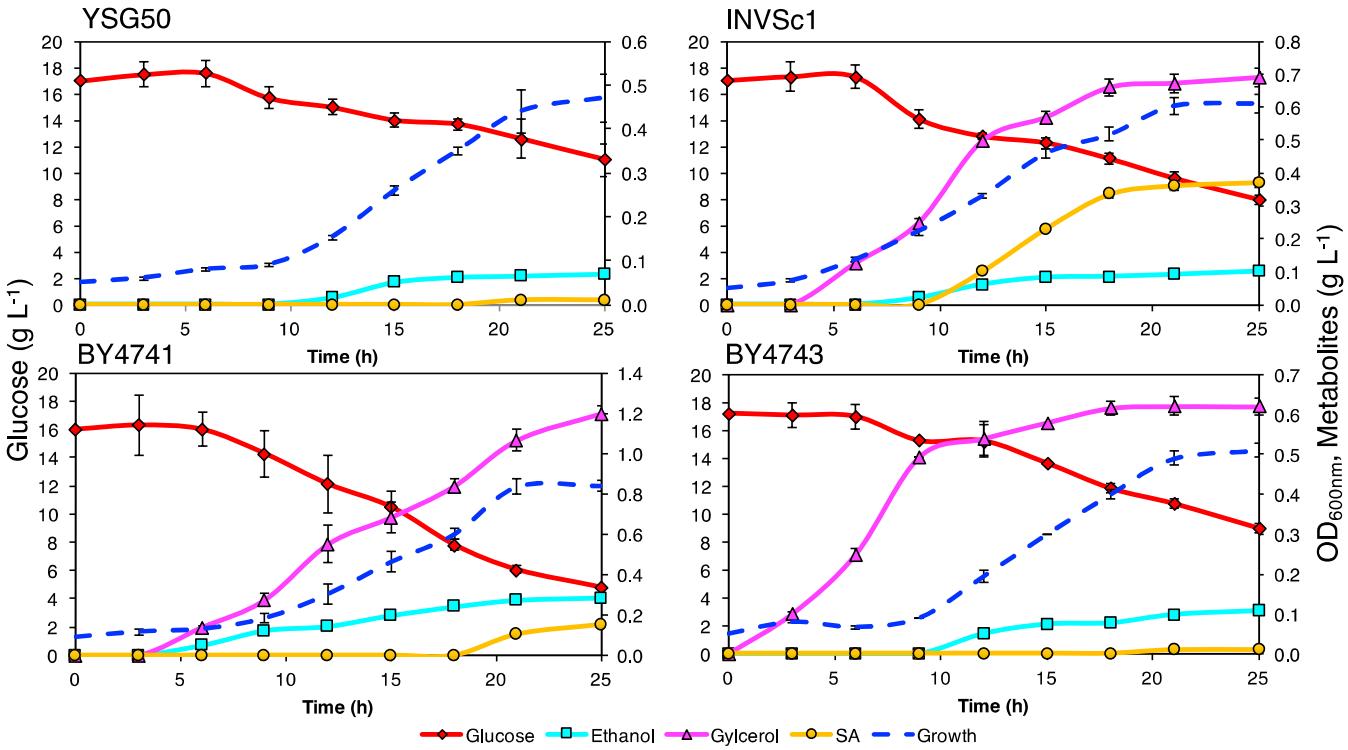

Fig. A.S5 Fermentation profiles of strain group SA2

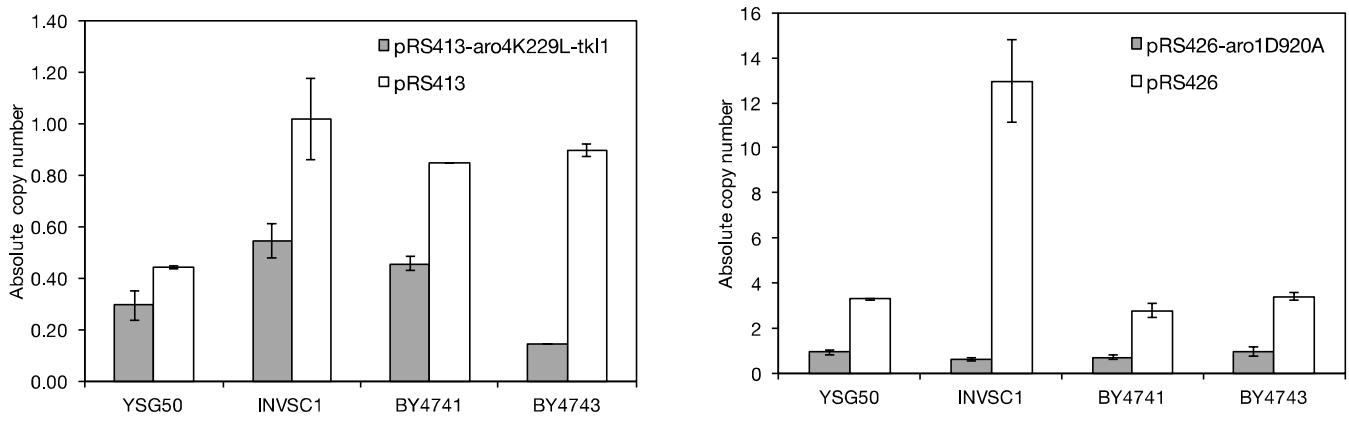

Fig. A.S6 Absolute copy number of plasmid in strains SA0 and SA2. a) Comparison between plasmids pRS413 and pRS413-*aro4*$_{K229L}$-*TKL1*. b) Copy number comparison between plasmids pRS426 and pRS426-*aro1*$_{D920A.}$

Table A.S1. Isotopic labeling patterns of SA2 strains.

Amino acid	Labeling pattern	YSG50		INVSc1		BY4741		BY4743	
		M-57	M-159	M-57	M-159	M-57	M-159	M-57	M-159
Ala	m0	0.51	0.49	0.49	0.47	0.48	0.46	0.51	0.49
	m1	0.32	0.34	0.34	0.35	0.35	0.35	0.32	0.34
	m2	0.03	0.17	0.03	0.18	0.02	0.19	0.03	0.17
	m3	0.14		0.14		0.15		0.14	
Gly*	m0	0.85	0.84	0.79	0.83	0.79	0.82	0.85	0.87
	m1	0.03	0.16	0.06	0.17	0.05	0.18	0.02	0.13
	m2	0.12		0.15		0.16		0.12	
Val	m0	0.32	0.31	0.27	0.28	0.26	0.26	0.32	0.31
	m1	0.29	0.28	0.31	0.30	0.29	0.27	0.29	0.28
	m2	0.19	0.25	0.21	0.25	0.21	0.31	0.19	0.25
	m3	0.12	0.13	0.12	0.13	0.15	0.13	0.12	0.13
	m4	0.05	0.03	0.07	0.03	0.06	0.04	0.05	0.03
	m5	0.03		0.02		0.03		0.03	
Leu	m0	0.94	0.95	0.96	0.94	0.94	0.95	0.93	0.95
	m1	0.06	0.04	0.04	0.05	0.06	0.04	0.06	0.03
	m2	0.00	0.01	0.00	0.01	0.00	0.01	0.01	0.01
	m3:6	0.00	0.00	0.00	0.00	0.00	0.00	0.00	0.00
Ile	m0	0.45	0.27	0.43	0.24	0.41	0.24	0.46	0.29
	m1	0.21	0.26	0.18	0.26	0.22	0.27	0.20	0.26
	m2	0.17	0.26	0.19	0.28	0.18	0.26	0.19	0.25
	m3	0.11	0.15	0.11	0.16	0.09	0.17	0.08	0.14
	m4	0.04	0.05	0.05	0.05	0.07	0.06	0.05	0.05
	m5	0.02	0.01	0.03	0.01	0.03	0.01	0.02	0.01
	m6	0.00		0.00		0.01		0.00	
Pro	m0	0.31	0.32	0.24	0.27	0.24	0.29	0.31	0.32
	m1	0.24	0.29	0.29	0.31	0.27	0.29	0.24	0.29
	m2	0.25	0.24	0.28	0.27	0.28	0.27	0.25	0.24
	m3	0.15	0.12	0.13	0.12	0.15	0.12	0.15	0.12
	m4	0.04	0.03	0.06	0.03	0.05	0.03	0.04	0.03

	m5	0.01		0.01		0.01		0.01	
Ser	m0	0.49	0.55	0.55	0.54	0.45	0.47	0.52	0.51
	m1	0.32	0.32	0.29	0.34	0.37	0.39	0.31	0.34
	m2	0.06	0.13	0.06	0.12	0.01	0.14	0.06	0.14
	m3	0.13		0.11		0.17		0.12	
Thr	m0	0.42	0.39	0.41	0.41	0.41	0.43	0.48	0.47
	m1	0.32	0.39	0.37	0.37	0.36	0.35	0.31	0.33
	m2	0.12	0.23	0.07	0.19	0.08	0.18	0.06	0.15
	m3	0.11	0.00	0.11	0.03	0.11	0.04	0.11	0.05
	m4	0.03		0.05		0.03		0.04	
Phe	m0	0.81	0.80	0.64	0.61	0.65	0.63	0.80	0.79
	m1	0.09	0.11	0.11	0.14	0.12	0.14	0.11	0.11
	m2	0.04	0.04	0.06	0.10	0.08	0.10	0.03	0.04
	m3	0.02	0.02	0.07	0.06	0.06	0.05	0.02	0.03
	m4	0.02	0.01	0.04	0.03	0.04	0.03	0.01	0.01
	m5	0.01	0.01	0.04	0.03	0.03	0.03	0.01	0.01
	m6	0.01	0.01	0.01	0.02	0.02	0.02	0.01	0.01
	m7	0.00	0.00	0.01	0.01	0.01	0.01	0.00	0.00
	m8:9	0.00	0.00	0.00	0.00	0.00	0.00	0.00	0.00
Asp	m0	0.43	0.45	0.40	0.41	0.40	0.43	0.42	0.43
	m1	0.30	0.34	0.33	0.33	0.37	0.36	0.36	0.33
	m2	0.12	0.17	0.12	0.21	0.06	0.16	0.09	0.19
	m3	0.13	0.04	0.12	0.05	0.12	0.06	0.10	0.05
	m4	0.02		0.03		0.04		0.03	
Glu	m0	0.27	0.29	0.23	0.23	0.20	0.23	0.31	0.32
	m1	0.29	0.26	0.28	0.33	0.30	0.31	0.22	0.26
	m2	0.20	0.28	0.27	0.29	0.28	0.29	0.23	0.28
	m3	0.18	0.15	0.15	0.12	0.16	0.12	0.20	0.11
	m4	0.06	0.03	0.05	0.03	0.05	0.04	0.05	0.03
	m5	0.00		0.01		0.01		0.00	
Lys	m0	0.24	0.25	0.17	0.17	0.17	0.17	0.24	0.25
	m1	0.18	0.23	0.20	0.21	0.21	0.22	0.18	0.23
	m2	0.27	0.23	0.24	0.30	0.26	0.31	0.27	0.23

	m3	0.19	0.20	0.23	0.21	0.22	0.20	0.19	0.20
	m4	0.09	0.07	0.12	0.08	0.08	0.08	0.09	0.07
	m5	0.04	0.02	0.03	0.02	0.05	0.01	0.04	0.02
	m6	0.00	-	0.01	-	0.01	-	0.00	-
Tyr	m0	0.66	0.57	0.52	0.52	0.48	0.44	0.66	0.57
	m1	0.10	0.19	0.17	0.17	0.16	0.18	0.10	0.19
	m2	0.09	0.11	0.09	0.13	0.11	0.15	0.09	0.11
	m3	0.05	0.04	0.07	0.07	0.10	0.09	0.05	0.04
	m4	0.05	0.04	0.05	0.04	0.06	0.06	0.05	0.04
	m5	0.03	0.02	0.05	0.04	0.04	0.03	0.03	0.02
	m6	0.02	0.01	0.02	0.02	0.03	0.03	0.02	0.01
	m7	0.01	0.01	0.01	0.01	0.01	0.01	0.01	0.01
	m8	0.01	0.00	0.01	0.00	0.01	0.00	0.01	0.00
	m9	0.00	-	0.00	-	0.00	-	0.00	-
Met	m0	0.27	0.33	0.26	0.28	0.82	0.88	0.27	0.33
	m1	0.34	0.34	0.30	0.36	0.15	0.09	0.34	0.34
	m2	0.19	0.22	0.23	0.23	0.02	0.00	0.19	0.22
	m3	0.11	0.08	0.12	0.11	0.00	0.02	0.11	0.08
	m4	0.09	0.02	0.07	0.02	0.01	0.00	0.09	0.02
	m5	0.01	-	0.02	-	0.00	-	0.01	-
SA	m0	-	-	0.2193	-	0.2255	-	0.2408	-
	m1	-	-	0.2932	-	0.3219	-	0.3317	-
	m2	-	-	0.1675	-	0.124	-	0.1341	-
	m3	-	-	0.153	-	0.1508	-	0.1417	-
	m4	-	-	0.0824	-	0.1074	-	0.078	-
	m5	-	-	0.0846	-	0.0705	-	0.0738	-

* The fragments for glycine were M-57 and M-85.

Appendix B: Supplementary Material of Chapter 3.4

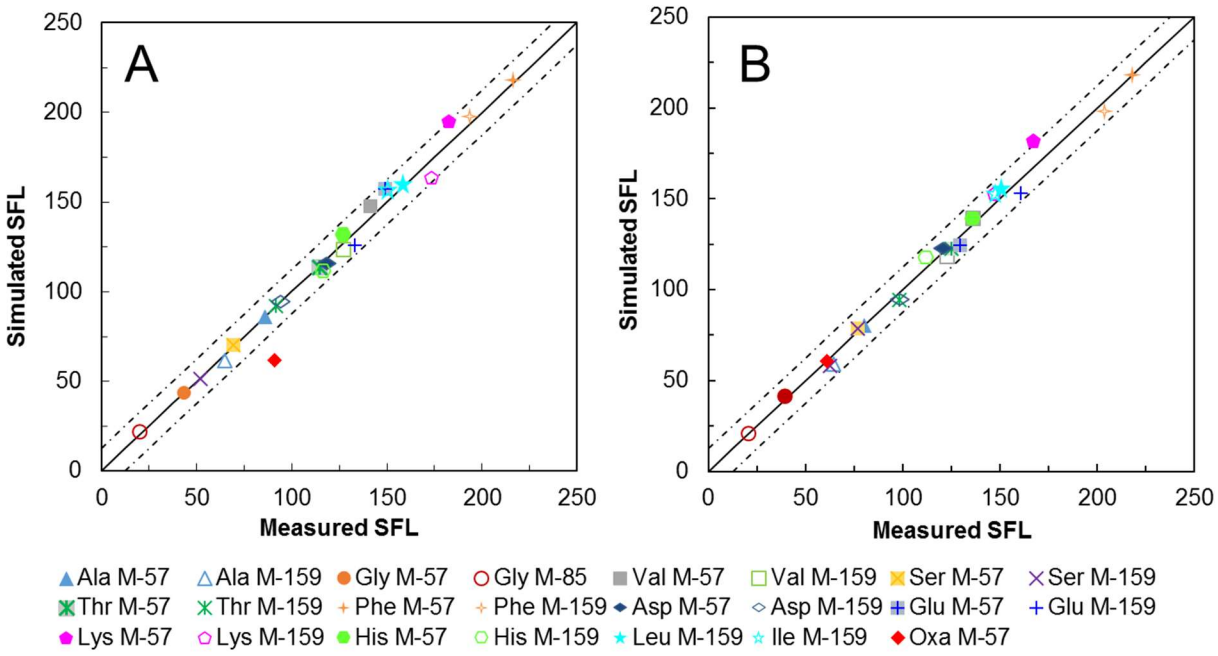

Fig. B.S1 Simulated isotopic labeled pattern fitting based on SFL calculation. (A) Low nitrogen condition (LN); (B) High nitrogen condition (HN)

Table B.S1. Metabolic flux distribution and central metabolic model.

No.	Reactions	Relative flux (LN)	[a]STDEV	Relative flux (HN)	[a]STDEV
1	GLC <-> G6P	100.0	0.0	100.0	0.0
2	G6P <-> F6P	36.7	2.2	41.5	0.8
3	F6P <-> DHAP + G3P	76.6	1.3	79.3	1.5
4	DHAP <-> G3P	76.6	1.3	79.3	1.5
5	G3P <-> PEP	167.3	0.1	163.3	0.1
6	PEP <-> PYRCYT	166.6	0.9	160.8	2.0
7	G6P <-> CO2 + P5P	60.1	5.3	56.7	0.9
8	P5P + P5P <-> S7P + G3P	20.0	1.7	18.9	0.3
9	S7P + G3P <-> F6P + E4P	20.0	1.7	18.9	0.3
10	P5P + E4P <-> F6P + G3P	19.9	1.8	18.9	0.3
11	PYRCYT <-> ACA + CO2	14.9	8.2	0.0	0.0
12	ACA <-> ETH	0.0	0.0	0.0	0.0
13	ACA <-> ACE	24.9	8.2	0.1	0.1
14	OAACYT <-> OXA + ACE	0.1	0.0	9.0	0.8
15	G3P <-> GLYC	5.5	4.3	1.8	0.1
16	ACE <-> ACCOACYT	24.7	8.0	0.0	0.0
17	PYRCYT + CO2 <-> OAACYT	96.4	7.3	52.8	0.9
18	PYRMIT <-> ACCOAMIT + CO2	98.8	5.3	125.8	0.5
19	OAAMIT + ACCOAMIT <-> ICIT	108.8	2.1	125.0	0.3
20	ICIT <-> AKG + CO2	99.5	2.3	124.8	0.3
21	ICIT <-> GOXA + SUC	9.2	0.2	0.2	0.0
22	GOXA <-> OXA	9.2	0.2	0.2	0.1
23	AKG <-> SUC + CO2	89.6	2.3	114.9	0.3
24	SUC <-> FUM	98.8	2.1	115.0	0.3
25	FUM + FUM <-> OAAMIT + OAAMIT	50.2	0.4	121.5	4.9
26	OAAMIT <-> FUM	1.6	1.3	127.9	10.1
27	GOXA + ACCOAMIT <-> OAAMIT	0.1	0.0	0.0	0.0
28	OAAMIT <-> OAACYT	-68.9	9.5	-28.3	0.1
29	ACCOACYT <-> ACCOAMIT	19.8	3.2	0.0	0.0
30	PYRCYT <-> PYRMIT	49.6	4.2	108.0	1.1
31	G3P <-> SER	0.0	0.0	11.8	2.5
32	SER <-> GLY + C1	0.0	0.0	9.5	0.2
33	OAACYT <-> THR	19.9	0.0	6.2	0.4
34	THR <-> GLY + ACA	10.0	0.0	0.1	0.1
35	OAAMIT <-> PYRMIT + CO2	59.1	9.5	18.3	0.2
36	G6P <-> G6POUT	3.2	3.1	1.8	1.8
37	P5P <-> P5POUT	0.2	0.2	0.0	0.0
38	E4P <-> E4POUT	0.1	0.1	0.0	0.0
39	G3P <-> G3POUT	0.2	0.2	0.6	0.5
40	PEP <-> PEPOUT	0.8	0.7	2.5	1.9

41	PYRMIT <-> PYRMITOUT	9.9	0.0	0.5	0.5
42	PYRCYT <-> PYRCYTOUT	5.6	4.3	0.0	0.0
43	OAACYT <-> OAACYTOUT	7.5	2.1	9.3	0.7
44	AKG <-> AKGOUT	9.9	0.0	10.0	0.0
45	ACCOACYT <-> ACCOACYTOUT	4.8	4.8	0.0	0.0
46	ACCOAMIT <-> ACCOAMITOUT	9.8	0.1	0.8	0.7
47	SER <-> SEROUT	0.0	0.0	2.3	2.3
48	GLY <-> GLYOUT	10.0	0.0	9.6	0.2
49	C1 <-> C1OUT	0.0	0.0	9.5	0.2
50	THR <-> THROUT	9.9	0.0	6.1	0.5
51	ETH <-> ETHOUT	0.0	0.0	0.0	0.0
52	ACE <-> ACEOUT	0.3	0.3	9.1	0.8
53	GLYC <-> GLYCOUT	5.5	4.3	1.8	0.1
54	CO2 <-> CO2OUT	325.6	1.5	387.7	0.2
55	OXA <-> OXAOUT	9.3	0.2	9.2	0.8

[a] Standard deviation

BLAST results of oxalate biosynthesis enzymes in *G. trabeum*

Table B.S2. BLAST results of *G. trabeum* from *Fomitopsis palustris*

Enzyme	Score	Expect	Identities	Gaps	Strand
Oxaloacetate acetylhydrolase (fpOAH)	722 bits(800)	0.0	711/918(77%)	0/918(0%)	Plus/Plus
Glyoxylate dehydrogenase (fpGLOXDH1)	385 bits(426)	2e-106	920/1373(67%)	45/1373(3%)	Plus/Plus

>gi|472338812|dbj|AB690578.1| Fomitopsis palustris FpOAH mRNA for oxaloacetate acetylhydrolase, complete cds

Gloeophyllum trabeum ATCC 11539 Phosphoenolpyruvate/pyruvate domain-containing protein partial mRNA

Sequence ID: ref|XM_007867946.1| Length: 1008 Number of Matches: 1

>gi|225636765|dbj|AB079662.1| Fomitopsis palustris FPGLOXDH1 mRNA for glyoxylate dehydrogenase, complete cds

Gloeophyllum trabeum ATCC 11539 hypothetical protein mRNA

Sequence ID: ref|XM_007868156.1| Length: 1750 Number of Matches: 1

Appendix C: Supplementary Material of Chapter 4

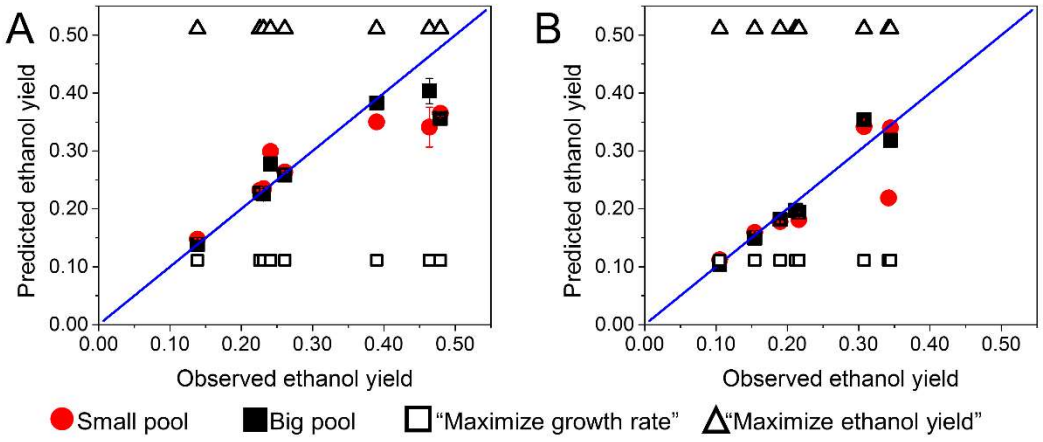

Fig. C.S1 Comparison of FBA prediction using dual objective function and the commonly used objective function.

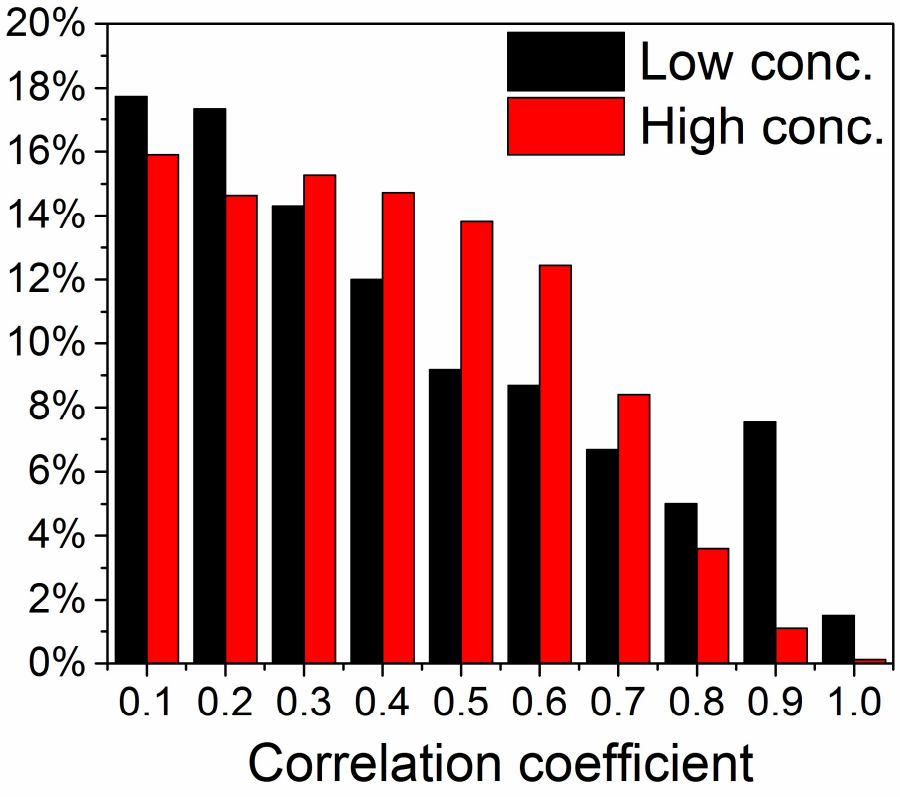

Fig. C.S2 Correlation coefficient (absolute value) between gene expression and phenotype-matched weighting factors at low glucose condition and high glucose condition.

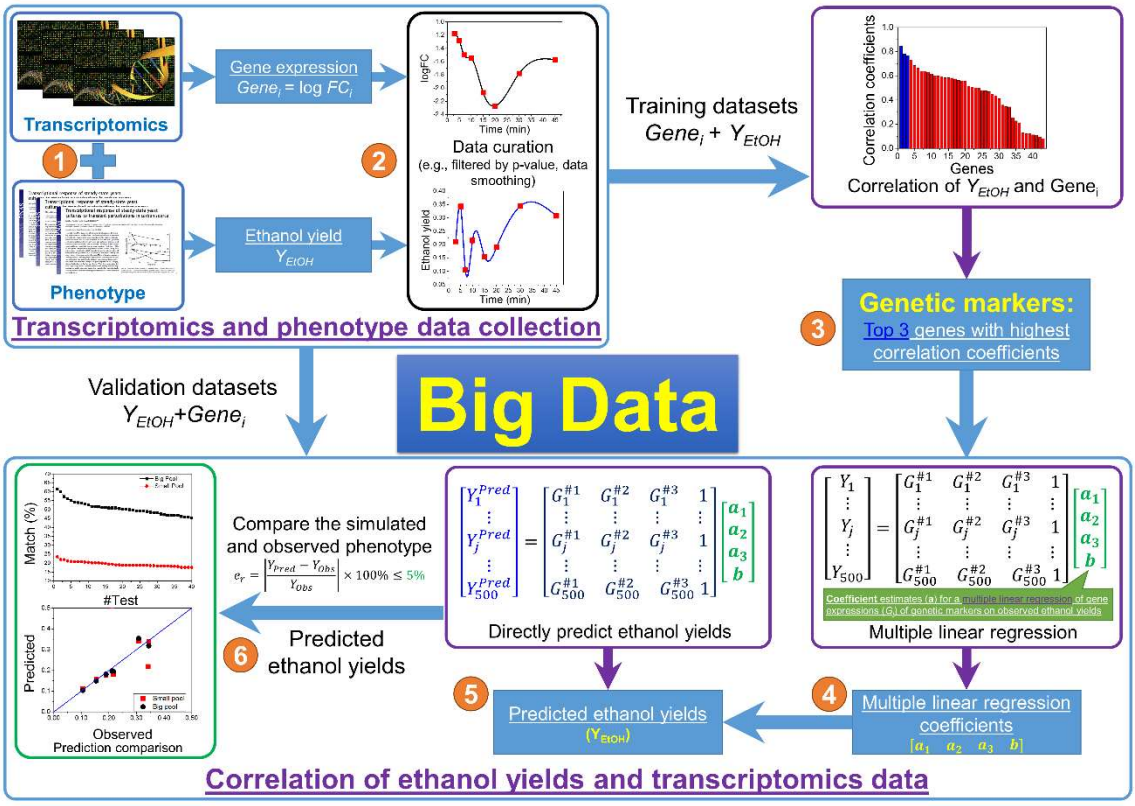

Fig. C.S3 Scheme for "Big Data" approach.

In general, we directly correlated the transcriptomics and the phenotype data from the training dataset using regression analysis. Based on this regression equation derived, we applied the transcriptomics data from validation dataset to predict the phenotype, and compared the predictions and observations to evaluate the prediction accuracy. To start, we used the same training and validation datasets for big data approach as the ones we used for omFBA. We next calculated the absolute value of correlation coefficients between the transcriptomics data of each gene and the ethanol yields, and ranked them to find the top 3 genes with highest absolute values of correlation coefficients as the genetic markers. The transcriptomics data of these genetic markers have been used for multiple linear regressions to connect the gene expression with ethanol yield. Then, based on the regression equation, the ethanol yields were predicted from the transcriptomics data in validation dataset.

Finally, the predicted ethanol yields were compared to the observed ethanol yields in the validation dataset. We repeated the “Big Data” regression approach for 40 times to make sure our predictions were statistically reliable.

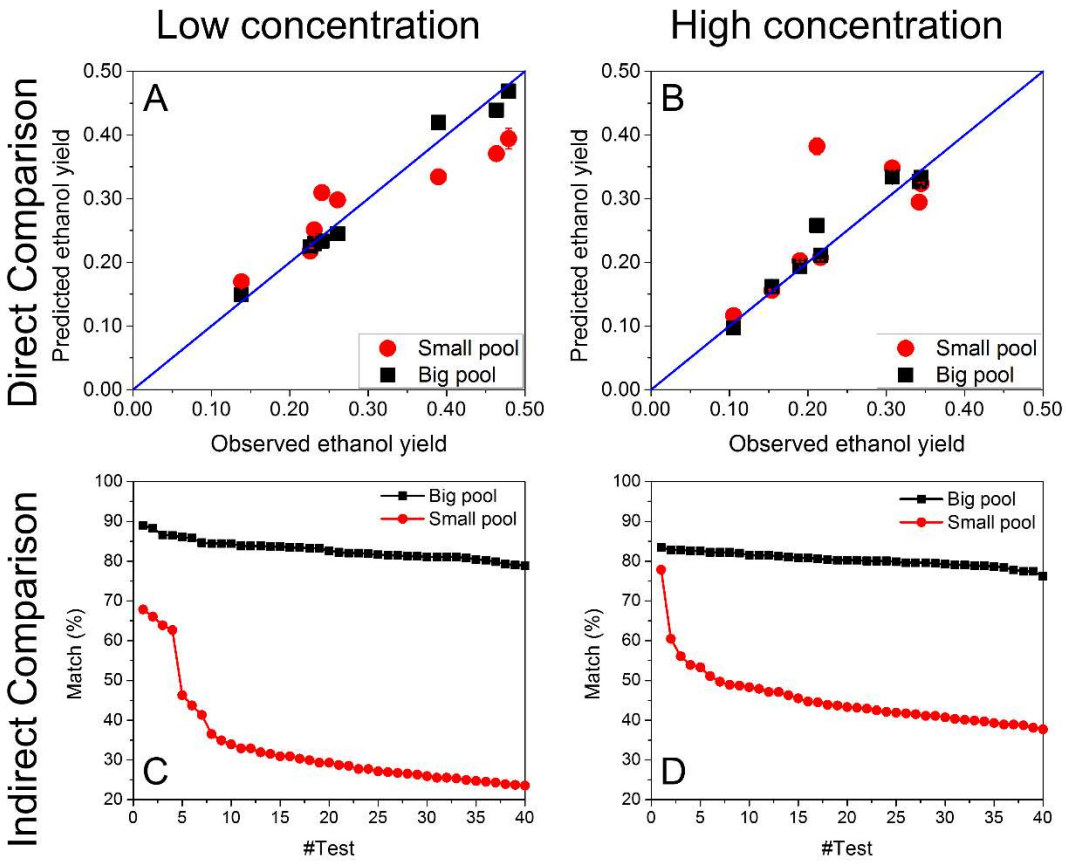

Fig. C.S4 Prediction accuracy of "Big Data" approach. Direct comparison of the predicted and observed ethanol yields in low (A) and high (B) glucose condition. The "Big Data" algorithm was repeated for 40 times and the proportions of matched predictions of "Big Data" algorithm were calculated and ranked for low (C) and high (D) glucose conditions.

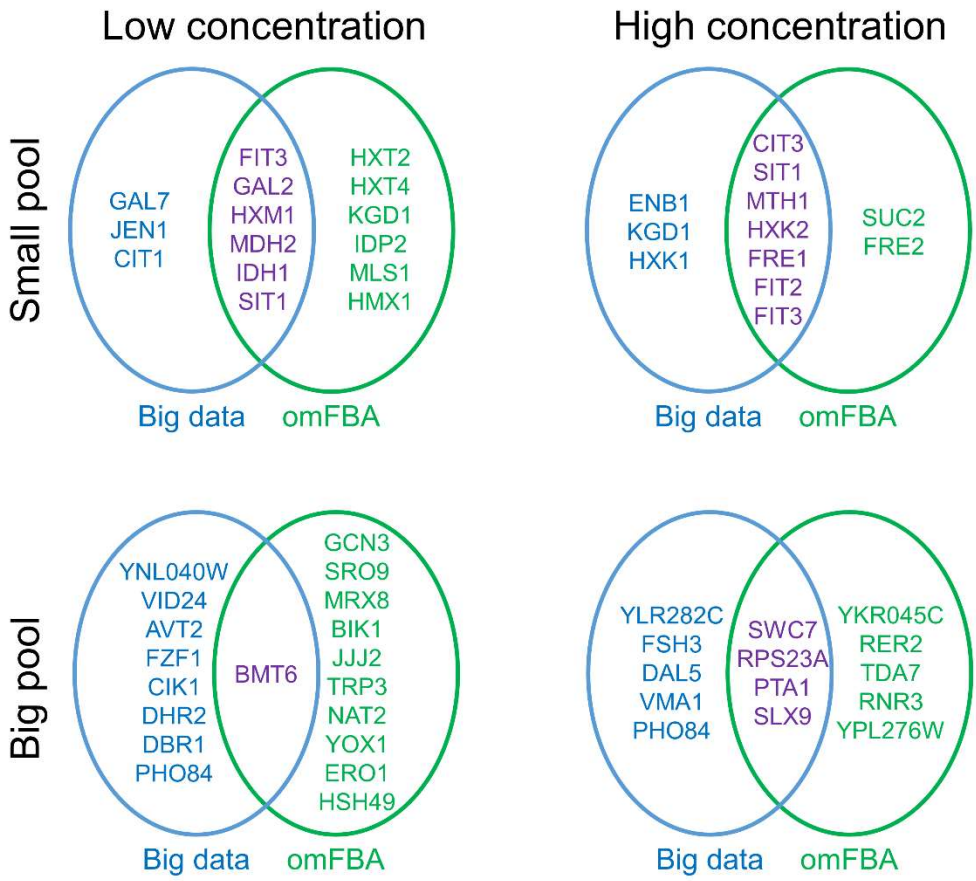

Fig. C.S5. Venn diagram for genetic markers identified by omFBA and "Big Data" using either "big pool" or "small pool" of genes for low and high concentration conditions. Top 10 genes with the highest absolute values of correlation coefficients were extracted from S1 Table and shown in this figure.

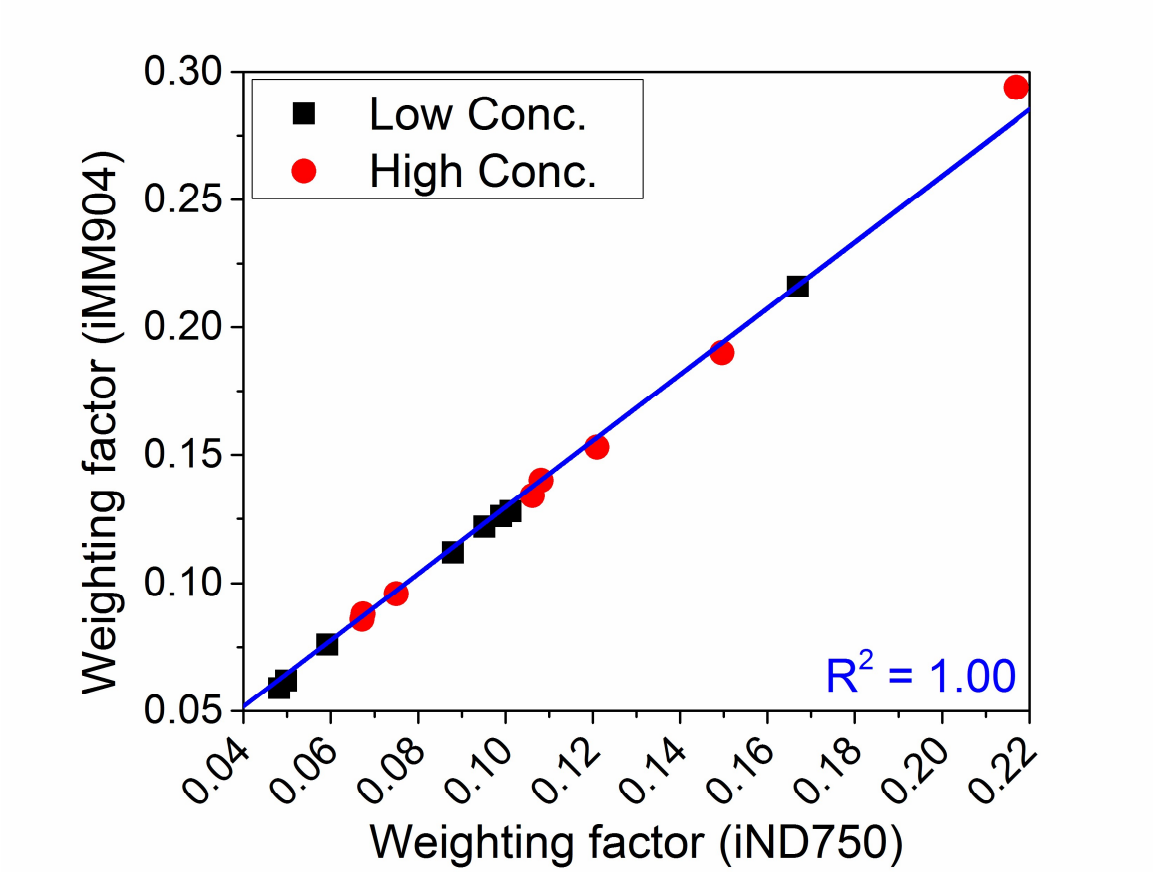

Fig. C.S6 Correlation of phenotype-matched weighting factors derived from two genome-scale metabolic models of S. cerevisiae: iMM904 and iND750.

Appendix D: Supplementary Material of Chapter 5

1. Binary regression decision tree model

1.1. Parameterization of guide RNAs

Nine key design parameters, i.e., location, GC content (GC%), minimal free energy (ΔG), number of base A, number of base G, AGG, TGG, CGG, and GGG, have been extracted from guide RNAs, respectively. Location is defined as the number of bases between the first base of guide RNA binding sequence and the A in the start codon (ATG). Therefore, the position of A in the ATG is considered as 0. The location of guide RNAs binding before the start codon is defined as negative, and vice versa. The GC content (GC%) is defined as the proportion of base G and base C in the guide RNA sequence. Minimal free energy (ΔG) is calculated by *rnafold* command in MATLAB. As a categorical parameter, AGG, TGG, CGG, and GGG are four bool parameters representing four types of the PAM site type. Each guide RNA has a set of key design parameters. The parameters are used to train and validate the decision tree model.

1.2. Setup of regression decision tree model

To train the binary regression decision tree model, "*fitrtree*" command in MATLAB was used with the default settings. In detail, the standard CART algorithm was used to select the best split predictor, which maximized the split-criterion gain over all possible splits of all predictors. The "*fitrtree*" grew the regression tree and estimated the optimal sequence of pruned subtrees based on the equally weighted mean squared errors, but did not prune the regression tree. During the tree growing, splitting nodes stopped when quadratic error per node dropped below 10^{-6} of the quadratic error for the entire data

computed before the decision tree was grown. To control the depth of the tree and avoid the over-fitting of the tree model, the maximu m splits number was the number of guide RNAs in training datasets.

1.3. Application of regression decision tree model

To apply our binary regression decision tree model, "*predict*" command in MATLAB was used to predict the fold changes of gene expression levels for specific guide RNAs. (https://www.mathworks.com/help/stats/compactregressiontree.predict.html?searchHighlight=predict&s_tid=doc_srchtitle). In general, the target guide RNA sequence will be first processed by customized functions (supplementary software) to calculate the corresponding design parameters. An input matrix will be generated for the tree model, which will be used to predict the corresponding fold change of the gene expression level.

1.4 CRISTINES software and its results

CRISTINES software is an offline MATLAB-based tool to provide the guide RNA designs to achieve gene up-regulation and down-regulation. The core algorithm is the binary regression decision tree model that uses the key design parameters of guide RNAs as the input. In the CRISTINES, the sequence of interest with the identification of the start codon ATG, is used as the source file. All the possible guide RNAs from the input sequence will be generated, and the nine design parameters, i.e., location, GC content, minimal free energy, number of base A, number of base G, AGG, TGG, CGG, and GGG, are calculated for each of guide RNAs. These design parameters will then be used in the binary regression decision tree model to calculate the regulatory effects (i.e., fold change of gene expression level) of guide RNAs. CRISTINES will report the top 5 guide RNA designs with highest

up- and down- regulation effects, respectively. The regulatory effects of all possible guide RNAs can be downloaded to the local folder in Excel file.

2. Calculation of metabolic fluxes in violacein pathway subject to dCas9-VP64 regulation

We hypothesized that the changes gene expression levels would quantitatively change the metabolic fluxes in the branches of violacein pathway, and thus, leading to different concentrations of various products. In detail, the flows through pathways governed by gene *vioA*, *vioB*, *vioC*, *vioD*, and *vioE*, are defined as f_A, f_B, f_C, f_D, and f_E, respectively. The predicted fold changes of gene *vioA*, *vioB*, *vioC*, *vioD*, and *vioE*, are defined as FC_A, FC_B, FC_C, FC_D, and FC_E, respectively. Similarly, the flows through the non-enzymatic pathways for producing the final colorful chemical, proviolacein, prodeoxyviolacein, violacein, and deoxyviolacein, are defined as f_{PV}, f_{PDV}, f_V, and f_{DV}, respectively. To calculate the effects of dCas9-VP64 on metabolic fluxes in violacein pathway, we assume a pseudo-steady state was achieved. Thus, based on the flux balance at steady state, the quantitative relations among these parameters were shown below:

$$f_A = f_B = f_E \quad \text{Eq. 1}$$

$$f_E = f_{DV} + f_{PDV} + f_D \quad \text{Eq. 2}$$

$$f_D = f_V + f_{PV} \quad \text{Eq. 3}$$

$$f_C = f_{DV} + f_V \quad \text{Eq. 4}$$

In addition, we hypothesized that the proportion between f_{DV} and f_V obeys the Hill equation as shown in Eq. 5 with Hill coefficient defined as n:

$$f_{DV} / f_V = 1 / (f_C^n + 1) \quad \text{Eq. 5}$$

The values of f_{PV}, f_{PDV}, f_V, and f_{DV} can be directly obtained from the HPLC measurements, which would serve as the experimental measurements. The constant n was calculated as 0.356 from the measurements of the control strain by using Eq. 4 and Eq. 5. The following methods were used to calculate the simulated f_{PV}, f_{PDV}, f_V, and f_{DV}.

1) If the dCas9-VP64 system regulates the gene expression of *vioA* or *vioE*, then $f_E = FC_A * f_{E,\,Control}$ or $f_E = FC_E * f_{E,\,Control}$, respectively; $f_D = FC_D * f_{D,\,Control}$, and $f_C = FC_C * f_{C,\,Control}$.
2) If the dCas9-VP64 system regulates the gene expression of *vioC*, then $f_C = FC_C * f_{C,\,Control}$, $f_E = f_{E,\,Control}$, and $f_D = f_{D,\,Control}$.
3) If the dCas9-VP64 system regulates the gene expression of *vioD*, then $f_D = FC_D * f_{D,\,Control}$, $f_E = f_{E,\,Control}$, and $f_C = f_{C,\,Control}$.
4) If the dCas9-VP64 system is regulating multiple gene expression in the violacein pathways, we assume that the regulation of each gene is independent to others. In other words, we hypothesized that the regulation of dCas9-VP64 system was independent on each gene and each pathway of the violacein pathways.

By knowing f_E, f_D, and f_C, we could then solve Eq 1-5 together to derive the simulated f_{DV}, f_V, f_{PV}, and f_{PDV} sequentially. We next compared the experimentally measured and simulated f_{DV}, f_V, f_{PV}, and f_{PDV} as shown in Fig. 3B and 3C.

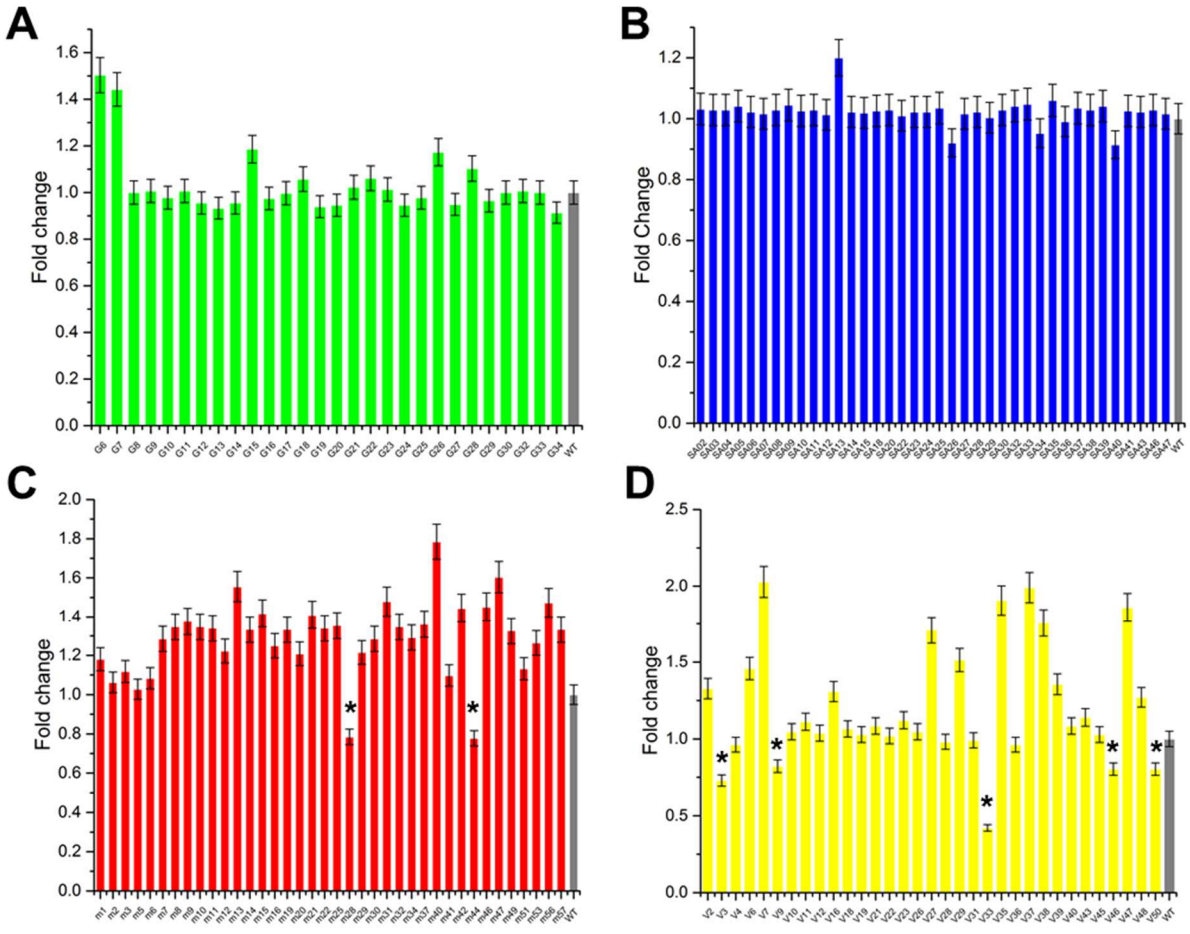

Fig. D.S1. The OD_{600} fold change for all the strains used for screening. (A) OD_{600} fold-change for GFP screening set. (B) OD_{600} fold-change for Sapphire screening set. (C) OD_{600} fold-change for mCherry screening set. (D) OD_{600} fold-change for Venus screening set. The results showed that no significant metabolic burden could be detected compared with wild type strain. The strains marked with (*) indicated a significant inhibition of growth (p<0.05).

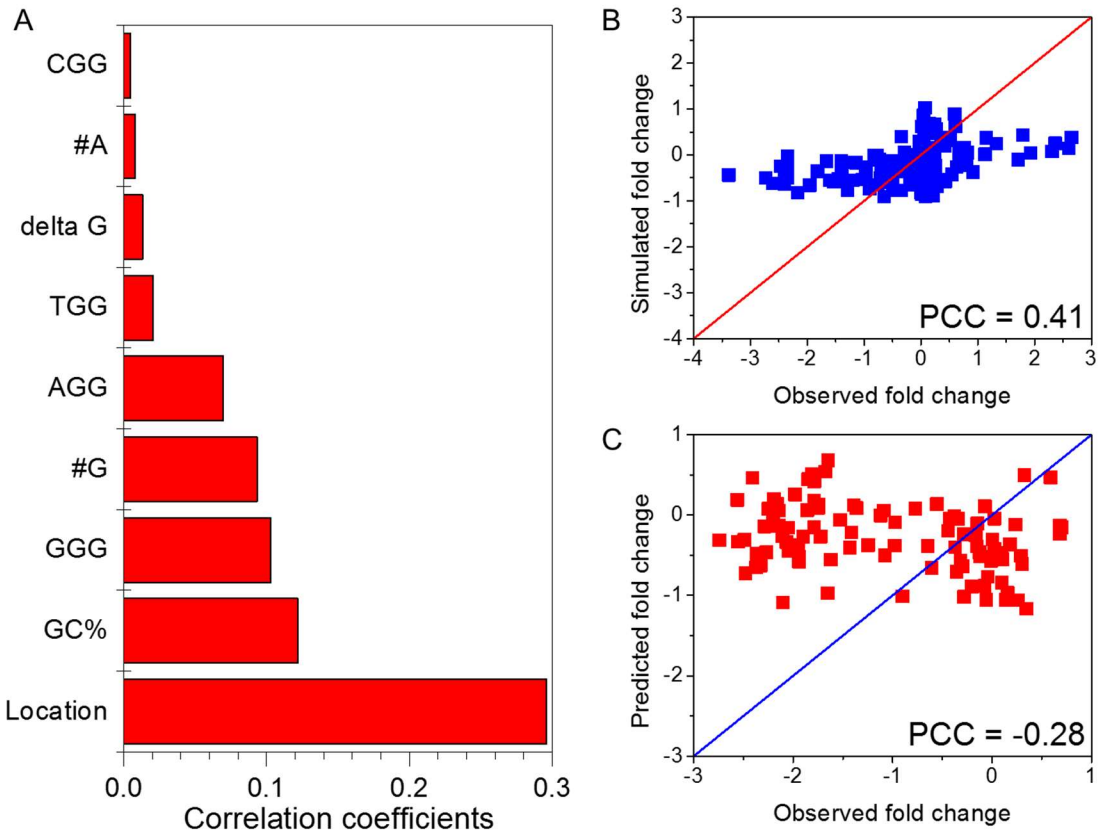

Fig. D.S2. Linear model for predicting transcriptional regulation by dCas9-VP64. (A) Pearson's correlation coefficients between each guide RNA design parameters and the fold changes of gene expressions from the screening data of the four synthetic genetic cassettes. (B) Simulation accuracy of the linear model. (C) Validation of the linear model by comparing the simulated and experimentally measured gene regulations on Eno2p-tdTomato cassette subject to dCas9-VP64 regulation.

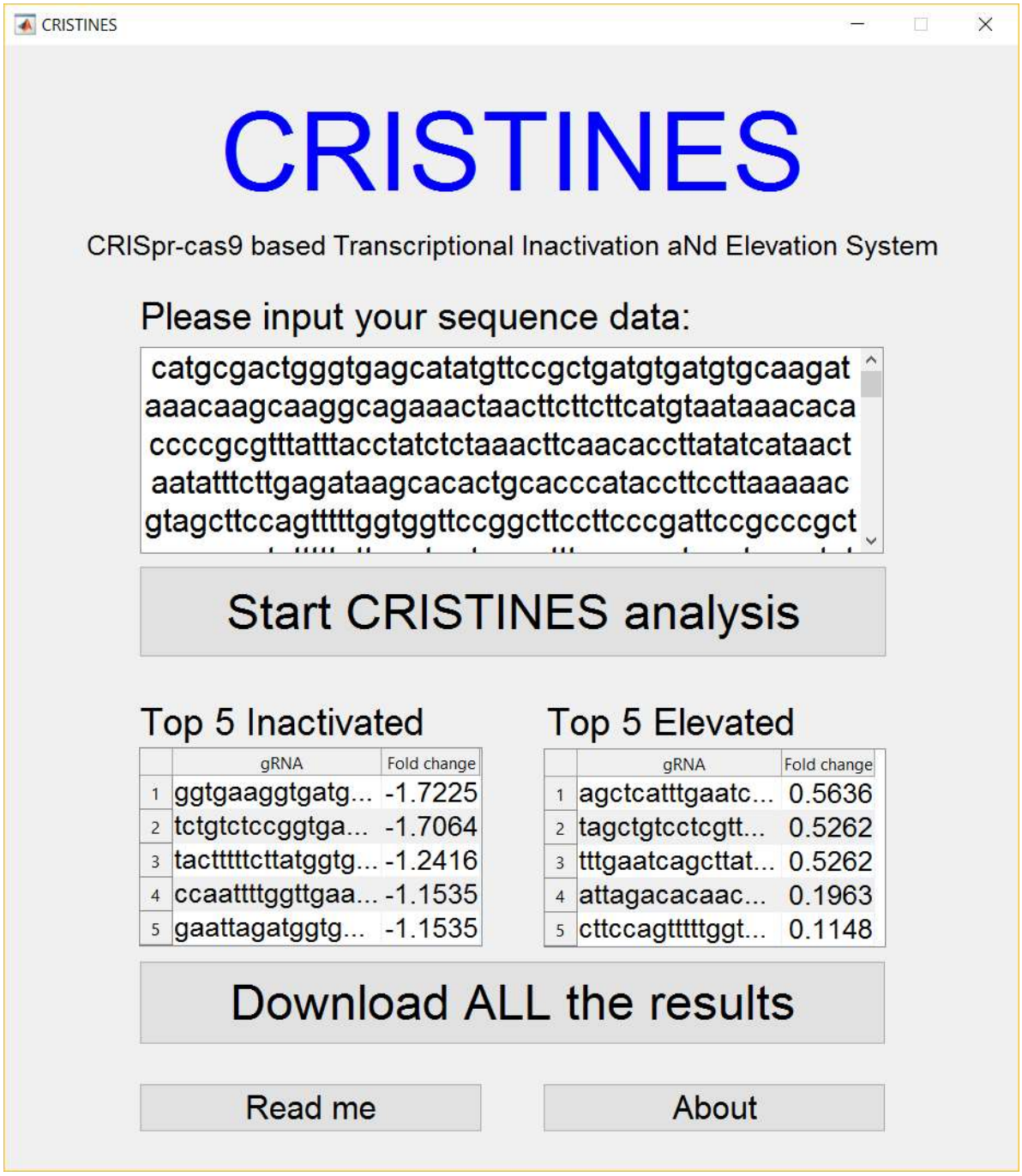

Fig. D.S3. Screenshot of CRISTINES software with a demo sequence.

Table D.S1. DNA sequences and plasmids used in this study.

DNA Name	Sequence (5'-3')
TEF1p	atagcttcaaaatgtttctactccttttttactcttccagattttctcggactccgcgcatcgccgtaccacttcaaaacacccaagca cagcatactaaatttcccctctttcttcctctagggtgtcgttaattacccgtactaaaggtttggaaaagaaaaaagagaccgcct cgtttctttttcttcgtcgaaaaaggcaataaaaatttttatcacgtttctttttcttgaaaatttttttttttgatttttttctctttcgatgacct cccattgatatttaagttaataaacggtcttcaatttctcaagtttcagtttcatttttcttgttctattacaacttttttacttcttgctcatta gaaagaaagcatagcaatctaatctaagttttaattacaaa
ENO2p	gtgtcgacgctgcgggtatagaaagggttctttactctatagtacctcctcgctcagcatctgcttcttcccaaagatgaacgcgg cgttatgtcactaacgacgtgcaccaacttgcggaaagtggaatcccgttccaaaactggcatccactaattgatacatctacaca ccgcacgccttttttctgaagcccactttcgtggactttgccatatgcaaaattcatgaagtgtgataccaagtcagcatacacctc actagggtagtttctttggttgtattgatcatttggttcatcgtggttcattaatttttttctccattgctttctggctttgatcttactatcat ttggatttttgtcgaaggttgtagaattgtatgtgacaagtggcaccaagcatatataaaaaaaaaaagcattatcttcctaccaga gttgattgttaaaaacgtatttatagcaaacgcaattgtaattaattcttatttttgtatctttttcttcccttgtctcaatcttttatttttattttat ttttcttttcttagtttctttcataacaccaagcaactaatactataacatacaataata
PDC1p	catgcgactgggtgagcatatgttccgctgatgtgatgtgcaagataaacaagcaaggcagaaactaacttcttcttcatgtaata aacacaccccgcgtttatttacctatctctaaacttcaacaccttatatcataactaatatttcttgagataagcacactgcacccata ccttccttaaaaacgtagcttccagtttttggtggttccggcttccttcccgattccgcccgctaaacgcatatttttgttgcctggtgg catttgcaaaatgcataacctatgcatttaaaagattatgtatgctcttctgacttttcgtgtgatgaggctcgtggaaaaaatgaata atttatgaatttgagaacaattttgtgttgttacggtattttactatggaataatcaatcaattgaggattttatgcaaatatcgtttgaata tttttccgacccttgagtacttttcttcataattgcataatattgtccgctgccccttttttctgttagacggtgtcttgatctacttgctatc gttcaacaccaccttatttttctaactatttttttttttagctcatttgaatcagcttatggtgatggcacatttttgcataaacctagctgtcc tcgttgaacataggaaaaaaaaatatataaacaaggctctttcactctccttgcaatcagatttgggtttgttccctttatttttcatatttc ttgtcatattccttttctcaattattatttttctactcataacctcacgcaaaataacacagtcaaatcaatcaaa
PGK1p	tcaggcatgaacgcatcacagacaaaatcttcttgacaaacgtcacaattgatccctccccatccgttatcacaatgacaggtgtc attttgtgctcttatgggacgatccttattaccgctttcatccggtgatagaccgccacagaggggcagagagcaatcatcacctg caaacccttctatacactcacatctaccagtgtacgaattgcattcagaaaactgtttgcattcaaaaataggtagcatacaattaaa acatggcgggcacgtatcattgcccttatcttgtgcagttagacgcgaatttttcgaagaagtaccttcaaagaatggggtctcatc ttgttttgcaagtaccactgagcaggataataatagaaatgataatatactatagtagagataacgtcgatgacttcccatactgtaa ttgcttttagttgtgtatttttagtgtgcaagtttctgtaaatcgattaatttttttttctttcctctttttattaaccttaatttttatttttagattcct gacttcaactcaagacgcacagatattataacatctgcacaataggcatttgcaagaattactcgtgagtaaggaaagagtgagg aactatcgcatacctgcatttaaagatgccgatttgggcgcgaatcctttattttggcttcaccctcatactattatcagggccagaa aaaggaagtgtttccctccttcttgaattgatgttaccctcataaagcacgtggcctcttatcgagaaagaaattaccgtcgctcgt gatttgtttgcaaaaagaacaaaactgaaaaaacccagacacgctcgacttcctgtcttcctattgattgcagcttccaatttcgtca cacaacaaggtcctagcgacggctcacaggttttgtaacaagcaatcgaaggttctggaatggcgggaaagggtttagtacca catgctatgatgcccactgtgatctccagagcaaagttcgttcgatcgtactgttactctctctctttcaaacagaattgtccgaatc gtgtgacaacaacagcctgttctcacacactcttttcttctaaccaagggggtggtttagtttagtagaacctcgtgaaacttacattt acatatatataaacttgcataaattggtcaatgcaagaaatacatatttggtcttttctaattcgtagtttttcaagttcttagatgctttct ttttctctttttttacagatcatcaaggaagtaattatctactttttacaacaaatataaaaca
TPI1p	tatatctaggaacccatcaggttggtggaagattacccgttctaagacttttcagcttcctctattgatgttacacctggacacccctt tttctggcatccagtttttaatcttcagtggcatgtgagattctccgaaattaattaaagcaatcacacaattctctcggataccacctc ggttgaaactgacaggtggtttgttacgcatgctaatgcaaaggagcctatataccttggctcggctgctgtaacagggaatata aagggcagcataatttaggagtttagtgaacttgcaacatttactatttttcccttcttacgtaaatatttttctttttaattctaaatcaatct ttttcaatttttttgtttgtattctttttcttgcttaaatctataactacaaaaaacacatacataaactaaaa
EGFP	atgtctaaaggtgaagaattattcactggtgttgtcccaattttggttgaattagatggtgatgttaatggtcacaaatttttctgtctcc ggtgaaggtgaaggtgatgctacttacggtaaattgaccttaaaatttatttgtactactggtaaattgccagttccatggccaacct tagtcactactttaacttatggtgttcaatgtttttctagatacccagatcatatgaaacaacatgacttttcaagtctgccatgccag aaggttatgttcaagaaagaactatttttttcaaagatgacggtaactacaagaccagagctgaagtcaagtttgaaggtgatacct tagttaatagaatcgaattaaaaggtattgattttaaagaagatggtaacattttaggtcacaaattggaatacaactataactctcac aatgtttacatcatggctgacaaacaaaagaatggtatcaaagttaacttcaaaattagacacaacattgaagatggttctgttcaat tagctgaccattatcaacaaaatactccaattggtgatggtccagtcttgttaccagacaaccattacttatccactcaatctgcctta tccaaagatccaaacgaaaagagagaccacatggtcttgttagaatttgttactgctgctggtattacccatggtatggatgaattg tacaaataa
tdTomato	atggtgagcaagggcgaggaggtcatcaaagagttcatgcgcttcaaggtgcgcatggagggctccatgaacggccacgag

	ttcgagatcgagggcgagggcgagggccgcccctacgagggcacccagaccgccaagctgaaggtgaccaagggcggc cccctgcccttcgcctgggacatcctgtccccccagttcatgtacggctccaaggcgtacgtgaagcaccccgccgacatccc cgattacaagaagctgtccttccccgagggcttcaagtgggagcgcgtgatgaacttcgaggacggcggtctggtgaccgtga cccaggactcctccctgcaggacggcacgctgatctacaaggtgaagatgcgcggcaccaacttcccccccgacggccccg taatgcagaagaagaccatgggctgggaggcctccaccgagcgcctgtacccccgcgacggcgtgctgaagggcgagatc caccaggccctgaagctgaaggacggcggccactacctggtggagttcaagaccatctacatggccaagaagcccgtgcaa ctgcccggctactactacgtggacaccaagctggacatcacctcccacaacgaggactacaccatcgtggaacagtacgagc gctccgagggccgccaccacctgttcctggggcatggcaccggcagcaccggcagcggcagctccggcaccgcctcctcc gaggacaacaacatggccgtcatcaaagagttcatgcgcttcaaggtgcgcatggagggctccatgaacggccacgagttcg agatcgagggcgagggcgagggccgcccctacgagggcacccagaccgccaagctgaaggtgaccaagggcggccccc tgcccttcgcctgggacatcctgtccccccagttcatgtacggctccaaggcgtacgtgaagcaccccgccgacatccccgatt acaagaagctgtccttccccgagggcttcaagtgggagcgcgtgatgaacttcgaggacggcggtctggtgaccgtgaccca ggactcctccctgcaggacggcacgctgatctacaaggtgaagatgcgcggcaccaacttcccccccgacggccccgtaatg cagaagaagaccatgggctgggaggcctccaccgagcgcctgtacccccgcgacggcgtgctgaagggcgagatccacca ggccctgaagctgaaggacggcggccactacctggtggagttcaagaccatctacatggccaagaagcccgtgcaactgcc cggctactactacgtggacaccaagctggacatcacctcccacaacgaggactacaccatcgtggaacagtacgagcgctcc gagggccgccaccacctgttcctgtacggcatggacgagctgtacaagtaa
Sapphire	atgtctaaaggtgaagaattattcactggtgttgtcccaattttggttgaattagatggtgatgttaatggtcacaaattttctgtctcc ggtgaaggtgaaggtgatgctacttacggtaaattgaccttaaaatttatttgtactactggtaaattgccagttccatggccaacct tagtcactacttttttcttatggtgttatggtttttgctagatacccagatcatatgaaacaacatgacttttcaagtctgccatgccaga aggttatgttcaagaaagaactatttttttcaaagatgacggtaactacaagaccagagctgaagtcaagtttgaaggtgatacctt agttaatagaatcgaattaaaaggtattgattttaaagaagatggtaacattttaggtcacaaattggaatacaactttaactctcaca atgtttacatcatggctgacaaacaaaagaatggtatcaaagctaacttcaaaattagacacaacattgaagatggtggttgttcaat tagctgaccattatcaacaaaatactccaattggtgatggtccagtcttgttaccagacaaccattacttatccattcaatctgccttа tccaaagatccaaacgaaaagagagaccacatggtcttgttagaatttgttactgctgctggtattacccatggtatggatgaattg tacaaataa
mCherry	atggttagcaaaggcgaggaagataacatggctataatcaaagagtttatgagattcaaagtacacatggagggttcagtgaat ggtcatgaatttgaaattgaaggcgaaggcgagggcagaccttacgaaggaactcaaacagcaaaacttaaggtaacaaaag gtggtcctctgccattcgcctgggacattctcagtccacaattcatgtacggttctaaagcgtacgtcaaacatccagcagacatt ccagattacttgaaattgtcttttccagaaggctttaagtgggaaagagttatgaacttcgaggatggaggggttgtgaccgttac gcaagattcctctttacaagatggtgagtttatctacaaggtcaaattaagggggactaattttccttcagacgggccagtcatgca gaaaaagactatgggatgggaagcctcttcagagagaatgtatcctgaagatggcgctctaaaaggagaaatcaagcaaagat tgaagttaaaggacggaggtcattatgatgcagaagtaaaaacaacctataaagctaaaaagccagttcaacttcctggtgccta caatgttaacatcaagctagacattacatcccataatgaagattacactatagtggaacagtatgaacgtgctgaaggtagacac agtacaggtggtatggatgaactgtacaagtaa
Venus	atgtctaaaggtgaagaattattcactggtgttgtcccaattttggttgaattagatggtgatgttaatggtcacaaattttctgtctcc ggtgaaggtgaaggtgatgctacttacggtaaattgaccttaaaattgatttgtactactggtaaattgccagttccatggccaacc ttagtcactactttaggttatggtttgcaatgttttgctagatacccagatcatatgaaacaacatgacttttcaagtctgccatgcca gaaggttatgttcaagaaagaactatttttttcaaagatgacggtaactacaagaccagagctgaagtcaagtttgaaggtgatac cttagttaatagaatcgaattaaaaggtattgattttaaagaagatggtaacattttaggtcacaaattggaatacaactataactctc acaatgtttacatcactgctgacaaacaaaagaatggtatcaaagctaacttcaaaattagacacaacattgaagatggtggtgtt caattagctgaccattatcaacaaaatactccaattggtgatggtccagtcttgttaccagacaaccattacttatcctatcaatctgc cttatccaaagatccaaacgaaaagagagaccacatggtcttgttagaatttgttactgctgctggtattacccatggtatggatga attgtacaaataa
VioA	atgaagcacagttctgatatttgcatagttggggcgggcatctcagggttgacctgcgcgagtcaccttcttgactctcctgcttgt cgtggcttatccctaagaatttttgatatgcaacaggaggctggaggtaggatcaggtctaagatgcttgatggcaaagcgagca ttgagttgggcgctggccgttattcccctcaacttcatcctcacttccaaagcgcgatgcaacactattcacagaagagtgaggttt atccgtttacacaattaaaattcaagagccatgtccagcagaagctaaagagagctatgaatgagctttccccccgtctaaagga gcacggaaaagaatcctttctacagtttgtgtctcgttaccaaggtcacgactccgcggtcggcatgatcaggtctatgggatatg acgcgctattccttccggacatatctgcagaaatggcatacgatattgttggcaaacatcccgagatccaaagtgttactgacaat gacgctaatcagtggtttgccgcagaaactgggttcgccgggcttattcaggggattaaggcgaaagtaaaggctgcaggtgc tagattttccctggggtataggttactgtcagtgaggacggacggggacggatacttgctgcaattagctggtgatgatggctgg aaacttgagcatagaacaagacatctaattcttgcaatacctccatcagctatggcgggactaaatgtagattttcctgaagcgtg gtcaggggccaggtatgggtcattaccgctatttaaaggcttcttaacttacggagagccatggtggttagattataagctagatg

	accaggtgctaattgtggataatccgcttagaaagatctactttaaaggcgataagtatttatttttttacacagactcagaaatggc aaattattggagaggctgtgtagcggagggcgaggatggttatttggaacaaatccgtactcacttggcctcagcgctaggaat cgttagggagcgtataccccaaccgttagcccatgttcacaagtattgggcacatggtgtcgagttttgcagggattcagatattg accacccatcagcccttagccaccgtgactccggaatcattgcgtgcagtgacgcctatactgaacattgcggatggatggagg ggggtcttttatctgcgagagaagccagcaggctgcttctacaaaggatagccgcctaa
VioB	atgagcattctggattttccacgcatccatttccgcggctgggcgcgggtcaacgcgcccaccgccaaccgcgatccgcacgg ccacatcgacatggccagcaatacggtggccatggcaggcgaaccgttcgacctcgcgcgccatccgaccgagttccaccg ccacctgcggtcgctggggccgcgtttcggcctggacggccgggctgacccggaagggccgttcagcctggccgagggct acaacgcggccggcaacaaccatttctcctgggagagcgccaccgtcagccacgtgcagtgggatggcggcgaagcggac cgcggcgacggcctggtcggcgccaggctggcgctgtgggggcattacaacgattacctgcgcaccaccttcaaccgcgcg cgctgggtggacagcgaccccaccgccgcgacgcggcgcagatctacgccgggcagttcacgatcagcccggccggcg ccggaccgggcacgccctggctgttcaccgccgacatcgacgacagccacggcgcgcgctggacgcgcggcggccacat cgccgagcgcggcggccatttcctggacgaggagttcggcctggcgcggctgttccagttctcggtgcccaaagaccatccg cacttcctgttccacccggggccattcgattccgaagcctggcgcaggctgcagctggcgctggaggacgacgacgtgctcg gcctgacggtgcagtacgcgctgttcaatatgtcgacgccgccgcaacccaactcgccggtgttccacgacatggtcggcgtg gtcggcctgtggcggcgcggcgaactggccagctacccggccggccggctgctgcgtccgcgccagcccgggctgggcg atctgacgctgcgcgtaagcggcggccgcgtggcgctgaatctggcctgcgccattccgttctccacccgggcggcgcagcc gtccgcgccggacaggctgacgcccgatctcggggccaagctgccgttgggcgacctgctgctgcgcgacgaggacggcg cgttgctggcgcgggtgccgcaggcgctttaccaggattactggacgaaccacggcatcgtcgacctgccgctgctgcgcga gcccaggggctcgctgacgctgtccagcgagctggccgaatggcgcgagcaggactgggtcacgcagtccgacgcctcca atctttatttggaagcgccggaccgccgccacggccgtttctttccggaaagcatcgcgctgcgcagctatttccgcggcgagg cccgcgcgcgcccggacattccccaccggatcgaggggatgggtctggtcggcgtggagtcgcgccaggacggcgatgcc gccgaatggcggctgaccggcctgcggcccggcccggcgcgcatcgtgctcgacgacggcgcggaggcgatcccgctgc gggtgctgccggacgactgggcgttggacgacgcgacggtggaggaggtcgattacgccttcctgtaccggcacgtgatgg cctattacgagctggtctacccgttcatgtccgacaaggtgttcagcctggccgaccgctgcaagtgcgagacctacgccagg ctgatgtggcagatgtgcgatccgcagaaccggaacaagagctactacatgcccagcacccgcgagctgtcggcgcccaag gccaggctgttcctcaaatacctggcccatgtcgagggccaggccaggctgcaggcgccgccgccggccgggccggcgcg catcgagagcaaggcccagctggcggccgagctgcgcaaggcggtggatctggagttgtcggtgatgctgcagtacctgtac gccgcctattccattcccaattacgcccagggccagcagcgggtgcgcgacggcgcgtggacggcggagcagctgcagct ggcctgcggcagcggcgaccggcgccgcgacggcggcatccgcgccgcgctgctggagatcgcccacgaggagatgatc cattacctggtggtcaacaacctgctgatggcgctgggcgagccgttctacgccggcgtgccgctgatgggcgaggcggcgc ggcaggcgttcggcctggacaccgaattcgcgctggagccgttctccgagtcgacgctggcgcgcttcgtccggctggaatg gccgcacttcatccctgcgccgggcaaatccatcgccgactgctacgccgccatccgccaggcctttctcgatctgcccgacct gttcggcggcgaggccggcaagcgcggcggcgagcaccacttgttcctcaacgagctgaccaaccgcgcccatcccggct accagctggaggtgttcgatcgcgacagcgcgctgttcggcatcgccttcgtcaccgaccagggcgagggcggggcgctgg actcgccgcattacgagcattcgcatttccagcggctgcgggagatgtcggccaggatcatggcgcagtccgcgccgttcgag ccggcgttgccggcgctgcgcaacccggtgctggacgagtcgccgggctgccagcgcgtggcggacggacgggcgcgc gcgctgatggcgctgtaccagggcgtgtacgagctgatgttcgcgatgatggcgcagcacttcgcggtcaagccgctgggca gcctcaggcgctcgcggctgatgaacgcggcgatcgacctgatgaccggcctgctcaggccgctgtcctgcgcgctgatgaa cctgccgtcgggcatcgccggacgcaccgccgggccgccgctgccggggccggtggatacccgcagctacgacgactac gcgctgggctgccggatgctggcgcggcgctgcgagcgcctgctggagcaggcgtcgatgctggagccgggctggctgcc cgacgcgcaaatggaactgctggatttctaccgccggcagatgctggatttggcttgtggaaagctttctagagaggcctaa
VioC	atgcagaaagccattatcgtgggaggcggcttagccggtggcttaacagctatttacctagcaaggcgtggctatgaggtacac gtagtagagaagaggggtgaccccttgcaagatctgtcatcttatgtcgacgcagtttccagtcgtgctatagggtaagtatga cggtcaggggcattaaagcggttttggccgctggtatccccagggctgagctggatcaatgtggagagccgatagttgggatg gcatttagtgtgggaggaaagttcaggatacgtgaattacaacctctggaagggctttctcccttgtccctgaatagggcagcctt tcagagactgttaaatcgtcacgcgaatcgtaatggggtgaggtatcatttcgagcacaaatgtcttgacgtcgacttggaaggc aagtccgtactgattcaaagcaaggacgggcaactacaaagactgcaaggtgatatggtaattggcgccgacggcgcacata gcgccgtaaggcaggcaatgcaaagtggtatgcgtaggttcgagttccaacagactttcttccgtcatggttataaaaccttagtt ctgccggatgccgaggctctgggttatagaaaagatttgttgtacttcttcggtatggattctggcggtctattcgcagggagagc agctaccatcccggacgggtcagtcagcatcgccgtgtgtctgccttatgaagggacgccctcccttgctacgcaggatagac aggcgatgaaagctttcttccaaaggtattttggttctctatcagacgcagttagggaggagatgttagagcaattcctagtgaaa cccagcaacgacctaataaatgttaggtccagcaccttccactacaaagggaacgttttattgcttggcgatgccgcccatgcca ctgcgccatttttgggccagggaatgaacatggcgctggaagacgcccacagcttcgtgaccctacttgatcaacattgtcacg atcaggagctggcattcgctgagtttacagcccaacgtaaagtgcaagctgatgcaatgcaagacatggcgcgtgcaaattac

	gatgtgttatcctgttcaaatcccatcttctttctgagggcgagatatactaggtacatgcacggaaaattcccggagctttatccac cagatatggcgcaaaagctatattttacgagtgaaccttacgacaaactacaaacaatacaaaagaaacagaacgtttggtacaa gctaggcagggtaaac
VioD	atgaagaagattttagttattggggctggacccgcgggtctggtgttcgcatcacagatgaagctagcgaaaccagattggcaa attagcatagctgagaagaacgatccggaggaggtcgctggttggggtgtagttttgccggggcgtcctggccagcatcctgc caaccctttgagctatttggagcatccggagaggcttgatccgcagttcctggaagacttcaaacttatacatcataacgaaccta acctgatgtctactggagtcctactttgcggggttgaacgtaggggcttgtccaggctctgcgtgagaggtgccagtctttggg gatcgcgatccactacgagagcccattactagccagggaacaattacctcttgatgactatgacttaatagtagctgcaaacggg gtgaatcataaaactagccacttcacggaagcgttggcaccgaaactggaatacgggggcaacaaatatatatggttcggtacc tcacaactgtttgaccaaatgaacttggtatttaggacacacggaaaagatatattcatcgcgcacgcatataagtattcaagcag aatgagtacattcgttgtcgagtgttccgaagaaaccttcgagcgtgcaaggttaggtgagatgtctgacgaagctagtgccga gtacgtagccggggtcttcagggcggagcttggtggtcacgggctggtcgcacaacctgggcttgggtggcgtaatttcatga ccctttcacacgataagtcttacgacggaaagttagttttaatcggcgacgctctgcaaagcggacacttcagtattgggcatggc acaacgatggcagtggtggctgcccagcttctagtcaaagctctgtgcgctgaagccagcgtccctgccgctctagcctcatttg acgcgagagcgatgccattagtaaagctgttttccgagcacgcgaattccagccgtgattggttcgagacggtcgatgatagaa tgcacctgtcaaacgcggaattcatgcagtccttcgacgcaagaaggaaagctttgcctcccttacccgaggcgttggcccgta atctaggctacgccttagataga
VioE	atggaaaatagagagcccccactgttaccagctcgttggtctagcgcatacgtgtcctattggtccccgatgctacccgacgacc agctgacatctggttattgctggtttgactatgaaagagatatatgcagaatcgatgggctatttaatccatggagcgaacgtgac accgggtatcgtttatggatgagtgaggtaggtaatgccgcgtctggcaggacctggaaacaaaaggtagcatacggtaggga gagaactgctcttggggagcagctgtgtgaacgtccactggacgatgaaactggcccgtttgctgaacttttttgccgagagat gttctgcgtagactaggcgcacgtcacataggacgtagagttgtattaggcagagaagccgatggatggaggtatcagaggcc gggaaagggcccatccaccctatatttggacgcagcatcaggcacccccttgagaatggtgacgggagacgaggccagtcgt gcgagtctaagagactttcccaatgtgagtgaagcagagatacctgatgctgtgttcgctgccaagcgctaa
dCas9_VP64	atgtctagagccccaaagaagaagagaaaagttagacccggggataagaaatactctattggtttggctatcggtacaaactct gttggttgggctgttattactgatgaatacaaggttccatccaagaagttcaaggttttgggtaacactgatagacactccatcaaa aagaacttgattggtgccttgttgttcgattctggtgaaactgctgaagctactagattgaaaagaaccgctagaagaagatacac cagaagaaagaacagaatctgctacttgcaagaaatcttctccaacgaaatggccaaggttgatgattcattcttccacagattgg aagaatccttcttggtcgaagaagataagaagcacgaaagacatccaatcttcggtaacatcgttgatgaagttgcttaccacga aaagtacccaactatctaccatttgagaaagaagttggttgactctaccgataaggctgatttgagattgatctatttggctttggcc cacatgattaagttcagaggtcatttcttgatcgaaggtgatttgaacccagataactccgatgttgataagttgttcatccaattagt ccaaacctacaatcaattattcgaagaaaacccaatcaacgcctctggtgttgatgctaaagctattttgtctgccagattgtccaa gtccagaagattagaaaatttgatcgcccaattaccaggtgaaaagaagaatggtttgttcggtaatttgattgccttgtctttgggt ttgactccaaacttcaagtccaatttcgatttggctgaagatgccaagttgcaattatctaaggatacctacgatgacgatttggata acttgttggctcaaatcggtgatcaatacgctgatttgtttttggctgctaagaacttgtccgatgccattttgttgtccgatattttgag agtcaacaccgaaattactaaggctccattgtctgcctctatgatcaaaagatacgatgaacaccaccaagacttgactttgttga aggctttggtcagacaacaattacctgaaaagtacaaagaaattttcttcgatcaatccaagaacggttacgccggttatattgatg gtggtgcttctcaagaagaattttacaagttcatcaagccaatcttggaaaagatggacggtactgaagaattattggtcaagttga acagagaagatttgttgagaaagcaaagaaccttcgacaacggttctattccacatcaaattcacttgggtgaattgcacgcaatt ttgagaagacaagaagatttttatccattcttgaaggacaacagagaaaagatcgaaaagattctgaccttcagaatcccttacta cgttggtccattggctagaggtaattcaagatttgcctggatgactagaaagtccgaagaaactattactccttggaacttcgaag aagttgtagataagggtgcttctgcccaatcctttattgaaagaatgaccaacttcgacaagaacttgccaaacgaaaaggttttg ccaaagcactctttgttgtacgaatacttcaccgtctacaacgaattgactaaggttaagtacgtcaccgaaggtatgagaaaacc agcttttttatccggtgaacaaaagaaggctatcgtcgatttgttgttcaagaccaacagaaaggttactgtcaagcaattaaaaga agattacttcaagaaaatcgaatgcttcgactccgttgaaatttctggtgtcgaagatagattcaatgcctctttaggtacttaccatg acttgttgaaaatcatcaaggacaaggatttcttggacaacgaagaaaacgaagatattttggaagatattgtcttgacattgacct tgtttgaagatagagaaatgattgaagaaagattgaaaacctacgcccacttgttcgatgataaggttatgaagcaattaaagaga agaagatacactggttggggtagattgtccagaaaattgattaacggtatcagagacaagcaatccggtaagaccattttggact ttttgaagtctgatggtttcgctaacagaaacttcatgcaattaatccacgacgattccttgactttcaaagaagatatacaaaaggc ccaagtctctggtcaaggtgattctttacatgaacatatcgctaacttggctggttctccagctattaagaagggtattttacaaacc gttaaggtcgttgacgaattggtcaaagttatgggtagacataagccagaaaacatcgttatcgaaatggctagagaaaatcaaa ccacccaaaagggtcaaaagaactccagagaaagaatgaagagaatcgaagaaggtatcaaagaattgggttcccaaattttg aaagaacacccagttgaaaacacccaattacaaaacgaaaagttgtacttgtactacttgcaaaacggtagagatatgtacgttg accaagaattggacatcaacagattgtctgattacgatgttgacgctatcgttccacaatctttttgaaggatgactccattgacaa caaggtcttgactagatccgataagaatagaggtaagtccgataacgttccatctgaagaagtcgttaagaaaatgaagaactat

	tggagacaattattgaacgccaagttgatcacccaaagaaagtttgacaatttgaccaaggctgaaagaggtggtttgtctgaatt ggataaggcaggtttcatcaaaagacaattagtagaaaccagacaaatcaccaagcacgttgctcaaattttggatagtagaatg aacactaagtacgacgaaaacgacaaattgatcagagaagttaaggtcattaccttgaagtccaagttggtttccgatttcagaaa ggacttccaattctacaaggtcagagaaatcaacaactaccatcatgcacatgatgcttacttgaatgctgttgttggtactgccttg attaagaagtatccaaagttggaatccgaatttgtctacggtgattacaaggtttacgacgttagaaagatgatcgccaagtccga acaagaaattggtaaagctactgccaaatacttcttctactccaatattatgaatttctttaagaccgaaatcactttggccaacggt gaaattagaaaaagaccattgattgaaactaatggtgaaacaggtgaaatcgtttgggataagggtagagattttgccactgttag aaaggtattgtccatgccacaagtaaacatcgtcaaaaagaccgaagttcaaactggtggtttctccaaagaatccattttgccta agagaaactccgataagttgatcgctagaaaaaaagactgggacccaaaaaagtacggtggttttgattctccaactgttgctta ctctgttttggttgttgctaaggtcgaaaagggtaagagtaagaagttgaagtccgtcaaagaattattaggtatcactatcatgga aagatcctcattcgaaaagaatcctatcgacttttggaagccaagggttacaaagaagtcaagaaggacttgatcattaagttgc caaagtacagtttgttcgaattggaaaatggtagaaagagaatgttggcttctgccggtgaattacaaaagggtaatgaattggct ttgccatccaagtacgttaatttcttatacttggcctcccactacgaaaaattgaaaggttctcctgaagataacgaacaaaagcaa ttatttgtcgaacaacacaagcactacttggacgaaatcattgaacaaatttccgaattttccaaaagagtcattttggctgacgcca atttggacaaagttttgtcagcttacaacaagcacagagataagccaattagagaacaagctgaaaacatcattcacttgttcactt tgactaacttgggtgctccagctgcttttaagtatttcgataccactatcgacagaaagagatacacctctaccaaagaagttttgg acgctactttgatccaccaatctattactggtttgtacgaaactagaatcgacttgtctcaattaggtggtgatggttctggtagatct ggagtcgacggtggaggttctgacgctttggacgacttcgacttggatatgctgggttctgatgcgctagatgactttgacctcga catgcttggaagtgacgccttagatgattttgacctggatatgcttggatcagacgctctggacgatttcgacttagacatgctttcc taa
gRNA expression cassette	gagctcgggggatctgccaattgaacataacatggtagttacatatactagtaatatggttcggcacacattaaaagtataaaaac tatctgaattacgaattacatatattggtcataaaaatcaatcaatcatcgtgtgttttatatgtctcttatctaagtataagaatatccat agttaatattcacttacgctacctttttaacctgtaatcattgtcaacaggatatgttaacgacccacattgataaacgctagtatttcttt ttcctcttcttattggccggctgtctctatactcccctatagtctgtttcttttcgtttcgattgttttacgtttgaggcctcgtggcgcaca tggtacgctgtggtgctcgcggctgggaacgaaactctgggagctgcgattggcagaagcttNNNNNNNNNNNNNNNNNNNgttttagagctagaaatagcaagttaaaataaggctagtccgttatcaacttgaaaaagtggcaccgagtcg gtgctttttttctcgagccatatccaacttccaatttaatctttcttttttaattttcacttatttgcgatacagaaagaaaaaagcgatagt aactattgaattttgtttggatttggttagattagatatggtttctcttatatttacatgctaaaaatgggctacaccagagatacataat tagatatatatacgccagtacaccttatcggcccaagccttgtcccaaggcagcgttttgttcttggaaacgctgccctacacgttc gctatgcttcaagaacttttctgagcacttcatgatgcatgtttgttccttattggttagctttgatgttgtgaagtcattgacacagtct gtgaaacatctttctaccagattagagtacaaacgcatgaaatccttcatttgcttttgttccactacttttttggaactcttgttgttcttt gg
Plasmid Name	**Description**
p4FP	pRS416-tef1p-GFP-tef1t-pdc1p-sapphire-pdc1t-tpi1p-mCHerry-tpi1t-pgk1p-Venus-pgk1t
pTomato	pRS416-eno2p-tdTomato-eno2t
pViolacein	pRS416- tef1p-VioA-tef1t- pgk1p-VioB-pgk1t- eno2p-VioC-eno2t- tpi1p-VioD-cyc1t-pdc1p-VioE-pdc1t
pCas9	pRS413-gal1p-dCas9_VP64-cyc1t
pgRNA(n)*	pRS425-rpr1p-gRNA-rpr1t

* All the gRNAs use the same structure except the 20bp targeting to different sites.

Table D.S2. Strains used in this study.

Name	Phenotype	Plasmid
TEF1p(H)	INVSc1: MATa his3D1 leu2 trp1-289 ura3-52 MAT his3D1 leu2 trp1-289 ura3-52	pViolacein, pCas9, pgRNA-TEF1p(H)
TEF1p(M)	Same as INVSc1	pViolacein, pCas9, pgRNATEF1p(M)
TEF1p(L)	Same as INVSc1	pViolacein, pCas9, pgRNATEF1p(L)
PDC1p(H)	Same as INVSc1	pViolacein, pCas9, pgRNAPDC1p(H)
PDC1p(M)	Same as INVSc1	pViolacein, pCas9, pgRNAPDC1p(M)
PDC1p(L)	Same as INVSc1	pViolacein, pCas9, pgRNAPDC1p(L)
TPI1p(M)	Same as INVSc1	pViolacein, pCas9, pgRNATPI1p(M)
TPI1p(L)	Same as INVSc1	pViolacein, pCas9, pgRNATPI1p (L)
ENO2p(H)	Same as INVSc1	pViolacein, pCas9, pgRNAENO2p(H)
ENO2p(M)	Same as INVSc1	pViolacein, pCas9, pgRNAENO2p(M)
ENO2p(L)	Same as INVSc1	pViolacein, pCas9, pgRNAENO2p(L)
ACD	Same as INVSc1	pViolacein, pCas9, pgRNATEF1p(H)-gRNAENO2p(H)-gRNATPI1p(L)
CD	Same as INVSc1	pViolacein, pCas9, pgRNAENO2p(H)-gRNATPI1p(L)
AD	Same as INVSc1	pViolacein, pCas9, pgRNATEF1p(H)-gRNATPI1p(L)

Table D.S3. Key parameters of guide RNAs used in this study for model training.

TEF1p-GFP

ATAGCTTCAAAATGTTTCTACTCCTTTTTTACTCTTCCAGATTTTCTCGGACTCCGCGC

ATCGCCGTACCACTTCAAAACACCCAAGCACAGCATACTAAATTTCCCCTCTTTCTTC

CTCTAGGGTGTCGTTAATTACCCGTACTAAAGGTTTGGAAAAGAAAAAAGAGACCGC

CTCGTTTCTTTTTCTTCGTCGAAAAAGGCAATAAAAATTTTTATCACGTTTCTTTTTCT
G1
TGAAAATTTTTTTTTTTGATTTTTTTCTCTTTCGATGACCTCCCATTGATATTTAAGTTA

ATAAACGGTCTTCAATTTCTCAAGTTTCAGTTTCATTTTTCTTGTTCTATTACAACTTTT
G2
TTTACTTCTTGCTCATTAGAAAGAAAGCATAGCAATCTAATCTAAGTTTTAATTACAAA

ATGTCTAAAGGTGAAGAATTATTCACTGGTGTTGTCCCAATTTTGGTTGAATTAGATG
G3 G4 G5 G6
GTGATGTTAATGGTCACAAATTTTCTGTCTCCGGTGAAGGTGAAGGTGATGCTACTTA
G7 G8 G9 G10
CGGTAAATTGACCTTAAAATTTATTTGTACTACTGGTAAATTGCCAGTTCCATGGCCAA
G11 G12 G13
CCTTAGTCACTACTTTAACTTATGGTGTTCAATGTTTTTCTAGATACCCAGATCATATGA
G14
AACAACATGACTTTTTCAAGTCTGCCATGCCAGAAGGTTATGTTCAAGAAAGAACTAT
G15
TTTTTTCAAAGATGACGGTAACTACAAGACCAGAGCTGAAGTCAAGTTTGAAGGTGA
G16 G17
TACCTTAGTTAATAGAATCGAATTAAAAGGTATTGATTTTAAAGAAGATGGTAACATTT
G18 G19
TAGGTCACAAATTGGAATACAACTATAACTCTCACAATGTTTACATCATGGCTGACAA
G20 G21 G22
ACAAAAGAATGGTATCAAAGTTAACTTCAAAATTAGACACAACATTGAAGATGGTTCT
G23 G24
GTTCAATTAGCTGACCATTATCAACAAAATACTCCAATTGGTGATGGTCCAGTCTTGTT
G25
ACCAGACAACCATTACTTATCCACTCAATCTGCCTTATCCAAAGATCCAAACGAAAAG

AGAGACCACATGGTCTTGTTAGAATTTGTTACTGCTGCTGGTATTACCCATGGTATGGA
G26 G27 G28
TGAATTGTACAAA

No.	Location	GC%	ΔG	AGG	TGG	CGG	GGG	#G	#A	Fold change (log2)
G1	-213	0.3	-9.1	1	0	0	0	2	4	0.00
G2	-114	0.1	-7.3	0	0	1	0	2	9	-0.02
G3	9	0.15	-9.3	1	0	0	0	1	9	-3.38
G4	27	0.3	-12	0	1	0	0	4	9	-0.29
G5	44	0.45	-11	0	1	0	0	4	3	0.01
G6	57	0.3	-7.8	0	1	0	0	4	6	0.07
G7	69	0.3	-7	0	1	0	0	6	7	0.03
G8	90	0.4	-8.4	0	0	1	0	3	4	-0.24

G9	96	0.4	-9.5	1	0	0	0	4	4	-0.50
G10	102	0.55	-10.8	1	0	0	0	7	3	-1.54
G11	117	0.45	-8.8	0	0	1	0	7	5	-0.09
G12	150	0.15	-10.4	0	1	0	0	1	7	-0.15
G13	169	0.45	-12.9	0	1	0	0	4	5	-0.24
G14	198	0.25	-8.6	0	1	0	0	1	6	0.07
G15	270	0.5	-9.9	1	0	0	0	4	5	-0.01
G16	309	0.2	-8	0	0	1	0	2	7	-0.19
G17	345	0.4	-10	1	0	0	0	6	7	-0.35
G18	378	0.2	-7.1	1	0	0	0	3	10	-0.04
G19	399	0.25	-7.9	0	1	0	0	5	8	0.05
G20	411	0.25	-10.8	1	0	0	0	4	9	0.08
G21	422	0.25	-8.1	0	1	0	0	2	8	-0.97
G22	458	0.35	-7.1	0	1	0	0	1	6	0.08
G23	477	0.35	-7.6	0	1	0	0	4	11	-0.31
G24	519	0.3	-7	0	1	0	0	3	10	0.13
G25	564	0.25	-8.1	0	1	0	0	0	10	-0.21
G26	653	0.4	-7	0	1	0	0	4	12	-0.12
G27	681	0.35	-8.9	0	1	0	0	4	4	0.00
G28	693	0.5	-14.5	0	1	0	0	4	4	0.21

TPI1p-mCherry

TATATCTAGGAACCCATCAGGTTGGTGGAAGATTACCCGTTCTAAGACTTTTCAGCTTC
M1 M2
CTCTATTGATGTTACACCTGGACACCCCTTTTCTGGCATCCAGTTTTTAATCTTCAGTG
M3 M4
GCATGTGAGATTCTCCGAAATTAATTAAAGCAATCACACAATTCTCTCGGATACCACCT
M5
CGGTTGAAACTGACAGGTGGTTTGTTACGCATGCTAATGCAAAGGAGCCTATATACCT
M6 M7 M8 M9
TTGGCTCGGCTGCTGTAACAGGGAATATAAAGGGCAGCATAATTTAGGAGTTTAGTGA
M10 M11 M12 M13 M14
ACTTGCAACATTTACTATTTTCCCTTCTTACGTAAATATTTTTCTTTTTAATTCTAAATCA

ATCTTTTTCAATTTTTTGTTTGTATTCTTTTCTTGCTTAAATCTATAACTACAAAAAACA

CATACATAAACTAAAAA**TG**GTTAGCAAAGGCGAGGAAGATAACATGGCTATAATCAA
M15 M16
AGAGTTTATGAGATTCAAAGTACACATGGAGGGTTCAGTGAATGGTCATGAATTTGAA
M17 M18 M19
ATTGAAGGCGAAGGCGAGGGCAGACCTTACGAAGGAACTCAAACAGCAAAACTTAA
M20
GGTAACAAAAGGTGGTCCTCTGCCATTCGCCTGGGACATTCTCAGTCCACAATTCATG
M21 M22 M23
TACGGTTCTAAAGCGTACGTCAAACATCCAGCAGACATTCCAGATTACTTGAAATTGT
M24
CTTTTCCAGAAGGCTTTAAGTGGGAAAGAGTTATGAACTTCGAGGATGGAGGGGTTG
M25 M26 M27
TGACCGTTACGCAAGATTCCTCTTTACAAGATGGTGAGTTTATCTACAAGGTCAAATT

M28

AAGGGGACTAATTTTCCTTCAGACGGGCCAGTCATGCAGAAAAAGACTATGGGATG

M29M30 M31 M32

GGAAGCCTCTTCAGAGAGAATGTATCCTGAAGATGGCGCTCTAAAAGGAGAAATCAA

M33

GCAAAGATTGAAGTTAAAGGACGGAGGTCATTATGATGCAGAAGTAAAAACAACCTA

M34 M35

TAAAGCTAAAAAGCCAGTTCAACTTCCTGGTGCCTACAATGTTAACATCAAGCTAGAC

ATTACATCCCATAATGAAGATTACACTATAGTGGAACAGTATGAACGTGCTGAAGGTA

M36

GACACAGTACAGGTGGTATGGATGAACTGTACAAG

M37 M38

No.	Location	GC%	Energy	AGG	TGG	CGG	GGG	#G	#A	Fold change (log2)
M1	-408	0.45	-11.8	0	1	0	0	4	6	2.36
M2	-405	0.55	-14.5	0	1	0	0	6	5	2.31
M3	-353	0.4	-8.2	0	1	0	0	2	4	2.65
M4	-314	0.3	-7.4	0	1	0	0	2	5	2.60
M5	-265	0.35	-8.2	0	0	1	0	1	8	1.79
M6	-253	0.45	-8.6	0	0	1	0	2	5	1.15
M7	-239	0.55	-10.7	1	0	0	0	4	5	0.35
M8	-236	0.55	-10.5	0	1	0	0	6	5	0.76
M9	-211	0.4	-11.4	1	0	0	0	4	6	0.81
M10	-194	0.4	-14.2	0	1	0	0	3	7	1.93
M11	-189	0.45	-12.2	0	0	1	0	4	4	0.10
M12	-176	0.55	-11.1	1	0	0	0	6	2	0.20
M13	-165	0.35	-7.4	1	0	0	0	5	8	0.26
M14	-150	0.3	-9.6	1	0	0	0	4	8	0.92
M15	2	0.2	-7	0	1	0	0	0	13	0.05
M16	29	0.45	-7	0	1	0	0	6	10	0.22
M17	68	0.3	-7	0	1	0	0	3	9	-0.29
M18	71	0.4	-7.5	1	0	0	0	5	8	0.15
M19	84	0.5	-7.7	0	1	0	0	7	6	-1.14
M20	116	0.5	-10.7	1	0	0	0	8	7	-0.17
M21	165	0.3	-7.2	1	0	0	0	3	11	-0.02
M22	168	0.3	-8.7	0	1	0	0	4	11	0.08
M23	187	0.65	-10.8	0	1	0	0	5	1	0.68
M24	216	0.4	-7	0	0	1	0	2	6	0.67
M25	282	0.3	-8.6	1	0	0	0	3	5	0.28
M26	314	0.4	-8.3	1	0	0	0	6	7	0.03
M27	322	0.4	-11.3	0	0	0	1	6	6	-0.05
M28	377	0.35	-10.3	1	0	0	0	5	6	0.22
M29	388	0.25	-7.1	1	0	0	0	2	8	0.17
M30	389	0.25	-7	0	0	0	1	2	9	0.18
M31	411	0.4	-9.9	0	0	1	0	4	5	-0.60
M32	442	0.4	-7.3	0	1	0	0	6	9	-0.07

M33	477	0.4	-7.2	0	1	0	0	6	8	-0.11
M34	518	0.3	-7	1	0	0	0	4	10	0.43
M35	525	0.4	-7.6	1	0	0	0	7	8	0.02
M36	647	0.25	-7.1	0	1	0	0	3	9	0.34
M37	687	0.5	-7.1	0	1	0	0	7	8	0.54
M38	692	0.45	-8.6	0	1	0	0	6	7	0.41

PDC1p-Sapphire

CATGCGACTGGGTGAGCATATGTTCCGCTGATGTGATGTGCAAGATAAACAAGCAAG
S1
GCAGAAACTAACTTCTTCTTCATGTAATAAACACACCCCGCGTTTATTTACCTATCTCT

AAACTTCAACACCTTATATCATAACTAATATTTCTTGAGATAAGCACACTGCACCCATA

CCTTCCTTAAAAACGTAGCTTCCAGTTTTTGGTGGTTCCGGCTTCCTTCCCGATTCCG
S2 S3 S4
CCCGCTAAACGCATATTTTTGTTGCCTGGTGGCATTTGCAAAATGCATAACCTATGCAT
S5 S6
TTAAAAGATTATGTATGCTCTTCTGACTTTTCGTGTGATGAGGCTCGTGGAAAAAATG
S7 S8
AATAATTTATGAATTTGAGAACAATTTTGTGTTGTTACGGTATTTTACTATGGAATAATC
S9 S10
AATCAATTGAGGATTTTATGCAAATATCGTTTGAATATTTTTCCGACCCTTTGAGTACTT
S11
TTCTTCATAATTGCATAATATTGTCCGCTGCCCCTTTTTCTGTTAGACGGTGTCTTGATC
S12
TACTTGCTATCGTTCAACACCACCTTATTTTCTAACTATTTTTTTTTTAGCTCATTTGAAT

CAGCTTATGGTGATGGCACATTTTTGCATAAACCTAGCTGTCCTCGTTGAACATAGGA
S13 S14
AAAAAAAATATATAAACAAGGCTCTTTCACTCTCCTTGCAATCAGATTTGGGTTTGTTC
S15
CCTTTATTTTCATATTTCTTGTCATATTCCTTTCTCAATTATTATTTTCTACTCATAACCTC

ACGCAAAATAACACAGTCAAATCAATCAAA**ATG**TCTAAAGGTGAAGAATTATTCACTG
S16
GTGTTGTCCCAATTTTGGTTGAATTAGATGGTGATGTTAATGGTCACAAATTTTCTGTC
S17 S18
TCCGGTGAAGGTGAAGGTGATGCTACTTACGGTAAATTGACCTTAAAATTTATTTGTA
S19 S20 S21 S22
CTACTGGTAAATTGCCAGTTCCATGGCCAACCTTAGTCACTACTTTTTCTTATGGTGTT
S23 S24 S25
ATGGTTTTTGCTAGATACCCAGATCATATGAAACAACATGACTTTTTCAAGTCTGCCAT

GCCAGAAGGTTATGTTCAAGAAAGAACTATTTTTTTCAAAGATGACGGTAACTACAA
S26 S27
GACCAGAGCTGAAGTCAAGTTTGAAGGTGATACCTTAGTTAATAGAATCGAATTAAAA
S28 S29
GGTATTGATTTTAAAGAAGATGGTAACATTTTAGGTCACAAATTGGAATACAACTTTAA
S30 S31 S32
CTCTCACAATGTTTACATCATGGCTGACAAACAAAAGAATGGTATCAAAGCTAACTTC
S33 S34
AAAATTAGACACAACATTGAAGATGGTGGTGTTCAATTAGCTGACCATTATCAACAAA

S35

ATACTCCAATTGGTGATGGTCCAGTCTTGTTACCAGACAACCATTACTTATCCATTCAA

S36

TCTGCCTTATCCAAAGATCCAAACGAAAAGAGAGACCACATGGTCTTGTTAGAATTTG

TTACTGCTGCTGGTATTACCCATGGTATGGATGAATTGTACAAA

S37 S38

No.	Location	GC%	Energy	AGG	TGG	CGG	GGG	#G	#A	Fold change (log2)
S1	-745	0.35	-8.4	1	0	0	0	4	10	-0.35
S2	-596	0.35	-10.1	0	1	0	0	3	6	-0.02
S3	-593	0.45	-11.2	0	1	0	0	5	3	-0.29
S4	-587	0.45	-10.7	0	0	1	0	5	1	0.15
S5	-541	0.35	-8.3	0	1	0	0	3	5	0.03
S6	-538	0.45	-10.4	0	1	0	0	5	2	-0.78
S7	-468	0.4	-8.3	1	0	0	0	5	2	-1.39
S8	-461	0.5	-9.6	0	1	0	0	7	2	-1.29
S9	-413	0.25	-11.6	0	0	1	0	4	6	-1.42
S10	-400	0.3	-8.5	0	1	0	0	4	4	-0.40
S11	-381	0.25	-7.1	1	0	0	0	3	9	-0.08
S12	-283	0.45	-9.2	0	0	1	0	3	2	-0.18
S13	-202	0.35	-10.1	0	1	0	0	3	6	1.13
S14	-196	0.35	-10	0	1	0	0	5	5	-0.02
S15	-103	0.4	-9	0	1	0	0	2	5	-0.02
S16	27	0.3	-12	0	1	0	0	4	9	-2.35
S17	57	0.3	-7.8	0	1	0	0	4	6	-2.40
S18	69	0.3	-7	0	1	0	0	6	7	-1.60
S19	90	0.4	-8.4	0	0	1	0	3	4	-1.40
S20	96	0.4	-9.5	1	0	0	0	4	4	-2.35
S21	102	0.55	-10.8	1	0	0	0	7	3	-1.45
S22	117	0.45	-8.8	0	0	1	0	7	5	-2.60
S23	150	0.15	-10.4	0	1	0	0	1	7	-1.45
S24	169	0.45	-12.9	0	1	0	0	4	5	-0.97
S25	198	0.25	-8.2	0	1	0	0	1	4	-0.71
S26	270	0.5	-9.9	1	0	0	0	4	5	-2.47
S27	309	0.2	-8	0	0	1	0	2	7	-0.82
S28	345	0.4	-10	1	0	0	0	6	7	-1.29
S29	378	0.2	-7.1	1	0	0	0	3	10	-0.76
S30	399	0.25	-7.9	0	1	0	0	5	8	-0.40
S31	411	0.25	-10.8	1	0	0	0	4	9	-0.65
S32	422	0.25	-8.1	0	1	0	0	2	8	-0.40
S33	458	0.35	-7.1	0	1	0	0	1	6	-0.82
S34	477	0.35	-7.6	0	1	0	0	4	11	-1.40
S35	519	0.3	-7	0	1	0	0	3	10	-0.06
S36	564	0.25	-8.1	0	1	0	0	0	10	-2.35

S37	681	0.35	-8.9	0	1	0	0	4	4	-2.17
S38	693	0.5	-14.5	0	1	0	0	4	4	-2.40

PGK1p-Venus

TCAGGCATGAACGCATCACAGACAAAATCTTCTTGACAAACGTCACAATTGATCCCTC

CCCATCCGTTATCACAATGACAGGTGTCATTTTGTGCTCTTATGGGACGATCCTTATTA
V1V2
CCGCTTTCATCCGGTGATAGACCGCCACAGAGGGGCAGAGAGCAATCATCACCTGCA
V3 V4 V5
AACCCTTCTATACACTCACATCTACCAGTGTACGAATTGCATTCAGAAAACTGTTTGC

ATTCAAAAATAGGTAGCATACAATTAAAACATGGCGGGCACGTATCATTGCCCTTATCT
V6 V7
TGTGCAGTTAGACGCGAATTTTTCGAAGAAGTACCTTCAAAGAATGGGGTCTCATCTT
V8
GTTTTGCAAGTACCACTGAGCAGGATAATAATAGAAATGATAATATACTATAGTAGAGA
V9
TAACGTCGATGACTTCCCATACTGTAATTGCTTTTAGTTGTGTATTTTTAGTGTGCAAG

TTTCTGTAAATCGATTAATTTTTTTTTCTTTCCTCTTTTTATTAACCTTAATTTTTATTTTA

GATTCCTGACTTCAACTCAAGACGCACAGATATTATAACATCTGCACAATAGGCATTTG

CAAGAATTACTCGTGAGTAAGGAAAGAGTGAGGAACTATCGCATACCTGCATTTAAA

GATGCCGATTTGGGCGCGAATCCTTTATTTTGGCTTCACCCTCATACTATTATCAGGGC
V10 V11
CAGAAAAAGGAAGTGTTTCCCTCCTTCTTGAATTGATGTTACCCTCATAAAGCACGTG
V12
GCCTCTTATCGAGAAAGAAATTACCGTCGCTCGTGATTTGTTTGCAAAAAGAACAAA

ACTGAAAAAACCCAGACACGCTCGACTTCCTGTCTTCCTATTGATTGCAGCTTCCAAT

TTCGTCACACAACAGGGTCCTAGCGACGGCTCACAGGTTTTGTAACAAGCAATCGAA
V13 V14 V15
GGTTCTGGAATGGCGGGAAAGGGTTTAGTACCACATGCTATGATGCCCACTGTGATCT
V16 V17
CCAGAGCAAAGTTCGTTCGATCGTACTGTTACTCTCTCTCTTTCAAACAGAATTGTCC

GAATCGTGTGACAACAACAGCCTGTTCTCACACACTCTTTTCTTCTAACCAAGGGGG
V18 V19
TGGTTTAGTTTAGTAGAACCTCGTGAAACTTACATTTACATATATATAAACTTGCATAAA

TTGGTCAATGCAAGAAATACATATTTGGTCTTTTCTAATTCGTAGTTTTTCAAGTTCTTA
V20
GATGCTTTCTTTTTCTCTTTTTTACAGATCATCAAGGAAGTAATTATCTACTTTTTACAA
V21
CAAATATAAAACAA**ATG**TCTAAAGGTGAAGAATTATTCACTGGTGTTGTCCCAATTTTG
V22 V23
GTTGAATTAGATGGTGATGTTAATGGTCACAAATTTTCTGTCTCCGGTGAAGGTGAA
V24 V25 V26 V27
GGTGATGCTACTTACGGTAAATTGACCTTAAAATTGATTTGTACTACTGGTAAATTGCC
V28

AGTTCCATGGCCAACCTTAGTCACTACTTTAGGTTATGGTTTGCAATGTTTTGCTAGAT

ACCCAGATCATATGAAACAACATGACTTTTTCAAGTCTGCCATGCCAGAAGGTTATGT

TCAAGAAAGAACTATTTTTTTCAAAGATGACGGTAACTACAAGACCAGAGCTGAAGT

CAAGTTTGAAGGTGATACCTTAGTTAATAGAATCGAATTAAAAGGTATTGATTTTAAAG

AAGATGGTAACATTTTAGGTCACAAATTGGAATACAACTATAACTCTCACAATGTTTAC

ATCACTGCTGACAAACAAAAGAATGGTATCAAAGCTAACTTCAAAATTAGACACAAC

ATTGAAGATGGTGGTGTTCAATTAGCTGACCATTATCAACAAAATACTCCAATTGGTG

ATGGTCCAGTCTTGTTACCAGACAACCATTACTTATCCTATCAATCTGCCTTATCCAAA

GATCCAAACGAAAAGAGAGACCACATGGTCTTGTTAGAATTTGTTACTGCTGCTGGTA

TTACCCATGGTATGGATGAATTGTACAAA

V29 V30 V31 V32 V33 V34

No.	Location	GC%	Energy	AGG	TGG	CGG	GGG	#G	#A	Fold change (log2)
V1	-1200	0.4	-13.6	0	1	0	0	5	2	0.18
V2	-1199	0.35	-13.9	0	0	0	1	4	2	0.42
V3	-1172	0.4	-12.6	0	0	1	0	1	3	0.11
V4	-1152	0.6	-12.3	0	0	0	1	6	6	0.07
V5	-1151	0.6	-12.1	0	0	0	1	7	6	0.60
V6	-1037	0.3	-7	0	1	0	0	3	10	0.05
V7	-1034	0.3	-7.9	0	0	1	0	3	10	0.24
V8	-965	0.35	-10.2	0	1	0	0	4	10	0.15
V9	-930	0.45	-8.9	1	0	0	0	4	5	0.22
V10	-645	0.35	-12.7	0	1	0	0	4	6	0.82
V11	-601	0.35	-7.7	1	0	0	0	0	5	0.27
V12	-589	0.4	-7	1	0	0	0	4	8	0.40
V13	-409	0.4	-7	1	0	0	0	1	7	0.01
V14	-397	0.5	-7	0	0	1	0	4	8	0.61
V15	-389	0.65	-10.3	1	0	0	0	6	4	0.51
V16	-356	0.45	-8.5	0	1	0	0	6	7	0.68
V17	-353	0.45	-9.6	0	0	1	0	7	6	0.63
V18	-199	0.35	-8.7	1	0	0	0	0	5	1.33
V19	-196	0.4	-9	0	0	0	1	2	4	0.51
V20	-132	0.15	-8.2	0	1	0	0	1	10	0.24
V21	-39	0.3	-7.1	1	0	0	0	1	5	1.71
V22	27	0.3	-12	0	1	0	0	4	9	-0.29
V23	44	0.45	-11	0	1	0	0	4	3	0.10
V24	57	0.3	-7.8	0	1	0	0	4	6	-1.82
V25	69	0.3	-7	0	1	0	0	6	7	-1.21
V26	90	0.4	-8.4	0	0	1	0	3	4	-0.17
V27	96	0.4	-9.5	1	0	0	0	4	4	0.21

V28	150	0.2	-8.6	0	1	0	0	2	7	-0.06
V29	192	0.4	-11.1	1	0	0	0	1	5	-1.66
V30	198	0.3	-7	0	1	0	0	3	5	-0.09
V31	270	0.5	-9.9	1	0	0	0	4	5	-0.27
V32	309	0.2	-8	0	0	1	0	2	7	0.09
V33	378	0.2	-7.1	1	0	0	0	3	10	-0.13
V34	399	0.25	-7.9	0	1	0	0	5	8	-0.49

Table D.S4. Key parameters of guide RNAs used in validation experiments (Eno2p-tdTomato).

CGCTCAGCATCTGCTTCTTCCCAAAGATGAACGCGGCGTTATGTCACTAACGACGTGC
T1
ACCAACTTGCGGAAAGTGGAATCCCGTTCCAAAACTGGCATCCCTAATTGATACATCT
T2 T3 T4
ACACACCGCACGCCTTTTTTCTGAAGCCCACTTTCGTGGACTTTGCCATATGCAAAAT
T5
TCATGAAGTGTGATACCAAGTCAGCATACACCTCACTAGGGTAGTTTCTTTGGTTGTA
T6 T7
TTGATCATTTGGTTCATCGTGGTTCATTAATTTTTTTCTCCATTGCTTTCTGGCTTTGAT
T8 T9 T10
CTTACTATCATTTGGATTTTTGTCGAAGGTTGTAGAATTGTATGTGACAAGTGGCACCA
T11 T12 T13
AGCATATATAAAAAAAAAAAGCATTATCTTCCTACCAGAGTTGATTGTTAAAAACGTAT

TTATAGCAAACGCAATTGTAATTAATTCTTATTTTGTATCTTTTCTTCCCTTGTCTCAATC

TTTTATTTTTATTTTATTTTTCTTTTCTTAGTTTCTTTCATAACACCAAGCAACTAATACT

ATAACATACAATAATA**ATG**GTGAGCAAGGGCGAGGAGGTCATCAAAGAGTTCATGCG

CTTCAAGGTGCGCATGGAGGGCTCCATGAACGGCCACGAGTTCGAGATCGAGGGCG
T14 T15 T16 T17 T18
AGGGCGAGGGCCGCCCCTACGAGGGCACCCAGACCGCCAAGCTGAAGGTGACCAA
T19T20 T21T22 T23T24 T25 T26
GGGCGGCCCCCTGCCCTTCGCCTGGGACATCCTGTCCCCCCAGTTCATGTACGGCTCC
T27 T28 T29 T30
AAGGCGTACGTGAAGCACCCCGCCGACATCCCCGATTACAAGAAGCTGTCCTTCCCC

GAGGGCTTCAAGTGGGAGCGCGTGATGAACTTCGAGGACGGCGGTCTGGTGACCGT
T31T32 T33 T34 T35 T36
GACCCAGGACTCCTCCCTGCAGGACGGCACGCTGATCTACAAGGTGAAGATGCGCGG
T37 T38 T39 T40
CACCAACTTCCCCCCCGACGGCCCCGTAATGCAGAAGAAGACCATGGGCTGGGAGG
T41 T42 T43 T44 T45
CCTCCACCGAGCGCCTGTACCCCCGCGACGGCGTGCTGAAGGCGAGATCCACCAG
T46 T47 T48
GCCCTGAAGCTGAAGGACGGCGGCCACTACCTGGTGGAGTTCAAGACCATCTACATG
T49
GCCAAGAAGCCCGTGCAACTGCCCGGCTACTACTACGTGGACACCAAGCTGGACATC
T50
ACCTCCCACAACGAGGACTACACCATCGTGGAACAGTACGAGCGCTCCGAGGGCCG
T51 T52 T53
CCACCACCTGTTCCTGGGGCATGGCACCGGCAGCACCGGCAGCGGCAGCTCCGGCA
T54 T55 T56 T57 T58 T59
CCGCCTCCTCCGAGGACAACAACATGGCCGTCATCAAAGAGTTCATGCGCTTCAAGG
T60 T61
TGCGCATGGAGGGCTCCATGAACGGCCACGAGTTCGAGATCGAGGGCGAGGGCGAG
T62 T63 T64 T65 T66
GGCCGCCCCTACGAGGGCACCCAGACCGCCAAGCTGAAGGTGACCAAGGGCGGCCC
T67 T68 T69 T70T71 T72
CCTGCCCTTCGCCTGGGACATCCTGTCCCCCCAGTTCATGTACGGCTCCAAGGCGTAC

T73T74 T75 T76
GTGAAGCACCCCGCCGACATCCCCGATTACAAGAAGCTGTCCTTCCCCGAGGGCTTC
T77T78
AAGTGGGAGCGCGTGATGAACTTCGAGGACGGCGGTCTGGTGACCGTGACCCAGGA
T79T80 T81 T82 T83 T84 T85
CTCCTCCCTGCAGGACGGCACGCTGATCTACAAGGTGAAGATGCGCGGCACCAACTT
T86
CCCCCCCGACGGCCCCGTAATGCAGAAGAAGACCATGGGCTGGGAGGCCTCCACCG
T87 T88 T89
AGCGCCTGTACCCCCGCGACGGCGTGCTGAAGGGCGAGATCCACCAGGCCCTGAAG
T90T91 T92
CTGAAGGACGGCGGCCACTACCTGGTGGAGTTCAAGACCATCTACATGGCCAAGAAG
T93 T94 T95 T96
CCCGTGCAACTGCCCGGCTACTACTACGTGGACACCAAGCTGGACATCACCTCCCAC
T97
AACGAGGACTACACCATCGTGGAACAGTACGAGCGCTCCGAGGGCCGCCACCACCT
T98 T99
GTTCCTGTACGGCATGGACGAGCTGTACAAG

No.	Location	GC%	Energy	AGG	TGG	CGG	GGG	#G	#A	Fold change (log2)
T1	-516	0.45	-7.9	0	0	1	0	3	6	-1.81
T2	-482	0.5	-8.6	0	0	1	0	4	6	0.59
T3	-475	0.55	-9.8	0	1	0	0	6	6	-1.79
T4	-456	0.5	-11.7	0	1	0	0	4	6	-1.85
T5	-397	0.45	-14.3	0	1	0	0	3	3	-1.86
T6	-338	0.45	-7.9	1	0	0	0	2	7	-1.67
T7	-325	0.45	-12.8	0	1	0	0	4	3	-1.53
T8	-308	0.3	-11.2	0	1	0	0	4	3	0.10
T9	-298	0.35	-7.8	0	1	0	0	4	4	-0.97
T10	-266	0.3	-7	0	1	0	0	1	1	-1.12
T11	-244	0.3	-10	0	1	0	0	2	4	-0.15
T12	-230	0.3	-8	1	0	0	0	4	4	-1.94
T13	-205	0.35	-8.4	0	1	0	0	6	7	-1.72
T14	56	0.6	-15.8	0	1	0	0	6	4	-1.41
T15	59	0.65	-14.4	1	0	0	0	8	3	-1.62
T16	72	0.6	-14.9	0	0	1	0	7	5	-1.43
T17	92	0.65	-9.7	1	0	0	0	7	4	-2.29
T18	93	0.6	-9.3	0	0	0	1	7	5	-1.36
T19	98	0.65	-12.7	1	0	0	0	9	4	-1.94
T20	99	0.6	-10.6	0	0	0	1	9	5	-1.90
T21	104	0.75	-10.8	1	0	0	0	11	4	-2.27
T22	105	0.7	-8.7	0	0	0	1	11	5	-1.79
T23	119	0.85	-16.2	1	0	0	0	9	2	-2.11
T24	120	0.8	-12.8	0	0	0	1	8	3	-1.98
T25	143	0.65	-8.3	1	0	0	0	4	6	-2.41
T26	152	0.6	-11.2	1	0	0	0	6	6	-2.15
T27	153	0.55	-10.2	0	0	0	1	6	7	-1.74
T28	156	0.55	-9.5	0	0	1	0	8	7	-1.25

T29	176	0.8	-10.9	0	0	0	1	4	0	-1.65
T30	204	0.55	-7.4	0	0	1	0	3	3	-2.16
T31	269	0.6	-9.8	1	0	0	0	4	4	-2.20
T32	270	0.55	-10.1	0	0	0	1	4	5	-2.19
T33	280	0.65	-11.1	0	1	0	0	5	3	-1.77
T34	302	0.6	-8.8	1	0	0	0	8	4	0.10
T35	306	0.55	-9.3	0	0	1	0	7	5	-0.13
T36	314	0.65	-11.8	0	1	0	0	8	4	-2.07
T37	344	0.7	-11.5	1	0	0	0	4	3	-1.39
T38	348	0.65	-14.4	0	0	1	0	5	4	-0.44
T39	365	0.6	-8.9	1	0	0	0	6	5	-0.28
T40	378	0.45	-8.7	0	0	1	0	6	7	-0.12
T41	399	0.7	-8.6	0	0	1	0	3	4	0.33
T42	425	0.45	-7	0	1	0	0	5	9	-0.42
T43	426	0.4	-9.7	0	0	0	1	5	9	0.68
T44	430	0.55	-7	0	1	0	0	7	7	0.70
T45	434	0.6	-9	1	0	0	0	9	6	-0.60
T46	465	0.75	-8.9	0	0	1	0	6	3	-1.75
T47	476	0.8	-11	1	0	0	0	7	2	0.68
T48	491	0.65	-10.4	1	0	0	0	7	5	-0.65
T49	548	0.45	-7	0	1	0	0	4	7	0.24
T50	599	0.55	-7.8	0	1	0	0	4	6	-1.09
T51	620	0.6	-7.9	1	0	0	0	3	6	-0.55
T52	635	0.55	-8.2	0	1	0	0	4	7	-0.77
T53	657	0.6	-8.4	0	0	0	1	6	6	-0.34
T54	679	0.7	-10.1	0	0	0	1	4	2	-2.56
T55	684	0.65	-10.3	0	1	0	0	5	3	-2.05
T56	690	0.65	-9.5	0	0	1	0	7	2	-2.33
T57	699	0.75	-9.7	0	0	1	0	8	4	-2.55
T58	705	0.8	-12.5	0	0	1	0	8	4	-2.74
T59	714	0.75	-12	0	0	1	0	7	4	-2.49
T60	731	0.8	-11	1	0	0	0	4	1	-2.14
T61	743	0.55	-9.7	0	1	0	0	3	7	-2.25
T62	782	0.6	-15.8	0	1	0	0	6	4	-2.48
T63	786	0.6	-9.6	0	0	0	1	7	4	-2.37
T64	818	0.65	-9.7	1	0	0	0	7	4	-2.37
T65	824	0.65	-12.7	1	0	0	0	9	4	-2.10
T66	830	0.75	-10.8	1	0	0	0	11	4	-1.65
T67	845	0.85	-16.2	1	0	0	0	9	2	-0.04
T68	846	0.8	-12.8	0	0	0	1	8	3	-0.17
T69	869	0.65	-8.3	1	0	0	0	4	6	0.03
T70	878	0.6	-11.2	1	0	0	0	6	6	-0.30
T71	879	0.55	-10.2	0	0	0	1	6	7	-0.98
T72	882	0.55	-9.5	0	0	1	0	8	7	-0.08
T73	901	0.85	-10.6	0	1	0	0	5	0	-0.07

T74	902	0.8	-10.9	0	0	0	1	4	0	-1.79
T75	930	0.55	-7.4	0	0	1	0	3	3	0.18
T76	938	0.55	-7.4	1	0	0	0	4	4	0.29
T77	995	0.6	-9.8	1	0	0	0	4	4	-1.08
T78	996	0.55	-10.1	0	0	0	1	4	5	0.01
T79	1006	0.65	-11.1	0	1	0	0	5	3	0.03
T80	1007	0.6	-9.4	0	0	0	1	5	3	-0.37
T81	1028	0.6	-8.8	1	0	0	0	8	4	-0.06
T82	1032	0.55	-9.3	0	0	1	0	7	5	0.16
T83	1035	0.55	-8.1	0	0	1	0	8	5	0.26
T84	1040	0.65	-11.8	0	1	0	0	8	4	0.10
T85	1055	0.7	-14.3	1	0	0	0	7	2	-0.90
T86	1074	0.65	-14.4	0	0	1	0	5	4	-0.36
T87	1125	0.7	-8.6	0	0	1	0	3	4	-0.38
T88	1157	0.55	-7.9	0	0	0	1	7	7	0.30
T89	1160	0.6	-9	1	0	0	0	9	6	0.35
T90	1202	0.8	-11	1	0	0	0	7	2	-0.29
T91	1203	0.75	-10.2	0	0	0	1	7	3	-0.15
T92	1217	0.65	-10.4	1	0	0	0	7	5	-0.20
T93	1232	0.65	-9.5	1	0	0	0	5	5	-0.32
T94	1236	0.6	-12.1	0	0	1	0	7	6	-0.28
T95	1239	0.65	-11.7	0	0	1	0	8	5	0.14
T96	1250	0.7	-10.8	0	1	0	0	7	5	-0.01
T97	1325	0.55	-7.8	0	1	0	0	4	6	-2.05
T98	1346	0.6	-7.9	1	0	0	0	3	6	-1.95
T99	1361	0.55	-8.2	0	1	0	0	4	7	-1.96

Table D.S5. Binary regression decision tree model.

Group	Value	Decision path
1	0.115	<6 → <4 → <-563
2	-0.871	<6 → <4 → ≥-563
3	2.122	<6 → ≥ 4 → <-13.45
4	-1.044	<6 → ≥ 4 → ≥-13.45 → <-408 → ≥-528
5	0.821	<6 → ≥ 4 → ≥-13.45 → <-408 → <-528 → <-12.5
6	0.597	<6 → ≥ 4 → ≥-13.45 → <-408 → <-528 → ≥-12.5 → ≥7
7	0.018	<6 → ≥ 4 → ≥-13.45 → <-408 → <-528 → ≥-12.5 → <7 → <-8.1
8	0.240	<6 → ≥ 4 → ≥-13.45 → <-408 → <-528 → ≥-12.5 → <7 → ≥ -8.1
9	2.364	<6 → ≥ 4 → ≥-13.45 → ≥-408 → <-404
10	0.053	<6 → ≥ 4 → ≥-13.45 → ≥-408 → ≥-404 → <4 → ≥7
11	0.564	<6 → ≥ 4 → ≥-13.45 → ≥-408 → ≥-404 → <4 → <7 → <-8.4
12	2.323	<6 → ≥ 4 → ≥-13.45 → ≥-408 → ≥-404 → <4 → <7 → ≥ -8.4
13	-0.755	<6 → ≥ 4 → ≥-13.45 → ≥-408 → ≥-404 → ≥4 → ≥-8.45
14	-0.401	<6 → ≥ 4 → ≥-13.45 → ≥-408 → ≥-404 → ≥4 → <-8.45 → <-394
15	0.526	<6 → ≥ 4 → ≥-13.45 → ≥-408 → ≥-404 → ≥4 → <-8.45 → ≥-394
16	-3.382	≥ 6 → <-9.15 → <838 → <0.525 → <18
17	0.319	≥ 6 → <-9.15 → <838 → <0.525 → ≥ 18 → = 1
18	0.055	≥ 6 → <-9.15 → <838 → <0.525 → ≥ 18 → = 0 → <4
19	-0.400	≥ 6 → <-9.15 → <838 → <0.525 → ≥ 18 → = 0 → ≥4 → ≥5
20	-0.542	≥ 6 → <-9.15 → <838 → <0.525 → ≥ 18 → = 0 → ≥4 → <5 → <0.275
21	-1.662	≥ 6 → <-9.15 → <838 → <0.525 → ≥ 18 → = 0 → ≥4 → <5 → ≥0.275 → <3
22	-1.097	≥ 6 → <-9.15 → <838 → <0.525 → ≥ 18 → = 0 → ≥4 → <5 → ≥0.275 → ≥3 → <-13.7
23	-0.606	≥ 6 → <-9.15 → <838 → <0.525 → ≥ 18 → = 0 → ≥4 → <5 → ≥0.275 → ≥3 → ≥-13.7 → <-12.5
24	-0.925	≥ 6 → <-9.15 → <838 → <0.525 → ≥ 18 → = 0 → ≥4 → <5 → ≥0.275 → ≥3 → ≥-13.7 → ≥-12.5 → <341
25	-0.596	≥ 6 → <-9.15 → <838 → <0.525 → ≥ 18 → = 0 → ≥4 → <5 → ≥0.275 → ≥3 → ≥-13.7 → ≥-12.5 → ≥ 341
26	-0.134	≥ 6 → <-9.15 → <838 → ≥0.525 → <585 → ≥346
27	-0.484	≥ 6 → <-9.15 → <838 → ≥0.525 → <585 → <346 → <2
28	-0.911	≥ 6 → <-9.15 → <838 → ≥0.525 → <585 → <346 → ≥ 2 → ≥ 9.6
29	-1.488	≥ 6 → <-9.15 → <838 → ≥0.525 → <585 → <346 → ≥ 2 → <9.6 → <82
30	-1.706	≥ 6 → <-9.15 → <838 → ≥0.525 → <585 → <346 → ≥ 2 → <9.6 → ≥ 82 → < 4
31	-2.083	≥ 6 → <-9.15 → <838 → ≥0.525 → <585 → <346 → ≥ 2 → <9.6 → ≥ 82 → ≥ 4
32	-1.654	≥ 6 → <-9.15 → <838 → ≥0.525 → ≥585 → ≥827
33	-2.290	≥ 6 → <-9.15 → <838 → ≥0.525 → ≥585 → <827 → =0
34	-2.528	≥ 6 → <-9.15 → <838 → ≥0.525 → ≥585 → <827 → =1
35	-0.953	≥ 6 → <-9.15 → ≥838 → <5
36	-0.009	≥ 6 → <-9.15 → ≥838 → ≥5 → ≥8
37	-0.980	≥ 6 → <-9.15 → ≥838 → ≥5 → <8 → ≥7
38	-0.628	≥ 6 → <-9.15 → ≥838 → ≥5 → <8 → <7 → <-13.2
39	0.157	≥ 6 → <-9.15 → ≥838 → ≥5 → <8 → <7 → ≥-13.2 → ≥-9.4
40	-0.273	≥ 6 → <-9.15 → ≥838 → ≥5 → <8 → <7 → ≥-13.2 → <-9.4 → =0
41	-0.018	≥ 6 → <-9.15 → ≥838 → ≥5 → <8 → <7 → ≥-13.2 → <-9.4 → =1
42	-1.983	≥ 6 → ≥-9.15 → ≥1243
43	0.028	≥ 6 → ≥-9.15 → <1243 → <147 → ≥8
44	-2.099	≥ 6 → ≥-9.15 → <1243 → <147 → <8 → ≥0.575
45	-0.604	≥ 6 → ≥-9.15 → <1243 → <147 → <8 → <0.575 → <5
46	-1.196	≥ 6 → ≥-9.15 → <1243 → <147 → <8 → <0.575 → ≥5
47	-1.242	≥ 6 → ≥-9.15 → <1243 → ≥147 → <4
48	0.193	≥ 6 → ≥-9.15 → <1243 → ≥147 → ≥4 → <1
49	0.324	≥ 6 → ≥-9.15 → <1243 → ≥147 → ≥4 → ≥1 → <-7.5 → =0 → ≥1141
50	0.036	≥ 6 → ≥-9.15 → <1243 → ≥147 → ≥4 → ≥1 → <-7.5 → =0 → <1141 → <6

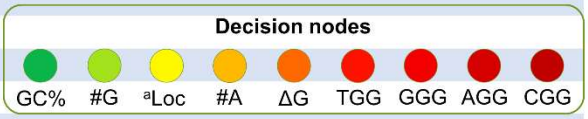

Cont. Table D.S5. Binary regression decision tree model.

Group	Value	Decision path
51	-0.206	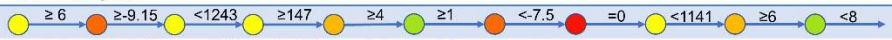
52	-0.605	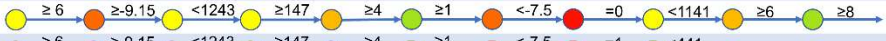
53	-0.209	
54	-0.745	
55	0.511	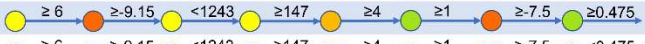
56	0.671	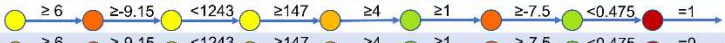
57	0.158	
58	0.178	
59	-0.067	
60	-0.252	

Table D.S6. Measured and predicted concentrations of products from violacein pathway

Strains	Measured concentrations (A.U.)				Predicted concentrations (A.U.)			
	PV	PDV	V	DV	PV	PDV	V	DV
TEF1p(H)	472.00	216.30	229.70	22.90	481.83	219.39	220.37	27.13
TEF1p(M)	392.70	206.80	294.00	32.30	422.47	191.06	191.92	24.63
TEF1p(L)	345.70	138.30	177.00	16.30	356.13	159.59	160.32	21.71
PDC1p(H)	408.30	188.60	222.50	23.50	835.91	390.75	392.48	40.50
PDC1p(M)	297.30	142.80	168.70	2.10	417.21	188.55	189.41	24.41
PDC1p(L)	55.10	40.70	60.70	0.10	85.92	35.23	35.40	7.36
TPI1p(M)	270.00	134.20	120.70	14.20	537.68	102.32	200.50	25.40
TPI1p(L)	342.20	120.00	132.90	15.90	239.27	400.73	200.50	25.40
ENO2p(H)	375.20	168.60	147.10	17.40	357.22	192.65	283.68	32.35
ENO2p(M)	337.80	156.20	199.20	19.90	425.71	198.31	215.19	26.69
ENO2p(L)	455.60	231.70	74.30	24.70	598.05	216.54	42.85	8.46
ACD	235.15	161.80	251.65	34.20	57.17	363.64	295.96	36.48
CD	219.75	149.10	245.45	28.10	57.17	297.88	295.96	36.48
AD	251.95	286.35	81.10	23.40	202.19	377.62	150.95	22.50

Note: PV: Proviolacein, PDV: Prodeoxyviolacein, V: Violacein, DV: Deoxyviolacein

Appendix E: Supplementary Material of Chapter 6.1

Table E.S1. Primers used in this study.

Name	Primer sequence
XF_FP_csXR_ADH1t	ATGAGCCCAAGCCCAATTCC
XF_FP_ctXDH_CYC1t	ATGACTGCAAACCCATCATT
XF_FP_ppXKS_ADH2t	ATGGTTACCAAAGAAATCCA
XF_RP_csXR_ADH1t	GCATGCCGGTAGAGGTGTGG
XF_RP_ctXDH_CYC1t	GCAAATTAAAGCCTTCGAGC
XF_RP_ppXKS_ADH2t	CTCACTAAAGGGAACAAAAGCTGGAGCTCCACCGCGGTGGAGCTACTAATAGGATAAATT
XF_FP_PDC1p	AACGACGGCCAGTGAGCGCGCGTAATACGACTCACTATAGCATGCGACTGGGTGAGCATA
XF_FP_TEF1p	CATGAGGTCGCTCTTATTGACCACACCTCTACCGGCATGCATAGCTTCAAAATGTTTCTA
XF_FP_ENO2p	GCTTGAGAAGGTTTTGGGACGCTCGAAGGCTTTAATTTGCGTGTCGACGCTGCGGGTATA
XF_RP_PDC1p	CGTTGTTCAACTTGAAAGCTGGAATTGGGCTTGGGCTCATTTTGATTGATTTGACTGTGT
XF_RP_TEF1p	CGTCAACTTTGTTAAGAACTAATGATGGGTTTGCAGTCATTTTGTAATTAAAACTTAGAT
XF_RP_ENO2p	TCATTGCTGAATTTCTATCTTGGATTTCTTTGGTAACCATTATTATTGTATGTTATAGTA

Table E.S2. Promoters used in this study

Name	Promoter Strength	Promoter sequence
TEF1p(H)	Strong	ATAGCTTCAAAATGTTTCTACTCCTTTTTTACTCTTCCGGATTTTCTCGGACTCCGCGC ATCGCCGTACCACCTCAAAACACCCAAGCACAGCATACTCAATTCCCCCTCTTTCTTC CTCTAGGGTGTCGTTAATTACCCGTACTAAAGGTTTGGAAAAGAAGAAAGAGACCG CCTCGTCTCTCTTTCTTCGTCGAAAAAGGCAATAAAAATTTTTATTACGTTTCTTTTTC TTGAAAATTTTCTTTTTTGATTTTTCTCTCTTTCGATGACCTCCCATTGATATTTAAGT CATTAAATGGTCTTCAATTTCTCAAGTTTCAGTTTCATTTTTCTTATTCTATTACGACT CTTTTTACCTCTTGCTCATTAGAAAGAAAGCATAGCAATCTAATCTAAGTTTTAATTA CAAA
TEF1p(M)	Medium	ATAGCTTCAAAATGTTTCTACTCCTTTTTTACTCTTCCAGATTTTCTCGGACTCCGCGC ACCGCCGTACCACTTCAAAACACCCAAGCACAGCATACTAAATTCCCCCTCTTTCTT CCTCTAGGGTGTCGTTAATTACCCGTACTAAAGGTTTGGAAAAGAAAAAAGAGACC GCCTCGTTTCTTTTTCTTCGTCGAAGAAGGCAATAAAAATTTTTATCACGTTTCGTTT TCTTGAAAACTTTTCTTTTTGATTCTTTTCTCTTTCGATGACCTCCCATTGATATTTAA GTTATTAGATGGTCTTCAATTTCTCAAGTTTCAGCTCCATTTTTCTTGTTCTATTACAA CTTTTTTTACTTCTTGCTCATTAGAAAGAAAGCATAGCAATCTAATCTAAGTTTTAAT TACAAA
TEF1p(L)	Low	ATAGCTTCAAAATGTTTCTACTCCTTTTTTACTCCTCCAGACTTCCTCGGACTCCGCG CATCGCCGTACCACTTCAAAACACCCAAGCACAGCATACTAAATTCCCCCTCTTTCTT CCTCTAGGGTGTCGTTAATTACCCGTACTAAAGGTTTGGAAAAGAAAAAAGAGACC GCCTCGTTTCTTTTCCTTCGTCGAAAAAGGCAATAGAAATTTTTATCACGTTTTTCCT TCTTGAAAATCTTTTTTTTTGATTTTTTTCTCTTTCGATGACCTCCCATTGACATTTAA GTTATTAAATGGTCTTCAATTTCTCAAGTTTCAGTTTCATTTTTCTTGTTCTATTACAA CTTTTTTTACTTCTTGCTCATTAGAAAGAAAGCATAGCAATCTAATCTAAGTTTTAAT TACAAA
TEF1p*	(Mutated)	ATAGCTTCAAAATGTTTCTACTCCTTTTTTACTCTTCCAGATTTTCTCGGACTCCGCGC ACCGCCGTACCACTTCAAAACACCCAAGCACAGCATACTAAATTCCCCCTCTTTCTT CCTCTAGGGTGTCGTTAATTACCCGTACTAAAGGTTTGGAAAAGAAAAAAGAGACC GCCTCGTTTCTTTTTCTTCGTCGAAGAAGGCAATAAAAATTTTTATCACGTTTCGTTT TCTTGAAAACTTTTCTTTTTGATTCTTTTCTCTTTCGATGACCTCCCATTGATATTTAA GTTATTAGATGGTCTTCAATTTCTCAAGTTTCAGCTCCATTTTTCTTGTTCTATTACAA CTTTTTTTACTTCTTGCTCATTAGAAAGAAAGCATAGCAATCTAATCTAAGTTTTAAT TACAAA
ENO2p(H)	Strong	GTGTCGACGCTGCGAGTATAGAAAGGGCTCTTTACTCTATAGTACCTCCTCGCTCGG CATCTGCTTCCTCCCAAAGATGAGCGCGGCGTCATGTCACTAACGACGTGCACCAAC TTGCGGAAAGTGGAATCCCGTTCCAAAACTGGCATCCACTAATTGATACATCTACAC ACCGCACGCCTTTTTTCTGAAGCCCACTTTCGTGGACTTTGCCATATGCAAAATTCAT GAAGTGTGACACTGAGTCAGCATACACCTCACTAGGGTAGTTTCTTTGGCTGTATTG ATCATTTGATTCATCGTGGTTCATTAATTTTTTTTCTCCACTGCTTTCTGGCTTTGATC TTACTATCATTTGGATTTTTGTCGAAGGTTGTAGAATTGTGTGTGACAAGTGGCACCA AGCATATATAAAAAAAAAAAGCATTATCTTCCCACCAGAGTTGATTGTTAAAAACGT ATTTATAGCAAACACAATTGTGATTAATTCTTATTTTGTATCTTTTCTTCCCTTGTCTC AATCTTTTATTTTCATTTTATTTTCCTTCTCTTAGTTTCTTTCATAACACCAAGCAACT AATACTATAACGTACAATAATA
ENO2p(M)	Medium	GTGTCGACGCTGCGGGTATAGAAAGGGTTCTTTACTCTATAGTACCTGCTCGCTCAG CACCTGCTTCTTCCCAAAGATGAACGCGGCGTTATGTCACTAACGACGTGCACCAAC TTGCGGAAAGTGGAATCCCGTTCCAAAACTGGCATCCACTAATTGATACACCTACAC ACTGCACGCCTTTTTTCCGAAGCCCACTTCCGTGGACTTTGCCATATGCAAAATTCAT GAAATGTGATACCAAGTCAGCATACACCTCACTAGGGCAGTTTCTTTGGTTGTATTG ATCATTTGGTTCATCGCGGTTCATTAATTTTTTTTCTCCATTGCTTTCTGGCTTTGATC TTACTATCATTTGGATTTTTGTCGAAAGTTGTAGAATTGTATGTGACAAGTGGCACCA AGCATATATAAAAGAAAAAAAGCATCATCTTCCTACCAGAGTTGATTGTTAAGAAC GTATTTATAGCAAACGCAGTTGTAGTTAATTCTTATTTTGTATCTTTTCTTCCCTTGTC CCGATCTTTTATTTTTATTTTATCTTTCTTTTCTTAGTTTCTGTCATAGCACCAAGCAA CTAATACTATAACGTACAATAATA
ENO2p(L)	Low	GTGTCGACGCTGCGGGTATAGAAAGGGTTCTTGACTCTATAGTACCTCCTCGCTCAG CATCTGCTTCTTCCCACAGATGAACGCGGCGTTATGTCACTAACGACGTGCACCAAC TTGCGGAAAGTGGAATCCCGTTCCAAAACTGGCATCCACGAATTGATAGATCTACAC ACCGCACGCCTTTTTTCTGAAGCCCACCTTCGTGGACTTTGCCATACGCAGAATTCGT

		GAAGTGTGATACCAAGTCAGCATACACCTCACCAGGGTAGTCTCTTTGGTTGTATTG ATCATTTGGTTCATCGTGGTTCATTAATTTTTTTTCTCTATTGCTTTCTGGCTTTGATC TTACTATCATTTGGATTCTTGTCGAAGGTTGTAGAATTGTATGTGACAAGTGGCACC AAGCATATATAAAAAAAAAAAGCATTATCTTCCTACCAGAGTTGATTGTTAAAAACG TATTTATAGCAAACGCAATTGTAATTAATTCTTATTTTGTGTCTTTTCTTCCCTTGTCT CAATCTTTTATCTTTGTTTTATTCTTCTTTTCTTAGTTTCCTTCATAACACCAAGCAAC TAACACTATAACATACAATAATA
ENO2p*	(Mutated)	GTGTCGACGCTGCGGGTATAGAAAGGGTTCTTTACTCTATAGTACCTCCTCGCTCAG CATCTGCTTCTTCCCAAAGATGAACACGGCGTTATGCCACTAACGGCGTGCACCGAC TTGCGGAAAGTGGAATCCCGTTCCAAAACTGGCATCCACTAATTGATACATCTACAC ACCGCACGCCTTTTCTCTGAAACCCACTTTCGTGGTGGACTTTGCCATATGCAAAATTTAT GAAGTGTGATACCAAGTCAGCATACACCTCACTAGGGTAGTTTCTTTGGTTGTGTTG ATCATTTGGTTCATCGTGGTTCATTAATTTTTTTTCTCCGTTGCTTTCTGGCCTTGATC TTACTATCATTTGGATTTTTGTCGAAGGTTGTAGAATTGTATGTGACAAGTGGCACCA AGCATATATAAAGAAAAAAAGCATTATCTTCCTACCAGAGTTGACTGCTAAAAACGT ATTTATAGCAAACGCAATTGTAATTGATTCTTATTTTGTATCTTTTCTTCCCTTGTCTC AATCTTTTATTTTTATTTTATTTTTCTTTTCTTAGTTTCTTTCATAACACCAAGCAACT AATACTATAACATACAATAATA
PDC1p(H)	Strong	CATGCGACTGGGTGAGCATATGTTCCGCTGGTGTGATGTGCAAGATAAACAAGCAA GGCAGAAACTAACTTCTTCTTCATGTAATAAACACACCCCGCGTTTATTTACCTATCT CTAAACTTCAACACCTTATATCATAACTAGTGTTTCTTGAGGTAAGCACACTGCACC CATACCTTCCTTAAAAACGTAGCTTCCAGTTTTTGGTGGTTCCGGCTTCCTTCCCGAT TCCGCCCGCTAGACGCATGTTTTTGTTGCCTGGCGGCATTTGTAAAGTGCATAACCTA TGCATTTAAAAGATTATGCATGCTCTTCTGACTCTTCGTGTGATGAGGCTCGTGGAA AAAATGAATAATTTATGAATTTGAGAACAATTTTGTGTTGTTACGGTATTTTACTATG GAATAATCAATCAATTGAGGATTTTATGCAAATATTGTTTGAATATTTTTCCGACCCT TTGAGTACTTTTCTTCATAATTGCATAATATTGTCCGCTGCCCCTTTTTCTGTTAGACG GTGTCTTGATCTACTTGCTATCGTTCAACACCACCTTATTTTCTAACTATTTTTTTTTT AGCTCATTTGAATCAGCTTATGGTGATGGCACATTTTTGCATAAACCTAGCTGTCCTC GTTGAACATAGGAAAAAAAAAATATATAAACACGGCTCTTTCACTCTCCTTGCAATC AGATTTGGGTTTGTTCCCTTTATTTTCATATTTCTTGTCATATTCCTTTCTCAATTATT ATTTTCTACTCATAACCTCACGCAAAATAACACAGTCAAATCAATCAAA
PDC1p(M)	Medium	CATGCGACTGGGTGAGCATATGTTCCGCTGATGTGATGTGCAAGATAAACAAGCAA GGCAGAAGCTAACTTCTTCTTCATGTGATAAACACACCCCGCGCTTATTTACCTATCT CTAAACCTCAACACCTTGTATCGTAACTAATATTTCTTGAGATAAGCACACTGCACC CATACCTTCCTTAAAAACGTAGCTTCCAGTTTTTGGTGGTTCCGGCTTCCTTCCCGAT TCCGCCCGCTAAACGCATGTTTTTGTTGCCTGGTGGCATTTGCAAAATGCATAACCTA TGCATTTAAAAGATTATGTATGCTCTTCTGACTTTTCGTGTGATGAGGCTCGTGGAAA AAATGAGTAATTTATGAACTTGAGAACAATTTTGTGTTGTTACGGTACTTTACTATGG AATAATCAATCAATTGAGGATTTTGTGTAAATATCGTTTGAATATTTCTCCGACCCTT TGAGTACTTTTCTTCATAATTGCATAATATTGTCCGCTGCCCCTTTTTCTGTTAGACG GCGTCTCGATCTACTTGCTGTCGTTCAACACCACCTTATTTTCTAACTATTTTTTTTTT AGCTCATTTGAATCGGCTTATGGTGATGGCACGTTTTTGCATAAACCTAGCTGTCCTC GTTGAACATAGGAAAAAAAAATATATAAACAAGGCTCTTTCACTCTCCTTGCAATCA GATTTGGGTTTGTTCCCTTTATTTTCATATTTCTTGCCATATTCCTTTCTCAATTATTAT TTTCTACTTATAACCTCACGCAAAATAGCACAGTCAAATCAGTCAAG
PDC1p(L)	Low	CATGCGACTGGGTGAGCATATGTTCCGCTGATGTGATGTACAAGATAAACAAGCAA GGCAGAAACTAACTTCCTCTTCATGTAATAAACACACCCCGCGTTTATTTACCTATCT CTAAACTTCAACCCCCTATATCATAACTAATATTTCTTGAGATAAGCACACTGCACC CATACCTTTCTTAAAAGCGCAGCTTCCAGTTTTTGGTGGTTCCGGCTTCCTTCCCGAT TCCGCCCGCTAAACGCATATTTTTGCTGCCTGGTGGCATTTGCAAAATGCATAACCT ACGCATTTAGAAGATTATGTATGCTCTTTTGATTTTTCGCGTGATGAGGCTCGTGGAG AAAATGGATAATTTATGAATTTGAGAACAATTTCATGTTGTTACGGTATTTTACTATG GAATAATCAATCAATTGAGGATTTTATGCAAATATCGTTTGAATATCTTTCCGACCCT TCGAGTACTTTTCTTCATAATTGCATAATATTGTCCGCAGCCCCTTTTTCTGTTAGAC GGTACCTTGATCTACTTGCTATCGTTCAACACCACCTTATTTTCTAACTATTTCTTCTT AGCTCATTTGAATCAGCCTGTGGTGATGGCACATTTTTGCACAAACCTAGCTGTCCTC GTTGAACATAGGAGGAAAAAACATATAAGCAGGGCTCTTTCACTCTCCTTGCAATCA GATTTGGGTTTGTTCCCTTTATTTCCATGCCTCTTGTCATATTCCTTTCTCAATTATTA TTTTCTACTCATAACCTCACGCAAAATAACACAGTCAAATTAACCAAA
PDC1p*	Mutated	CATGCGACTGGGTGAGCATATGTTCCGCTGATGTGGTGTGCAAGATAAACAAGCAA GGCAGAAGCTAACTTCTTCTTCATGTGATAAACACACCCCGCGCTTATTTACCTATCT CTAAACCTCAACACCTTGTATCGTAACTAATATTTCTTGAGATAAGCACACTGCACC CATACCTTCCTTAAAAACGTAGCTTCCAGTTTTTGGTGGTTCCGGCTTCCTTCCCGAT

TCCGCCCGCTAAACGCATGTTTTTGTTGCCTGGTGGCATTTGCAAAATGCATAACCTA
TGCATTTAAAAGATTATGTATGCTCTTCTGACTTTTCGTGTGATGAGGCTCGTGGAAA
AAATGAGTAATTTATGAACTTGAGAACAATTTTGTGTTGTTACGGTACTTTACTATGG
AATAATCAATCAATTGAGGATTTTGTATAAATATCGTTTGAATATTTCTCCGACCCTT
TGAGTACTTTTCTTCATAATTGCATAATATTGTCCGCTGCCCCTTTTTCTGTTAGACG
GCGTCTCGATCTACTTGCTGTCGTTCAACACCACCTTATTTTCTAACTATTTTTTTTTT
AGCTCATTTGAATCGGCTTATGGTGATGGCACGTTTTTGCATAAACCTAGCTGTCCTC
GTTGAACATAGGAAAAAAAAATATATAAACAAGGCTCTTTCACTCTCCTTGCAATCA
GATTTGGGTTTGTTCCCTTTATTTTCATATTTCTTGCCATATTCCTTTCTCAATTATTAT
TTTCTACTTATAACCTCACGCAAAATAGCACAGTCAAATCAGTCAAG

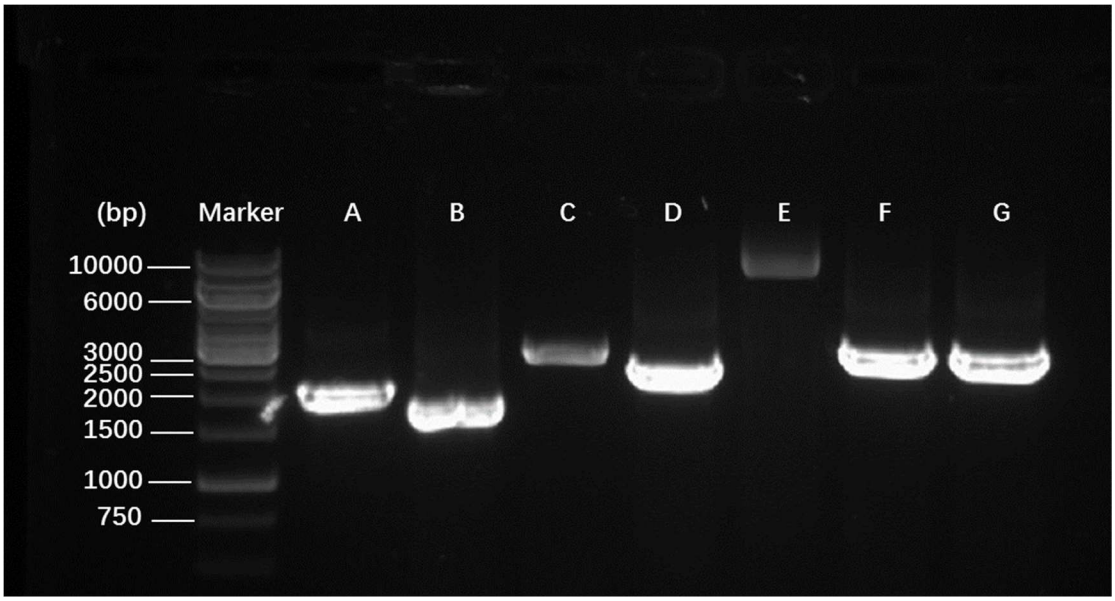

Fig. E.S1. DNA electrophoresis confirmed that all of the cassettes in both xylose pathway and 1-hexadecanol pathway existed in the evolved strains (second generation). (A) XR cassette (2160 bp) in pXF3X03; (B) XDH cassette (1730 bp) in pXF3X03; (C) XK cassette (2800 bp) in in pXF3X03; (D) TaFAR cassette (2503 bp) in pTaFAR_ACC1; (E) ACC1 cassette (7615 bp) in pTaFAR_ACC1; (F) ACL cassette1 (2840 bp) in pYlACL; (G) ACL cassette2 (2850 bp) in pYlACL.

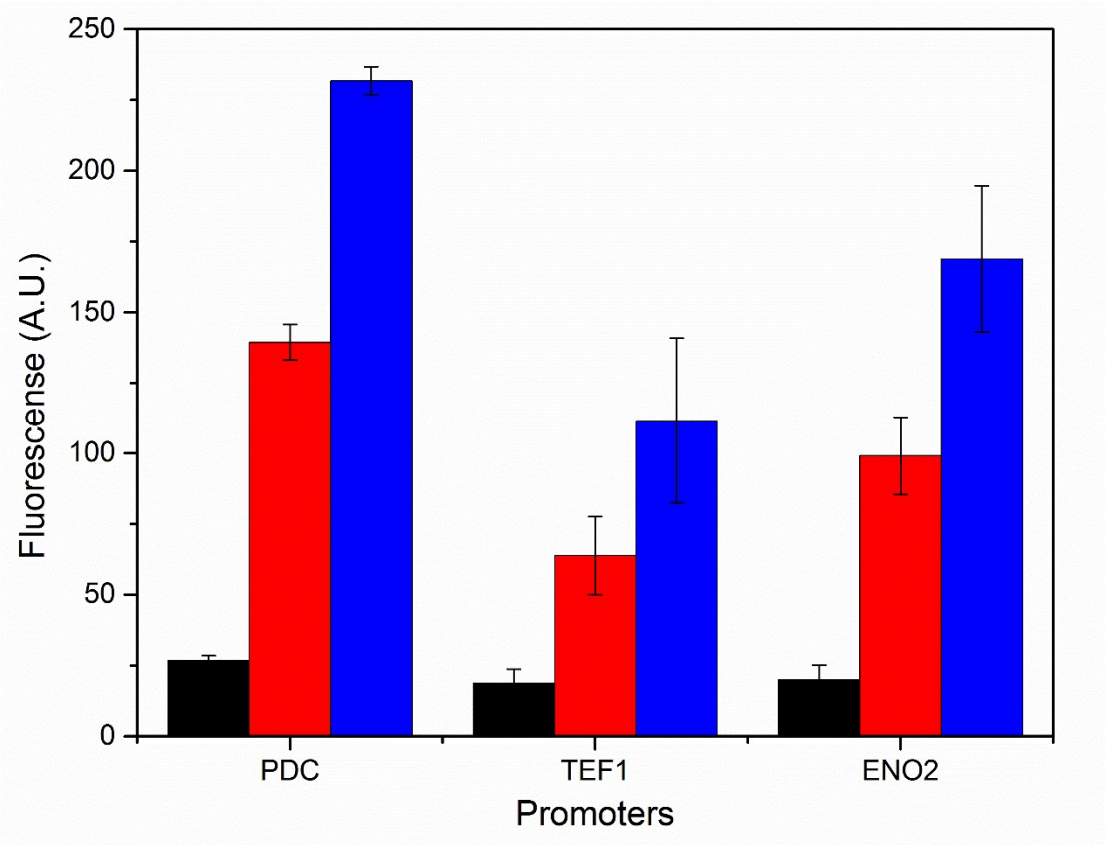

Fig. E.S2. The strengths of PDC1, TEF1, and ENO2 promoters in front of EGFP. The strength of wild-type PDC1, TEF1, and ENO2 promoter was normalized into 100. Black, red, and blue bars represent the promoters with low, medium, and high strength, respectively.

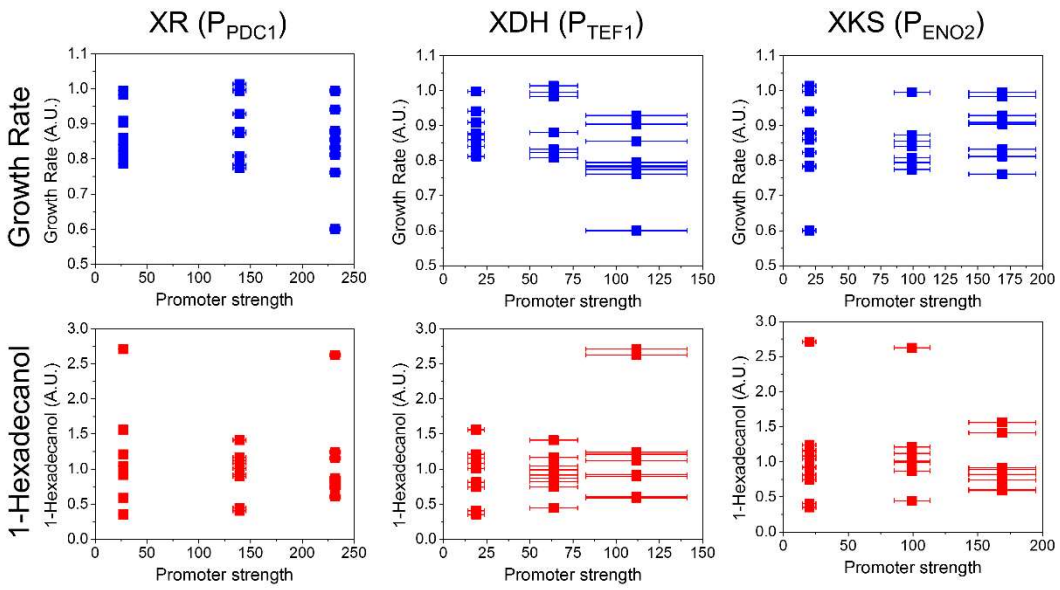

Fig. E.S3. Correlations between the promoter strengths in front of XR, XDH and XKS in xylose utilization pathways and the growth rates (blue dots) as well as 1-hexadecanol concentrations (red dots). The unit of promoter strength was the same as that was used in Figure S2, i.e., normalized fluorescence (A.U.) of EGFP expressed by PDC1, TEF1 and ENO2 promoters, respectively. No correlation was observed between promoter strength and 1-hexadecanol concentration. Similarly, no correlation was observed between promoter strength and growth.

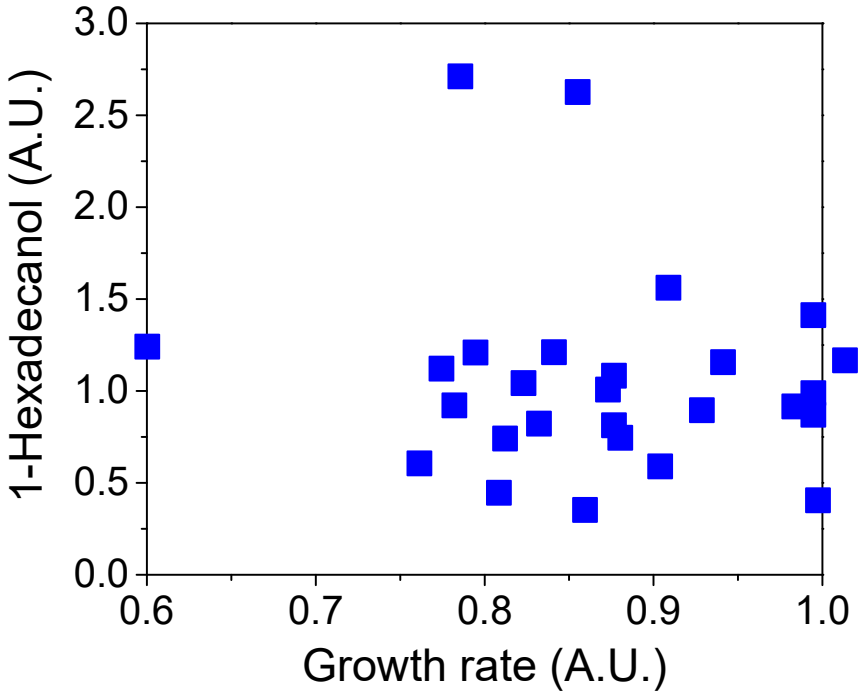

Fig. E.S4. Correlation between the growth rates and the 1-hexadecanol titers for the combinatorial promoter engineering.

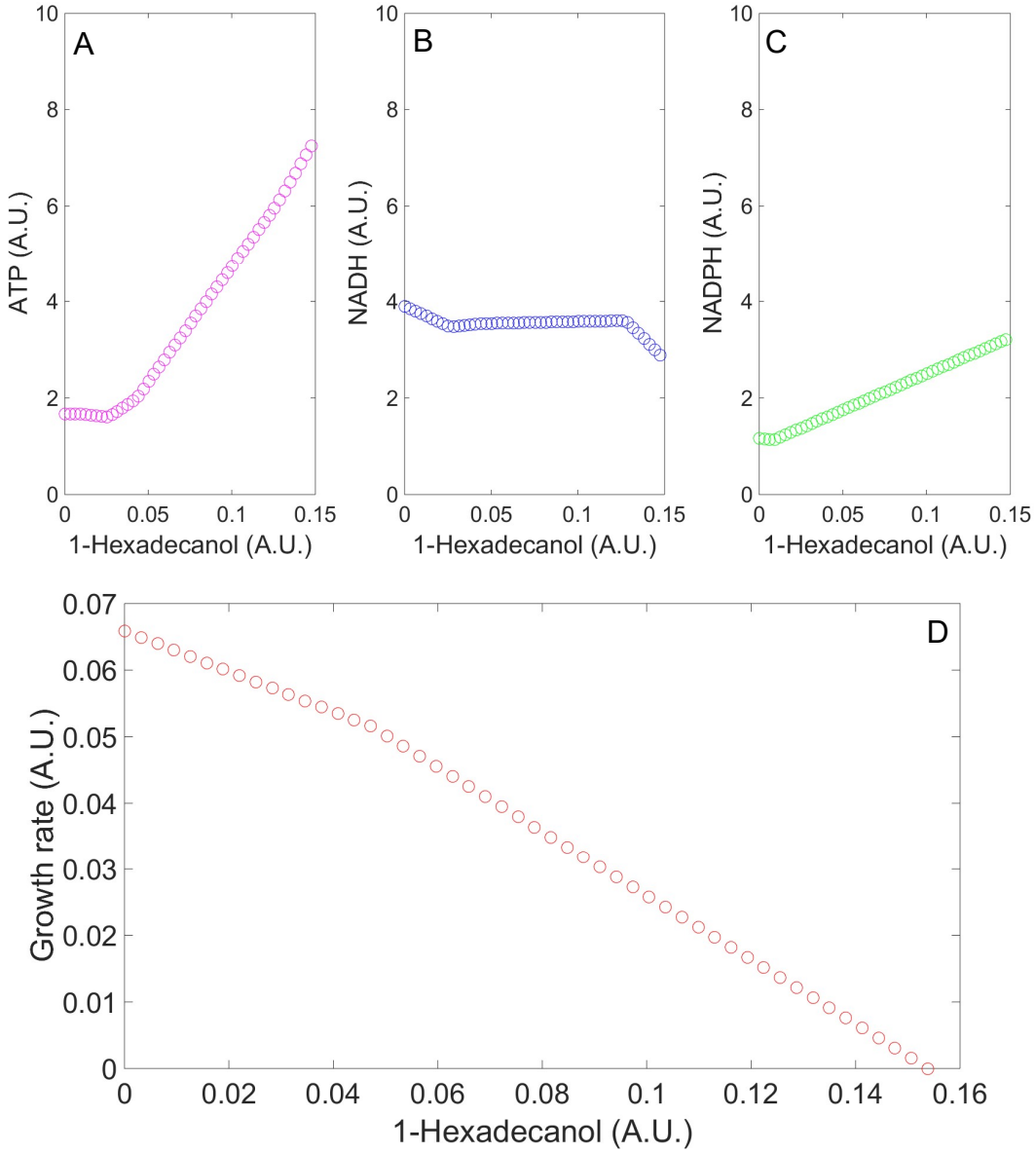

Fig. E.S5. Flux balance analysis revealed correlation between the 1-hexadecanol production and ATP (A), NADH (B), NADPH (C), and growth rate (D).